Doctoral theses at NTNU, 2023:25

Tichaona Mukono

Ferromanganese Production from Pretreated Manganese Ores: From Laboratory scale to Pilot scale.

Doctoral thesis

NTNU
Norwegian University of Science and Technology
Thesis for the Degree of
Philosophiae Doctor
Faculty of Natural Sciences
Department of Materials Science and Engineering

NTNU
Norwegian University of
Science and Technology

Tichaona Mukono

Ferromanganese Production from Pretreated Manganese Ores: From Laboratory scale to Pilot scale.

Thesis for the Degree of Philosophiae Doctor

Trondheim, January 2023

Norwegian University of Science and Technology
Faculty of Natural Sciences
Department of Materials Science and Engineering

NTNU
Norwegian University of
Science and Technology

NTNU
Norwegian University of Science and Technology

Thesis for the Degree of Philosophiae Doctor

Faculty of Natural Sciences
Department of Materials Science and Engineering

ISBN 978-82-326-6532-7 (printed ver.)
ISBN 978-82-326-6929-5 (electronic ver.)
ISSN 1503-8181 (printed ver.)
ISSN 2703-8084 (online ver.)

Doctoral theses at NTNU, 2023:25

Printed by NTNU Grafisk senter

Dedicated to my late mum Marian and daddy Ephias Damian, who never saw this adventure.

Preface

This thesis is submitted to the Norwegian University of Science and Technology (NTNU) as a partial fulfilment of the requirements for the degree of Philosophiae Doctor.

The work has been carried out at the Department of Material Science and Engineering (IMA) under the supervision of Professor Merete Tangstad in the period between March 2019 and October 2022. This work is part of the PreMa project, which has received funding from the European Union's Horizon 2020 Research and Innovation Programme under Grant Agreement No 820561 and industry partners: Eramet, Ferrogroble, Transalloys, OFZ and Outotec. The author greatly acknowledges the financial support from the PreMa project.

The main aim of this work was to investigate effect of manganese ore pretreatment on furnace performance in ferromanganese production. Collaboration with SINTEF on pilot work and a master student on lab scale experiments was also part of the thesis work.

Trondheim, January 2023

Tichaona Mukono

List of Publications

Parts of the work presented in this thesis has been included in the following journal and conference publications:

Journal Publications:

- **T. Mukono**, H.S. Reiersen, T.L. Schanche, M. Wallin, and M. Tangstad, "Prereduction Behavior of Manganese Ores with Solid Carbon and in CO/CO_2 Gas Atmosphere", *Metall. Mater. Trans. B*, 2022, doi:10.1007/s11663-022-02611-5.

- **T. Mukono**, M. Wallin, and M. Tangstad, "Phase Distribution During Slag Formation in Mn Ferroalloy Production," *Metall. Mater. Trans. B*, 2022, doi: 10.1007/s11663-022-02441-5.

Conference publications:

- **T. Mukono**, J. E. Gjøvik, H. Gaertner, T. A. Larssen, M. Wallin, E. Ringdalen, and M. Tangstad, "Utilization of Pretreated Mn-Ore in a Pilot-Scale Ferromanganese Furnace: Effect of Ore Pretreatment on Carbon and Energy Consumption.", in *Proceedings of the 61st Conference of Metallurgists,* COM *2022,* Montreal, Canada, Springer Nature. doi: 10.1007/978-3-031-17425-4.

- **T. Mukono**, M. Wallin and M. Tangstad, "Slag Reduction and Viscosities Interaction in Ferromanganese Process". In: Steenkamp, J.D., Gregurek, D., Reynolds, Q.G., Alvear Flores, G., Joubert, H., Mackey, P.J. (eds) Furnace Tapping, 2022. The Minerals, Metals & Materials Series. Springer, Cham. https://doi.org/10.1007/978-3-030-92544-4_12

- **T. Mukono**, J. E. Gjøvik, H. Gærtner, M. Wallin, E. Ringdalen, and M. Tangstad, "Extent of Ore Prereduction in Pilot-scale Production of High Carbon Ferromanganese," in *16th International Ferroalloys Congress*, 2021, Trondheim, Norway, pp. 1–14, doi: 10.2139/ssrn.3926275.

- **T. Mukono**, M. Wallin, and M. Tangstad, "Molten ferromanganese slag production from Mn-ores". *In Proceedings of the 11th International Conference on Molten Slags, Fluxes and Salts*, 2021, South Korea-virtual conference.

Acknowledgements

I am immensely grateful for having Prof. Merete Tangstad as my supervisor and mentor. During our first meeting, I vividly remember her saying, 'before we start talking about your PhD work, let's talk about clothing'. This was important since I had no prior experience of living in cold countries, and it is an example of how she immensely cares for her student's welfare. She has provided me with tremendous opportunities to better my knowledge of process metallurgy. I am grateful for her constant guidance, support, and discussions we have had over the PhD period. I am also thankful to my co-supervisor, Dr Maria Wallin who helped me to settle in and I appreciate her support and comments during my PhD period. Next, I am grateful to Dr. Eli Ringdalen (SINTEF Industry) for her encouragements and inspiring discussions.

I greatly appreciate collaborating with engineers and scientists at SINTEF industry. Pilot campaigns had special moments of trouble shooting and success which would have never been possible without the resilient and clever minds of Jonas E. Gjøvik, Ingeborg Solheim, Heiko Gærtner, Michal Ksiazek, Trine Larssen, Nicholas Smith-Hanssen, Steinar Prytz and Sarina Bao, all from SINTEF Industry. I also had the privilege of working with master's students whom I greatly appreciate for their good work ethics. Thanks to Henrik Stensdal Reiersen (fantastisk) for teaching me Fityk software, Mika Serna Malmer and Kseniia Koseniuk for giving a hand during pilot furnace post experimental work.

I would like to thank the engineering staff at the Department of Material Science and Engineering at NTNU for trainings, practical advice, and supply of consumables for experimental work in various furnaces and equipment. Special mention to Morten Peder Raanes for EPMA analysis, Dmityr Slizovisky, Arman Hoseinpur-Kermani, Ivar Ødegård, Berit Kramer, Marit Odde and Pål Skaret, for their technical assistance. A special thanks goes to administrators and professors in the SiMnTi group i.e., Prof. Gabriella Tranell, Jafar Safarian, Kristian Etienne Einarsrud and Ragnhild Elizabeth. Thank you for steering the SiMnTi meetings, I have learnt a lot from all members' contributions.

I am also grateful to all my friends; Vlad, Adamantia, Alicia, Hossein, Dmitry Sukhomlinov, Azam, Hamideh, James, Gerrit, Didier, Sergey, Kamilla, Ece & Tino. Gym time with Trygve Storm Aarncæs and Vincent Canaguier was always interesting and fun. Special thanks to Trygve Lindahl Schanche, my officemate and coworker in the

field of ferromanganese production. I cherish the coffee breaks, power play and encouragements we had especially in the last days of completing thesis work.

I am thankful to Anne Grethe Lindseth, Paul Calvert, Erik Aareskjold, and the entire process team at Eramet Norway Sauda (i.e., Cedrik Brozek, Henrietta Isakkson Oyvind Viland and Astrid Lone) for providing me additional time to complete my thesis prior to commencing work in Sauda.

Finally, I would like to thank my loving wife Gracious and son Adiel for always being there for me, profound understanding, and amazing patience over such a long period of time.

Abstract

The production of high carbon ferromanganese (HCFeMn) alloys is an energy intensive process where manganese ores are smelted in a submerged arc furnace (SAF) using carbon reductants thereby generating CO_2 emissions. In the prereduction zone of the SAF, higher manganese oxides in the ore are reduced to MnO through solid-gas exothermic reactions and at a temperature around 800 °C, the unwanted endothermic Boudouard reaction is also active. As such, the total coke and energy consumption is highly dependent on if the prereduction occurs by CO gas or solid C. Improvement of existing SAF ferromanganese process in resource and energy efficiency as well as reduction of CO_2 emission through ore pretreatment in a separate unit is being explored in this work. A successful pretreatment limits the extent of Boudouard reaction thereby reducing the carbon and energy footprint of the process. Pretreated raw materials are expected to give a more stable and predictable furnace operation and in addition, contribute to lowering CO_2 emissions. However, the effect of utilizing pretreated ores on the SAF process is not known and this work seeks to increase and contribute to the knowledge about furnace performance from use of pretreated ores in ferromanganese production.

Experimental investigations were carried out at both laboratory and pilot scale. Firstly, laboratory scale experiments were carried out to investigate the prereduction behavior of manganese ores and to gain knowledge on the effect of extent of prereduction on the high temperature metal producing reaction i.e., MnO+C=Mn+CO. Three commercial ores used in industry, namely Comilog, Nchwaning and UMK were studied. Secondly, pilot-scale experiments have been conducted at SINTEF/NTNU in a 440 kVA AC electric furnace using different feed mixtures of untreated manganese ore, manganese ore preheated in air and manganese ore prereduced with solid carbon. Comilog and Nchwaning ores in both untreated and pretreated forms were used in the experiments. In addition, untreated UMK ore and a blend of untreated UMK and Kudumane referred to as Mintek mix, were used in separate pilot experiments. In total, 8 pilot experiments were carried out. Post experimental investigations were carried out on the pilot experiments, through digouts of the prereduction zone and excavations of the cokebed zone. Focus was on establishing the prereduction behavior of the various ores and establishing the effect of using pretreated ores on the metal producing reactions. Lastly, accounting material and energy balance calculations for the 8 pilot experiments were then calculated in HSC Chemistry software. Through mass and energy balances, carbon and energy consumption were established based on the offgas composition and the degree of degree of prereduction was estimated.

TGA data showed that the extent of ore prereduction will not have any effect on the metal producing reaction i.e., MnO + C = Mn + CO. Any remaining prereduction will be completed in the low temperature range 1200 – 1400 ℃ prior to the metal producing reaction. This was in agreement with findings from pilot experiments, were pretreatment of manganese ores was seen to have no effect on the metal producing reaction. Phase development in untreated and pretreated charge mixtures of Comilog, Nchwaning, UMK and Kudumane ores, which is dependent on temperature and composition of the ore, showed that the initial slag formed is mainly liquid + solid monoxide phase and slag reduction will occur on top of the coke bed with an increased dissolution of monoxide in slag rendering the slag fluid enough to trickle down the coke bed. The coexistence of a solid phase and a liquid slag phase explains the high MnO activity in the slag as well as affect the viscosity of the slag. Therefore, low reduction extent will occur inside the coke bed area due to the lower MnO activity which emanates from complete dissolution of solid monoxide phase. Hence, the final slag for example in untreated, pretreated and prereduced Comilog ores, will be tapped at compositions which are in the same region in the stable period of the furnace operation.

In laboratory experiments, the prereduction of ores mixed with solid carbon i.e., coke in the induction furnace improved the extent of prereduction. The decomposition of carbonates leads to better prereduction due to the CO produced in the Boudouard reaction. Hence, UMK ore was found to have a better prereduction compared to Nchwaning which is low in carbonates and Comilog which is known to have a higher CO reactivity at similar CO contents. However, in TGA experiments were the CO/CO_2 gas flow is high and stable, Comilog is seen to have a higher extent of prereduction followed by UMK and lastly Nchwaning. Contrastingly, in pilot furnace digouts, UMK ore was seen to have a lowest O/Mn ratio with increasing furnace depth, followed by Comilog and lastly Nchwaning. Pretreatment of Comilog ore was not seen to affect the degree of prereduction, which correlates well with laboratory scale results and energy calculations. Pretreatment of Nchwaning ore was seen to increase the extent of prereduction compared to untreated Nchwaning ore, when looking at the extent of prereduction adjacent the electrode. On the other hand, no differences were observed for Nchwaning ore adjacent the furnace lining. As such, we see an increased extent of prereduction for preheated Nchwaning in digout of pilot experiments but we do not see it based on the offgas composition and mass and energy calculations. It is believed that furnace digouts are subject to uncertainties. The furnace is shutdown 40kWh after the last tapping and the chemical reactions in the cokebed area are expected to stop within minutes of shutdown since metal producing reactions in the cokebed are highly endothermic. However, it is possible that exothermic reduction in the prereduction zone will continue as the furnace cools.

Based on furnace offgas composition, mass, and energy calculations, preheated and prereduced Comilog experiments show more stable operation compared to untreated Comilog experiment. As such pretreatment in Comilog series gives a stable operation. However, for Nchwaning ore, ore preheating does not show stable operation. For a fixed charge the lower CO_2 to ($CO + CO_2$) ratio in the offgas indicates higher CO_2 consumed in the Boudouard reaction and consequently higher carbon and energy consumption. Offgas measurements in the Comilog series show that the use of untreated Comilog ore leads to considerably lower CO/CO_2 off-gas composition compared to pretreated Comilog ores, largely related to the high oxygen level of Comilog ore. For untreated and preheated Nchwaning there was no significant differences in the offgas composition. The degree of prereduction is generally high for Comilog series, followed by UMK and Mintek mix and lastly Nchwaning experiments. As such Comilog will have the lowest carbon and energy consumption. The degree of prereduction in UMK was significantly higher compared to Nchwaning series experiments, hence the total carbon consumption was lower for UMK. Carbonates will have a double effect consuming both energy on decomposition and energy by Boudouard reaction and as such Mintek mix had the highest energy and carbon consumption.

Due to the higher amount of exothermic reactions, the untreated Comilog ore will give lower energy consumption compared to pretreated ore if added cold in the SAF. However, charging hot pretreated ore will result in lowering of the energy consumption in SAF by 300kWh/ton alloy. Prereduced Comilog did not have any significant difference from preheated Comilog with regards to energy and carbon consumption owing to insignificant change in oxygen level when Comilog is prereduced with solid carbon. The degree of prereduction in the Comilog series is in the same area within the uncertainties of the experiment. This gives the same carbon consumption and hence the overall CO_2 emissions.

Contents

Preface iii
List of Publications iv
Acknowledgements v
Abstract vii
List of Figures xiv
List of Tables xxvi
1 Introduction 1
1.1 Introduction 1
1.2 Ferromanganese production 1
1.2.1 Prereduction zone 3
1.2.2 Coke bed zone 4
1.3 Energy and carbon consumption 5
1.3.1 Boudouard reaction 6
1.3.2 Effect of trace elements and moisture on carbon and energy consumption 9
1.3.3 Summary of factors affecting carbon and energy consumption 10
1.4 Thesis scope 11
2 Theory and Literature Review 15
2.1 Manganese Ores 15
2.2 Prereduction reactions 17
2.2.1 Thermodynamics of reduction reactions 18
2.2.2 Prereduction mechanism and kinetics 22
2.2.3 Effect of different parameters on the prereduction rate of Mn-ores 25
2.3 High temperature reduction 28
2.3.1 Reduction of slag to metal – the thermodynamics 29
2.3.2 Phase composition and reduction of complex slags 35
2.3.3 Reduction mechanism and kinetic considerations 40
2.4 Excavation of pilot and industrial furnaces 44
3 Laboratory scale experiments 49
3.1 Introduction 49
3.2 Materials and methods 50

3.2.1 Raw materials 50
3.2.2 Induction furnace experiments 51
3.2.2.1 Experimental set up 51
3.2.2.2 Thermal conditions 54
3.2.2.3 Excavation of the crucible 56
3.2.3 TGA-Disvadri furnace experiments 57
3.2.3.1 Experimental setup 58
3.2.3.2 Theoretical weight loss and experimental TGA data 59
3.2.4 TGA furnace (TF1) experiments 61
3.2.4.1 Experimental setup and temperature schedule 61
3.2.4.2 Analyses of reduction degree – weight loss and EPMA analyses 65
3.2.5 Analytical techniques 66
3.2.5.1. Chemical analysis 66
3.2.5.2 Porosity measurements 67
3.2.5.3 Electron probe microanalyser (EPMA) 67
3.2.5.4 ImageJ® 68
3.2.5.5 Equilibrium Calculations 69
3.2.6 Overview of experimental work 69
3.3 Results 72
3.3.1 P-Series: Slag reduction from induction furnace experiments 72
3.3.1.1 Phase development and compositions for Comilog ore 72
3.3.1.2 Phase development and compositions for Nchwaning ore 76
3.3.1.3.Phase development and compositions for UMK ore 78
3.3.1.4 Calculated equilibrium phases during reduction of Comilog, Nchwaning and UMK 81
3.3.2 Q series: Slag reduction from TF1 furnace experiments 86
3.3.2.1 Reduction behavior 86
3.3.2.2 Slag phase development 93
3.3.3 R-series: Prereduction behavior in induction furnace 98
3.3.3.1 Variation of O/Mn ratio with temperature 98
3.3.3.2 Porosity development and carbonates decomposition 99
3.3.4. S-series: Manganese ore prereduction in CO/CO_2 atmosphere 101
3.3.4.1 Weight reduction behavior and change in O/Mn ratio 101

3.3.4.2 Reduction rate and decomposition of carbonates 103
3.4 Discussion 105
3.4.1 Reduction of MnO from slag 105
3.4.1.1 Overview 105
3.4.1.2 Monoxide phase development and its dissolution in slag 107
3.4.1.3 Slag reduction path 111
3.4.1.4 Effect of extent of prereduction on slag reduction 113
3.4.2 Prereduction behavior of Manganese ores 116
3.5 Summary 123
4 Pilot Scale Furnace 125
4.1 Introduction 125
4.2 Experimental 126
4.2.1 Raw Materials and charge mixtures 126
4.2.2 Pilot Furnace description and operation 130
4.2.3 Electrical parameters 132
4.2.4 Off-gas measurements 140
4.2.5 Post Experimental Work 144
4.2.5.1 Dig out of prereduction zone 144
4.2.5.2 Excavation of the cokebed zone 146
4.3 Results 148
4.3.1 Comilog Series 148
4.3.1.1 Analyses of tapped slag and alloy 148
4.3.1.2 Composition of prereduced samples 153
4.3.1.3 Composition of excavated samples from the cokebed zone 155
4.3.2. Nchwaning series 164
4.3.2.1 Analyses of tapped slag and alloy 164
4.3.2.2 Composition of prereduced samples 168
4.3.2.3 Composition of excavated samples from the cokebed zone 170
4.3.3. UMK and Mintek mix 178
4.3.3.1 Analyses of tapped slag and alloy 178
4.3.3.2 Composition of prereduced samples 182
4.3.3.3 Composition of excavated samples from the cokebed zone 184

4.4 Discussion 188
4.4.1 Prereduction in pilot furnace 188
4.4.2 Furnace interior and cokebed relations 191
5 Mass and Energy Considerations 197
5.1 Introduction 197
5.2 Data from Pilot experiments 197
5.3 Mass and energy calculations 199
5.4 Comparison of carbon and energy consumption in different scenarios. 205
5.5 Summary 209
6 Conclusions and Further work 211
References 215
Appendix A: TGA data smoothing in Excel 224
Appendix B: Calculation of slag composition of reduced charges 225
Appendix C – Chemical composition of phases measured by EPMA 226
Appendix D – Chemical composition of samples from prereduction zone 228
Appendix F: Material Balances 234

List of Figures

Figure 1.1: Schematic illustration of the submerged arc ferromanganese furnace showing example of charge mix quantities per tonne of alloy production and composition of products. (Quantitative data from Olsen et al., [2]). 2
Figure 1.2: Energy consumption and off-gas analyses versus carbon consumption for a fixed charge mixture [16]. 7
Figure 1.3: Energy consumption versus degree of prereduction for different manganese ores (Data from Kalenga et al.,[18]).....9
Figure 1.4: A sketch of pretreatment prior to SAF process in PreMa project..... 12

Figure 2.1: Standard Gibbs energies of prereduction reactions of higher oxides of Mn and Fe by CO gas, carbonate decomposition and reduction of MnO, FeO and SiO_2 by C versus temperature (data from HSC Chemistry® software[6]). 18
Figure 2.2: The oxygen partial pressure of practical gas mixtures (green lines) superimposed on the Mn-O and Fe-O stability diagrams, showing oxygen partial pressure versus temperature (Equilibrium values calculated from HSC Chemistry® software[6]) 19
Figure 2.3: Isothermal section of the Fe-Mn-O system at 1273 K. (MW = $(Fe,Mn)_{1-x}O$, C.Sp = $(Fe,Mn)_3O_4$, T.Sp = $(Mn,Fe)_3O_4$, Cor = $(Fe,Mn)_2O_3$, Bix = $(Mn,Fe)_2O_3$, and five metallic phases (CBCC,CUB, FCC, BCC, Liq.)) [60] 20
Figure 2.4: Experimental points and calculated oxygen potential in $MnFe_nO_x$ at 1242 K. The wustite ($Fe_{1-x}O$) and manganosite ($Mn_{1-x}O$) phases are isomorphous both having the NaCl-type structure with generic name halite.[61]..... 20
Figure 2.5: Calculated phase diagram of the Fe–Mn–O system at (a) 600 °C and (b) 800 °C at 1 atm by Schanche and Tangstad [63]. The highlighted areas show the equilibrium pO_2 for the experimental gas mixtures used in their work and the vertical line is the average Mn/(Mn+Fe) ratio based on chemical analysis of Nchwaning ore [63]..... 21
Figure 2.6: Schematic of the shrinking core model 23
Figure 2.7: Reaction progress for lumpy MnO_2 ore during gradual heating [2] 23
Figure 2.8: Weight loss as a function of time, respectively for Comilog ore (a) and Nchwaning ore (b) [73], [75]. 27
Figure 2.9: Reaction rate as a function of time for Comilog ore (a). Reaction rate as function of time and temperature for Nchwaning ore(b) [73], [75]..... 27

Figure 2.10: Reduction curves as a function of temperature for several manganese sources[17]. 28
Figure 2.11: Standard Gibbs energies for reduction of MnO, FeO, SiO_2, Al_2O_3, CaO and MgO by C versus temperature (data from HSC Chemistry® software[8]). 29
Figure 2.12: Calculated phase and liquidus relations for the MnO-SiO_2-CaO system. As an example, the reduction of a slag of initial composition **X** along the basicity line to liquidus composition **Y** and further reduction to equilibrium point **Z** is indicated. (Calculated in FactSage 8.1 [87]) 30
Figure 2.13: Equilibrium constant of MnO, FeO and SiO_2 reduction as a function of temperature. according to reactions (1) and (2) (calculated from HSC Chemistry v.10). 31
Figure 2.14: Activity of MnO(s) in liquid slag at 1400 ℃ depending on the slag basicity (wt.% CaO/wt.% SiO_2), MgO, and Al_2O_3 content. (a) Influence of Al_2O_3 content, and (b) influence of MgO content [11]. 33
Figure 2.15: (a) Curves of %MnO of the slag at liquidus temperature, calculated from liquidus relations for the MnO–SiO_2–CaO system for representing Nchwaning slags. (b) Curves of %MnO of the slag at liquidus temperature, calculated from liquidus relations for MnO–SiO_2–CaO–Al_2O_3 (Al_2O_3/SiO_2=1.24) system representing Comilog slags. The dots are experimental points, and the (S) marks where spherical MnO phase is observed [95]. 34
Figure 2.16: Activities and isoactivity lines of MnO in MnO-SiO_2-Al_2O_3 melts at 1823 K. (a) Influence of Al_2O_3/SiO_2 ratios on MnO activity. (b) Dependency of MnO activity on MnO concentration [92]. 34
Figure 2.17: The MnO-SiO_2 binary phase diagram highlighting the FeMn slag system. (Calculated in FactSage v8.1[87]). 35
Figure 2.18: Melting behavior of ore being heated in argon on a carbon substrate[98] 37
Figure 2.19: Variation of Initial melting for various Mn sources with % acid oxides. (Based on figure in Tangstad et al., (2021)[94] adapted from Brynjulfsen (2013)[103] and Ringdalen (2015)[102]). 37
Figure 2.20: Melting and flow behavior of ore heated in CO sitting in a graphite canyon[98] 38
Figure 2.21: (a) Calculated liquidus relations for the MnO–SiO_2–CaO system to predict reduction paths in Nchwaning slag. (b) Calculated liquidus relations for MnO–SiO_2–CaO–Al_2O_3 (Al_2O_3/SiO_2 = 1.24) system to predict reduction paths in Comilog slag. Green lines represent the reduction paths for Nchwaning and Comilog charges

with different basicities, red dots represent the starting points after pre-reduction [95]. 40
Figure 2.22: Rate of reduction of MnO presented as weight loss curves for slag starting from 72 to 73 pct MnO with Al_2O_3/SiO_2 ratio of 0.25 and basicity of 0.67[94]. 42
Figure 2.23: Slag composition in HCFeMn production. Calculated slag composition are based on the thermodynamic equilibrium calculations with carbon saturation at 1400 -1500 °C[11] 43
Figure 2.24: Left side: image of the furnace cross section. Right side: schematic illustration of the plate with corresponding zones. The cavity, metal, and softened ore particles are marked with color. The other zones are marked as follows: I-electrode, II-charge materials, III-cokebed zone, IV-coke-slag mixture, V-slag layer, VI-lining material. Numbers 1 to 9 depicts position of the core drills [119]. 45
Figure 2.25: Selected sampling localities. (a) Furnace plan view at roof level and (b) a view in elevation through electrode 1[130] 46
Figure 2.26: Sketch of one of the electrodes and the surrounding zone of a 75MVA furnace excavated by Barcza et al,. [130]. 46
Figure 2.27: Excavation results from a FeMn furnace. (a) overview over metal salamander and MnO-slag zone indicating plane b and c, (b) View of plane through the centre, (c) View of plane through the B electrode [132]. 47

Figure 3.1: Overview of furnaces, experiments, and analysis methods in relation to the simulated furnace zones. 49
Figure 3.2: Sketch of induction furnace and graphite crucible containing raw materials 53
Figure 3.3: A photograph of the 75kW induction furnace and the crucible used in this work 53
Figure 3.4: Temperature profiles in induction furnace (IF75) experiments with final temperatures on top of the cokebed at 1200 °C, 1300 °C, 1400 °C and 1500 °C. 55
Figure 3.5: Vertical temperature gradients inside the crucible with top of cokebed as reference point 55
Figure 3.6: Photographs of (a) crucible containing materials prior to 'digout' and (b) crucible interior after 'digout' of prereduction showing the sintered materials of the cokebed zone. 56
Figure 3.7: Typical pictures of the crucible interiors, and schematic illustration of sampling positions for the excavations from Nchwaning experiments with cokebed temperatures (a) 1220 °C, (b) 1413 °C and (c) 1505 °C. 57

Figure 3.8: Schematics of the experimental setup: 1 – furnace, 2 – gas flasks, 3 – gas mass flow controllers, 4 – gas inlet, 5 – gas outlet, 6 – gas analyzer, 7 – off-gas, 8 – solid charge, 9 – K-type thermocouple (sample), 10 – S-type thermocouple (furnace), 11 –eurotherm regulator/furnace controller, 12 – thermobalance, 13 – computer. (Dashed lines show the linkages between auxiliary components and the solid line arrows indicate gas flow) 59
Figure 3.9: Schematic of the TF1 furnace[136] 62
Figure 3.10: Photographs of TF1 furnace: (a) closed furnace and (b) opened furnace illustrating the crucible hooked to the furnace balance and suspended by a molybdenum wire. 62
Figure 3.11: Typical temperature profile in the furnace for measurements T1-T3. Indicated is the position of B-type thermocouple at 0.5cm below the bottom of crucible. 63
Figure 3.12: Illustration of temperature schedules for experiments. Dashed black line is sample temperature for experiments with 30 minutes holding time at 1200 °C to ensure complete prereduction and the blue solid line indicates the schedule without holding temperature at 1200 °C 64
Figure 3.13: Illustration of the TF1 crucible; (a) before cutting, (b) cross-section of vertically cut crucible and (c) epoxy mounted materials after heating 66
Figure 3.14: Quantification of phases using ImageJ software. (a) Original backscattered micrograph from EPMA showing all the phases present. The subsequent area fractions of the different phases are shown in (b), (c) and (d). 68
Figure 3.15: BSE images of Comilog slag samples CM-1, CM-2, CM-3, and CM-4 collected from positions on top of the coke bed with temperatures 1217 °C, 1277 °C, 1410 °C and 1475 °C, respectively. Legend: A = alloy, M = monoxide; T = tephroite and G = galaxite 73
Figure 3.16: BSE images of Comilog slags CM-5 and CM-6 collected from positions 5cm below top of the coke with reference coke bed temperatures at 1410 °C and 1475 °C, respectively. Legend: A = alloy, T = tephroite and G = galaxite. 74
Figure 3.17: BSE images of Nchwaning slag samples Nch-1, Nch-2, Nch-3, and Nch-4 collected from positions on top of the coke with temperatures 1220 °C, 1270 °C, 1413 °C and 1505 °C, respectively. Legend: A = alloy, M= monoxide; S = slag matrix. 76
Figure 3.18: BSE images of Nchwaning slag Nch-5 (a) collected from positions 5cm below the top of the coke bed with reference coke bed temperature at 1505 °C and the area inside of the red rectangular line is higher magnification (b). Legend: A = alloy, LG = light grey phase and DG = dark grey slag matrix 77

Figure 3.19: BSE images of UMK slag samples UMK-1, UMK-2, UMK-3, UMK-4, UMK-5, and UMK-6 collected from positions on top of the coke with temperatures 1156 ℃, 1180 ℃, 1223 ℃, 1226 ℃, 1308 ℃ and 1367 ℃, respectively. Legend: A = alloy, M= monoxide; LG = light grey phase and DG = dark grey phase.....79
Figure 3.20: Equilibrium phase distribution with increasing temperature that shows: (a) Phases in primary Comilog slag, (b) Phases when Comilog is in equilibrium with solid carbon, (c) Phases in primary Nchwaning slag, (d) Phases when Nchwaning is in equilibrium with solid carbon, (e) Phases in primary UMK slag, & (d) Phases when UMK is in equilibrium with solid carbon 82
Figure 3.21: Comparison of weight loss behavior of Comilog charge mixture i.e., Q1-series, with (pathway 1) and without holding temperature at 1200 ℃ (pathway 2). 87
Figure 3.22: Comparison of weight loss behavior of Nchwaning charge mixture i.e., Q2-series, with (pathway 1) and without holding temperature at 1200 ℃ (pathway 2).....87
Figure 3.23: Comparison of weight loss behavior of UMK charge mixture i.e., Q3-series, with (pathway 1) and without holding temperature at 1200 ℃ (pathway 2). 87
Figure 3.24: Weight loss curves during slag reduction for Comilog charge (Q1 series). The temperature profile is shown. 89
Figure 3.25: Weight loss curves during slag reduction for Nchwaning charge (Q2 series). The temperature profile is shown. 89
Figure 3.26: Weight loss curves during slag reduction for UMK charge (Q3 series). The temperature profile is shown.....89
Figure 3.27: Calculated reduction rate and temperature profile, all as a function of time for Comilog 'Q1' series. 91
Figure 3.28: Calculated reduction rate and temperature profile, all as a function of time for Nchwaning 'Q2' series. 91
Figure 3.29: Calculated reduction rate and temperature profile, all as a function of time for Comilog 'Q1' series. 92
Figure 3.30: (a) Reduction rate comparison for Comilog, Nchwaning and UMK series experiments for experiment with final temperature at 1550 ℃. Temperature profile is shown. (b) Reduction rate curves for completely prereduced Comilog, Nchwaning and UMK ores are shown on a different scale to indicate the differences in heating rate at T<1450 ℃. 93
Figure 3.31: BSE images of Comilog slag samples in 'Q1' series experiments. Legend: A = alloy, M = monoxide; T = tephroite and G = galaxite. 94

Figure 3.32: BSE images of Nchwaning slag samples in 'Q2' series experiments. Legend: A = alloy, M= monoxide; S = slag matrix..... 96
Figure 3.33: BSE images of UMK slag samples in 'Q3' series experiments. Legend: A = alloy, M= monoxide; S = slag matrix. 97
Figure 3.34: Variation of O/Mn ratio in manganese ores as a function of temperature for (a) Comilog ore, (b) Nchwaning ore, (c) UMK ore and (d) a comparison of the three ores. 98
Figure 3.35: The development of porosity and decomposition of carbonates as a function of temperature for (a) Comilog, (b) Nchwaning and (c) UMK ores. 100
Figure 3.36: Weight loss (wt.%) as a function of (a) temperature and (b) time. O/Mn ratio as a function of (c) temperature and (d) time, all for Comilog, Nchwaning and UMK ores (10 to 12.5 mm particles). The TGA and calculated O/Mn curves are at heating rates of 3, 6 and 9 ℃/min all at 70 % CO and 30 % CO_2. 101
Figure 3.37: Variation of rate (wt. %/sec) with temperature for Comilog, Nchwaning and UMK ores (10 to 12.5 mm), heated at 3, 6 and 9 ℃/min in a 70 wt.% CO and 30 wt.% CO_2 atmosphere. 104
Figure 3.38: Fraction of carbonates decomposed in Nchwaning and UMK as a function of temperature. Legend: ore type-final temperature (℃) e.g., Nch-900.....105
Figure 3.39: A schematic illustration of the interactions in the slag-coke bed system 106
Figure 3.40: Composition of the monoxide phase as a function of temperature in Comilog ore. Experimental measured values from EPMA analysis are shown for both IF75 and TF1 experiments. 109
Figure 3.41: Composition of the monoxide phase as a function of temperature in Nchwaning ore. Experimental measured values from EPMA analysis are shown for both IF75 and TF1 experiments. 110
Figure 3.42: Composition of the monoxide phase as a function of temperature in UMK ore. Experimental measured values from EPMA analysis are shown for both IF75 and TF1 experiments.....110
Figure 3.43: Calculated equilibrium content of MnO versus temperature for the liquid phase in the presence of carbon. Experimental MnO contents versus temperature in the liquid phase relative to their position within the coke bed zone are indicated. 113
Figure 3.44: Calculated liquidus relations for the MnO-SiO_2-CaO slag system calculated in FactSage 8.3. The starting composition after prereduction are represented by red and green dots and the subsequent reduction paths are represented by red and green lines with basicities indicated for Nchwaning and UMK, respectively.....115

Figure 3.45: Contribution of water evaporation and prereduction reactions to the overall rate of prereduction for Comilog ore heated at (a) 3 °C/min, (b) 6 °C/min and 9 °C/min in a 70/30 CO/CO_2 atmosphere. 118
Figure 3.46: Reaction steps during non-isothermal (6 °C/min) reduction of Comilog ore (11.2 -15.0 mm) in 50/50 CO/CO_2 [75]. 119
Figure 3.47: Contribution of various ore constituents to the overall rate of prereduction for Nchwaning ore heated at (a) 3 °C/min, (b) 6 °C/min and 9 °C/min in a 70/30 CO/CO_2 atmosphere. 120
Figure 3.48: Contribution of prereduction reactions and decomposition of carbonates to the overall rate of prereduction for UMK ore heated at (a) 3 °C/min, (b) 6 °C/min and 9 °C/min in a 70/30 CO/CO_2 atmosphere. 121

Figure 4.1: O/Mn ratio for different manganese sources 127
Figure 4.2: Schematic drawing of the pilot furnace 130
Figure 4.3: A photograph of the pilot furnace in operation 130
Figure 4.4: Electrode tip position and resistance as a function of time in the untreated, preheated and prereduced Comilog experiments. Start of charging and the tappings thereafter are indicated for each experiment. 133
Figure 4.5: Voltage, power and current as function of time in the untreated Comilog experiment 133
Figure 4.6: Voltage, power and current in the preheated Comilog experiment 134
Figure 4.7: Voltage, power and current in the prereduced Comilog experiment 134
Figure 4.8: Electrode tip position and resistance as a function of time in the untreated, preheated and prereduced Nchwaning experiments. Start of charging for all the experiments are indicated. 135
Figure 4.9: Voltage, power and current as function of time in the untreated Nchwaning experiment 136
Figure 4.10: Voltage, power and current as function of time in the preheated Nchwaning experiment. 136
Figure 4.11: Voltage, power and current as function of time in the prereduced Nchwaning experiment 137
Figure 4.12: Electrode tip position and resistance as a function of time in the untreated UMK experiment. Start of charging, end of experiment and tappings (in brackets) for all the experiment are indicated. 138
Figure 4.13: Voltage, power and current as function of time in the untreated UMK experiment. Tappings are shown in brackets. 138

Figure 4.14: Electrode tip position and resistance as a function of time in the untreated Mintek mix experiment. Start of charging, end of experiment and tappings (in brackets) for the experiment are indicated. 139
Figure 4.15: Voltage, power and current as function of time in the untreated Mintek mix experiment. Tappings are shown in brackets 139
Figure 4.16: Micro-GC Thermal Conductivity Detector (TCD) principle[150]. 140
Figure 4.17: CO concentration in the offgas measured from pilot experiments in the Comilog series 141
Figure 4.18: CO_2 concentration in the offgas measured from pilot experiments in the Comilog series 141
Figure 4.19: CO concentration in the offgas measured from pilot experiments in the Nchwaning series. 142
Figure 4.20: CO_2 concentration in the offgas measured from pilot experiments in the Nchwaning series. 143
Figure 4.21: CO concentration in the offgas measured from untreated UMK and Mintek mix pilot experiments 143
Figure 4.22: CO_2 concentration in the offgas measured from untreated UMK and Mintek mix pilot experiments 144
Figure 4.23: (a) A schematic illustration of the sampling regions during the furnace digout and a plan view of the SINTEF/NTNU Pilot furnace. (b) Photographs of furnace top prior to dig-out & (b) interior of the furnace and top of cokebed after complete digout of the prereduction zone. 145
Figure 4.24: Cross - section of the interior part of the cokebed zone 147
Figure 4.25: (a) Schematic showing core drilling of excavated cokebed furnace interior. (b) Cores from the drilling. 147
Figure 4.26: Comparison of the slag/alloy ratios for the whole experiments and tappings 7 to 12 with values from HSC mass balance calculation and the planned slag/alloy ratio in the untreated, preheated and prereduced Comilog experiments. 149
Figure 4.27: Variation of slag and alloy composition with tapping number for Comilog series experiments. Untreated Comilog (a & b), preheated Comilog (c & d) and prereduced Comilog (e & f). 150
Figure 4.28: MnO_x as a function of depth from the top of charge material. (a) Untreated Comilog (UCom), (b) Preheated Comilog (HCom), (c) Prereduced Comilog (RCom) & (d) Comparison of MnO_x vs depth for the three experiments assuming a 70/30 Electrode/Furnace ratio of flow material in each experiment. 154

Figure 4.29: Sample positions in the cross-section of cokebed in Comilog series experiments. (a) Untreated Comilog samples 1-11 (named UC1-UC11), (b) preheated Comilog samples 1-11 (named HC1-HC11), & prereduced Comilog samples 1-22 (named RC1-RC22).....155
Figure 4.30: Backscattered electron micrographs of untreated Comilog samples UC-1, UC-2, UC-3, UC-4, and UC-5 collected from positions 5cm vertically adjacent the electrode. Legend: DG = dark grey phase; LG = light grey phase.....157
Figure 4.31: Backscattered electron micrographs of untreated Comilog samples UC-6, UC-7, UC-8, and UC-9 collected from positions 10cm vertically adjacent the electrode. Samples UC-10 and UC-11 are from below the tip of the electrode and close to the taphole, respectively. Legend: DG = dark grey phase; LG = light grey phase.....158
Figure 4.32: Backscattered electron micrographs of preheated Comilog samples HC-1, HC-2, HC-3, and HC-4 from positions 5cm vertically adjacent the electrode. Legend: DG = dark grey phase; LG = light grey phase.....160
Figure 4.33: Backscattered electron micrographs of preheated Comilog samples HC-5, HC-6, HC-7, and HC-8 collected from positions 10cm vertically adjacent the electrode. Samples HC-9, HC-10 and HC-11 are from positions inside the cokebed and close to the taphole.....161
Figure 4.34: Backscattered electron micrographs of prereduced Comilog samples RC-1 to RC-7 from positions 5cm vertically adjacent the electrode. Legend: DG = dark grey phase; LG = light grey phase. 162
Figure 4.35: Backscattered electron micrographs of prereduced Comilog samples RC-8 to RC-13 from positions 10cm vertically adjacent the electrode. Legend: DG = dark grey phase; MG = medium grey phase & LG = light grey phase. 163
Figure 4.36: Comparison of experimental slag/alloy ratios with values from HSC mass balance calculation and the planned slag/alloy ratio in the untreated, preheated and prereduced Nchwaning experiments.....165
Figure 4.37: Variation of slag and alloy composition with tapping number for Comilog series experiments. Untreated Nchwaning (a & b), preheated Nchwaning (c & d) and prereduced Nchwaning (e & f).....166
Figure 4.38: MnO_x as a function of depth from the top of charge material. (a) Untreated Nchwaning (UNch), (b) Preheated Nchwaning (HNch), (c) Prereduced Nchwaning (RNch) & (d) Comparison of MnO_x vs depth for the three experiments assuming a 70/30 Electrode/Furnace ratio of flow material in each experiment..169
Figure 4.39: Sampling positions in the cross-section of cokebed in Nchwaning series experiments. (a) Untreated Nchwaning samples 1-10 (named UN1-UN10), (b)

preheated Nchwaning samples 1-11 (named HN1-HN11), & prereduced Nchwaning samples 1-9 (named RN1-RN9). 171
Figure 4.40:Backscattered electron micrographs of untreated Nchwaning samples UN-1 – UN-5 collected from positions 5cm vertically adjacent the electrode. Legend: DG = dark grey phase; MG = medium grey phase & LG = light grey phase. 172
Figure 4.41: Backscattered electron micrographs of untreated Nchwaning samples UN-5 – UN-8 from positions 10cm vertically adjacent the electrode. Samples UN-9 and UN-10 are from close to the taphole and below the tip of the electrode, respectively.....173
Figure 4.42:Backscattered electron micrographs of preheated Nchwaning samples HN-1 – HN-4 collected from positions 5cm vertically adjacent the electrode. Legend: DG = dark grey phase & LG = light grey phase.....174
Figure 4.43: Backscattered electron micrographs of preheated Nchwaning samples HN-5 – HN-8 from positions 10cm vertically adjacent the electrode. Samples HN-9 – HN-11 are from close to the taphole. 175
Figure 4.44: Backscattered electron micrographs of prereduced Nchwaning samples RN-1 to RN-5 from positions 5cm vertically adjacent the electrode. Legend: DG = dark grey phase; MG = medium grey phase & LG = light grey phase. 177
Figure 4.45: Backscattered electron micrographs of prereduced Nchwaning samples RN-6 – RN-9 from positions 10cm vertically adjacent the electrode.....178
Figure 4.46: Slag/alloy ratios in whole experiment, tappings in the last half of the experiment and planned theoretical slag/alloy ratio in the untreated UMK and Mintek mix experiments.....179
Figure 4.47: Variation of slag and alloy composition with tapping number for untreated UMK and Mintek mix experiments. Untreated UMK (a & b) and Mintek mix (c & d). 180
Figure 4.48: MnO_x as a function of depth from the top of charge material. (a) Untreated Mintek, (b) untreated Mintek & (c) comparison of MnO_x vs depth for the two experiments assuming a 70/30 Electrode/Furnace ratio of flow material in each experiment. 183
Figure 4.49: Decomposition of carbonates during prereduction as a function of furnace depth for (a) UMK and (b) Mintek mix experiments. 183
Figure 4.50: Sampling positions in the cross-section of cokebed in UMK and Mintek mix experiments. (a) Untreated UMK samples 1-8 (named UMK1-UMK8) & (b) untreated Mintek mix samples 1-10 (named MN1-MN10). 184

Figure 4.51: Backscattered electron micrographs of untreated UMK samples UMK-1 – UMK-4 taken from positions 5cm vertically adjacent the electrode. Legend: DG = dark grey phase, MG = medium grey phase & LG = light grey phase.....185
Figure 4.52: Backscattered electron micrographs of untreated UMK samples UMK-5 – UMK-8 from positions 10cm vertically adjacent the electrode. 186
Figure 4.53:Backscattered electron micrographs of Mintek mix samples MN-1 – MN-6. Samples MN-1 – Mn-3 and MN-4 – MN-6 were collected respectively from positions 5cm and 10cm vertically adjacent the electrode. Legend: DG = dark grey phase & LG = light grey phase. 187
Figure 4.54: Backscattered electron micrographs of Mintek mix samples MN-7 – MN-10 from positions inside the cokebed close to the taphole.....187
Figure 4.55: Comparison of MnO_x from digout of the prereduction zone of pilot experiments. (a) MnOx adjacent electrode, (b) MnO_x adjacent furnace lining and (c) Variation of MnOx with depth at an electrode/furnace wall material distribution ratio of 70/30.....189
Figure 4.56: Average CO and CO_2 concentration in the offgas measured in the last 100 minutes for all pilot experiments. 191
Figure 4.57: Schematic illustration of the interior of the furnace showing the O/Mn ratio (prereduction zone) and wt.% MnO in slag (cokebed zone) in (a) untreated Comilog experiment, (b) preheated Comilog experiment and (c) prereduced Comilog experiment.....192
Figure 4.58: Schematic illustration of the interior of the furnace showing the O/Mn ratio (prereduction zone) and wt.% MnO in slag (cokebed zone) in (a) untreated Nchwaning experiment, (b) preheated Nchwaning experiment and (c) prereduced Nchwaning experiment.....193
Figure 4.59: Schematic illustration of the interior of the furnace showing the O/Mn ratio (prereduction zone) and wt.% MnO in slag (cokebed zone) in (a) untreated UMK experiment and (b) untreated Mintek mix experiment.....194
Figure 4.60: Ternary phase diagram representing the $MnO\text{-}SiO_2\text{-}Al_2O_3\text{-}CaO\text{-}MgO$ slag system with Al_2O_3/SiO_2 at 1.3 and MgO/CaO at 0.05 calculated in FactSage 8.3. 195

Figure 5.1: The relationship between energy consumption, $CO_2/(CO_2+CO)$ ratio and carbon consumption for production of 1 tonne of alloy using charge mixtures with (a) untreated Comilog (b) preheated Comilog and (c) prereduced Comilog ore.....200
Figure 5.2: The relationship between energy consumption, $CO_2/(CO_2+CO)$ ratio and carbon consumption for production of 1 tonne of alloy using charge mixtures with (a)

untreated Nchwaning (b) preheated Nchwaning and (c) prereduced Nchwaning ore. 202
Figure 5.3: The relationship between energy consumption, $CO_2/(CO_2+CO)$ ratio and carbon consumption for production of 1 tonne of alloy using charge mixtures with (a) untreated UMK and (b) Mintek mix 204
Figure 5.4: Minimum stoichiometric and total carbon consumption. The percentage of carbon above the minimum stoichiometric is shown on the vertical secondary axis for each experiment. 206
Figure 5.5: Energy consumption per ton of alloy for ore blends with untreated, preheated and prereduced ores, with input temperatures at 25 °C and 600 °C. ..207

Figure A.1: TGA reduction curve superimposed with smoothed Fityk curve 224

List of Tables

Table 1.1: Theoretical fixed carbon requirements in the cokebed (Calculated using HSC Chemistry® software[6]) per ton alloy for the different ASTM standard A99-03 grades of HCFeMn. 5
Table 1.2: Summary of increase in carbon and energy consumption due to reactions in the prereduction zone 11

Table 2.1: Typical manganese minerals [33]–[36] 16
Table 2.2: Typical composition of some commercial ores and sinters (dry basis) [2], [57] 17

Table 3.1: Chemical composition of raw materials (wt. pct) 50
Table 3.2: Raw material particle size range with type of experiment 51
Table 3.3: Quantities of ores used to fill 200mm height in crucible 52
Table 3.4: Calculated theoretical weight loss from ores (wt. %) based on Table 3.1 60
Table 3.5: Calculated primary slag composition after complete prereduction 65
Table 3.6: Overview of the induction furnace experiments in P-series were samples within the cokebed were excavated. Ore particle size was 9.5 -16 mm. 70
Table 3.7: Overview of TGA Q-series experiments conducted in TF1 furnace. Ore and coke particle size was 3.15 - 4 mm in all experiments. The experiments were conducted with repeated parallels 70
Table 3.8: Overview of the induction furnace experiments in R-series were samples within the prereduction were excavated. Ore and coke particle size was 9.5 -16 mm[9]. 71
Table 3.9: Overview of TGA non-isothermal S-series experiments conducted in 70/30 CO/CO_2 atmosphere. Ore particle size was 10 -12.5 mm for the three ores in all experiments[9]. 71
Table 3.10: Summary of the average compositions of the phases experimentally observed from Comilog slags (CM-1) – (CM-4) from top of the coke bed and (CM-5) – (CM-6) are 5cm into the coke bed. 75
Table 3.11: Calculated liquid slag composition based on measured area fraction by ImageJ® and EPMA phase analysis for Comilog slags (Samples (CM-1) – (CM-4) were on top of the coke bed and (CM-5) – (CM-6) are 5cm into the coke bed) 75

Table 3.12: Average compositions of the phases experimentally observed from Nchwaning slags (Nch-1) – (Nch-4) from top of the coke bed and slag Nch-5 from 5cm below top of coke bed. 78
Table 3.13: Calculated liquid slag composition based on measured area fraction by ImageJ® and EPMA phase analysis for Nchwaning slags (Slags (Nch-1) – (Nch-4) were on top of the coke bed and Nch-5 is 5cm into the coke bed) 78
Table 3.14: Average compositions of the phases experimentally observed from UMK slags (UMK-1) – (UMK-5) from top of the coke bed. 80
Table 3.15: Calculated liquid slag composition based on measured area fraction by ImageJ® and EPMA phase analysis for UMK slags (Slags (UMK-2) – (UMK-5) were on top of the coke bed). 81
Table 3.16: Calculated primary slag composition assuming prereduction of higher manganese and iron oxides to MnO and FeO 81
Table 3.17: Composition (wt. %) of the monoxide phase during heating of Comilog, Nchwaning and UMK (FactSage 8.1). (Note: No carbothermic reduction of slag) 84
Table 3.18: Composition (wt. %) of the monoxide phase during carbothermic reduction of Comilog, Nchwaning and UMK (FactSage 8.1) 84
Table 3.19: Calculated equilibrium composition (wt. %) of liquid slag phase in coexistence with monoxide phase and solid carbon for Comilog, Nchwaning and UMK reduction (FactSage 8.1) 85
Table 3.20: Calculated equilibrium composition (wt. %) of the liquid alloy for the reduction of Comilog, Nchwaning and UMK slags (FactSage 8.1) 85
Table 3.21: Prereduction mass loss for Comilog, Nchwaning and UMK experiments with and without holding for 30 minutes at 1200 ℃ 88
Table 3.22: Calculated final slag composition based on weight loss results (TGA data) at 1400, 1500 and 1550 ℃. 90
Table 3.23: Calculated liquid slag composition based on measured area fraction by ImageJ® and EPMA phase analysis for Comilog slags in 'Q1' series 95
Table 3.24: Calculated liquid slag composition based on measured area fraction by ImageJ® and EPMA phase analysis for Nchwaning slags in 'Q2' series 96
Table 3.25: Calculated liquid slag composition based on measured area fraction by ImageJ® and EPMA phase analysis for UMK slags in 'Q3' series 97
Table 3.26: Chemical analysis of Comilog, Nchwaning and UMK samples exposed to non-isothermal reduction. 103
Table 3.27: Chemical analysis of Nchwaning heated up to 900 ℃ and UMK samples heated up to 700, 800 and 900 ℃ 104

Table 4.1: Chemical composition of ores and sinter for pilot experiments. (Analysed by SINTEF Norlab). (Note: Com = Comilog, Nch = Nchwaning, Kud = Kudumane and UMK = United Manganese of Kalahari) 127
Table 4.2: Targeted slag basicity, slag/alloy ratio and chemical composition of slag and alloy products. (Note: Com = Comilog, Nch = Nchwaning, UMK = United Manganese of Kalahari, and Mint = Mintek mix) 128
Table 4.3: Charge blend for each pilot experiment in the Comilog series (Each batch had a total weight of 30kg).....129
Table 4.4: Charge blend for each pilot experiment in the Nchwaning series (Each batch had a total weight of 30kg).....129
Table 4.5: Charge blend for the UMK and Mintek mix pilot experiments (Each batch had a total weight of 30kg).....129
Table 4.6: Weight of tapped slag and alloy for the experiments with untreated, preheated and prereduced Comilog charge mixtures 148
Table 4.7: Measured slag composition for untreated Comilog experiment.....151
Table 4.8: Measured slag composition for preheated Comilog experiment 151
Table 4.9: Measured slag composition for prereduced Comilog experiment 152
Table 4.10: Alloy composition for untreated and preheated Comilog experiments 153
Table 4.11: Alloy composition for prereduced Comilog experiments 153
Table 4.12: Calculated liquid slag composition based on measured area fraction by ImageJ® and EPMA phase analysis for samples from untreated Comilog experiment. 159
Table 4.13: Calculated liquid slag composition based on measured area fraction by ImageJ® and EPMA phase analysis for samples from preheated Comilog experiment 161
Table 4.14: Calculated liquid slag composition based on measured area fraction by ImageJ® and EPMA phase analysis for samples from prereduced Comilog experiment 163
Table 4.15: Weight of tapped slag and alloy for the experiments with untreated, preheated and prereduced Nchwaning charge mixtures. 164
Table 4.16: Measured slag composition for untreated Nchwaning experiment 167
Table 4.17: Measured slag composition for preheated Nchwaning experiment.....167
Table 4.18: Measured slag composition for prereduced Nchwaning experiment ..167
Table 4.19: Alloy composition for untreated and preheated Nchwaning experiments 168
Table 4.20: Alloy composition for prereduced Nchwaning experiment 168

Table 4.21: Calculated liquid slag composition based on measured area fraction by ImageJ® and EPMA phase analysis for samples from untreated Nchwaning experiment 173
Table 4.22:Calculated liquid slag composition based on measured area fraction by ImageJ® and EPMA phase analysis for samples from preheated Nchwaning experiment 175
Table 4.23: Calculated liquid slag composition based on measured area fraction by ImageJ® and EPMA phase analysis for samples from prereduced Nchwaning experiment 176
Table 4.24: Weight of tapped slag and alloy for the experiments with untreated, preheated and prereduced Nchwaning charge mixtures 179
Table 4.25: Measured slag composition for untreated UMK experiment 180
Table 4.26: Measured slag composition for untreated Mintek mix experiment 181
Table 4.27: Alloy composition for untreated UMK and Mintek mix experiments 182
Table 4.28: Calculated liquid slag composition based on measured area fraction by ImageJ® and EPMA phase analysis for samples from untreated UMK experiment 185
Table 4.29: Calculated liquid slag composition based on measured area fraction by ImageJ® and EPMA phase analysis for samples from Mintek mix experiment 188

Table 5.1: Composition of tapped slag and alloy from the pilot experiments. (UCom = untreated Comilog ore, HCom = preheated Comilog ore, RCom = prereduced Comilog ore, UNch = Untreated Nchwaning ore, HNCh = preheated Nchwaning ore and RNch = prereduced Nchwaning ore). 198
Table 5.2: Measured range of CO/CO_2 in the offgas in the stable period 100 minutes prior to furnace shutdown and the calculated $CO_2/(CO_2 + CO)$ (*Note: Only CO/CO_2 for RNch was from first 100 minutes) 198
Table 5.3: Comparison between results of untreated, preheated and prereduced Comilog experiments. (NB: UCom – untreated Comilog, HCom – preheated Comilog and RCom – prereduced Comilog) 201
Table 5.4: Comparison between results of untreated, preheated and prereduced Nchwaning experiments. (NB: UNch – untreated Nchwaning, HNch – preheated Nchwaning and RNch – prereduced Nchwaning) 203
Table 5.5: Comparison between results of untreated UMK and Mintek mix experiments. 205

Table B.1: Calculated slag composition after reduction of Comilog at 1400 and 1550 °C. 225

Table C.1: Phase composition for Comilog slags in 'Q1' series analyzed by EPMA. 226
Table C.2: Phase composition for Nchwaning slags in 'Q2' series analyzed by EPMA 226
Table C.3: Phase composition for UMK slags in 'Q3' series analyzed by EPMA.....227

Chapter 1

1 Introduction

1.1 Introduction

Due to increased growth of the world population, stainless steel remains and is envisaged to continue to be a crucial material for modern civilization. Manganese is one of the most common commercial metals and it is an important alloying element in the stainless-steel manufacture. Its significance is primarily on improving the workability of steel and production of advanced high strength steel. About 10 – 15 % of Mn content in steel is required to achieve the production of ultrahigh Mn steels, such as transformation-induced plasticity (TRIP) and twinning-induced plasticity (TWIP) alloys[1]. Mn-ferroalloys are also used as a deoxidizer and improves the negative effect of S in the steel. Therefore, the demand for ferromanganese (FeMn) alloys in steel industry will continue to grow over time. At the same time this industry is focusing on a more sustainable production, as such, process improvements with regards to energy consumption and CO_2 emissions from the primary production of FeMn are of paramount importance.

1.2 Ferromanganese production

Commercial production of HCFeMn is through carbothermic reduction of manganese ores, with more than 90% of its production primarily being produced in the submerged arc furnace (SAF). The SAF is charged with a constant supply of raw materials such as manganese ore, sinter, metallurgical coke, and flux blended in predetermined ratios[2]. Metallurgical coke is the most common source of reductant and typical fluxes added to adjust the composition of the slag are dolomite and limestone. These basic fluxes are added to give the slag suitable chemical properties, altering liquidus temperatures and viscosity in-order to secure good and stable furnace operation and a high manganese recovery. Studies [3], [4] have shown that choice of slag composition is paramount in HCFeMn production as an appropriate slag will result in high metallic yield and smooth furnace operation. The composition of slag determines the

slag/metal equilibrium and kinetic relations, including the MnO content of the final slag and slag viscosity. Typically, several ores together with sinter can be used as the Mn-source and their selection is highly dependent on availability, relative cost, the desired Mn/Fe ratio in the alloy product, content of impurities such as phosphorus.

The actual ways in which reductants take part in the reduction reactions are mainly; gasification (Boudouard reaction) to form CO which can react high in the furnace, direct reduction reaction of solid carbon with MnO in the slag and dissolution of carbon in the metal product [5]. In-order to satisfy the above-mentioned reactions, a high-quality reductant is desirable. A good quality metallurgical coke should possess a low reactivity of solid carbon with CO_2 gas, as this is to a larger extent decisive for the total consumption of coke and electric energy[2].

Figure 1.1 shows a schematic illustration of the SAF for HCFeMn production showing typical quantities per tonne of alloy production, energy input and characteristic composition of products.

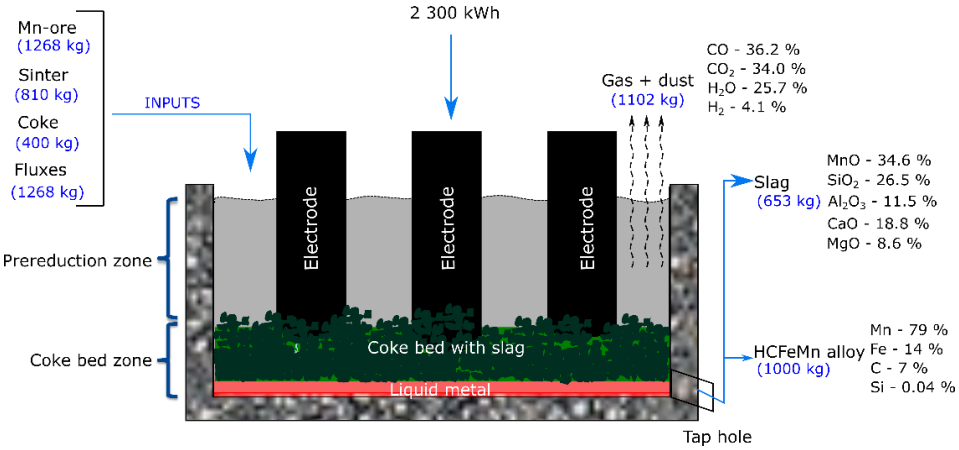

Figure 1.1: Schematic illustration of the submerged arc ferromanganese furnace showing example of charge mix quantities per tonne of alloy production and composition of products. (Quantitative data from Olsen et al., [2]).

Energy for the process is supplied by conversion of electrical energy into heat at the electrode tip through resistive heating of the coke bed to attain smelting temperatures. The formed liquid slag and liquid metal is periodically tapped at the bottom of the furnace during production. A temperature gradient develops in the furnace through heat exchange between descending burden materials and hot ascending CO-rich gas generated from the smelting reactions. The furnace is typically

divided into two main zones namely, the prereduction zone (200 – 1200 ℃) and the coke-bed zone (1200 – 1600 ℃).

1.2.1 Prereduction zone

The prereduction zone is mainly characterized by solid-gas reactions. Initially, iron oxides and higher manganese oxides (MnO_2, Mn_2O_3 and Mn_3O_4) are prereduced in the prereduction zone by means of CO gas to metallic Fe and MnO. The typical process reactions in the prereduction zone and their corresponding standard reaction enthalpies calculated using HSC Chemistry® software[6] are presented as follows:

$$2MnO_2 + CO(g) = Mn_2O_3 + CO_2(g), \quad \Delta H^0_{298} = -202 \text{ kJ/mol.} \tag{1.1}$$

$$3Mn_2O_3 + CO(g) = 2Mn_3O_4 + CO_2(g), \quad \Delta H^0_{298} = -177 \text{ kJ/mol.} \tag{1.2}$$

$$3Fe_2O_3 + CO(g) = 2Fe_3O_4 + CO_2(g), \quad \Delta H^0_{298} = -40 \text{ kJ/mol.} \tag{1.3}$$

$$Mn_3O_4 + CO(g) = 3MnO + CO_2(g), \quad \Delta H^0_{298} = -53 \text{ kJ/mol.} \tag{1.4}$$

$$Fe_3O_4 + 4CO(g) = 3Fe + 4CO_2(g), \quad \Delta H^0_{298} = +37 \text{ kJ/mol.} \tag{1.5}$$

$$CaCO_3 = CaO + CO_2(g), \quad \Delta H^0_{298} = +178 \text{ kJ/mol.} \tag{1.6}$$

$$C + CO_2(g) = CO(g), \quad \Delta H^0_{298} = +172 \text{ kJ/mol.} \tag{1.7}$$

The solid - gas prereduction reactions (reactions (1.1)-(1.5)) are mostly exothermic and produce CO_2.

Carbonates in the charge mixture typically consist of Ca, Mg and Mn bearing carbonates or dolomite which decompose to produce CO_2. The resultant CO_2 gas from prereduction of Mn_3O_4 and decomposition of carbonates, may react with solid carbon according to the highly endothermic Boudouard reaction (reaction (1.7)) at temperatures greater than 800 ℃. The exothermic solid-gas prereduction reactions are beneficial as they contribute to charge heating, whereas decomposition of carbonates will have a double negative effect, first requiring energy on the decomposition and next to increase energy and coke consumption according to Boudouard reaction[7]. As an example, UMK (United Manganese of Kalahari) ore, a Mamatwan type-ore, which is enriched in Mn-bearing carbonates would exhibit a high energy consumption compared to Nchwaning which contains less carbonates[8], [9].

1.2.2 Coke bed zone

At sufficiently high temperatures in the coke bed zone (1200 – 1600 ℃) a primary slag will form, that is a mixture of solid and liquid phases. MnO formed from the prereduction of high Mn-oxides dissolves into the slag. Carbothermic reduction of the formed primary slag occurs with subsequent formation of alloy. The following chemical reactions take place in the coke bed zone:

$$MnO(l) + C(s) = Mn(l) + CO(g), \quad \Delta H^0_{298} = +258.7 \text{ kJ/mol} \tag{1.8}$$

$$FeO(l) + C(s) = Fe(l) + CO(g) \quad , \quad \Delta H^0_{298} = +146.5 \text{ kJ/mol} \tag{1.9}$$

$$SiO_2(l) + 2C(s) = Si(l) + 2CO(g), \quad \Delta H^0_{298} = +751.0 \text{ kJ/mol} \tag{1.10}$$

The MnO content in the end slag is determined by the basicity, and may typically be around 40%, in a process known as high-MnO slag practice[2].

Typically, this MnO rich slag from the HCFeMn process is blended with manganese ores, quartzite, recyclables, and coke as charge material for the silicomanganese (SiMn) process. In contrast to high MnO slag practice, HCFeMn alloy can also be produced in a discard slag process where the process is operated at higher basicity around 1.0 compared to basicity of 0.8 typical for the high MnO practice[2]. The discard slag process generates a slag low enough in MnO to be discarded, typically contains about 15 to 20 % MnO. In general, the slag will contain unreduceable oxides from the charge materials and the remaining oxides from carbothermic reduction constituting of MnO, SiO_2, CaO, Al_2O_3, MgO as well as S and other trace elements. The composition of the slag is usually defined by the basicity of the slag i.e., ratio of basic oxides over acid oxides as presented the equation:

$$\text{Basicity (B)} = (CaO + MgO)/(SiO_2 + Al_2O_3) \tag{1.11}$$

Slag composition is important for the physicochemical properties of slag, such as melting behavior and viscosity. In addition, as mentioned, slag basicity directly influences the composition of liquid HCFeMn alloy[2], [11]. Typical grades for HCFeMn alloys vary in terms of their Mn-content. ASTM standard A99-03[10] defines the typical grades as; Grade A ranging from 78 % to 82 % Mn, Grade B from 76 % to 78% and Grade C from 74 % to 76 % Mn.

1.3 Energy and carbon consumption

The FeMn production process is energy intensive with requirements ranging between 2.0 and 3.5 MWh per tonne alloy produced[2], [12]–[14]. In the coke bed zone, the necessary quantity of carbon and energy requirements to produce FeMn alloy by direct reduction (reactions (1.8 -1.11)) of the prereduced ore is fixed for a specific alloy composition. Table 1.1 shows the calculated minimum fixed carbon consumption in the coke bed for the different ASTM standard A99-03 grades of HCFeMn. Total carbon consumption in industrial furnaces is typically above the minimum fixed carbon consumption in the coke bed as shown in Table 1.1. In a material and energy balance study by Tangstad and Olsen[7], total carbon consumption in producing an alloy of composition 79% Mn, 14% Fe, 7% C and 0.04%Si was estimated to be 329 kg C/ton alloy, for a charge mixture composed of 17.57kmol Mn, dolomitic limestone, 10% water and MnO_x with x=1.7. Swamy et al.,[12] studied the factors affecting carbon consumption in the production of HCFeMn and also highlighted that most smelting operations consume more carbon than the theoretically required for cokebed zone, with consumptions varying from about 305 – 380 kg C/ton of smelted alloy which translate to about 10 – 30% more. In another study, Ahmed et al.,[13] investigated the parameters affecting energy consumption for producing HCFeMn in a closed SAF and reported carbon requirements of 394 kg C/ton HCFeMn alloy produced. Lindstad *et al.*,[15] also reported that all smelting operations consume 10 - 30% more than the carbon needed to reduce MnO and FeO to metal and the carbon contained in the alloy. The consensus from many investigations[7], [12]–[15] is that the additional carbon consumption above the theoretical required in the smelting zone, is occurring in the burden or prereduction zone and do vary depending on furnace conditions as well as raw material properties. As such the total amount of carbon that will be consumed in producing 1 tonne of alloy will depend upon the extent of reactions in the prereduction zone and do vary over a wide range.

Table 1.1: Theoretical fixed carbon requirements in the cokebed (Calculated using HSC Chemistry® software[6]) per ton alloy for the different ASTM standard A99-03 grades of HCFeMn.

Reaction	Element	Elements (Wt. %) per alloy grade			kg C/ton of alloy (HCFeMn grades)		
		A	B	C	A	B	C
$MnO+C = \underline{Mn}+CO$	Mn	82.0	78.0	76.0	179.3	170.5	166.2
$FeO+C = \underline{Fe}+CO$	Fe	10.5	14.7	16.1	22.6	31.6	34.6
$SiO_2+2C = \underline{Si}+2CO$	Si	0.5	0.3	0.9	4.3	2.6	7.7
$C = \underline{C}$	C	7.0	7.0	7.0	70.0	70.0	70.0
Total minimum theoretical carbon requirements					**276.2**	**274.7**	**278.5**

1.3.1 Boudouard reaction

Additional carbon consumption in the prereduction zone is mainly dependent on the degree of prereduction, and hence the extent of the Boudouard reaction (reaction 1.7). The extent of the Boudouard reaction is dependent on the amount of CO_2 present from the prereduction and decomposition reactions at temperatures above about 800 °C. The extent of prereduction is influenced by factors such as the ability of oxygen above MnO in the ore to react with CO to produce MnO and CO_2; reactivity of the coke in the burden mix and the depth of the burden mix, which is influenced by furnace design, among other factors[2]. The degree of prereduction defined by Tangstad[16] is a measure of the extent of some of the CO_2 producing reactions (reduction of Mn_3O_4 to MnO, FeO to Fe and decomposition of carbonates), where the produced CO_2 is not reacting with the carbon according to Boudouard reaction. The Boudouard reaction which is active at temperatures above 800 °C, was observed by several researchers to be fast at high CO_2 concentrations ($(CO_2/(CO_2+CO)>30\%$) and high temperatures[12], [13]. A higher degree of prereduction reflected by high gas CO_2 content in the off-gas results in lower coke and energy consumption. When all the Mn_3O_4 from the reduction of higher manganese oxides is reduced at low temperatures before the Boudouard reaction is activated, the degree of prereduction is defined to be 100%. If all CO_2 from the reduction of Mn_3O_4 is consumed by the Boudouard reaction, the degree of prereduction is 0%. As such, the total carbon and energy consumption is highly dependent on the extent of gaseous reduction of higher manganese oxides in the prereduction zone and the extent of the Boudouard reaction. Hence, the gas-solid reactions in the prereduction zone are to a large extent decisive for the variations of both coke and energy in ferromanganese production [17]. This will hence also affect the total CO_2 emissions from the process.

Considering that the following reaction (sum of reaction (1.4) and (1.7)) is occurring above 800 °C because of lower degree of prereduction:

$$Mn_3O_4 + 4C = 3Mn + 4CO(g),\ \Delta H^0_{298} = +262\ \text{kWh/kmol}\ Mn_3O_4 \qquad (1.12)$$

This reaction consumes 0.017 kg C/kg Mn_3O_4. If 2 tonnes of ore are required to produce 1 tonne of HCFeMn alloy using an ore containing 80% MnO_2, then 702 kg Mn_3O_4 is produced per tonne of ore. Theoretically, the CO_2 gas produced by the reduction of Mn_3O_4 could react with carbon according to the Boudouard reaction leading to additional carbon consumption. If all the CO_2 produced by the gaseous reduction of 80% of the Mn_3O_4 occurs in the Boudouard active region and reacts

according to Boudouard reaction, it will increase both carbon and energy consumption by 58.9 kg C/t alloy and 230.2 kWh/t alloy, respectively.

The Boudouard reaction described by equation (1.7) is highly endothermic and consumes 0.27 kg C/kg of CO_2. Considering an operation which utilizes limestone ($CaCO_3$) flux to achieve the desired slag properties and that 120kg $CaCO_3$ per ton of ore is used which decomposes according to reaction (1.6) producing 52.8kg of CO_2 per ton of alloy, then it would consume 14.4 kg C/t of alloy, assuming all the produced carbon dioxide reacts with carbon according to the Boudouard reaction. The energy consumption would be ultimately increased by 56.2kWh/t alloy in addition to the energy requirements for the decomposition of the carbonates.

The degree of prereduction reflect the $CO_2/(CO_2+CO)$ ratio of the off-gas and is inversely related to the coke and energy consumption. Tangstad[16] plotted a graph that describes the close connection between carbon consumption and off-gas analyses in relation to the extent of the Boudouard reaction (1.7) as shown in Figure 1.2 for a fixed charge mixture.

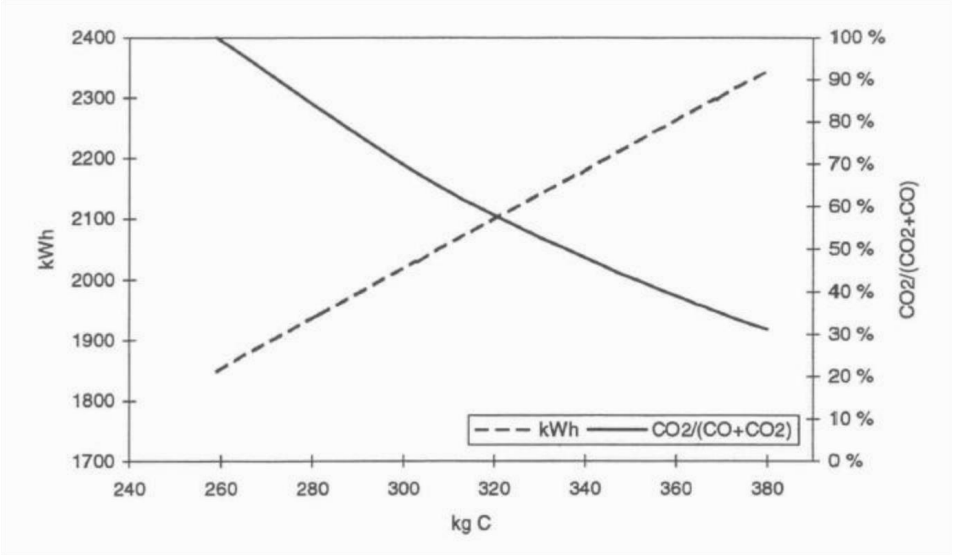

Figure 1.2: Energy consumption and off-gas analyses versus carbon consumption for a fixed charge mixture [16].

Figure 1.2 shows that an increase in carbon consumption results in an increase in the energy consumption. When all Mn_3O_4 is reduced in the direct reduction, approximately 380 kg C/ton alloy is consumed based on the charge mix considered in the work by Tangstad[16]. On the other hand, the minimum carbon consumption of

259 kg C/t alloy is required when the ore is completely reduced to MnO in the gas reduction zone. It was then concluded, that the maximum and minimum amounts of carbon are given by the extent of the Boudouard reaction. Similar relationship of offgas analyses, carbon and energy consumption with regards to the extent of the Boudouard reaction have been reported in a study by Ahmed et al.,[13] based on industrial data. Ahmed *et al.*,[13] reported that a portion of CO gas from direct reduction reactions in the coke bed zone is consumed in the indirect gaseous reduction of higher oxides of manganese and iron (i.e., MnO_2 and Fe_2O_3). Consequently, a higher amount of CO in the offgas than expected as a result of direct and indirect reactions should be a result of endothermic Boudouard reaction. Therefore, as the carbon monoxide content of the offgas increases, the energy consumption due to the Boudouard reaction increases. The main conclusion on this part of the work shows that the lower CO_2 to ($CO + CO_2$) ratio in the offgas indicates higher CO_2 consumed in the Boudouard reaction, and consequently, higher carbon and energy consumption.

Kalenga *et al.*,[18] assessed the impact of chemical compositions of raw materials and degree of prereduction on the energy requirements in HCFeMn for three different ores. Mn_2O_3 based ores namely Nchwaning 1, Nchwaning 2 and Gloria ores were assessed, in which Gloria ore was the only carbonates containing ore compared to the other two. They reported that the carbonate containing ore i.e., Gloria ore has an energy consumption higher than the two other ores mainly because of the effect of carbonate decomposition on the Boudouard reaction. The energy consumption increased with a decrease in the degree of prereduction and the results are presented in Figure 1.3. In their assessment the researchers assumed an off-gas temperature of 25 °C of which temperature magnitudes around 200 °C are typical in practical operations, as such their reported energy consumptions are relatively lower compared to consumptions reported in other investigations based on data of industrial SAF plants [2], [7], [12], [13].

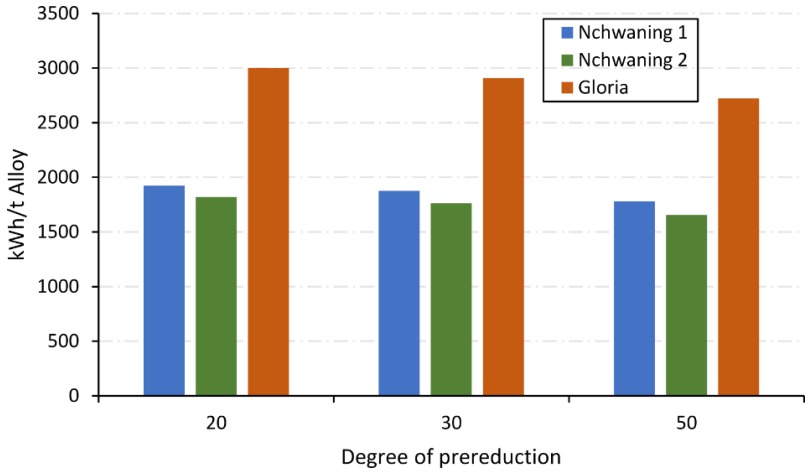

Figure 1.3: Energy consumption versus degree of prereduction for different manganese ores (Data from Kalenga et al.,[18])

1.3.2 Effect of trace elements and moisture on carbon and energy consumption

Manganese ores often contain small amounts of trace elements oxides such as potassium (K_2O), phosphorus (P_2O_5) and sodium (Na_2CO_3) which can affect the total carbon and energy consumption when reduced. Various investigations on different aspects have been conducted with ores containing K_2O in the range 1.1-2.3% [19]–[22]. The reduction of K_2O occurs in the coke bed according to the reaction:

$$K_2O(l) + 2C = 2K(g) + CO(g),\ \Delta H^0_{298} = +70.2\ \text{kWh/kmol}\ K_2O \qquad (1.13)$$

However, the formed potassium is vaporized due to the prevailing high temperatures in the cokebed. The vaporized potassium rises to the cooler regions i.e., above the cokebed where it reacts with CO_2 gas and condenses as K_2O according to the reaction:

$$2K(g) + CO_2(g) = K_2O + 2CO(g),\ \Delta H^0_{298} = -11.1\ \text{kWh/kmol K} \qquad (1.14)$$

Ultimately, potassium recycles in the furnace whilst consuming carbon and the evidence of its accumulation has been reported[12], [16]. The major difficulty observed was the predictability of the net effect of alkali circulation regarding carbon and energy consumption. It has been reported that the two step recirculation reactions (1.13) and (1.14) are equivalent to a single step Boudouard reaction (1.7) and as such their overall effect is difficult to distinguish. Swamy *et al.*,[12] reported a recirculating

potassium load of 9.0 times the input potassium in the ore. Tangstad and Olsen[7] estimated alkali accumulation at 15% K_2O which is approximately 7.5 times the input potassium in the ore and emphasis was placed on the fact that even a low alkali content of 5 – 10% will contribute significantly to the energy transfer. The potassium reduction reaction (1.13) consumes 0.128 kg C/kg K_2O. Assuming 7 times input potassium as the recirculating load, this will consume 35.7 kg C/t alloy and the energy consumption will be increased by 184kWh/t alloy. Typically, the calculated carbon consumption is subject to uncertainty.

More so, the kinetics of the Boudouard reaction is enhanced in the presence of alkalies. Lindstad *et al.*, [15] studied the reaction between CO_2 and ordinary metallurgical coke or coke impregnated with potassium at temperatures from 800 to 1100 °C in a thermobalance apparatus. The objective of this work was to establish the influence of alkalies on the Boudouard reaction. The main finding was that ordinary coke did not react to any extent at temperatures up to 1000 °C, whereas addition of potassium (2 – 10 %) resulted in a huge increase in reaction rates. The results from this work are in agreement with earlier findings from Alam and Debroy [23] where the presence of 2 wt.% Na_2CO_3 in the coke, at a temperature of 850 °C and pure CO_2 atmosphere increased the rate of Boudouard reaction by 8 times.

In a study of the effect of moisture, chemically bound water, and volatile elements on fixed carbon requirements in a ferromanganese furnace, Hongjie and Robertson [24], reported that the chances of free moisture and chemically bound water in manganese ore to reach the lower part of the furnace i.e., cokebed zone are very low and considered negligible. It was concluded that the consumption of carbon as a result of the direct reduction with water in the lower part of the furnace is very low unless the residence time of a fraction of the solid charge in the upper part of the furnace is less than 1.8 hours. Swamy *et al.*, [12] postulated a burden slumping that could make the chemically bound water to reach the lower part of the furnace and react directly with carbon consuming 0.67 kg C/kg of water.

1.3.3 Summary of factors affecting carbon and energy consumption

In view of the propositions asserted in this report, the potential increase in carbon consumption and energy consumption as well as energy consumption in producing an ASTM grade A HCFeMn alloy is summarized in Table 1.2. As previously discussed, the effect of alkali circulation on carbon and energy is equivalent to a single step Boudouard reaction. As such these two carbon consuming phenomena are not additive.

In consideration of this, increase in carbon consumption is 73.3 kg C/t alloy based on the propositions made. Therefore, a total of 354.9 kg Fix C/t alloy is consumed which is approximately 26% over the stoichiometric amount needed to produce 1 tonne of ASTM grade A HCFeMn alloy. This is within the range of 10 – 30% more carbon required to reduce MnO and FeO to metal and carbon contained in the alloy, as reported in literature [7], [12], [13], [15]. This is a good indication that carbon consumption depends on furnace conditions and the extent of carbon consuming reactions varies extensively. Therefore, management of the gaseous solid-state reduction of higher manganese ores is paramount in managing carbon consumption and consequently energy consumption which is determined by the net effect of exothermic and endothermic reactions in the process, as well as the enthalpy of the materials going in and out of the materials.

Table 1.2: Summary of increase in carbon and energy consumption due to reactions in the prereduction zone

Propositions for ore with 80% MnO_2 (Assuming 2 tonnes ore per 1 tonne alloy)	**Carbon consumption Kg C/t alloy**	**Energy consumption kWh/t alloy**
1. Minimum carbon consumption (fixed in cokebed zone)	281.6	
2.Boudouard reaction of all CO_2 from the decomposition of $CaCO_3$ (120kg $CaCO_3$/t ore)	14.4	56.2
3. All CO_2 from gaseous reduction of 80% Mn_3O_4 reacting according to the Boudouard reaction	58.9	230.2
4. P_2O_5 reduction in the coke bed (4kg P_2O_5 in ore/t alloy)	1.7	7.1
5. Recirculating potassium	35.7	184
Total increase excluding recirculating alkalies	**73.3**	**286.4**

1.4 Thesis scope

This work forms part of an EU funded H2020 project called PreMa, which is a collaborative project with partners from industry and research institutions. PreMa is focused on developing energy efficient, production of manganese ferroalloys through pretreatment of manganese ores prior to the submerged arc furnace (SAF). The project is aimed at demonstrating innovative technologies in ore pretreatment to reduce

energy consumption and CO_2 emissions from ferromanganese production. Figure 1.4 shows the PreMa concept of ore pretreatment prior to SAF. Pretreatment which entails preheating and/or prereduction, gives the possibility of using sustainable energy sources such as CO-rich offgas from the SAF, biocarbon and solar thermal energy[25]. As such, pretreatment has the potential to change Mn_3O_4 reactivity with CO when prereduced up to 600 °C and will thus contribute to lowering extra carbon and energy consumption through Boudouard reaction.

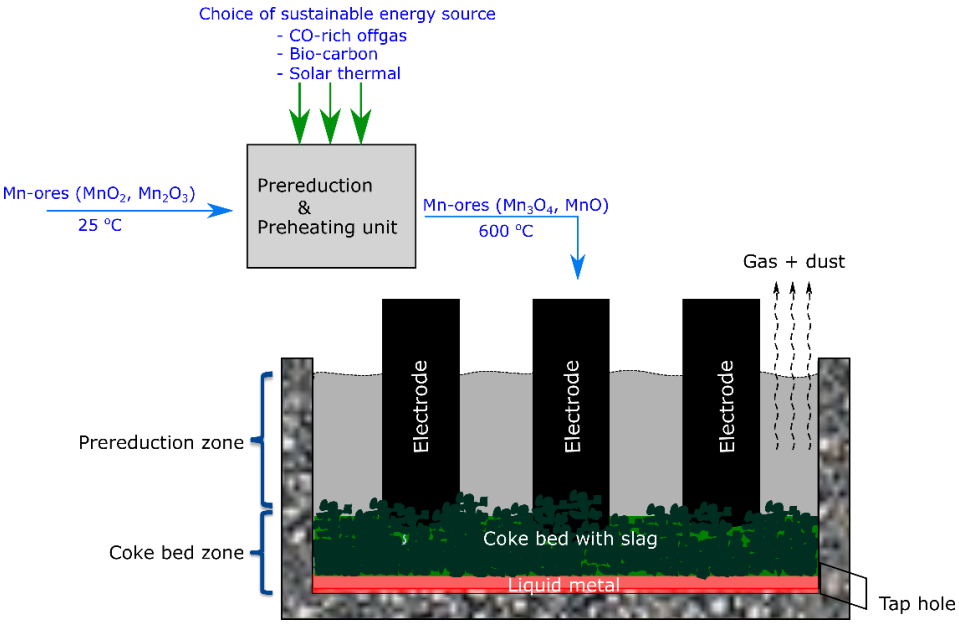

Figure 1.4: A sketch of pretreatment prior to SAF process in PreMa project

Some studies have been conducted to investigate the use of a dedicated separate unit in pretreatment of manganese ores[25]–[32]. In a study by Tangstad *et al.*, [25] on the pretreatment unit at CDK Kashima Works Japan, it was shown that the application of a separate unit could lower the electrical power consumption by 20% of the total energy consumption which translate to energy decreases of about 400-500 kWh/ton of alloy. In this work it is shown that the major benefit of a prereduction unit is the heating of raw materials up to 600 – 700 °C including the water evaporation where for every 100 degrees of increased temperature, the electrical energy consumption would be reduced by more than 80 kWh/ton. Pretreatment is mostly suited for Mn_2O_3 ores and Mn_3O_4 charges whereas, if a large amount of MnO_2 is used, the reduction of energy will be much less compared to the conventional standalone electric furnace. Furthermore, pretreated raw materials are expected to

give a more stable and predictable furnace operation and in addition, contribute to lowering CO_2 emissions. However, the effect of utilizing pretreated ores on the SAF process is not known and this work seeks to increase and contribute to the knowledge about furnace performance from utilization of pretreated ores. Therefore, the objectives of this PhD work are:

1) to gain more knowledge on the prereduction behavior of Mn-ores.
2) to evaluate the effect of varying degree of prereduction on the high temperature reaction $MnO + C = Mn + CO$.
3) to compare effect of untreated and pretreated ores on the change in inner structure and reaction path of the SAF through digout of the prereduction zone and excavation of the coke bed zone of the pilot experiments.
4) to assess the carbon and energy consumption based on mass and energy balances of pilot experiments when utilizing untreated and pretreated Mn ores.

The following chapters will be included in this thesis:

- **Chapter 2** describes the theory and literature review of ferromanganese process. The main focus is on prereduction behavior of manganese ores, carbothermic reduction of slag, carbon, and energy consumption in ferromanganese production.
- **Chapter 3** describes the methods and materials used in the small-scale and medium-scale experiments performed in the laboratory. In addition, the results are described and discussed.
- **Chapter 4** describes the pilot furnace experiments; its operation and details of the experiments conducted. In addition, the methods describing the digout of the prereduction zone and excavation of the coke bed zone of the pilot furnace is described. The main findings from the pilot furnace post experimental investigations i.e., digout of the prereduction zone and excavation of the coke bed zone are also described. Results of the inner structure and reactions in the furnace based on untreated and pretreated ores are discussed.
- **Chapter 5** gives the results and detailed discussion of accounting mass and energy balance calculations. The carbon and energy consumption per ton alloy is discussed highlighting the effect of ore pretreatment.
- **Chapter 6** gives a summary of the main results and conclusions in conjunction with recommendations for further work.

Chapter 2

2 Theory and Literature Review

2.1 Manganese Ores

Manganese (Mn) is the 10th most abundant element and third most abundant transition metal in Earth's crust and has the largest number of oxidation states of third row elements of the periodic table[33], [34]. Mn oxide or hydroxide (generally referred to as Mn oxide) minerals are found in a wide variety of geological settings. These oxides are the predominant ore minerals in most of today's commercially important Mn deposits, commonly formed by weathering of Mn-rich silicates or carbonates[33]. These Mn oxides have been extensively studied for the past several decades [33]–[36]. Surveys of geological manganese deposits clearly shows that there are significant manganese mineral variations in different deposits, with redox state of manganese in these minerals varying from Mn(II) to Mn(III) to Mn(IV)[2], [33]. This accounts for the complexity and impressive variety of Mn oxide minerals as they display a remarkable diversity of atomic architectures which accommodates a wide assortment of other metal cations of elements such as Ca, Mg, Si, Na, Al, Fe etc. [33]. Table 2.1 shows some of the most important Mn oxide minerals.

Manganese deposits have been described from different parts of the world and some of the world's largest land-based repositories of manganese ore are in Kalahari basin in South Africa, Groote Eylandt (GE) in Australia, Moanda deposit in Gabon as well as deposits in Brazil, India, and China.

The manganese deposits in South Africa has been studied by several researchers [36]–[40]. The Mn-rich Kalahari deposit has been mineralogically subdivided into two specific types namely Mamatwan-type (e.g., the Mamatwan and Gloria deposits) and Wessels-type (e.g., Nchwaning deposits). The ores from these regions exhibit considerable differences in mineral distributions and are dominated by divalent and trivalent Mn minerals, such as bixbyite, braunite and hausmannite[36], [41]. In addition, these ores have gangue and lower Mn content ore mineralogy dominated by carbonates such as calcite (often Mn-bearing), kutnohorite and dolomite as well as notable hematite in some cases. Mamatwan type ores are enriched in Mn-

bearing carbonates with typical minerals such as kutnahorite, hematite, rhodochrosite, jacobsite and hausmannite. The Wessels type ores contains both braunite-I and braunite-II, more bixbyite, more hematite (Fe_2O_3) and less carbonate minerals compared to Mamatwan types[36], [41]. Wessels type ore tends to have a more coarse microcrystalline structure and both ore types are characterized by particles with low levels of intra- and inter-crystal microporosity[41]. In general, these ores have an oxygen level close to that of Mn_2O_3 and are classified as semi-oxidized, with lower Mn/Fe ratio compared to higher oxidized ores i.e., MnO_2 based ores. In general, iron in manganese ores has been found in the forms of free hematite (Fe_2O_3), goethite (FeOOH) and bixbyite ($(Mn,Fe)_2O_3$)[19], [42]–[46].

Table 2.1: Typical manganese minerals [33]–[36]

Classification	Mineral	Chemical formula
Higher oxides	Pyrolusite	MnO_2
	Ramsdellite	MnO_2
	Nsutite	$Mn(O,OH)_2$
	Cryptomelane	$K_x(Mn^{4+},Mn^{3+})_8O_{16}$
	Todorokite	$(Ca,Na,K)_x(Mn^{4+},Mn^{3+})_6O_{12}\cdot 3.5H_2O$
Hydroxides	Manganite	γ-$Mn^{3+}O(OH)$
	Pyrochroite	$Mn^{2+}(OH)_2$
	Feitknechtite	β-$Mn^{3+}O(OH)$
Lower oxides + silicates	Bixybite	$(Mn^{3+},Fe^{3+})_2O_3$
	Jacobsite	$(Mn^{2+},Fe^{3+},Mg)(Fe^{3+},Mn^{3+})_2O_4$
	Braunite I	$Mn^{2+}Mn^{3+}{}_6SiO_{12}$
	Braunite II	$Ca(Mn^{3+},Fe^{3+})_{14}SiO_{24}$
	Hollandite	$Ba(Mn_{4+},Mn_{2+})_8O_{16}$
	Manganosite	MnO
	Rhodonite	$MnO\cdot SiO_2$
	Tephroite	$2MnO\cdot SiO_2$
Carbonates	Rhodochrosite	$Mn^{2+}CO_3$
	Kutnahorite	$Ca(Mn^{2+},Mg,Fe^{2+})(CO_3)_2$

Ostwald J.[35], [47] extensively studied the mineralogy of the Groote Eylandt (GE) deposit in Australia. The mineralogical description of GE includes minerals such as pyrolusite, nsutite, cryptomelane, todorokite and manganite. Similar to GE, the Moanda Mn ore deposit in Gabon is also dominated by tetravalent Mn oxides[41]. These ores also tend to have a high proportion of the gangue minerals present as clay (kaolinite or illite), quartz and goethite and exhibit relatively higher levels of microporosity. Moanda deposit in Gabon produces a globally shipped lumpy ore known as Comilog, which is more porous than Groote Eylandt lump ore. Ore porosity significantly determines moisture content in these ores and influences ore reactivity and

decrepitation behavior during prereduction in the solid-gas region of the electric furnace [2], [48], [49].

Other commercial ores are the Azul and Urucum deposits in Brazil which have a mineralogy which is quite similar to GE and Comilog[50]–[52]. These deposits are predominantly composed of cryptomelane and pyrolusite, with less braunite, todorokite and nsutite. The Azul lump ore is a high-grade ore and is more porous compared to Urucum containing some hematite, goethite and quartz[53], [54]. Ores from India are dominated more by divalent and trivalent Mn minerals, such as bixbyite, braunite and hausmannite[55], [56]. Table 2.2 shows some of the commercial manganese ores and sinters.

Table 2.2: Typical composition of some commercial ores and sinters (dry basis) [2], [57]

Composition (wt. %)		**Mn-source**					
	Comilog Ore	**Comilog Sinter**	**Mamatwan Ore**	**Groote Eylandt**	**Nchwaning ore**	**Amapa Sinter**	**CVRD Sinter**
Mn/Fe	16.5	16.7	8.2	11.6	4.6	5.1	11.5
$Mn_{,tot}$	51.0	58.5	38.2	48.8	46.4	49.1	54.5
$Fe_{,tot}$	3.1	3.5	4.67	4.21	10.0	9.63	4.73
MnO_2	76.4	19.7	26.5	73.9	34.6	18.6	22.5
MnO	3.5	59.6		2.6	31.6	45.7	52.0
CaO	0.4	0.1	13.3	0.1	5.9	0.8	1.9
MgO	0.1	-	3.17	0.1	1.4	0.5	0.5
SiO_2	3.5	7.0	0.08	6.9	6.7	7.6	5.4
Al_2O_3	5.6	6.5	0.74	4.2	0.5	7.6	8.7
K2O	0.7	0.75	0.08	2.0	0.0	0.3	1.4
P	0.1	0.12	0.02	0.09	-	0.10	0.11
CO_2	0.1	-	14.0	0.5	3.0	-	0.2
O/Mn	1.94	1.21	1.44	1.96	1.47	1.24	1.26

2.2 Prereduction reactions

Ores with reduceable oxides, mainly oxides of Mn and Fe with a typical Mn/Fe weight ratio of higher than 6.2, are usually used for production of HCFeMn production in SAF [2], [58]. The main manganese oxides of interest are MnO_2, Mn_2O_3, Mn_3O_4 and MnO and iron oxides are, Fe_2O_3, Fe_3O_4, and FeO. In a conventional closed SAF for manganese ferroalloy production, the furnace gas is mainly CO/CO_2 gas at atmospheric pressures, with CO gas acting as a reductant and CO_2 as a product of solid-gas reactions. The CO gas is generated from the metal formation reactions in the high temperature zone of the furnace and from the endothermic Boudouard reaction. In Figure 2.1 the equilibrium reduction reactions of the various manganese and iron

oxides, as well as the decomposition of carbonates are shown. It can be seen that the related standard Gibbs energies of the gaseous reactions by CO gas show negative values from very low temperatures and indicates that these prereduction reactions are thermodynamically feasible at lower temperatures. The gaseous reduction of oxides of Fe_3O_4 to Fe is feasible at temperatures approximately below 550 °C, whereas above 550 °C FeO is stable as will be discussed later.

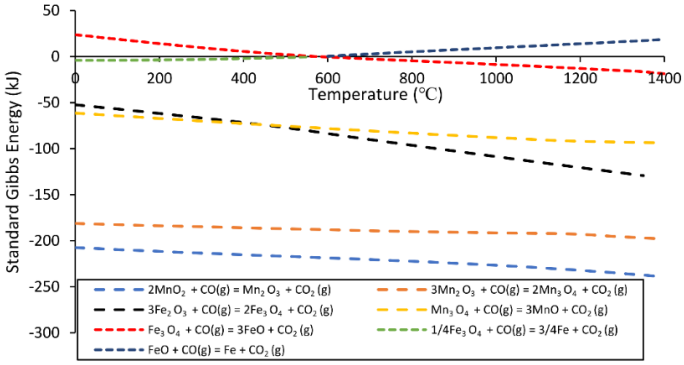

Figure 2.1: Standard Gibbs energies of prereduction reactions of higher oxides of Mn and Fe by CO gas, carbonate decomposition and reduction of MnO, FeO and SiO_2 by C versus temperature (data from HSC Chemistry® software[6]).

2.2.1 Thermodynamics of reduction reactions

The stability of the reduceable oxides of Mn and Fe as a function of partial pressure of oxygen (pO_2), and temperature is illustrated in Figure 2.2. The equilibrium partial pressure of oxygen (pO_2) which signifies the reduction potential of the gas is defined by the CO/CO_2 gas composition given by equilibrium reaction (2.1) and calculated using equation (2.2).

$$2CO(g) + O_2(g) = CO_2(g) \qquad \Delta H^0_{298} = -565.9 kJ/mol \qquad (2.1)$$

$$\log p(O_2) = 2 \log \left(\frac{p_{CO_2}}{p_{CO}} \right) - \frac{67890}{T} + 20.900 \qquad (2.2)$$

The equilibrium for gas composition with CO content from 20 – 80 % are superimposed on the Mn-O and Fe-O stability diagram as shown in Figure 2.2. According to the stability diagram higher manganese oxides of MnO_2 and Mn_2O_3 can be reduced in air to Mn_2O_3 and Mn_3O_4 at temperatures above 486 and 873 °C, respectively, and in a reducing atmosphere these oxides can be reduced at lower

temperatures. Previously, Olsen *et al.*, calculated the stability diagram using FactSage software and showed decomposition temperatures of MnO_2 and Mn_2O_3 oxides at 510 and 981 °C, respectively[2]. The main reason for these temperature differences is attributed to be due to differences in databases utilized for calculating equilibrium constants.

A very low oxygen partial pressure is required for metallization of Mn, and this is unlikely to be reached with CO gas. The oxygen partial pressure for production of metallic Mn depends on temperature, and evidently lower partial pressures of oxygen are required at lower temperatures as shown in Figure 2.2. For the higher oxygen pressures, the stable phase is MnO for the Mn-O binary system for all CO gas concentrations. Depending on the equilibrium oxygen partial pressure and temperature, the stable phases for the Fe-O system can be either Fe_3O_4 at high pO_2 gas concentration i.e., at 20 to 30% CO or Fe at very low pO_2 i.e., 70 to 80% CO. These relations are valid for pure oxides as the Fe-O binary system is superimposed on the Mn-O system. However, there is potential formation of solid solutions considering the complexity and variations of minerals in manganese ores.

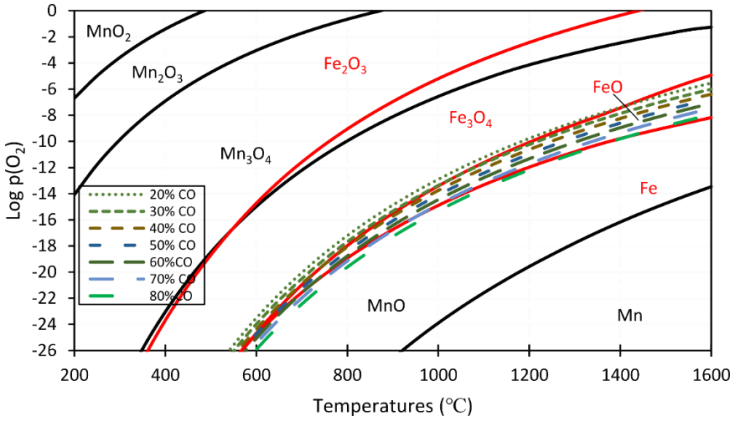

Figure 2.2: The oxygen partial pressure of practical gas mixtures (green lines) superimposed on the Mn-O and Fe-O stability diagrams, showing oxygen partial pressure versus temperature (Equilibrium values calculated from HSC Chemistry® software[6])

Several works have been reported on the thermodynamics of the Fe-Mn-O system[59]–[63]. Kang and Jung provided a critical evaluation of experimental data and thermodynamic optimization for the Fe-Mn-O system[60]. This work explains that the solid phases are inherently solution phases. The degree of solubility between the different oxides is clearly visible as presented by the isothermal section of the Fe-Mn-O system at 1273 K as shown in Figure 2.3. The following phases are found in this system: manganowüstite ($(Fe,Mn)_{1-x}O$), cubic spinel ($(Fe,Mn)_3O_4$), tetragonal spinel

($(Mn,Fe)_3O_4$)), corundum ($(Fe,Mn)_2O_3$), bixbyite ($(Mn,Fe)_2O_3$), and two metallic phases (β-metal CUB, γ-metal FCC). In similar works, Kjellqvist and Selleby provided very thorough data for the thermodynamics of the Fe-Mn-O system and reported the pO_2 as a function of oxygen content in a Fe-Mn solid solution, $MnFenO_x$[61]. The amount of oxygen in the solid solution has been reported to change as a function of oxygen partial pressure as shown in Figure 2.4.

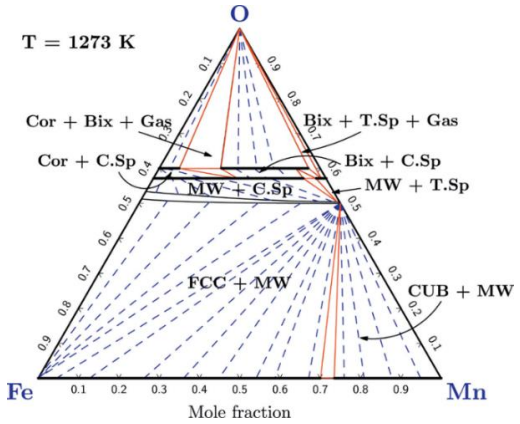

Figure 2.3: Isothermal section of the Fe-Mn-O system at 1273 K. (MW = $(Fe,Mn)_{1-x}O$, C.Sp = $(Fe,Mn)_3O_4$, T.Sp = $(Mn,Fe)_3O_4$, Cor = $(Fe,Mn)_2O_3$, Bix = $(Mn,Fe)_2O_3$, and five metallic phases (CBCC,CUB, FCC, BCC, Liq.)) [60]

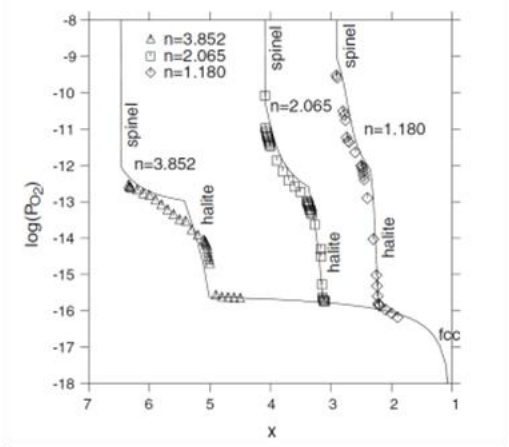

Figure 2.4: Experimental points and calculated oxygen potential in $MnFe_nO_x$ at 1242 K. The wustite ($Fe_{1-x}O$) and manganosite ($Mn_{1-x}O$) phases are isomorphous both having the NaCl-type structure with generic name halite.[61]

Most recently, Schanche and Tangstad[63], [64] calculated the phase stability in the Mn-Fe-O system (oxygen partial pressure versus metallic ratio) at (a) 600 °C and (b) 800 °C as shown in Figure 2.5.

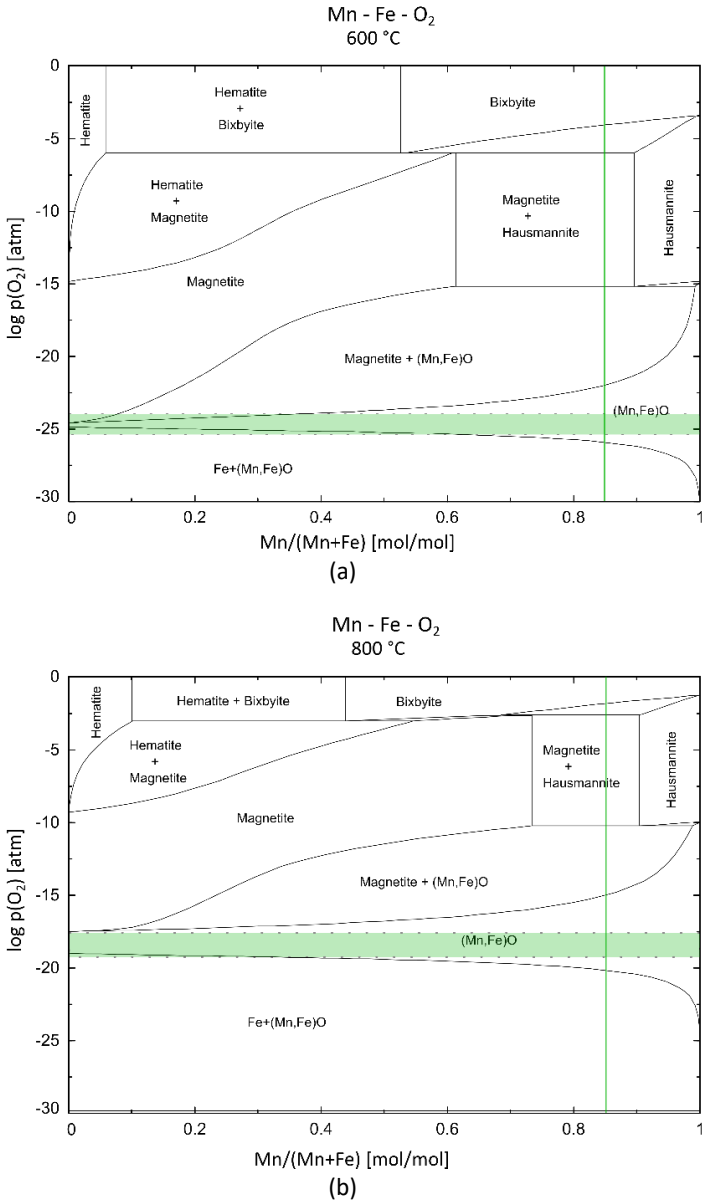

Figure 2.5: Calculated phase diagram of the Fe–Mn–O system at (a) 600 °C and (b) 800 °C at 1 atm by Schanche and Tangstad [63]. The highlighted areas show the equilibrium pO_2 for the experimental gas mixtures used in their work and the vertical line is the average Mn/(Mn+Fe) ratio based on chemical analysis of Nchwaning ore [63].

It can be seen from Figure 2.3 to Figure 2.5 that the oxides of manganese and iron display a wide range of solid solutions. The stable equilibrium phase of the manganese and iron oxides within the experimental range investigated by Schanche

and Tangstad is (Mn,Fe)O[63]. The formation of metallic iron was not confirmed experimentally in this work[64]. The X-ray diffraction revealed that bixbyite and braunite (I and II) were reduced to manganosite with no or limited formation of hausmannite. Reduction of iron oxides ended with wüstite, which is stabilized by manganese in the monoxide phase, and hydrogen was seen to improve the reduction of iron oxides. In another study, the prereduction of manganese ores with natural gas was investigated by Cheraghi *et al.*,[46]. Characterization of the ores, calcined ores, and reduced samples were carried out using X-Ray Diffraction, X-Ray Fluorescence, and Scanning Electron Microscopy techniques. Iron oxide and co-existing MnO produced during prereduction were also observed to dissolve in each other at high temperatures, forming (Mn,Fe)O solutions. Fahim *et al*,. [43] investigated the reactivity of the different ores carried out through pre-reduction of the selected ores using thermobalance at 900 ℃ and 1100 ℃ and mixture of CO and CO_2 gases. Most recently, Larssen *et al.*,[65] studied the reduction of manganese ores in CO/CO_2 atmospheres utilizing a thermogravimetric furnace up to 1100 ℃. The morphological observations in these studies[43], [65] were in agreement with reduction of iron oxides ending with wüstite, which is stabilized by manganese in the monoxide phase.

2.2.2 Prereduction mechanism and kinetics

Production of high carbon ferromanganese from manganese ores follows the step of solid-state reduction with CO gas in the prereduction zone of the submerged arc furnace prior to smelting in the cokebed zone. As such, CO gas plays an important role in the prereduction zone in the SAF, and most of the literature works on gaseous reduction were dedicated to reduction by CO-containing gases, with either presence or absence of a solid carbon source [20], [30], [44], [65]–[77]. Hence, in this chapter the solid-state reaction mechanism of manganese ores with CO/CO_2 containing gases are discussed.

The progress and determination of the kinetics of pre-reduction of high manganese oxides has been extensively described using the stepwise shrinking core model[76]–[79]. This model is often used for the gas-solid reactions and in this model, the outer layer of the particle is firstly reacted with the fluid, and by diffusion of the fluid front towards the center, converted materials are left behind, and the unreacted core of the particle contracts by the reaction progression[80]. This model visualizes five successive steps occurring during a gas-solid reaction as illustrated in Figure 2.6:

1. Diffusion of the reactant gas through a gas boundary layer towards the solid surface
2. Diffusion of the reactant gas through the particle surface
3. The chemical reaction of the gaseous reactant and the material
4. Diffusion of the gaseous products of the chemical reaction back to the particle surface
5. Diffusion of the gaseous products through the gas boundary layer to the main fluid body

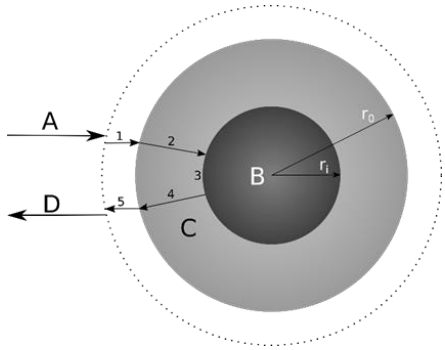

Figure 2.6: Schematic of the shrinking core model

The shrinking core model, as applied to prereduction of higher manganese oxides is illustrated by the schematic presented in Figure 2.7.

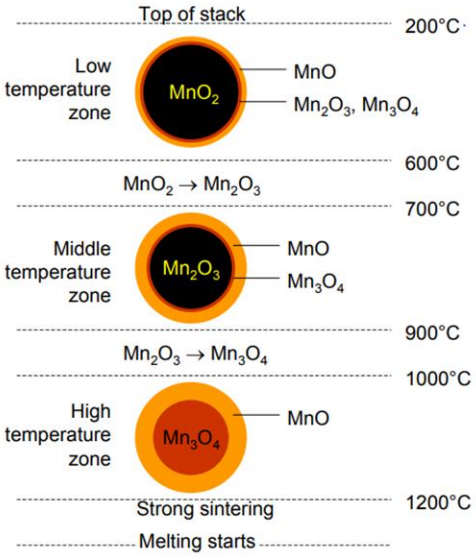

Figure 2.7: Reaction progress for lumpy MnO_2 ore during gradual heating [2]

The schematic indicates the reduction of a spherical MnO_2 particle to lower manganese oxides following a temperature gradient that exist in the SAF. Lower Mn oxides are seen to form stepwise with increasing temperature, however, as has been observed experimentally by Berg[76], the reduction of Mn_2O_3 to Mn_3O_4 was so fast that it was hardly detected during reduction.

In view of the shrinking core model, many researchers have agreed that the pre-reduction of higher manganese ores progress through very rapid chemical reactions, where the kinetics is limited by mass transfer of the CO reductant to the reaction interface and CO_2 product from the reaction interface[2], [77], [81], [82]. This mass transfer effect was investigated by Berg and Olsen[77], whereupon they established that MnO production on a shell adjacent to an unreduced Mn_3O_4 layer constraints diffusion by acting as a barrier and ultimately offers a significant resistance to the overall Mn_3O_4 to MnO reduction rate. However, ores with high porosity or small particle size would reduce more rapidly, where, if diffusion through product shell is rate-limiting then an MnO layer greater than 1mm would impact the reduction efficiencies[2], [81]. Industrially, gas flow within the furnace is highly impeded by smaller ore sizes and as such these are not preferable. Henceforth, a highly porous ore with considerable strength offers greater improvements in the prereduction of higher manganese ores to MnO. The shrinking core model is controlled by chemical reaction, pore diffusion, or a mixture [83].

Kor[68] studied the rate of reduction of Mn_3O_4 by CO and carbonaceous reductants namely; coconut charcoal, coke and pure graphite in the temperature range 900 to 1200 °C. The rate of reduction in CO was determined to be fast and the overall rate of reduction by a carbonaceous reductant was influenced by the oxidation of the carbon by CO_2. The oxidation of carbon by CO_2 was found to be significantly pronounced when the reductant was either carbon or coke and in addition, catalyzed by Mn_3O_4. Halim *et al.*,[70] studied the pre-reduction reactions for a 57.2% MnO_2 ore in a rotary kiln at 800-1100 °C. They used large sample sizes (3kg) with particle sizes (100 to 400 µm) mixed with Pet Coke. The coke (carbon) was mixed at 1.25 times the stoichiometric ratio for reducing iron and manganese. The crucible was kept in an inert atmosphere of argon during the experiment. Micro TGA was also used to measure weight loss for 1 gram of pelletized samples, also mixed with coke. The gas emissions were measured in a different experiment with 1 gram of pelletized samples heated isothermally in a horizontal tube furnace. With these experiments they concluded that the prereduction of manganese ores takes place by gaseous reduction mechanism and Boudouard reaction as the rate controlling step.

2.2.3 Effect of different parameters on the prereduction rate of Mn-ores

Since the prereduction reactions are highly decisive on the total carbon, and energy consumption of the ferromanganese process, understanding the prereduction behavior from ore characteristics and furnace conditions is of paramount importance. Characteristics of the prereduction process differ and are significantly dependent on the ore type used. This is mainly because manganese ores used by industry in the production of FeMn alloys have different origin and therefore differ in mineralogy, chemical, and physical properties. The prereduction behavior and extent of solid-gas reactions is dependent on several factors which are correlated, and these include porosity of the burden mix, CO reactivity of the ore, ore particle sizes, alkalie recirculating, moisture content, carbonates, hydroxides, and the reactivity of the coke in the burden mix.

The effect of porosity of feed raw materials on prereduction has been studied by several researchers[20], [48], [84], [85] and has been found to have an impact on the CO reactivity of feed materials. It has been shown that heat treated materials like sinter and pellets exhibit lower CO reactivity as compared to lumpy ores and briquettes[84]. This is mainly due to lower porosity in sinters and pellets. In another study of the kinetics of prereduction of manganese ores, Tangstad *et al.*,[20] established that ores with higher manganese oxides are reduced faster than others. In this study, it was shown that ores such as Comilog and BHP ore have minerals pyrolusite (MnO_2) and kryptomelane ($K_2Mn_8O_{18}.xH_2O$) which form bixbyite ($(Mn,Fe)_2O_3$) exhibiting a higher reduction rate than ores such as Wessels, Mamatwan and Assmang which contain braunite minerals ($3(Mn,Fe)_2O_3.MnSiO_3$,$7(Mn,Fe)_2O_3.CaSiO_3$). It can also be noted in this case that the mineralogy and porosity is correlated, that is the Comilog ore, and the BHP ore have higher porosity than the South African ores.

Turkova *et al.*,[48] studied correlation between CO-reactivity and porosity for three different manganese ores, CVRD, Assmang (Nchwaning) and Gabonese (Comilog). They used 200 g +/- 30g samples heated in a vertical tube furnace with a heating rate of 10 °C/min. They used a gas composition of 70/30 CO/CO_2 with a flow rate of 4 L/min. The ores were heated to three different max temperatures of 400, 800, and 1100 °C. The authors found that ores with higher initial porosity will have a higher CO-reactivity, and that for Assmang (Nchwaning), a low porosity ore, an agglomerate with higher porosity will give a higher CO-reactivity. In addition, porosity increase below 400 °C was reported to be caused by the removal of bound water and in the temperature range 400 – 800 °C, the porosity increase was an effect

of the pre-reduction of higher manganese oxides, swelling of the particle due to heating, and decomposition of carbonates.

De Jesus & Tangstad[69] investigated the CO reactivity for lump manganese ore and briquettes at 1100 °C. A macro TGA was used with a gas composition of 70/30 CO/CO_2 and heating rate of 10 °C/min. The lumpy ore was in the size range of 9-15 mm, while the briquettes were made of -250 µm fines mixed with either molasses or clay. The authors concluded porosity was the biggest factor in CO reactivity, with molasses in briquettes decomposing at lower temperatures causing pores to form which resulted in the highest reactivity. Recently, extensive work on the reduction of Comilog and Nchwaning ores in CO/CO_2 atmospheres and the analysis of the reaction rate of these ores has been carried out by Larssen *et al.*,[65], [73]. They obtained thermogravimetric data for the reduction of Comilog and Nchwaning ore in CO/CO_2 atmosphere were temperature, particle size and CO-concentration were investigated variables. It was reported that an increasing partial pressure of CO in CO/CO_2 atmosphere promoted the reaction rate with an order of 0.7 and 1.5 for Comilog and Nchwaning ores, respectively. The obtained reaction orders were for Comilog ore in particle size range 11.2 to 15.0 mm heated in 30, 40, 50 and 80 pct CO concentrations whereas similar particle size for Nchwaning ore were heated in 30, 50 and 80 pct CO concentrations. Activation energies of 17 kJ/mol and 63 kJ/mol were estimated for Comilog and Nchwaning ore, respectively. Carbonates in Nchwaning were found to decompose at temperature range 800 °C to 1000 °C and in addition, decreasing particle size promoted reaction rate for both ores. Figure 2.8 and Figure 2.9 shows the effects of partial pressure of CO in CO/CO_2 and particle size on the prereduction reaction rate for Comilog and Nchwaning ores, from work by Larssen[73], [75].

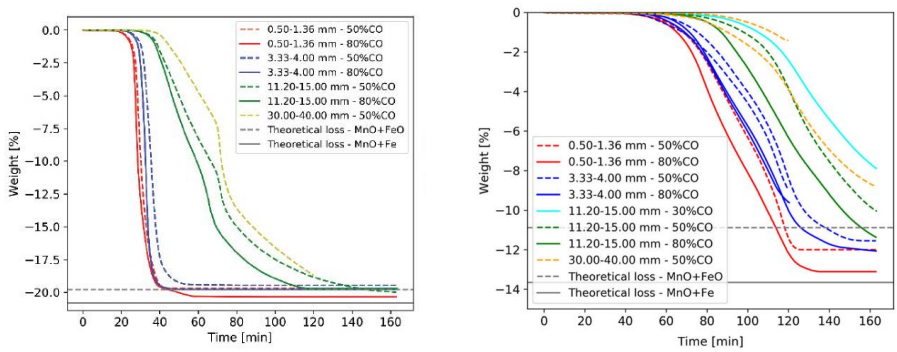

(a) (b)

Figure 2.8: Weight loss as a function of time, respectively for Comilog ore (a) and Nchwaning ore (b) [73], [75].

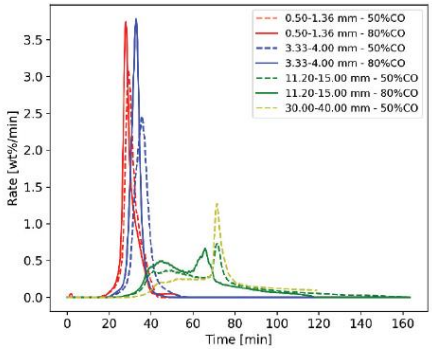

(a)

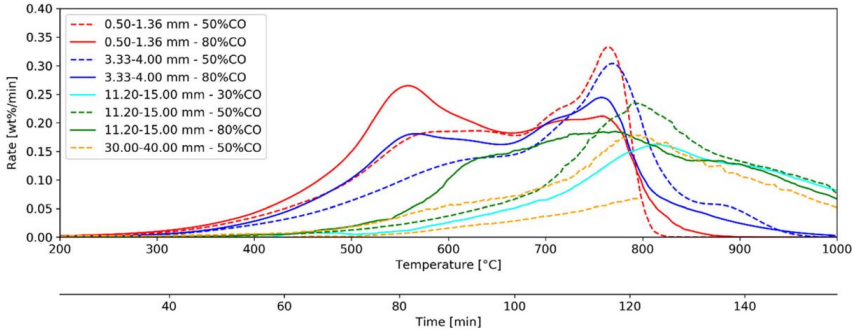

(b)

Figure 2.9: Reaction rate as a function of time for Comilog ore (a). Reaction rate as function of time and temperature for Nchwaning ore(b) [73], [75].

Ishak and Tangstad [17] studied degree of prereduction in industrial furnaces and reported that degree of prereduction is typically between 10 – 40%, but can be

as high as 60% in good operational periods. In this study, a series of laboratory scale experiments were performed to measure the CO reactivity of industrial ores resulting in a plot presented in Figure 2.10.

The Boudouard reaction is more pronounced at temperatures above 800 °C and it follows from Figure 2.10 that at this temperature Comilog ore has the lowest oxygen level, followed by Comilog sinter, Mamatwan ore, Assmang ore and Mamatwan sinter. As such Comilog ore has better degree of prereduction and should give the lowest amount of Boudouard reaction. Similar results were obtained by Larssen [75] in her PhD study focusing on the gaseous reduction of Comilog and Nchwaning ores. Comilog ore was found to be completely prereduced at 600 °C, whereas reduction of Nchwaning ore was not complete at 800 °C and the results were highly repeatable. Results from these investigations indicate that the use of highly reducible ores leads to increased indirect reduction of Mn_3O_4 at temperatures below the temperatures where the Boudouard reaction is active and thus, leads to lower carbon consumption.

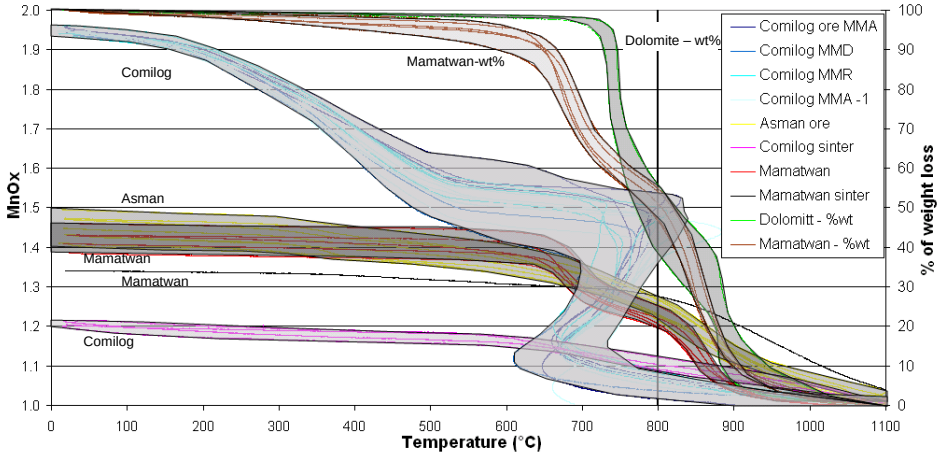

Figure 2.10: Reduction curves as a function of temperature for several manganese sources[17].

2.3 High temperature reduction

In the cokebed the carbothermic reduction to metal occurs. Liquid slag is formed and is reduced to produce liquid metal and CO gas which ascends into the prereduction zone subsequently prereducing the ores above this zone. In this multicomponent zone, slag composition is important for the physiochemical properties of the slag, such as

liquidus temperature and viscosity as well as the reactivity. In general, the performance of a pyrometallurgical process is highly influenced by proper knowledge and control of the slag and thus, the importance of a good slag can be summed up by the old adage, ''look after your slag and the metal will look after itself''[86]. Hence, the composition of liquid metal is hence directly influenced by the chemistry of the slag. Therefore, this section is a review of some aspects critical in influencing the metal formation reactions and stability of furnace operation.

2.3.1 Reduction of slag to metal – the thermodynamics

The main components in the FeMn slag system after prereduction are MnO-FeO-SiO_2-Al_2O_3-CaO-MgO. Figure 2.11 shows the equilibrium standard Gibbs free energies versus temperature for the reduction of these oxides.

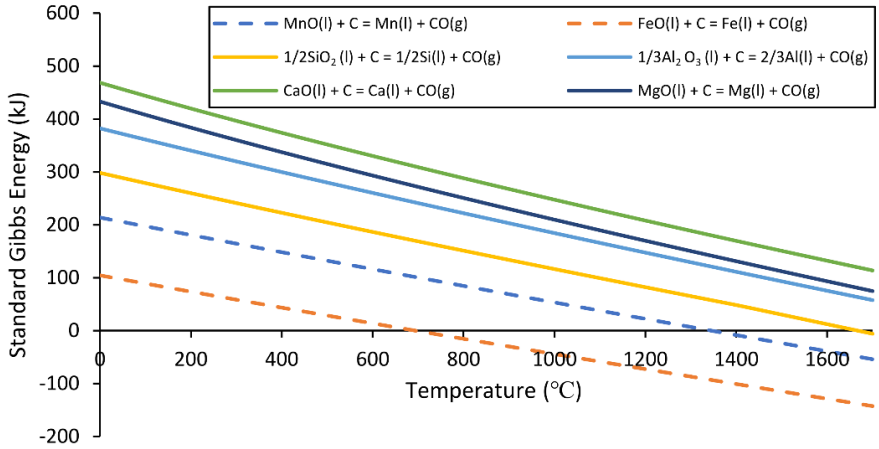

Figure 2.11: Standard Gibbs energies for reduction of MnO, FeO, SiO_2, Al_2O_3, CaO and MgO by C versus temperature (data from HSC Chemistry® software[8]).

The reduction of oxides of FeO and MnO by solid carbon show negative standard Gibbs energy at temperatures greater than 650 °C and 1350 °C, respectively, whereas the reduction of SiO_2, Al_2O_3, CaO and MgO requires higher temperatures as presented in Figure 2.11. This implies that all the Fe in the charge materials will end up in the metal as shown in Figure 2.11, where standard Gibb's energy is negative at temperatures well below furnace operating temperatures whereas, all Al_2O_3, CaO, MgO and most of the SiO_2 will report to the slag phase in FeMn process. The Gibbs energy is most usable for comparison when all species are

in their standard state. One still uses the Gibbs energy to get a first approximation of the system, even when the species are not in their standard state. In the FeMn process both the oxides, the alloy and the gas will be a solution of several elements, and a more detailed analysis must be done.

The reduction Of MnO can be illustrated by the ternary phase diagram for the MnO-CaO-SiO_2 slag system shown in Figure 2.12. The primary slag after complete prereduction will contain liquid slag in coexistence with solid MnO. As such, the reduction of MnO starts in the two-phase area as illustrated in Figure 2.12. Considering a slag with an initial composition X, MnO reduction will proceed with simultaneous dissolution of solid MnO until liquidus point Y along a fixed basicity line. During this period, the activity of MnO will remain constantly high. Further reduction will occur in the liquid phase and the activity of MnO will decrease rapidly as composition of slag will move from liquidus composition Y towards equilibrium point Z.

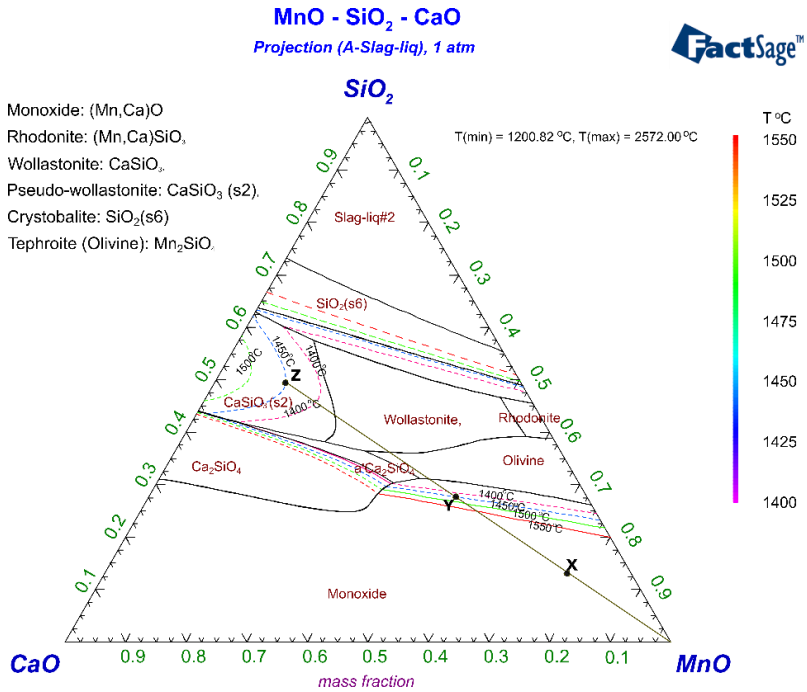

Figure 2.12: Calculated phase and liquidus relations for the MnO-SiO_2-CaO system. As an example, the reduction of a slag of initial composition **X** along the basicity line to liquidus composition **Y** and further reduction to equilibrium point **Z** is indicated. (Calculated in FactSage 8.1 [87]).

At equilibrium, the distribution of Mn in alloy and in slag from reaction (1.8) can be described by the equilibrium constant given by equation (2.3). Note, reaction (1.8) is repeatedly shown for easy readability.

$$MnO(l) + C(s) = Mn(l) + CO(g) \qquad \Delta H^0_{298} = +258.7\ kJ/mol \tag{1.8}$$

$$K = \frac{a_{Mn} \cdot p_{CO}}{a_{MnO} \cdot a_C} = \frac{a_{Mn} \cdot p_{CO}}{X_{MnO} \cdot \gamma_{MnO} \cdot a_C} \tag{2.3}$$

where K is the equilibrium constant of reaction (1.8), aMn is the activity of Mn in the metal, a_{MnO} is the activity of MnO in the slag, p_{CO} is the partial pressure of CO in the gas phase, a_C is the activity of solid carbon or carbon dissolved in alloy, X_{MnO} is the mole fraction of MnO in slag and γ_{MnO} is the activity coefficient of MnO in the slag.

The top part of the cokebed zone is where the reduction occurs with coke particles and CO gas as previously discussed. The partial pressure of CO in equilibrium with solid carbon can be considered as $p_{Total} = p_{CO} = 1atm$, and as the metal composition is fixed at a fixed temperature, aMn is fixed. The metal composition at the end state is fixed as it is the tapped metal composition. The activity of carbon is close to 1 as there exists solid carbon. The equilibrium expression can then be simplified and the amount of MnO in slag can be determined by equation (2.4)

$$X_{MnO} = \frac{1}{K} \cdot \frac{a_{Mn}}{\gamma_{MnO}} \tag{2.4}$$

The MnO content in slag is mainly affected by the activity coefficient of MnO i.e., γ_{MnO} and the equilibrium constant K which is temperature dependent as shown in Figure 2.13. Therefore, a lower MnO content during reduction is achieved at higher temperatures and basicity, as will be discussed below.

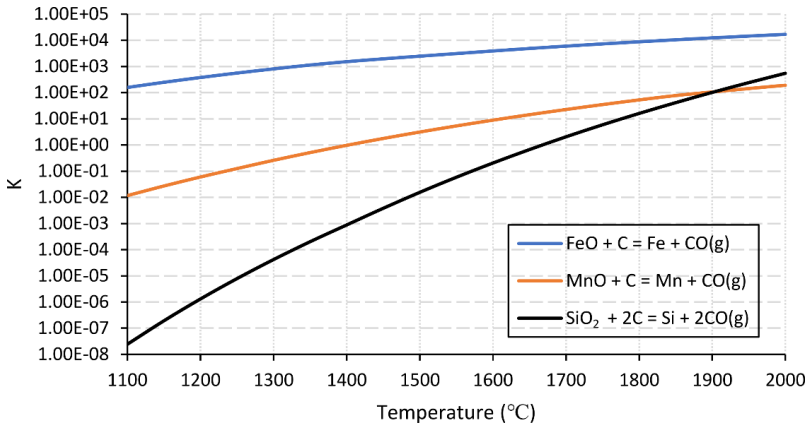

Figure 2.13: Equilibrium constant of MnO, FeO and SiO_2 reduction as a function of temperature. according to reactions (1) and (2) (calculated from HSC Chemistry v.10).

The chemistry of the slag is usually changed by varying input flux composition which alters the basicity of the slag. The main aim of slag composition adjustment through ore blending and mainly fluxing is to achieve an optimum condition of smelting temperature (liquidus), metallurgical quality and viscosity to operate an effective and efficient process with a high metal yield and high efficiency in tapping of products[2]. By definition basicity is simply the ratio between basic and acidic oxides and different formulas are used to express slag basicity in high carbon ferromanganese process[2], [58], [88], [89]. There are several definitions of slag basicity that can be used to describe the slag composition and the simplest expression is the CaO/SiO_2 ratio:

$$\text{Basicity} = CaO/SiO_2 \tag{2.5}$$

When the slag produced has a significant amount of MgO, it is expressed as:

$$\text{Basicity} = (CaO + MgO)/SiO_2 \tag{2.6}$$

If the smelting process produces slag containing a significant amount of Al_2O_3, it is expressed as:

$$\text{Basicity} = (CaO + MgO)/(SiO_2 + Al_2O_3) \tag{2.7}$$

The following extended basicity formula is used when all basic oxides such as BaO and K_2O are included:

$$\text{Basicity} = \frac{\sum \text{Basic oxides}}{(SiO_2+Al_2O_3)} = \frac{(100\text{-}SiO_2\text{-}Al_2O_3\text{-}MnO)}{(SiO_2+Al_2O_3)} \tag{2.8}$$

Basicity affects the activity coefficient of MnO, γMnO, in liquid slag. As presented in equation 1.8, when the activity coefficient of MnO in the liquid slag is changed with changing slag composition, the final MnO content in slag and the Mn content in liquid alloy can be changed. The higher activity of MnO in the slag results in a higher Mn yield. Several studies[3], [11], [88] have shown that choice of slag composition is paramount in HCFeMn production as an appropriate slag will result in high metallic yield and smooth furnace operation. Composition of slag determines slag/metal equilibrium relations including the MnO content of the final slag and slag viscosity [4], as such choice of fluxes is paramount in HCFeMn production.

The phase relations in the $MnO\text{-}SiO_2\text{-}Al_2O_3\text{-}CaO\text{-}MgO$ system and the activities of MnO in slag has been studied by several researchers[2], [11], [90]–[93]. Nam *et al.*,[11] simulated through thermodynamic calculations the effect of basicity on the activity of MnO in slag by varying amounts of CaO, MgO and Al_2O_3 contents. The results were plotted as shown in Figure 2.14.

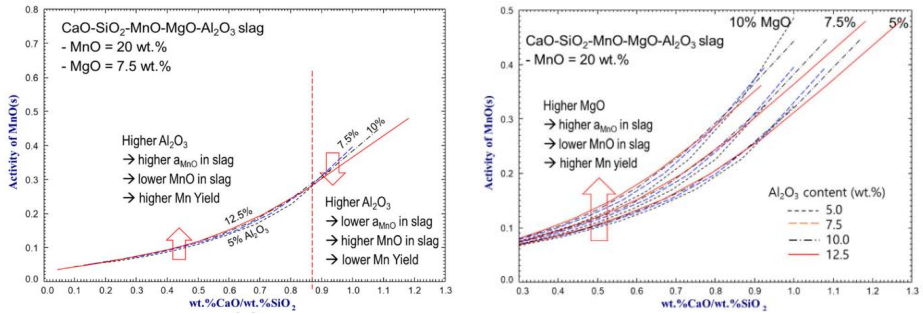

Figure 2.14: Activity of MnO(s) in liquid slag at 1400 °C depending on the slag basicity (wt.% CaO/wt.% SiO_2), MgO, and Al_2O_3 content. (a) Influence of Al_2O_3 content, and (b) influence of MgO content [11].

The activity of MnO is be seen to decrease significantly with decreasing the CaO/SiO_2 in the slag because γMnO decreases significantly with increasing SiO_2 content. Al_2O_3 shows the amphoteric nature of the MnO activity. In the low CaO/SiO_2 slag region (acidic slag), Al_2O_3 increases γ_{MnO}, while it decreases γ_{MnO} in high CaO/SiO_2 slag (basic slag). This is because Al_2O_3 behaves like a basic component in acidic slag, while it behaves like an acidic component in basic slag. As shown in Figure 2.14(b), γ_{MnO} increases noticeably with increasing MgO content which is a basic slag component. The influence of MgO on γ_{MnO} is much more significant than that of Al_2O_3. In addition, the amphoteric transition point (CaO/SiO_2 in slag) of Al_2O_3 is decreasing with increasing MgO content. Additional CaO, was reported to increase the reduction of MnO oxide in liquid slag to Mn metal i.e., Mn yield, up to a maximum point above which Ca_2SiO_2 solid phase is formed. Hence, choice of amount of CaO should be in such a way that it avoids formation of Ca_2SiO_2 solid phase as this is detrimental to sound tapping of the slag after SAF process. The activity coefficient of MnO will increase with basic oxides CaO and MgO, and decrease with acid oxides SiO_2 and Al_2O_3[94].

The content of MnO in slag is a function of basicity and temperature when two variables are fixed e.g., fixing Al_2O_3/SiO_2 and % MgO. Li *et al.*,[95] in their study on the reduction and dissolution behavior have shown the variation of % MnO in slag as a function of temperature and basicity for charge mixtures of Comilog and Nchwaning ores, as plotted in Figure 2.15. The trends are in agreement with other studies[16], [94] were increase in basicity and temperature results in low MnO content in slag. On the other hand, the rate of reduction in the two-phase area i.e., solid MnO + liquid slag, decreases with increasing basicity of the slag due to higher amount of

solid phase and hence the higher total viscosity. In the completely liquid area, it increases with increasing basicity, and thus also decreasing viscosity [16].

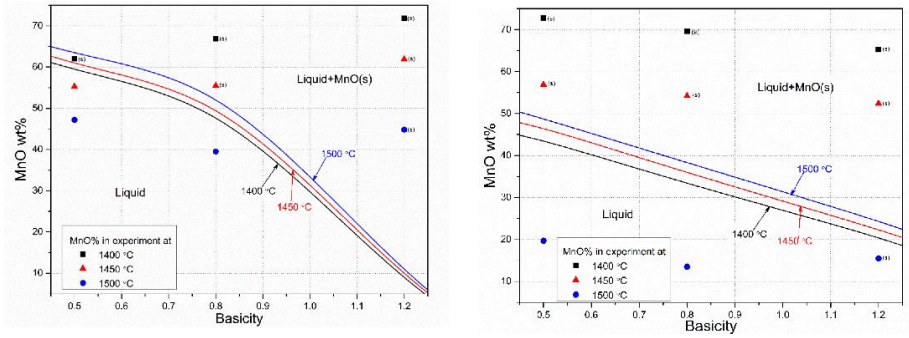

Figure 2.15: (a) Curves of %MnO of the slag at liquidus temperature, calculated from liquidus relations for the MnO–SiO_2–CaO system for representing Nchwaning slags. (b) Curves of %MnO of the slag at liquidus temperature, calculated from liquidus relations for MnO–SiO_2–CaO–Al_2O_3 (Al_2O_3/SiO_2=1.24) system representing Comilog slags. The dots are experimental points, and the (S) marks where spherical MnO phase is observed [95].

Woo *et al.*,[92] conducted a thermodynamic study of the MnO-SiO_2-Al_2O_3 slag system at 1823 K by equilibrating melts of different compositions with a Pt-Mn alloy and oxygen bearing gas phase. The activities and isoactivity lines of MnO in at 1823 K are shown in Figure 2.16.

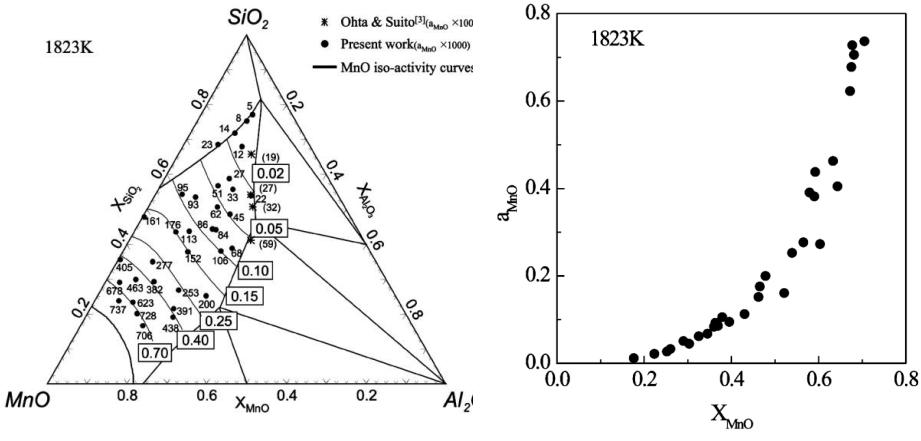

Figure 2.16: Activities and isoactivity lines of MnO in MnO-SiO_2-Al_2O_3 melts at 1823 K. (a) Influence of Al_2O_3/SiO_2 ratios on MnO activity. (b) Dependency of MnO activity on MnO concentration [92].

It can be seen from the MnO iso-activity lines, that the dependency of activity of MnO on the ratio of SiO_2 to Al_2O_3 is not large. However, the activities of MnO

increases rapidly with MnO concentration when the mole fraction exceeds about 0.5. The trends are visibly seen from Figure 2.16 (b) where the activity of MnO is plotted against MnO concentration. Note that the effect of basicity on activity and importance of its control will be categorically discussed in detail as it affects activity of MnO in slag, slag reduction rate and final composition of MnO in reduced slag.

2.3.2 Phase composition and reduction of complex slags

After prereduction, the MnO is reduced in the coke bed zone from liquid slag to Mn metal by means of solid carbon [2], [96]. Hence, the melting of the raw materials to form a primary slag and the subsequent reduction to ferromanganese alloy are closely related. Therefore, the melting behavior of ores to form liquid and phase compositions should be initially considered since the reduction of MnO occurs in liquid state. Figure 2.17 shows the MnO-SiO_2 binary phase diagram illustrating the formation of liquid slag in FeMn slag system as highlighted. According to the MnO-SiO_2 binary system, the melting of prereduced manganese ores in FeMn process will start above 1330 °C, neglecting the effects of other components in the ore. The primary slag formed will therefore consist of a liquid with a solid MnO phase and this will have an impact on the slag flow properties and activity of MnO as will be discussed later[2], [94].

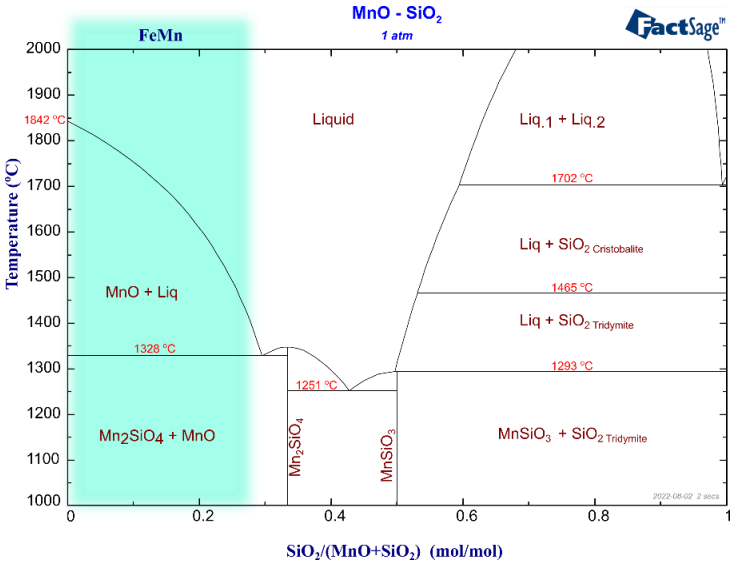

Figure 2.17: The MnO-SiO_2 binary phase diagram highlighting the FeMn slag system. (Calculated in FactSage v8.1[87]).

Olsen *et al.*,[2] showed that the typical content of MnO after prereduction is usually around 80 % and the sum of MnO, SiO_2 and Al_2O_3 is about 90% in acid ores such as Comilog, Groote Eyland and Amapa. Tangstad *et al.*,[94] showed that the MnO content for basic ores after prereduction is lower than acid ores and can be as low as 68 %.The pre-reduced oxide materials will sinter, soften and melt as the temperature increases in the cokebed zone. The melting behavior of various ores used in industrial operations have been studied by several authors[97]–[101]. The melting of the manganese ore has been in previous studies assessed in three different ways:

- Start melting, the temperature at which liquid was visible on the surface of the manganese ore
- Finish melting when the manganese ore appeared to be completely liquid
- Start reduction, when the first gas bubbles were visible on the surface of the manganese slag.

Gaal *et al.*,[98] investigated the melting phenomena in FeMn production focusing on the temperature that describes the flow characteristics of Nchwaning and Comilog ores. The description was centered on the temperature where the first liquid appears and the temperature where the ores behave as liquid. Separate experiments were conducted by heating prereduced manganese ore particles at 250 °C/min to 950 °C, then 30 °C/min to 1100 °C and finally at 5 °C/min until the test was stopped. Typical sample weight varied between 20 – 60 mg and was heated with continues purging of 0.5 Nl/min of Ar or CO gas at atmospheric pressure. The experiments were conducted whilst the shape of the particles was photographed every second, as can be seen in Figure 2.18 showing prereduced Comilog ore particle on a graphite substrate heated in Ar gas. Typical smelting ranges on graphite in a CO atmosphere were 1450-1490 °C for Comilog and 1430-1570 °C for Nchwaning. The main difference was considered to be low and attributed to the MnO content, as well as differences in ore mineralogy. The results were in close agreement with later findings from work by Ringdalen *et al.*,[101] where were melting behavior of Comilog, Nchwaning and CRVD ore as well as CRVD sinter was investigated under similar experimental investigations.

In general, the temperature of melting of manganese ores is lower than the melting of pure phases mainly because of the formation of other phases during prereduction as postulated in the work by Ringdalen *et al.*,[99], [101]. For example, the melting of pure MnO is 1842 °C [6] and the temperature for initial melting measured for several Mn sources using sessile drop show that the temperature where

the Mn sources start to melt, the softening temperature vary between the different Mn-sources from around 1250 °C to nearly 1600 °C [97], [98], [102], [103]. As presented in Figure 2.19, the initial melting temperature decreases with increasing amount of acidic oxides in the ore and subsequently increase the reduction rate[94].

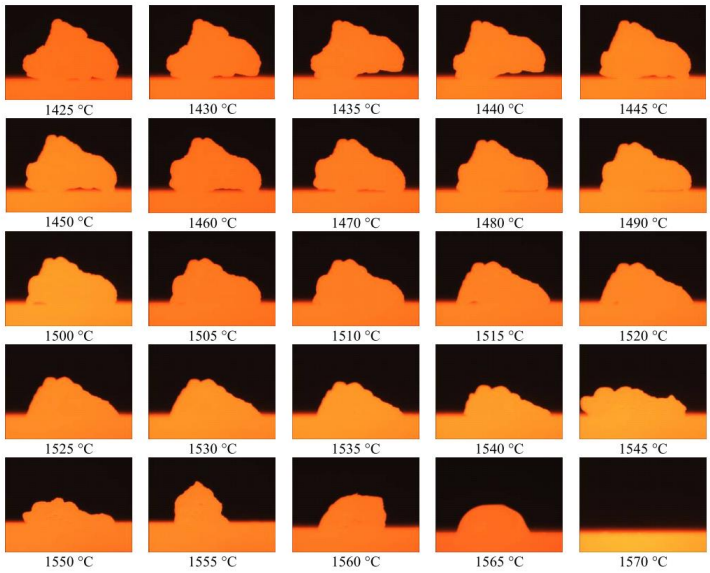

Figure 2.18: Melting behavior of ore being heated in argon on a carbon substrate[98]

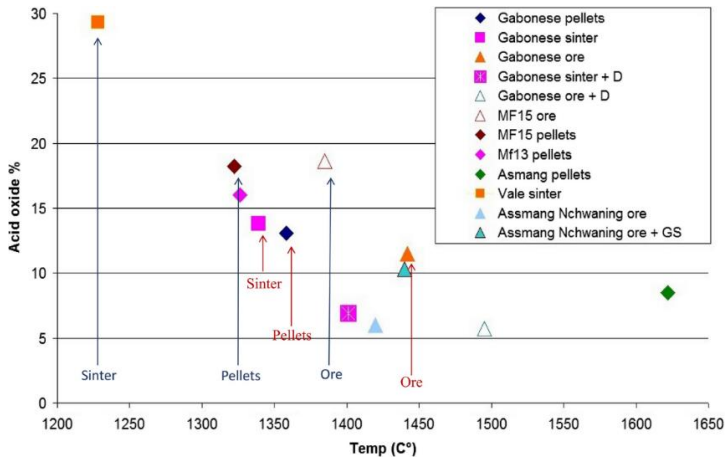

Figure 2.19: Variation of Initial melting for various Mn sources with % acid oxides. (Based on figure in Tangstad et al., (2021)[94] adapted from Brynjulfsen (2013)[103] and Ringdalen (2015)[102]).

Figure 2.20 shows the melting and flow behavior of Comilog heated in CO gas sitting on a graphite canyon with a gap diameter of 0.6mm from work by Gaal *et al.,* [97]. Comilog was observed to start to melt at 1425 °C and appeared completely molten at 1500 °C, after which the ore continued to react with graphite. As soon as the droplet was molten, small particles were seen to fall from the bottom of the suspended droplet of ore, which was most likely small metal prills reduced from the ore. These prills were very small, indicating that there was little attraction between the slag and metal. The experiment was stopped at 1600 °C, when only a small piece of molten ore remained suspended in the canyon. The results from this work indicated that most of the reduction occurs with flow of metal product as the slag droplet is suspended, which implies that the surface tension of the slag is sufficiently high to impede slag flow. With sufficient dissolution of solid monoxide phase the slag is expected to flow through the channel. This has also been reported from pilot scale experiments where it was found that most of the MnO reduction is found on top of the coke bed [16]. The MnO content in slag through microprobe analysis was found to be 41 % MnO[98].

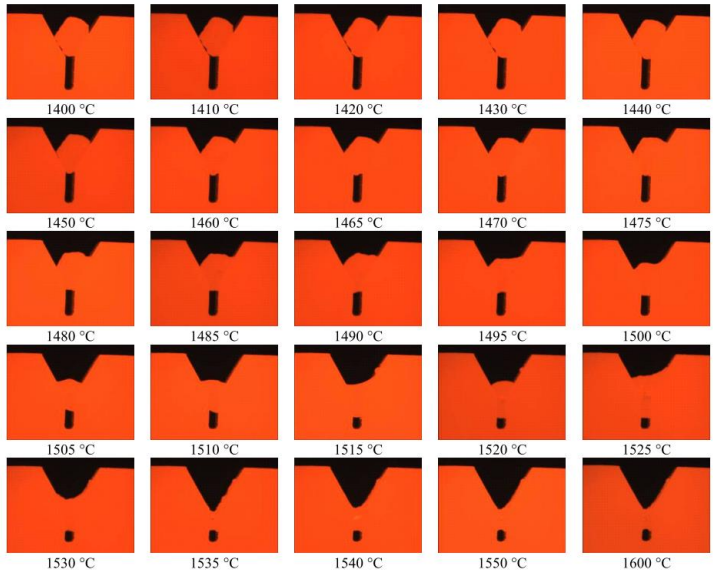

Figure 2.20: Melting and flow behavior of ore heated in CO sitting in a graphite canyon[98]

In view of the melting properties of Mn sources, the following two processes occur while the ore is being heated: firstly, a change in the chemical and phase compositions because of the changing temperature, and secondly a reduction of iron and manganese oxides from the ore. The prereduced manganese ore, upon heating to between 1100 °C and 1200 °C and higher, contains the solid monoxide phase,

which is predominantly manganese monoxide[104]. The subsequent reduction process includes the dissolution of solid MnO into the liquid slag and the dissolved MnO is then reduced to Mn metal thereby creating a potential for further dissolution of solid MnO. The morphological structure of primary slag formed in ferromanganese which consist of solid plus liquid slag and its subsequent reduction and dissolution of solid MnO phase has been reported by many researchers[16], [21], [93], [95], [105], [106].

Li *et al.,* [95] studied the reduction and dissolution behavior of manganese slag from Comilog and Nchwaning (Assmang) in the FeMn process. The extent of manganese ore reduction as a function temperature with variations in basicity were determined by using a thermo-gravimetric (TG) balance. Morphology of ores and its change during reduction was examined by scanning electron microscopy (SEM) and the dissolution behaviors of Nchwaning and Comilog slags were simulated in FactSage and verified by experiments. The liquidus relations for MnO–SiO_2–CaO system and MnO–SiO_2–CaO–Al_2O_3 (Al_2O_3/SiO_2 = 1.24) systems were calculated and applied to predict Nchwaning slag and Comilog slag dissolution behavior, respectively as shown in Figure 2.21. The ores start to reduce in a liquid + solid phase area and as the reduction proceeds with subsequent dissolution of MnO in slag until liquidus is reached. The liquidus content of MnO decreases with increasing basicity. For example, at 1500 °C, the reduction of Comilog charge mix with a basicity of 0.8 will take place from about 80 wt.% MnO in presence of two stable phases, manganosite + liquid slag down to the liquid composition at about 40 wt.% MnO. Further reduction takes place through the galaxite area down to the final composition. In general, FeMn charges will be reduced from a primary slag to a slag with MnO content in tapped slag around 15 to 45 wt.% MnO [2], [94], [105], [107], [108]. In addition, the tapped slag is close to the liquidus MnO content, which is depended on slag basicity, for instance, the composition can be 30 to 40 wt.% MnO for a basicity of 0.7 and about 20 wt.% MnO at basicities of 1.1[94]. Slag basicity influences the activity of MnO as will be discussed later.

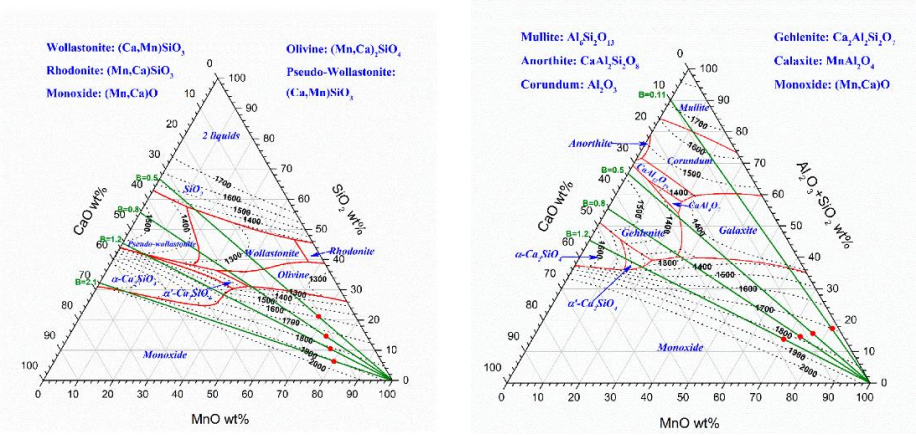

(a) (b)

Figure 2.21: (a) Calculated liquidus relations for the MnO–SiO_2–CaO system to predict reduction paths in Nchwaning slag. (b) Calculated liquidus relations for MnO–SiO_2–CaO–Al_2O_3 (Al_2O_3/SiO_2 = 1.24) system to predict reduction paths in Comilog slag. Green lines represent the reduction paths for Nchwaning and Comilog charges with different basicities, red dots represent the starting points after pre-reduction [95].

2.3.3 Reduction mechanism and kinetic considerations

The cokebed zone is the hottest part of the submerged arc furnace in HCFeMn production. In this zone, the main metal formation takes place i.e., reduction of MnO to Mn through the interaction of high MnO containing silicate slag (MnO-CaO-SiO_2-MgO-Al_2O_3-FeO) according to reaction (1.8). As discussed above, the primary slag formed contain a liquid phase and solid monoxide phase on melting. Thus, reduction will commence within the two-phase region. The solid monoxide is predominantly solid MnO and can form a solid solution of MnO-FeO-MgO with reported MgO content of less than 20 % depending on the mineralogy of the charge mixtures[16].

The mechanism of reduction in the two phase is well known and has been broadly described[71], [109]–[112]. Earlier, Eric and Burucu[112] studied the mechanism and kinetics of the carbothermic reduction of Mamatwan. In this work, metallization was observed to start with nucleation of iron, which subsequently was carburized around MnO grains inside the particle. The metallic iron that was formed was an intermediate product and transformed to iron carbide (Fe_3C) by carburization in the presence of excess carbon as the reduction proceeded. The metallic nuclei grew by spreading over rounded MnO-rich oxide grains. The metallic nuclei at the earlier stages of reduction contained more iron than manganese. It is believed that the reduction by carbon dissolved in iron is important in initiating the reduction of MnO in the second stage. The reduction rate of MnO is rapid when MnO is present in solid

state, due to the high and constant activity of MnO. In this stage, because the slag consists of a mixture of solid MnO plus liquid slag and contain molten metal, the relative position of the phases to each other and reduction interface location are dynamic[105], [113], [114]. Further reduction of MnO through the homogenous liquid slag phase will take place at a rapidly decreasing rate due to decreasing activity of MnO[16], [21], [95]. Therefore, the reduction rate is divided into two steps; a rapid reduction step in the liquid slag with solid MnO followed by a slower reduction from a liquid slag.

The kinetics of MnO in FeMn slag has been extensively studied[16], [72], [95], [109], [110], [115] and the reduction rate generally described using equation (2.9), assuming that the reaction is a first-order reaction controlled by chemical reaction.

$$R_{MnO} = k \cdot A \cdot \left(a_{MnO} - a_{MnO,eq}\right) = k_0 \cdot \exp\left(-\frac{E}{RT}\right) \cdot A \cdot \left(a_{MnO} - \frac{a_{Mn} \cdot p_{CO}}{K_T}\right) \quad (2.9)$$

where R_{MnO} is the reduction rate (g/min), k is the rate constant (g/min·cm^2), k_0 is the frequency factor, A is the contact area (cm^2), E is the activation energy (kJ/mol), R is the gas constant, T is the temperature (K), a_{MnO} is the activity of MnO in the slag phase, $a_{MnO,eq}$ is the equilibrium activity of MnO in the slag phase, a_{Mn} is the activity of Mn in the metal phase, p_{CO} is the partial pressure of CO (g) and K_T is the equilibrium constant at temperature T. Equation (2.9) shows that the kinetics of reduction of MnO is highly influenced by slag properties affecting the rate constant, the interfacial area between carbon reductant and slag and the driving force, which is the difference between the total MnO content and the MnO content at equilibrium i.e. ($a_{MnO} - a_{MnO,eq}$). Therefore, the activity which influences the driving force will hence be high in the two-phase area during reduction, and when reaching the one phase liquid area, the reduction rate will decrease due to lower MnO activity[94], [110]. It is widely accepted that this metal formation reaction (Equation (1.8)) in the coke bed is controlled by the interfacial chemical reaction and the mass-transfer resistance in the slag phase may be neglected[16], [111].

The effects of temperature on the rate of reduction of MnO and final content of MnO in slag has been described by Tangstad *et al.*,[94] as shown in Figure 2.22. The reduction rate increases with increase in temperature which results in higher weight loss and lower MnO content in the final slag. The dissolution of solid monoxide phase to a point where only dissolved MnO remains in the liquid slag phase has been previously reported by Tangstad and Olsen [21] to slow down the kinetics of the

reduction reaction. This is mainly because of the drop in the chemical potential difference that drives the rate of reduction which is a consequence of the drop in the activity of MnO.

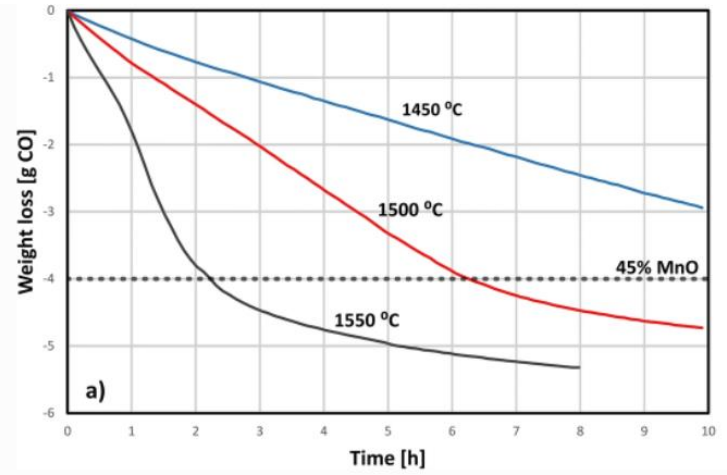

Figure 2.22: Rate of reduction of MnO presented as weight loss curves for slag starting from 72 to 73 pct MnO with Al_2O_3/SiO_2 ratio of 0.25 and basicity of 0.67[94].

In a study on thermodynamic and energy balance analysis in production of ferromanganese in SAF, Nam *et al.*,[11] calculated the slag compositions at 1400 - 1500 °C under carbon saturation conditions from various plant input data. The results are plotted as shown in Figure 2.23 and it was found that the higher the temperature, the lower the MnO content in the slag. In addition, furnace operational temperature was found to influence Mn yield. Mn yield which is defined as the ratio of Mn reduced to metal to total amount of Mn in ores was calculated to increase significantly with temperature increase at about 4% for every 50K.

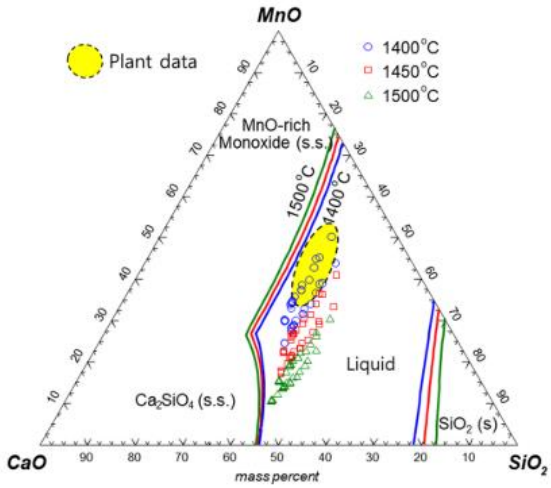

Figure 2.23: Slag composition in HCFeMn production. Calculated slag composition are based on the thermodynamic equilibrium calculations with carbon saturation at 1400 -1500 ℃[11]

Jafar *et al.,* [109] studied the kinetics and mechanism of simultaneous carbothermic reduction of FeO and MnO from HCFeMn slag. A synthetic slag of 38.7 wt.% MnO was studied using a sessile drop wettability technique in Ar at 1600 ℃. The authors observed that the carbothermic reduction of FeO and MnO takes place simultaneously and the initial rate of the FeO reduction was fast and then followed by a slow reduction rate. The MnO reduction is slow in the rapid FeO reduction stage and then the speed increases significantly. A number of studies [96], [106], [112], [113], [116], [117] presented clear evidence that the initial iron metal prills formed during formation and reduction of primary slag are enriched in Mn and C as MnO reduction proceeds. As such, if there is FeO in the slag, this is reduced initially and then a Fe-Mn-C_{sat} alloy is produced through further MnO reduction[109].

Yasreboff *et al.*, [72], [118] investigated reduction of Groote Eylandt (Australia) manganese ore as well as siliceous manganese fines, FeMn slag and pure MnO by graphite (30 % excess) in graphite crucibles in various gas atmospheres, by means of TGA coupled with IR analysis of CO/CO_2 ratio in the off gas. Groote Eylandt ore contains manganese (>50 %) predominantly in the Mn4+ oxidation degree, some silica, alumina, barium oxide, and iron oxides. Prior to reduction, the ore was sized between 50 and 150 µm and calcined at 1000 ℃ in argon, in samples of around 0.5 g. The experimental temperature range was 1000 to 1450 ℃. The reduction of Groote Eylandt ore to MnO and metallic iron was reported to be fast (within 85 min) at 1000 ℃ and the rate of the reduction process was controlled by the rate of the

Boudouard reaction (carbothermic reduction in inert atmosphere), since the reduction proceeds via CO gas. While at the higher temperatures carbon monoxide introduced to the system was reported to hinder carbothermic reduction of pure MnO as well as Mn-ore, compared to the carbothermic reduction in protective atmosphere of argon or helium. This effect was reported to be less prominent with increasing temperature. Silica was reported to hinder the rate of manganese oxide reduction. The authors suggested that in the experimental conditions, the rate of the carbothermic reduction of MnO (as well as Mn-ore) was mix-controlled, i.e., by the interfacial chemical reaction and CO mass transfer from the reaction interface to the gas phase.

2.4 Excavation of pilot and industrial furnaces

Pilot scale experiments have been utilized to test smelting in FeMn production simulating the industrial process. Several studies[16], [58], [119]–[123] have been conducted at pilot scale and, in many cases, it is possible to make direct and informed comparison of various parameters with operation of industrial furnaces. Eissa *et al,*. [58] designed and carried out pilot plant experiments out to determine the optimum conditions for smelting HCFeMn through investigating some parameters affecting the smelting process including Mn/Fe ratio of the blend, coke ratio, slag basicity and dolomite/limestone ratio of the flux. The results of pilot plant experimental heats to obtain a standard HCFeMn alloy containing minimum 75% Mn showed that using Mn blend with high Mn/Fe ratio of greater than 6.2 decreased the consumption of charging materials: Mn ores, coke, and fluxing materials (limestone and dolomite). Other pilot studies which investigated several parameters related to manganese alloy production include; Eidem [123], [124] who investigated the electrical properties of the cokebed, Tangstad[16] studied the effect of electrode position on furnace operation, Monsen *et al.,* [125] investigated use of charcoal as a reducing agent, Ringdalen and Tangstad [126] studied the effect of different raw materials in SiMn production and Brynjulfsen [120] studied the utilization of sinter and ore blends in ferromanganese production. In order to investigating the complex patterns of chemical reactions and physical phenomena, post experimental studies have been conducted through excavations of pilot furnaces.

Tangstad *et al,*.[119] studied the production of ferroalloys using heat-treated Mn nodules. In this study, a top and bottom electrode furnace operated at about 150 kW was shut down at the end of the experiments and allowed to cool. The excavation

was performed by casting the furnace with epoxy and cutting a furnace cross- section. Figure 2.24 shows the furnace interior from the excavation.

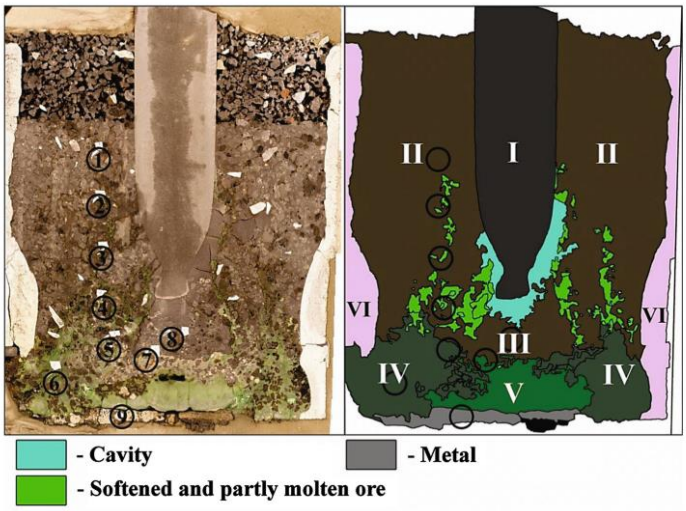

Figure 2.24: Left side: image of the furnace cross section. Right side: schematic illustration of the plate with corresponding zones. The cavity, metal, and softened ore particles are marked with color. The other zones are marked as follows: I-electrode, II-charge materials, III-cokebed zone, IV-coke-slag mixture, V-slag layer, VI-lining material. Numbers 1 to 9 depicts position of the core drills [119].

The physical changes of the charge mixture can be clearly seen from the excavation in Figure 2.24. As typically found in many such excavations, the furnace can be divided in two main zones namely the prereduction zone and cokebed zone. The prereduction zone is where the charge is solid (Zone II) and cokebed zone or the high temperature zone (zone III, IV and V) is mainly characterized by slag-coke mixture and metal at the bottom of the electrode. This type of excavation can also give information such as the position of the electrode and size of the cokebed. This is a typical experiment with a too small cokebed observed and areas with completely reduced slag i.e., zone V can be seen as well as an electrode with uneven shape. The uneven shape of the electrode mainly emanates from electrical currents which were forced through the sides of the lower part of the electrode. Samples were core drilled at different positions as shown in Figure 2.24 and the slag composition analyzed in EPMA (Electron Probe Mirco-analyzer) mainly to evaluate the degree of reduction versus position. In this pilot excavation, the furnace interior after the experiment with Mn nodules was observed to be similar to the furnace interior after HCFeMn experiments with other Mn source as, e.g., Comilog ore. The Mn nodules were reported to melt into a liquid phase and a solid MnO phase on top of the cokebed and the

reduction will occur on top of the cokebed until all the solid MnO is reduced. The tapped slag was at the composition close to the liquidus composition, as observed for other Mn-raw materials, and thus, also follow the well-known rule of lower MnO content in the slag with higher basicity.

Industrially, a number of excavations were conducted for different ferroalloys furnaces focusing on studying process patterns and prevailing reaction zones[127]–[131]. For FeMn a detailed excavation and analysis of the furnace interior of a 75MVA furnace was done by Barcza *et al,*. [130] . Figure 2.25 shows the sampling localities and the detailed description of the various zones of the furnace delineated by discrete boundaries is as shown in Figure 2.26.

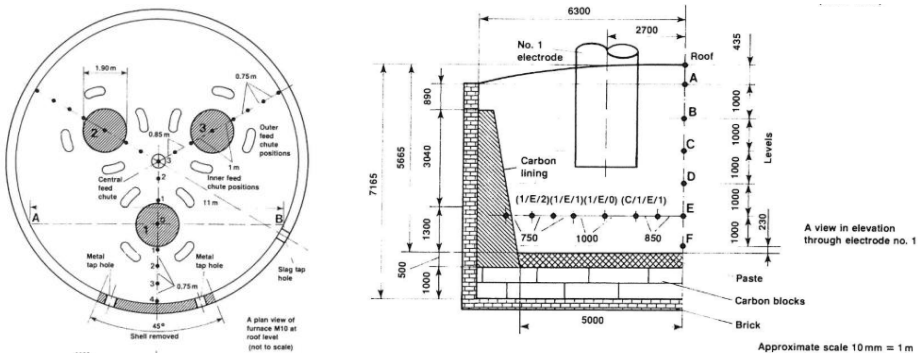

(a) (b)

Figure 2.25: Selected sampling localities. (a) Furnace plan view at roof level and (b) a view in elevation through electrode 1[130]

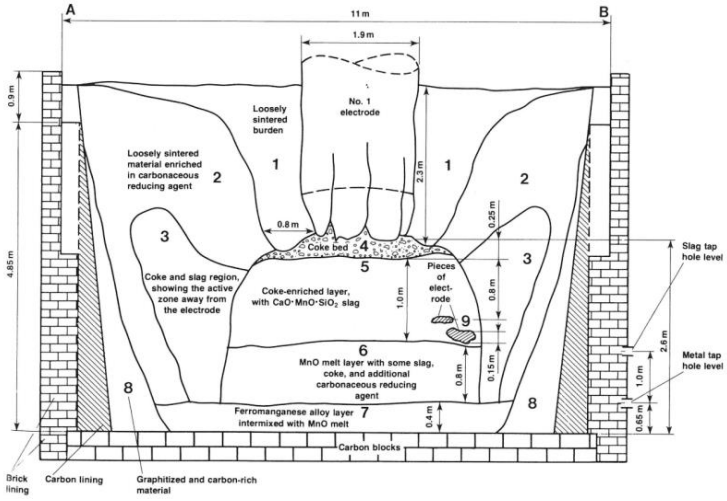

Figure 2.26: Sketch of one of the electrodes and the surrounding zone of a 75MVA furnace excavated by Barcza *et al,*. [130].

The different zones as shown in Figure 2.26 were based on both physical characteristics as well as the analyses of the materials sampled in the different regions. Both the prereduction zone (zones 1, 2 and 3) and the coke bed zone (zones 4, 5 and 6) were identified and are shown with their inherent variations subject to prevailing conditions in the different regions. In the prereduction zone, regions adjacent the electrode i.e., zone 1, were observed to be characterized by rapid material descent and therefore burden of raw materials in this region were loosely sintered. The active zones of the furnace in which most of the carbothermic reduction occurs were limited to the regions surrounding the electrodes. Zone 5 consists of slag and coke, while zone 6 consists of some slag and reducing agents and a layer of unreacted MnO, caused by the reduced furnace load. The MnO melt in zone 6 was reported to be due to poor operating conditions. Zone 7 consists mostly of FeMn alloy, mixed with some MnO melt, slag and flakes of graphite. The authors reported that the furnace was erratic prior to it being switched off and the slow cooling prior to excavation might have enhanced some phase separation[130]. Therefore, the interior of the furnace could not be expected to represent the conditions under normal operating conditions. Nevertheless, a stable operation with fewer disturbances is envisaged to reflect to a greater degree the process patterns during furnace operations. Most recently, Tangstad *et al.*,[132] carried work on the excavation of a HC FeMn furnace and an MnO layer was also found below the tapping hole level surrounding the metal salamander as illustrated in Figure 2.27.

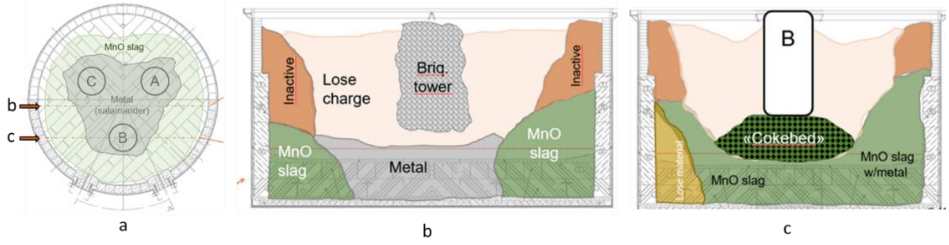

Figure 2.27: Excavation results from a FeMn furnace. (a) overview over metal salamander and MnO-slag zone indicating plane b and c, (b) View of plane through the centre, (c) View of plane through the B electrode [132].

Chapter 3

3 Laboratory scale experiments

3.1 Introduction

The main aims of the laboratory scale experiments presented in this chapter were to investigate the prereduction behavior of Mn-ores and to evaluate the effect of varying degree of prereduction on the high temperature reaction MnO + C = Mn + CO. Two research themes centered around the two zones of the industrial furnace i.e., the prereduction zone (up to 1200 °C) and the cokebed zone (1200 – 1550 °C) were investigated. The SAF was simulated in the medium scale induction furnace and small-scale controlled experiments for both prereduction zone and cokebed zone were performed in thermogravimetric furnaces. Figure 3.1 shows an overview of the furnaces, experiments conducted, analyses techniques and software.

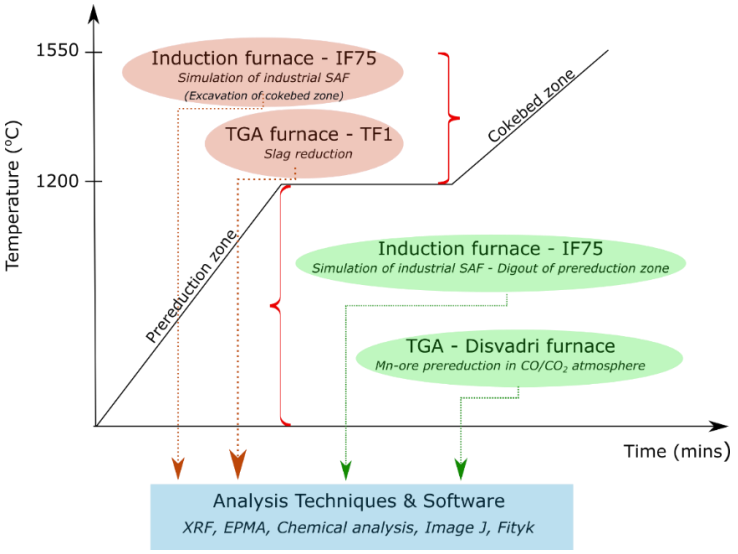

Figure 3.1: Overview of furnaces, experiments, and analysis methods in relation to the simulated furnace zones.

As can be seen, three types of furnaces commonly known as IF75, TF1 and Disvadri in the Department of Material Science at NTNU, were used in laboratory scale experiments. Firstly, an open induction furnace (IF75) was used to simulate the industrial furnace. Post experimental investigations were focused on the prereduction and cokebed zones of the induction furnace experiments. Secondly, a thermogravimetric (TGA) furnace known as Disvadri was utilized to study the prereduction behavior of ores in CO/CO_2 gas atmosphere. Lastly, a TGA furnace known as TF1 was used to study the effect of varying degree of prereduction on the metal producing reaction. This chapter includes details of the experimental work in these furnaces. As a part of this work an MSc student[9] was engaged and conducted experiments in the Induction furnace simulating the SAF and focused on the prereduction zone. In addition, prereduction of the ores in a controlled CO/CO_2 atmosphere was investigated in the Disvadri furnace. The student was supervised by the author and the more interesting findings are reported and discussed.

3.2 Materials and methods

3.2.1 Raw materials

The manganese ores investigated were Comilog, Nchwaning and UMK (United Manganese of Kalahari) ores. The reductant used was Polish coke. Comilog exhibit high level of porosity and is mainly composed of pyrolusite (β-MnO_2), nsutite ($(Mn^{4+})_{(1-x)}(Mn^{2+})O_{(2-2x)}(OH)_{2x}$ (x=0.06–0.07)) and cryptomelane ($K(Mn^{4+}_7,Mn^{3+})O_{16}$) minerals. UMK and Nchwaning contains both braunite-I ($(Mn^{2+},Mn^{3+})_6(SiO_4)O_8$) and braunite-II ($Ca(Mn^{3+},Fe^{3+})_6(SiO_4)O_8$) minerals, Nchwaning contains more bixbyite ($(Mn^{3+},Fe^{3+})_2O_3$) and hematite (Fe_2O_3) and less carbonate minerals compared to UMK ore [41]. The raw materials were chemically analyzed by SINTEF Norlab[133]. The chemical composition of the industrial raw materials is shown in Table 3.1.

Table 3.1: Chemical composition of raw materials (wt. pct)

	MnO_2	Mn_{tot}	Fe_{tot}	SiO_2	Al_2O_3	K_2O	CaO	MgO	CO_2	Fix C	LOI	O/Mn ratio
Comilog	79.6	51.2	2.9	3.3	5.8	0.7	0.4	0.1	-	-	12.6	1.93
Nchwaning	37.9	47.5	10.4	4.2	0.38	0.10	7.4	1.4	4.45	-	4.39	1.50
UMK	26.5	38.2	4.67	6.54	0.74	0.08	13.3	3.17	15.9	-	16.7	1.45
Coke	-	-	-	5.05	3.31	0.27	0.34	0.21	-	88.4	-	-

The different ore sizes of the different raw materials for the different type of experiments were prepared by crushing the ore in a steel mortar and pestle and sieving through sieve sizes between 1 to 16 mm. The different raw material sizes were selected for the different laboratory experiments as shown in Table 3.2. Experiments conducted with both ore and coke had a same size range selected.

Table 3.2: Raw material particle size range with type of experiment

Particle size [mm]	Experiments	Raw materials
9.15 - 16	Induction furnace IF75	Ore + coke
10 – 12.5	TGA-Disvadri	Ore only
3.15 – 4	TGA-TF1	Ore + coke mix

3.2.2 Induction furnace experiments

3.2.2.1 Experimental set up

A 75-kVA open induction furnace was used to investigate the prereduction behavior as well as the smelting and reduction of Comilog, Nchwaning and UMK ores in a set-up which simulates the industrial ferromanganese furnace. Experiments focused on investigating the prereduction behavior of ores were conducted by Reiersen[9], whereas those focused on the smelting and reduction of ores were conducted by the author. The author designed the study and supervised the MSc student (Reiersen[9]) with main contributions on experimental design, data analysis, interpretation and reviewing and editing MSc thesis.

The induction furnace has an induction coil of a total height of 310 mm from the bottom and the interior of the furnace chamber is refractory lined as seen in Figure 3.2. A high frequency current approximately 3 000 kHz is used. During induction heating, a temperature gradient develops with the highest temperature at the bottom of the furnace with decreasing temperature towards the furnace top. This simulates the temperature profile of an industrial ferromanganese furnace.

Graphite crucibles of grade EG-92 with a bulk density of 1.74 g/cm^3, electrical resistivity at 7 μΩm and 1.6 coefficient of thermal expansion, were used to contain the raw materials and acts as a heating element in the induction furnace. The dimensions of the graphite crucibles were 150 mm outer diameter, 115mm inner diameter, 400 mm outer height and approximately 380 mm inner depth. The raw

materials in each experiment were stratified as layers into the graphite crucible and two setups were used. The first setup consisted of a 100 mm coke layer in the bottom of the crucible working as the coke bed in industrial furnace, a 200 mm ore layer placed on top of the coke bed and lastly, a 50 mm coke layer on the top of the ore working as insulation and inhibits charge re-oxidation. In the second setup, the 200mm ore layer was replaced by a mixture of 90 wt.% ore + 10 wt.% coke reductant. Figure 3.2 shows a sketch of the induction furnace and graphite crucible containing the raw materials in the first setup. Table 3.3 shows the quantities and porosity values of ores used to fill the 200 mm height in the crucible. It can be seen as presented in Table 3.3, that the density is highest for Nchwaning followed by UMK and lowest for Comilog. As such, the weight of ore to occupy the 200 mm height in the setup is highest for Nchwaning, followed by UMK and lastly Comilog. The density of Polish coke used was 0.597 g/cm^3 and this would translate to 499 g and 249 g of coke occupying the 100 mm and 50 mm height in crucible, respectively. The weights of the charge materials were measured with Sartorius CP34000 (Germany) scale with a sensitivity at $\pm$0.05 g. The IF75 induction furnace, together with auxiliary equipment as well as the crucible used in this work, is shown in Figure 3.3.

Table 3.3: Quantities of ores used to fill 200mm height in crucible

Code	Ore type	Porosity (%)	Density of ore (g/cm^3)	Quantity of ore used to fill 200mm height in crucible (g)
Com	Comilog	3.5 – 13.2	1.97	3 290
Nch	Nchwaning	0 – 1.0	2.44	4 070
UMK	UMK	0 -2.8	2.17	3 623

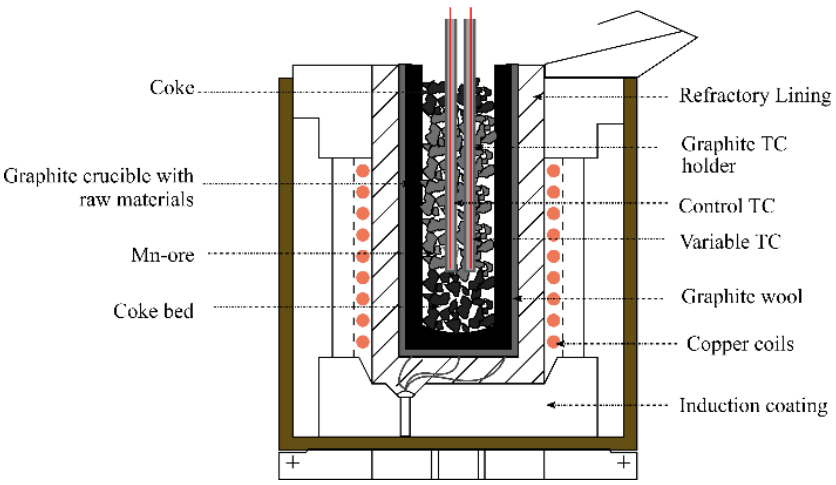

Figure 3.2: Sketch of induction furnace and graphite crucible containing raw materials

Figure 3.3: A photograph of the 75kW induction furnace and the crucible used in this work

3.2.2.2 Thermal conditions

The furnace crucible was heated gradually at 25 °C per minute up from 25 °C to 1200 °C on top of the coke bed. Temperature was held constant at 1200 °C for 30 minutes to ensure complete ore prereduction before the last heating step. Final target temperatures were 1200 °C, 1300 °C, 1400 °C and 1500 °C on top of the coke bed. Heating to target temperatures was done at 20 °C per minute and final target temperatures were held for 60 minutes on top of the coke bed. Experiments were conducted at different coke bed temperatures to investigate the temperature dependence on melting and reduction.

During each experiment, temperature in the crucible was measured using two type C tungsten/rhenium thermocouples encapsulated by alumina and graphite insulation tubes. Type C thermocouples are designed for extreme high temperatures up to 2315 °C and are encapsulated by alumina protective sheath to prevent failure from oxidation. As shown in Figure 3.2, the control thermocouple was located at the top of the coke bed and gives the reference temperature measurement. Likewise, the variable thermocouple, initially positioned on top of the coke bed, was used to measure temperatures at 20 mm interval distances away from the coke bed up to the top of the charge thus establishing the temperature gradient of the system. Stable temperatures at each point were established by holding the thermocouple fixed at that position for 3 minutes. The stable temperature at each 20 mm interval distance was measured in 2 runs i.e., away from the coke bed and towards the coke bed whilst maintaining a constant target coke bed temperature for 60 minutes. Figure 3.4 shows the temperature profile of the experiments during heating, isothermal periods and temperature gradient measurement periods which can be seen as V-shaped staircase steps. The typical temperature gradients shown in Figure 3.5 were measured whilst maintaining constant coke bed temperatures at 1200 °C, 1400 °C and 1500 °C. The temperature gradient is approximately in the range 27 °C to 35 °C per cm vertically across the charge material and the variations at constant setpoint are approximately ±20 °C in the center of the crucible as seen in Figure 3.5.

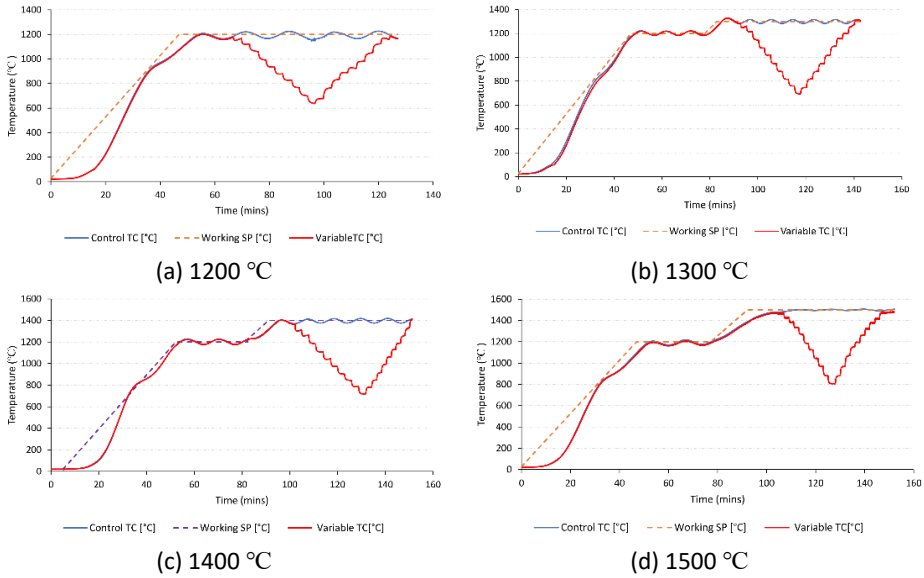

Figure 3.4: Temperature profiles in induction furnace (IF75) experiments with final temperatures on top of the cokebed at 1200 °C, 1300 °C, 1400 °C and 1500 °C.

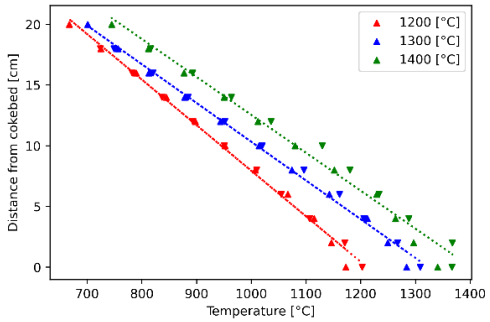

Figure 3.5: Vertical temperature gradients inside the crucible with top of cokebed as reference point.

As can be seen from Figure 3.5, the highest temperature is measured on top of the cokebed and the temperature at 20 cm height from the cokebed is within 700 °C to 800 °C. This creates a temperature gradient similar to the vertical temperature gradients in industrial operation and replicates the stages Mn ores go through in an industrial furnace. As such, as temperature rises the Mn-ore is reduced and a primary slag is formed in the high temperature zone. The slag is reduced to produce an alloy, which together with the formed slag, drain into the cokebed. This will allow the remaining solid material to subside along with thermocouples and as such at the end of the experiment the level of charge material will have shifted from the original

positions. This was taken into consideration when excavating the crucibles as will be discussed later.

3.2.2.3 Excavation of the crucible

At the end of each experiment the furnace was shut down and the crucible was cooled for 24 hours. After cooling the crucible, samples were excavated differently for the prereduction zone- and the cokebed zone- experiments. Reiersen[9], a masters student working in the project conducted experiments in the induction furnace and excavated the prereduction zone. In the prereduction zone, samples were excavated by digging out samples manually from the same levels where the temperatures were measured, while the material in-between the temperature measurement points were discarded. A level then corresponds to the particles excavated at a given height inside the crucible. Approximately 90 grams of sample materials were taken from each layer. The final layer excavated through digging out the prereduction zone was just above where sintering had occurred since the ores were glued together and this was considered to be the end of the prereduction zone. The collected samples were taken for chemical analysis and porosity measurements. Figure 3.6 shows the crucible containing raw materials before and after digging out samples.

(a) (b)

Figure 3.6: Photographs of (a) crucible containing materials prior to 'digout' and (b) crucible interior after 'digout' of prereduction showing the sintered materials of the cokebed zone.

Excavations targeted for the cokebed zone were done by filling the crucible with epoxy and cutting the crucible vertically in the middle. Figure 3.7 show typical excavations showing the interior of the crucibles and illustrations showing the physical characteristics of the ores in relation to the position in the crucible which corresponds

to the temperature gradients. It can be seen that the ores have distinct colour differences. These colour differences indicates the variation in prereduction extent with depth. The ore particles are seen to be green for fully prereduced ore particles. Melted and reduced ore samples were core-drilled out from selected areas close to the coke bed and further studied using Electron Probe Micro Analyser (EPMA) coupled with Wavelength Dispersive Spectrometry (WDS).

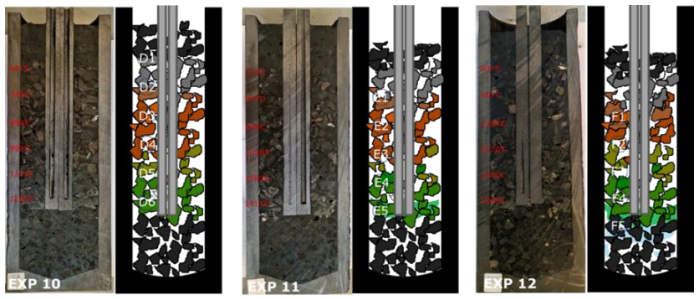

(a) (b) (c)

Figure 3.7: Typical pictures of the crucible interiors, and schematic illustration of sampling positions for the excavations from Nchwaning experiments with cokebed temperatures (a) 1220 °C, (b) 1413 °C and (c) 1505 °C.

3.2.3 TGA-Disvadri furnace experiments

The prereduction of the UMK, Nchwaning and Comilog ores in CO/CO_2 atmosphere was investigated quantitatively by the thermogravimetric analysis (TGA) technique. Total weight loss of the ore during prereduction was measured as a function of heating rate. The use of a TGA was meant to simulate the pre-reduction zone in an industrial ferromanganese furnace, with a constant supply of reducing gas CO/CO_2. Ore particles in the size range 10 – 12.5 mm were subject to different heating rates and a peak temperature of 1000 °C in a 70/30 CO/CO_2 atmosphere. In the industrial furnace, most of the heat is developed around the electrode thereby giving a higher heating rate for particles close to the electrode, and lower heating rate for particles close to the furnace lining. To study the effect of heating rate in the furnace it was chosen to use three different heating rates chosen as, 3 °C/min, simulating the condition closer to the furnace lining; 6 °C/min, in the middle between electrode and furnace lining; and 9 °C/min, close to the electrode.

3.2.3.1 Experimental setup

An Entech VTF 80/15 vertical resistance tube furnace, called the Disvadri furnace, was used for the solid-gas reactions study. Ores occupying 80 mm height of the crucible were placed in a gas-tight stainless-steel double-wall crucible which is 450 mm high and has an inner diameter of 48 mm. The crucible was suspended from a scale (Mettler Toledo PR2003DR, Switzerland,10 mg), with flexible gas inlet and outlet hoses connected at the top. The crucible was freely suspended, while the position of the furnace was adjustable vertically along a rail. The crucible was inside the furnace hot zone during the heating, while at the cooling stage the furnace was moved down. Furnace heating was regulated by an Eurotherm PID controller measured with a calibrated S-type thermocouple (Furnace Temperature), while charge temperature was measured with a K-type thermocouple (Crucible Temperature) sheathed in an alumina tube positioned in the center of the charge. Figure 3.8 shows the schematics of the experimental setup. The gases used in the experiments had a purity for CO, CO_2, and Ar, of 99.97, 99.9992, and 99.999 vol%, respectively. The gas flow in all experiments was regulated at 4 L/min 70/30 CO/CO_2 by mass flow controllers (Bronkhorst High-Tech El-flow, Netherlands). As illustrated in Figure 3.8, the furnace is designed in such a way that inlet gases are heated as they descend through the double-walled sides of the crucible. Upon reaching the bottom of the furnace, the gas flows upwards through the sample material and finally, the off-gas flow out of the top of the crucible through the gas outlet tubes.

The furnace was programmed to heat the sample from 25 °C until 1000 °C at the given heating rates and the charge was then cooled under Ar flow to avoid reoxidation of the prereduced samples. In addition, the weight of the solid charge was measured with an external scale Ohaus Pioneer PA4202 (US) before and after the prereduction to confirm the net weight loss acquired from the TGA data. The sensitivity of the external scale was ±0.01 g. After the experiments, prereduced ore samples were taken for chemical analysis. The decomposition of carbonates was investigated using the same experimental procedure at heating rate of 9 °C/min with experiments ending at 700 °C, 800 °C and 900 °C for UMK ore and 900 °C for Nchwaning ore.

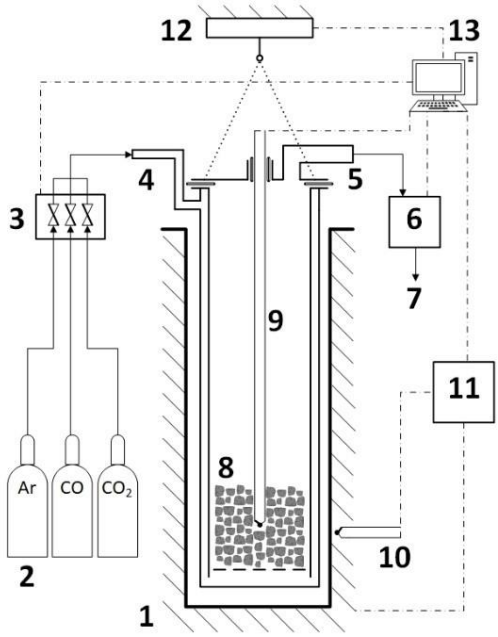

Figure 3.8: Schematics of the experimental setup: 1 – furnace, 2 – gas flasks, 3 – gas mass flow controllers, 4 – gas inlet, 5 – gas outlet, 6 – gas analyzer, 7 – off-gas, 8 – solid charge, 9 – K-type thermocouple (sample), 10 – S-type thermocouple (furnace), 11 –eurotherm regulator/furnace controller, 12 – thermobalance, 13 – computer. (Dashed lines show the linkages between auxiliary components and the solid line arrows indicate gas flow)

3.2.3.2 Theoretical weight loss and experimental TGA data

Oxides of manganese and iron display a wide range of solid solutions. Iron oxide (FeO) and co-existing MnO produced in prereduction has been observed by several researchers to dissolve in each other at high temperatures, forming FeO-MnO solutions[43], [63], [65]. Larssen *et al*,.[65] studied the reduction of manganese ores in 80/20 CO/CO_2 atmospheres utilizing a thermogravimetric furnace up to 1000 ℃. The morphological observations in these studies[43], [65] were in agreement with reduction of iron oxides ending with wüstite (FeO), which is stabilized by manganese in the monoxide phase. As such, the theoretical net weight loss of the ores during prereduction was estimated based on the chemical composition of the ore and corresponding equilibrium phases i.e., MnO and FeO at 1000 ℃ in the CO-containing gas atmosphere. The chemical composition of the ores in Table 3.1, shows that Comilog has a high oxidation level (O/Mn ratio) equal to 1.93 (≈ MnO_2), whereas Nchwaning and UMK are semi oxidized ores (predominantly Mn_2O_3) with oxygen level to 1.50 and 1.45, respectively. Similar oxygen levels have been reported in previous studies [64], [73], [134]. Fe concentration in manganese ores as measured by XRF was

converted to Fe_2O_3, assuming that it is present in the ore as Fe(III). On complete prereduction, Fe concentration was converted to FeO, assuming that it is present there as Fe(II). The theoretical weight loss was calculated using O/Mn ratio, and Fe content of the ores, while accounting for the decomposition of carbonates as shown by equation (3.1). The water content was calculated by subtracting the CO_2 content given in the chemical analysis and calculated weight loss change from MnO_x to Mn_3O_4 from the measured LOI. Table 3.4 shows the calculated theoretical weight loss for the ores.

$$Theoretical\ weight\ loss\ (wt.\%) = wt.\%\ (MnO_x \rightarrow MnO) + wt.\%\ (Fe_2O_3 \rightarrow FeO) + wt.\%\ CO_2 + wt.\%\ H_2O\ (chemically\ bound\ water) \quad (3.1)$$

Table 3.4: Calculated theoretical weight loss from ores (wt. %) based on Table 3.1

	Comilog	Nchwaning	UMK
Mn prereduction (MnO_x to MnO)	14.0	6.92	4.24
Fe-prereduction (Fe_2O_3 to FeO)	0.50	1.49	0.65
Carbonate decomposition	0.11	4.45	16.0
Water evaporation	3.80	-	-
Total	18.4	12.9	20.9

The theoretical weight loss presented in Table 3.4 varies slightly when compared to calculated values from previous studies[57], [134], [75]. Recently, Larssen [75] estimated the higher theoretical weight loss to be 20.7 wt. % and 13.7 wt. % for Comilog and Nchwaning, respectively. The discrepancy of the calculated weight loss compared to previous studies is mainly due to heterogeneity in ore compositions in particular Mn/Fe ratio and content of chemically bound moisture in ore. As an example the water content in Comilog in this work has been estimated to be 3.8 wt. %, however in several other studies by Tangstad *et al.*,[57], Ngoy[134] and Larssen[75], the chemically bound moisture in Comilog has been estimated to be approximately 5 wt. %. Addition of the 1.2 wt. % H_2O difference will place the weight loss in Comilog at the same level as previous studies. However, the variations are within acceptable ranges.

The experimental data acquired from the thermo-gravimetric setup are reported in the form of weight change curves (wt.%) and its first derivative, the reaction rate (wt.%/s) as a function of temperature and time. To analyze the contribution to the overall weight loss of prereduction reactions, decomposition of carbonates and water evaporation, Fityk [135] was used to decompose the rate curves into these constituents. Fityk is a general-purpose peak fitting program, which

was used to analyze isothermal TGA data where reaction models are fitted to the experimental data and the model giving the best fit is assumed to be representative. The rate curves were automatically described using Gaussian curves, with the only limitation of no negative curves. The curves were checked by integrating the assumed contribution and verifying it against expected weight loss presented in Table 3.4. The weight loss based on gas measurements only considers weight loss from reaction changing the CO/CO_2 ratio, meaning only decomposition and prereduction. One prereduction reaction removes one mole of oxygen while producing one mole of CO_2, whereas decomposition reaction removes one mole of CO_2. Therefore, considering the molecular weights, the CO_2 from decomposition reactions weighs 2.75 times more than oxygen removal from prereduction reactions. As such, for the rate curves analysis, the carbonate decomposition contribution was multiplied by the CO_2 factor of 2.75.

3.2.4 TGA furnace (TF1) experiments

TF1 was used to investigate the reaction rate of the metal producing reaction. The main goal was to investigate if varying degree of prereduction would affect the metal producing reaction.

3.2.4.1 Experimental setup and temperature schedule

Experiments were conducted in a vertical graphite tube furnace equipped with thermo-gravimetric (TGA) balance. The filled graphite crucibles with a perforated closing lid were hooked to the balance and suspended inside the furnace chamber by a molybdenum (Mo) wire. Figure 3.9 shows the schematic of the TF1 furnace. The photographs of the furnace when closed, and open showing the suspended crucible, are shown in Figure 3.10.

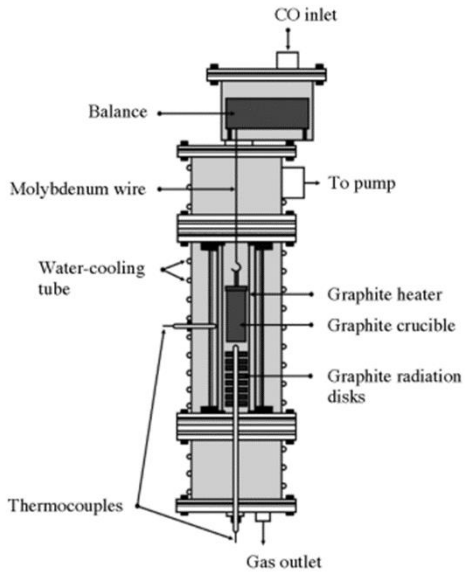

Figure 3.9: Schematic of the TF1 furnace[136]

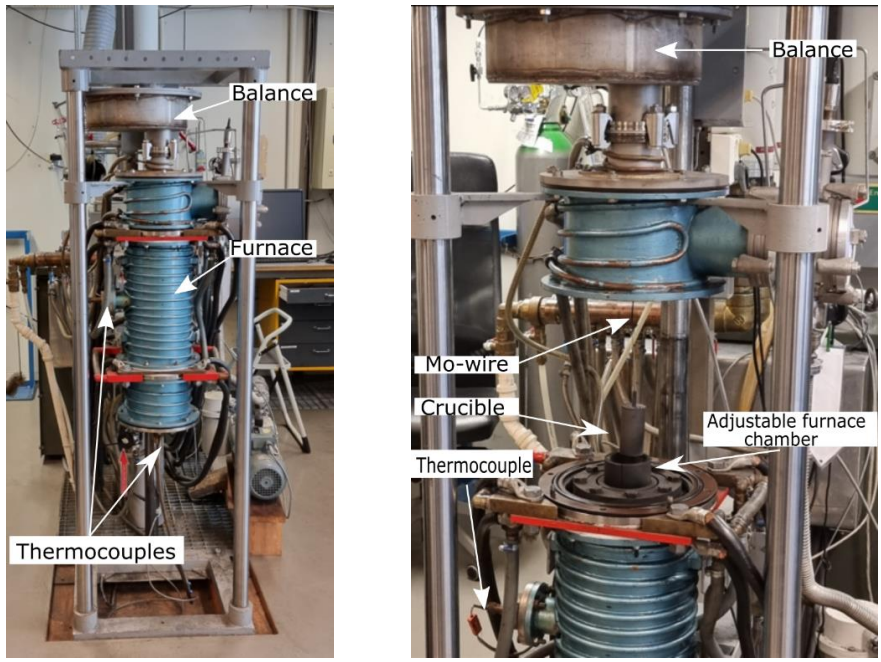

(a) (b)

Figure 3.10: Photographs of TF1 furnace: (a) closed furnace and (b) opened furnace illustrating the crucible hooked to the furnace balance and suspended by a molybdenum wire.

Temperature measurements were recorded in two locations as shown in Figure 3.9, with B-type thermocouple recording temperature in the hot zone at approximately 0.5 cm below the bottom of the graphite crucible and S-type thermocouple measuring furnace wall temperature. The S-type thermocouple was used to control the heating rate and temperature. Type B thermocouple can be used for temperatures up to 1800 °C with an uncertainty of 0.5K, whereas S-type thermocouple is applicable up to 1700 °C with an uncertainty of 0.3K at temperatures below 1000 °C and uncertainty of 1K for temperatures above 1000 °C. Prior to experiments, three measurements of the temperature profiles were measured in the furnace without crucible present. A typical temperature profile is as shown in Figure 3.11. As can be seen in Figure 3.11, the thermocouple is positioned at 0.5 cm below the bottom of the crucible and is in the area where the highest temperature is recorded. A temperature gradient exists ranging between 0 – 10 °C/cm, hence the charge materials will be within 0 to 10 °C from the measured value since the height of charge material was below 2 cm in all the experiments.

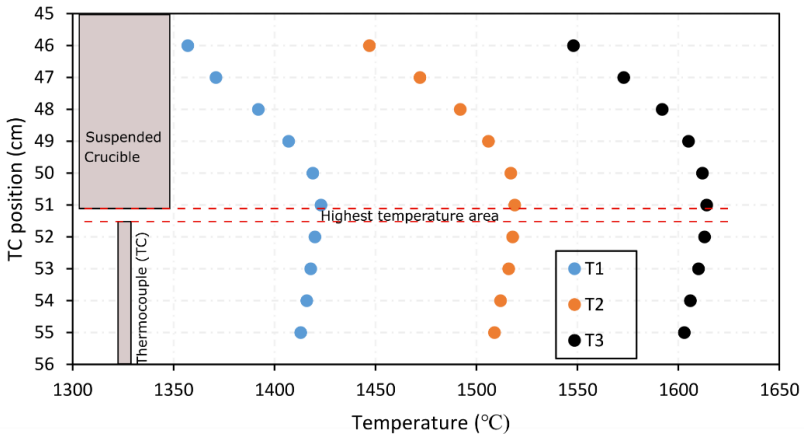

Figure 3.11: Typical temperature profile in the furnace for measurements T1-T3. Indicated is the position of B-type thermocouple at 0.5cm below the bottom of crucible.

The atmosphere in the furnace chamber was initially evacuated using a vacuum pump and subsequently replaced by a high purity 99.99 % Ar gas stream up to 1atm pressure. The gas flow was regulated by high range Alicat Scientific mass flow controllers with a 10 ms measurement response time. The Ar gas stream at 0.5 L/min was replaced by a high purity 99.97 % CO gas at 0.5 L/min during the heating stage upon reaching 500 °C. Ar was reintroduced at the end of the experiment when

the temperature had cooled down to 900 °C. Two alternative heating schedules were conducted as illustrated in Figure 3.12.

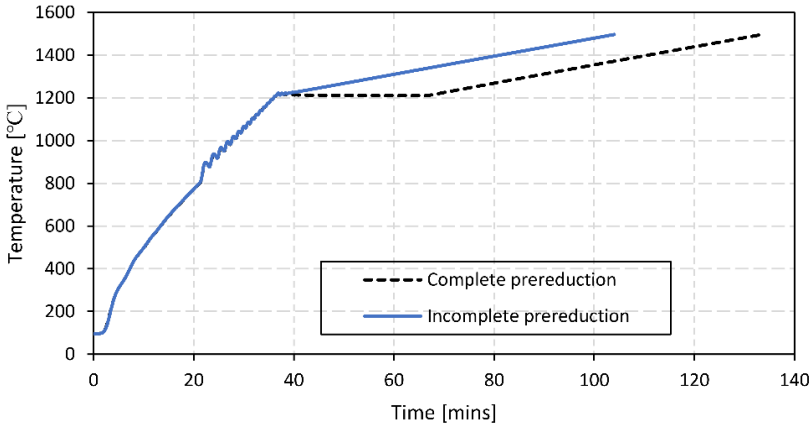

Figure 3.12: Illustration of temperature schedules for experiments. Dashed black line is sample temperature for experiments with 30 minutes holding time at 1200 °C to ensure complete prereduction and the blue solid line indicates the schedule without holding temperature at 1200 °C.

The samples were rapidly heated at 25 °C/min up to 1200 °C and temperature held at 1200 °C for 30 minutes followed by a slow heating step at 4.5 °C/min. Alternatively, the fast-heating stage was subsequently followed by a slow heating stage without holding temperature at 1200 °C. The two heating regimes were conducted to ascertain the effect of extent of prereduction on the final metal formation reactions. Final target temperatures were 1400 °C, 1500 °C and 1550 °C for the two heating regimes. The initial rapid heating stage up to 1200 °C represents the prereduction of manganese oxides and iron oxides (MnO_2, Mn_2O_3, Mn_3O_4 to MnO and Fe_2O_3, Fe_3O_4, FeO to Fe, evaporation of bound water and decomposition of carbonates) and the calculated composition of a completely prereduced charge are shown Table 3.5. Further heating to target temperatures represent the non-isothermal reduction of MnO in slag by carbon to form FeMn alloy.

The weight of the sample is recorded every 5 seconds. The total weight of crucible plus charge material is measured with an external scale Ohaus Pioneer PA4202 (US) before and after reduction experiments to confirm the net weight loss acquired from the TGA data. After cooling, the crucibles containing reacted slag are casted in epoxy resin and then cut to expose the slag and metal for EPMA analyses.

Table 3.5: Calculated primary slag composition after complete prereduction

Charge	MnO	SiO_2	CaO	MgO	Al_2O_3	Total	*Basicity
Com	83.2	6.44	0.36	0.23	9.76	100	0.04
Nch	79.19	9.61	8.43	1.52	1.25	100	0.92
UMK	66.39	9.43	18.66	4.09	1.43	100	2.09

*Basicity = (CaO+MgO) /(SiO_2+Al_2O_3)

3.2.4.2 Analyses of reduction degree – weight loss and EPMA analyses

Thermogravimetric (TGA) data which entails mass change as a function of temperature and time is the main information from experimental runs. The TGA data is important in understanding the behavior for different manganese ores. Since the reduction degree of MnO is different for charges heated up to different temperatures, analysis of the slag and alloy phases were done in EPMA to establish the end chemical composition after reduction. As such, crucibles were cut to get samples for EPMA analysis. Figure 3.13 illustrates the vertically cut crucible showing its cross-section and sample as it appears at the end of the experiment. The degree of MnO reduction can be estimated by analyzing the composition of slag phases. Various phases were subjected to three-point analysis and an average composition was obtained. Backscattered micrographs obtained from EPMA were post processed using ImageJ® software to quantify the phase distribution of different phases based on their contrast threshold. The total composition of the slag was then calculated based on the measured area fraction and the chemical composition of each phase as determined by EPMA. Three area fractions were measured for every slag sample and a 1.5 % average standard deviation of the area fraction was obtained in 18 slag samples.

The degree of reduction, expressed by the MnO content, was calculated based on the material analyses (Table 3.5.) and the weight loss measured by the thermobalance. The removed oxygen from MnO was assumed to leave as CO within the slag reduction temperatures. The calculated MnO content was verified with the MnO content in reduced slag as analyzed by EPMA.

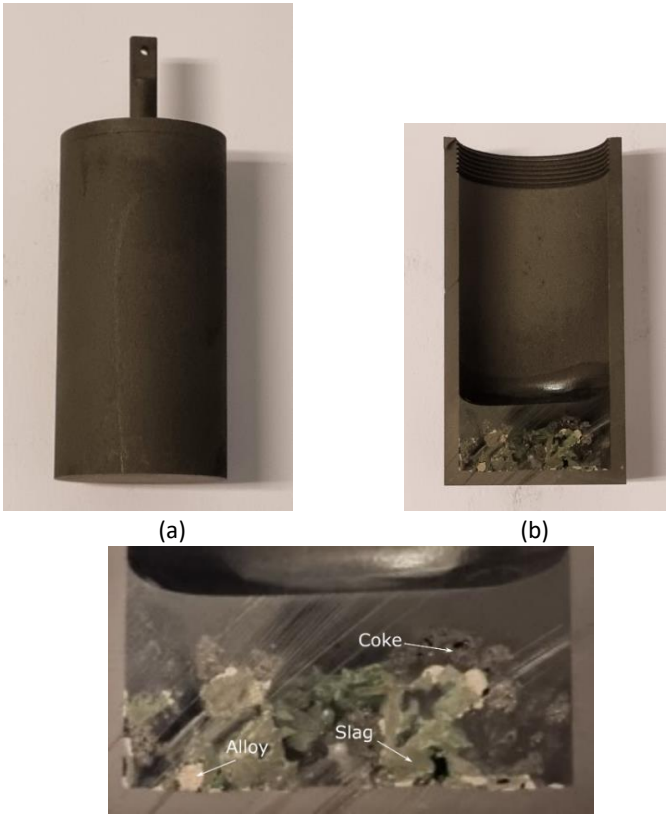

Figure 3.13: Illustration of the TF1 crucible; (a) before cutting, (b) cross-section of vertically cut crucible and (c) epoxy mounted materials after heating.

3.2.5 Analytical techniques

This section presents a detailed description of various techniques, equipment and software packages which were utilized in the analysis of raw materials, prereduced ores, slag, and alloy phases.

3.2.5.1. Chemical analysis

The chemical composition of raw and prereduced ore samples were measured by SINTEF Norlab. Techniques used for characterization of the raw materials and prereduced ore samples include X-ray fluorescence (XRF), permanganometric titration, thermogravimetric and combustion-IR methods. Elemental analysis (Mn, Fe, Si, Al, Ca, Mg, P, S, Ti, K, and Ba) was measured with X-Ray fluorescence (XRF) fused bead technique by employing a Bruker AXS S4 Pioneer X-Ray fluorescence spectrometer

(Billerica, US). Mn and Fe were given as total contents of the ores and other elements were converted into concentrations of their corresponding oxides, i.e., SiO_2, Al_2O_3, CaO, MgO, TiO_2, K_2O, and BaO in accordance with the stable oxides' forms with a specific oxidation degree. The oxygen level (O/Mn ratio) of manganese ores and prereduced products was determined by permanganometric titration (ASTM 465-11:2017)[137], in which excess oxygen above MnO is expressed as MnO_2. The analysis of carbon concentration was done with a LECO (Combustion-IR) instrument, and the measured concentration of carbon was converted to CO_2 concentration according to the stoichiometry, assuming that all carbon in the ore is in the form of CO_2. Loss on ignition (LOI) was measured to a constant weight at 950 °C in air, thermogravimetrically. It is assumed that during the analysis, all carbonates are fully decomposed, water is evaporated, while the stable forms of manganese and iron are Mn_3O_4 and Fe_2O_3, respectively.

3.2.5.2 Porosity measurements

The porosity of the solids ((1-(Apparent density/Absolute density)) was determined from the measurement of the absolute density (particle density) with Accupyc 1330 helium pycnometer and the measurement of the bulk density (apparent density) using a GeoPyc 1360 pcynometer. The analysis was done for three particles from each sample from the induction furnace trials. The porosity measurements were done at SINTEF Industry.

3.2.5.3 Electron probe microanalyser (EPMA)

Electron probe microanalyzer was used to determine the composition of the different phases present in the manganese slag and metal. Prior to EPMA analysis, metallographic sample preparation and polishing was conducted to produce smooth surfaces. Samples were embedded using epoxy resin curing for 12 hours and the surface of the samples were initially ground using a SiC grinding paper, grit 220 before polishing using polyurethane-based pads as the polishers (i.e., MD-Dac, 200 mm and MD-Nap, 300 mm) and an abrasive suspension, diamond water-based type as the polishing agent gradually decreased from 9, 3 and 1 µm particle size. The polished samples were cleaned with tap water using a cotton swab and dried in an oven for 12 hours. Thereafter, the specimen surfaces were coated in carbon prior to analysis to prevent charge build-up during electron analysis. After metallographic preparation and carbon coating, a high-resolution electron probe micro-analyzer (EPMA) JEOL JXA 8500TM, supported by wavelength dispersive spectroscopy (WDS) was used. EPMA/WDS provides high accuracy on quantitative analysis of the elements in observed phases of the samples as well as it can be used for imaging. Using an

electron gun, an electron probe micro-analyser (EPMA) provides chemical analysis of localized areas of a sample. Data were obtained from EPMA analysis which includes quantitative data regarding the chemical composition from three-point analysis and backscattered electron images which give an indication of the morphology of the specimens.

3.2.5.4 ImageJ®

ImageJ® is an open-source image processing software. Post processing of the backscattered images from EPMA was done using ImageJ® software to quantify the phase distribution of different phases based on their contrast threshold. Subsequently, the overall composition of the assumed liquid phase at high temperature, based on phase area fraction and chemical analyses was calculated assuming that the slag is homogeneous. Initially, the backscattered micrographs are converted to grey scale 8-bit type images. This action converts each phase pixel's colour information into brightness measurement. Secondly, a threshold dialogue is used to adjust the threshold of the selected phase which highlights the pixels of the selected phase in an image and the pixels which represent the selected phase turns red as can be seen in Figure 3.14. Lastly, the area of the selected phase is analysed within the limits of the threshold. As the ranges of pixels values that represent the different phases are unique, the software is manipulated to highlight the pixels that represent each phase and measure the area covered by the phase as illustrated in Figure 3.14.

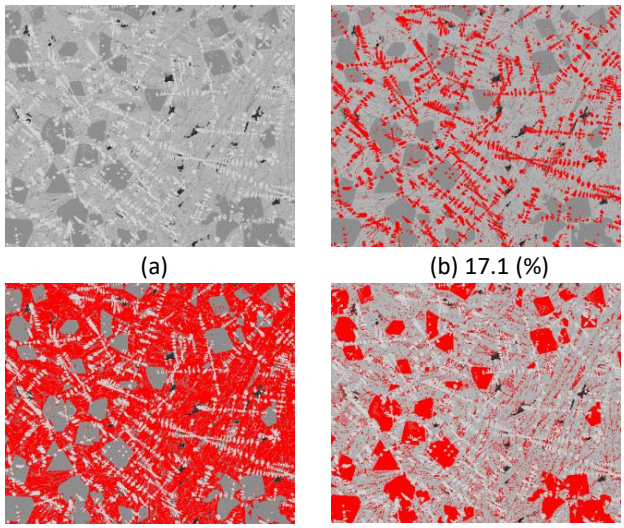

Figure 3.14: Quantification of phases using ImageJ software. (a) Original backscattered micrograph from EPMA showing all the phases present. The subsequent area fractions of the different phases are shown in (b), (c) and (d).

3.2.5.5 Equilibrium Calculations

FACTSage 8.1 thermochemical software[87] was used to calculate equilibrium phases and compositions in the reduction process of UMK, Comilog and Nchwaning ores. The equilibrium module in FACTSage 8.1 was used to calculate the equilibrium phase relations in the system MnO-SiO_2-Al_2O_3-FeO-CaO-MgO. The equilibrium relations were calculated for the ores mixed with excess carbon in a carbon monoxide (CO) atmosphere as a function of temperature in the range 1100 ℃ to 1600 ℃ at intervals of 10 ℃ and atmospheric pressure set to 1 atm. The FactPS, FToxid and FTmisc databases were used in all calculations. In addition, phase distribution was calculated in the absence of carbon reductant for the temperature range 1100 ℃ to 2000 ℃. The six component oxide compositions for UMK, Comilog and Nchwaning ores were calculated by mass balance assuming higher oxides of manganese and iron to be prereduced down to MnO and FeO, respectively, and that all other oxides (SiO_2, Al_2O_3, CaO and MgO) remain unreacted. The calculated oxide compositions of the prereduced UMK, Comilog and Nchwaning ores were used as starting input values for equilibrium calculations. The phase equilibrium calculations are key in understanding phase development and reduction of slag as a function of temperature and were conducted to support and evaluate results obtained from slag reduction experiments.

3.2.6 Overview of experimental work

An overview of laboratory scale experiments conducted in this study are presented in this section. As previously mentioned, a master's student performed experiments were digout of the prereduction zone was carried out and prereduction of the ores in TGA furnace. The results of this work are mainly used for comparison with digout of pilot scale experiments as they form the basis of understanding ore prereduction behavior under small-scale controlled conditions. For clear readability, all laboratory scale experiments are highlighted following two themes namely, slag reduction and prereduction experiments.

Experiments conducted to investigate slag reduction are categorized into P-series and Q-series. Table 3.6 shows the P-series experiments conducted in the induction furnace to investigate phase development during slag reduction in the high temperature region of the cokebed. Samples were generally excavated on temperature measurement points on top of the cokebed and 5 cm into the cokebed. Table 3.7 shows an overview of Q-series experiments conducted in TGA furnace (TF1)

focusing on evaluation of the effect of varying degree of prereduction on the high temperature reaction MnO + C = Mn + CO.

Table 3.6: Overview of the induction furnace experiments in *P-series* were samples within the cokebed were excavated. Ore particle size was 9.5 -16 mm.

Experiment ID	Ore	Target temperatures on top of cokebed (℃)	Samples
P1	Comilog	1200, 1400, 1500	CM1-CM6
P2	Nchwaning	1200, 1400, 1500	Nch1-Nch6
P3	UMK	1200, 1300, 1400	UMK1-UMK5

Table 3.7: Overview of TGA Q-*series* experiments conducted in TF1 furnace. Ore and coke particle size was 3.15 - 4 mm in all experiments. The experiments were conducted with repeated parallels.

Experiment ID	Charge (Ore type [g]+ Polish coke [g])	Experiments conducted (Ore-temperature-holding time (mins) at 1200 ℃)
Q1	Comilog [10g] + coke [2g]	Com-1400-30, Com-1400-0, Com-1500-30, Com-1500-0, Com-1550-30, Com-1550-0
Q2	Nchwaning [10g] + coke [2g]	Nch-1400-30, Nch-1400-0, Nch-1500-30, Nch-1500-0, Nch-1550-30, Nch-1550-0
Q3	UMK [10g] + coke [2g]	UMK-1400-30, UMK-1400-0, UMK-1500-30, UMK-1500-0, UMK-1550-30, UMK-1550-0

Experiments conducted to investigate ore prereduction are categorized into *R-series* and *S-series*. Table 3.8 and Table 3.9 shows an overview of the *R-series* and *S-series* experiments, respectively. *R-series* experiments focused on prereduction ores under simulation conditions of the ferromanganese process and evaluate the effect of solid carbon on the extent of prereduction within the temperature gradient that exists in furnaces. *S-series* experiments were conducted to investigate the effect of heating rate on the prereduction behavior of three ores in 70/30 CO/CO_2 gas atmosphere and to evaluate the extent of decomposition of carbonates in Nchwaning and UMK ores.

Table 3.8: Overview of the induction furnace experiments in *R-series* were samples within the prereduction were excavated. Ore and coke particle size was 9.5 -16 mm[9].

Experiment ID	Charge	Cokebed temperature (°C) [# of Experiments]	Total number of samples
R1	Comilog ore	1200 [1] 1300 [1] 1400 [1]	13
R2	Comilog ore + coke	1200 [2]	14
R3	Nchwaning ore	1200 [1] 1300 [1] 1400 [1]	21
R4	Nchwaning ore + coke	1200 [2]	18
R5	UMK ore	1200 [1] 1300 [1] 1400 [1]	25
R6	UMK ore + coke	1200 [2]	18

Table 3.9: Overview of TGA non-isothermal *S-series* experiments conducted in 70/30 CO/CO_2 atmosphere. Ore particle size was 10 -12.5 mm for the three ores in all experiments[9].

Experiment ID	Ore type	Heating rate (°C/min)	Final temperature (°C)
S1	Comilog	3	1000
		6	1000
		9	1000
S2	Nchwaning	3	1000
		6	1000
		9	1000
		9	900
S3	UMK	3	1000
		6	1000
		9	1000
		9	700
		9	800
		9	900

3.3 Results

The results from laboratory scale experiments are presented in this section in accordance with the series introduced in the overview of experiments (section 3.2.6)). The main results from slag reduction studies are presented for both the induction and TGA furnace experiments. As previously stated, experiments on the prereduction behavior of manganese ores with solid carbon in the induction furnace and in a CO/CO_2 were conducted by a master student as a part of this work[9], [66]. The present work reports some of the results as they offer a basis and a support to the discussion on prereduction behavior of these ores in Pilot experiments as will be presented in Chapter 4. Further details on the prereduction work can be found in Reiersen's reports [9], [66].

3.3.1 P-Series: Slag reduction from induction furnace experiments

In this work, Comilog Nchwaning and UMK slag samples at temperatures higher than 1200 °C from a setup which simulates the SAF have been studied to show phase development during the formation and reduction of slag from the high temperature regions of the furnace. Melted and reduced ore samples core-drilled out from selected areas close to the coke bed are named CM-x, Nch-x, and UMK-x for Comilog, Nchwaning and UMK experiments.

3.3.1.1 Phase development and compositions for Comilog ore

Figure 3.15 shows the backscattered micrographs for Comilog slags CM-1, CM-2, CM-3, and CM-4 from top of the cokebed at temperatures 1217 °C, 1277 °C, 1410 °C and 1475 °C, respectively. The samples show a variety of phases. Comilog slags CM-1, CM-2 and CM-3 show the microstructure of slag samples containing spherical manganosite (MnO) phases and the co-existence of a medium grey matrix which is tephroite ($2MnO{\cdot}SiO_2$) phase, a dark grey galaxite ($MnO{\cdot}Al_2O_3$) phase and bright alloy phase. It is believed that at high temperatures, the slag would be a mixture of the spherical manganosite in co-existence with a liquid, where the liquid has precipitated to the tephroite and galaxite phase. For sample CM-4, the spherical MnO phase has been completely dissolved and some dendrites have precipitated during cooling and a large region of MnO depleted slag is observed. In this case, increasing temperature results in increased dissolution of solid monoxide phase into the liquid. The composition of the alloy phase varies considerably as size increases, with the Mn/Fe ratios increasing with increase in alloy particle size. The observed Mn/Fe ratios

for the Comilog experiments were on average approximately 0.04, 0.96 and 12.1 for the metal prills (<10µm), beads (10-100µm) and bulk phase (>100µm), respectively.

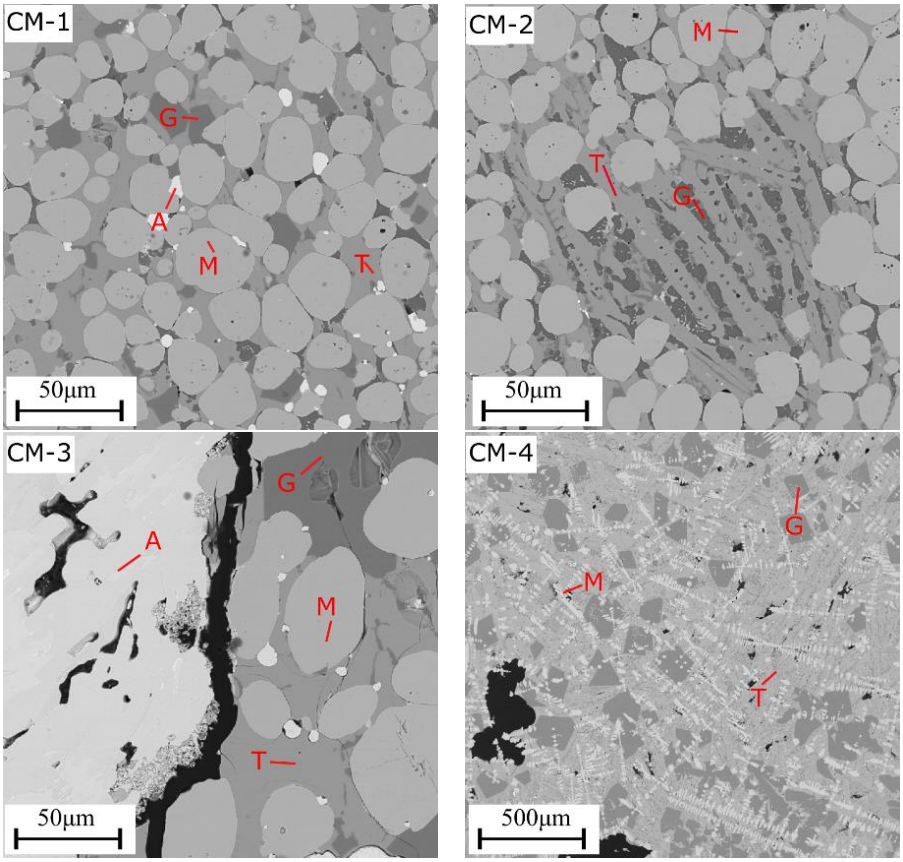

Figure 3.15: BSE images of Comilog slag samples CM-1, CM-2, CM-3, and CM-4 collected from positions on top of the coke bed with temperatures 1217 °C, 1277 °C, 1410 °C and 1475 °C, respectively. Legend: A = alloy, M = monoxide; T = tephroite and G = galaxite.

The micrographs for Comilog slags CM-5 and CM-6 taken from 5cm below the top of the cokebed are shown in Figure 3.16. The measured cokebed reference temperatures were 1410 °C and 1475 °C, respectively for CM-5 and CM-6. As can be seen in the micrographs, slags CM-5 and CM-6 were depleted of MnO i.e., all the solid MnO has dissolved into the liquid phase during reduction. The phases in the slags are mainly close to tephroite and galaxite phase. The bulk alloy was mainly FeMn alloy with Mn/Fe ratios at 11.7 and 9.7, respectively for slags CM-5 and CM-6.

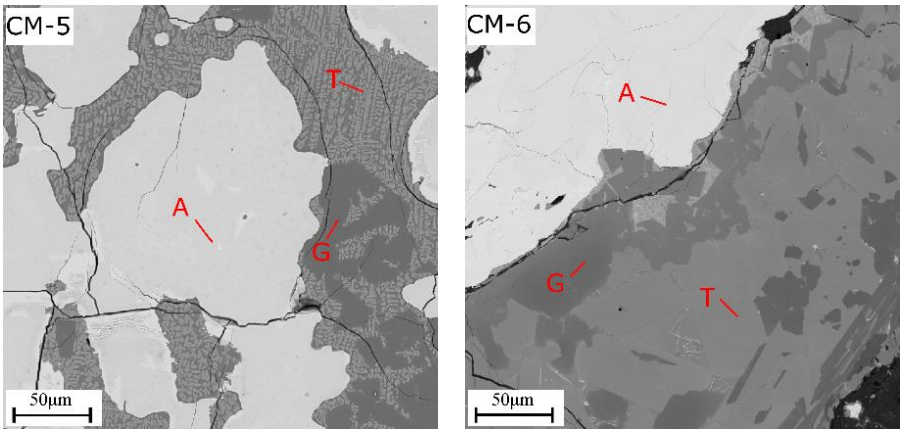

Figure 3.16: BSE images of Comilog slags CM-5 and CM-6 collected from positions 5cm below top of the coke with reference coke bed temperatures at 1410 °C and 1475 °C, respectively. Legend: A = alloy, T = tephroite and G = galaxite.

The composition of the phases in all the Comilog slags as determined by wavelength dispersive spectroscopy (WDS) in EPMA, are presented in Table 3.10. Details of the composition of the liquid phases calculated based on area fraction and composition of the phases are shown in Table 3.11. There is a significant decrease in the fraction of solid monoxide phase with increasing temperature and the total MnO content in the liquid slag phase was about 45.5 wt.% and 52.1 wt.% at 1410 °C and 1475 °C, respectively. Phase development and reduction of Comilog slag show that the solid MnO phase will be present in the slag on top of the coke bed and the slag will hence not flow into the coke bed until the solid spherical MnO is dissolved. However, CM-4 on top of the cokebed is an exception since it has been completely liquid on top of the cokebed. This is so because the whole Comilog ore charge subsidized with continuous melting and reduction on top of the cokebed, leading to complete melting of the whole ore charge layer.

Table 3.10: Summary of the average compositions of the phases experimentally observed from Comilog slags (CM-1) – (CM-4) from top of the coke bed and (CM-5) – (CM-6) are 5cm into the coke bed.

Identified Phase	Sample ID	Temperature (°C)	wt. pct						Total
			MnO	SiO_2	Al_2O_3	MgO	CaO	FeO	
Manganosite	CM-1	1217	100.4	0.10	0.17	0.28	0.01	0.58	101.5
	CM-2	1277	97.8	0.13	0.19	0.13	-	4.02	102.3
	CM-3	1410	100.9	0.10	0.34	0.40	0.02	0.24	102.0
	CM-4	1475	94.4	0.35	0.29	0.20	0.04	0.22	95.5
Tephroite	CM-1	1217	70.2	27.0	0.90	0.53	0.22	0.35	99.2
	CM-2	1277	69.3	27.6	0.94	0.24	0.12	1.53	99.7
	CM-3	1410	70.4	27.5	0.71	0.56	0.45	0.16	99.8
	CM-4	1475	65.3	30.0	0.65	0.35	0.35	0.14	96.8
	CM-5	>1410	52.8	30.6	11.7	0.18	0.89	0.21	96.4
	CM-6	>1475	61.7	30.0	1.07	0.28	2.81	0.22	96.1
Galaxite	CM-1	1217	41.1	0.18	58.5	1.16	-	0.36	101.3
	CM-2	1277	41.4	0.28	57.6	0.29	0.01	0.16	99.7
	CM-3	1410	41.1	0.10	60.0	1.37	0.02	0.12	102.7
	CM-4	1475	37.6	0.20	57.7	0.99	0.01	0.08	96.6
	CM-5	>1410	40.2	0.42	58.6	1.43	0.04	0.15	100.8
	CM-6	>1475	33.5	0.09	60.5	3.26	0.02	0.14	97.5

Table 3.11: Calculated liquid slag composition based on measured area fraction by ImageJ® and EPMA phase analysis for Comilog slags (Samples (CM-1) – (CM-4) were on top of the coke bed and (CM-5) – (CM-6) are 5cm into the coke bed)

Slag sample		CM-1	CM-2	CM-3	CM-4	CM-5	CM-6
Temperature (°C)		1217	1277	1410	1475	>1410	>1475
% Area fraction	Monoxide	64.6	66.7	62.7	15.8		
	Tephroite	25.5	25.7	21.9	59.1	41.5	66.1
	Galaxite	9.90	7.64	15.4	25.1	58.5	33.9
Total MnO (wt pct)		86.8	86.1	85.0	62.9	45.5	52.1
Liquid composition	MnO	62.1	62.7	58.3	62.9	45.5	52.1
	FeO	0.36	1.96	0.15	0.14	0.18	0.19
	SiO_2	19.2	21.3	16.2	17.8	12.9	19.9
	Al_2O_3	16.9	13.8	25.2	14.9	39.1	21.2
	CaO	0.16	0.17	0.27	0.21	0.39	1.86
	MgO	0.70	0.24	0.89	0.49	0.91	1.29
	BaO	0.02	0.05	0.05	0.05	0.65	0.24
	TiO_2	0.19	0.21	0.25	0.45	0.39	0.19
	Total	99.7	100.2	101.3	96.9	100.	97.0

3.3.1.2 Phase development and compositions for Nchwaning ore

Figure 3.17, shows the typical microstructure for Nchwaning slags Nch-1, Nch-2, Nch-3, and Nch-4 from top of the cokebed at temperatures 1220 °C, 1270 °C, 1413 °C and 1505 °C, respectively.

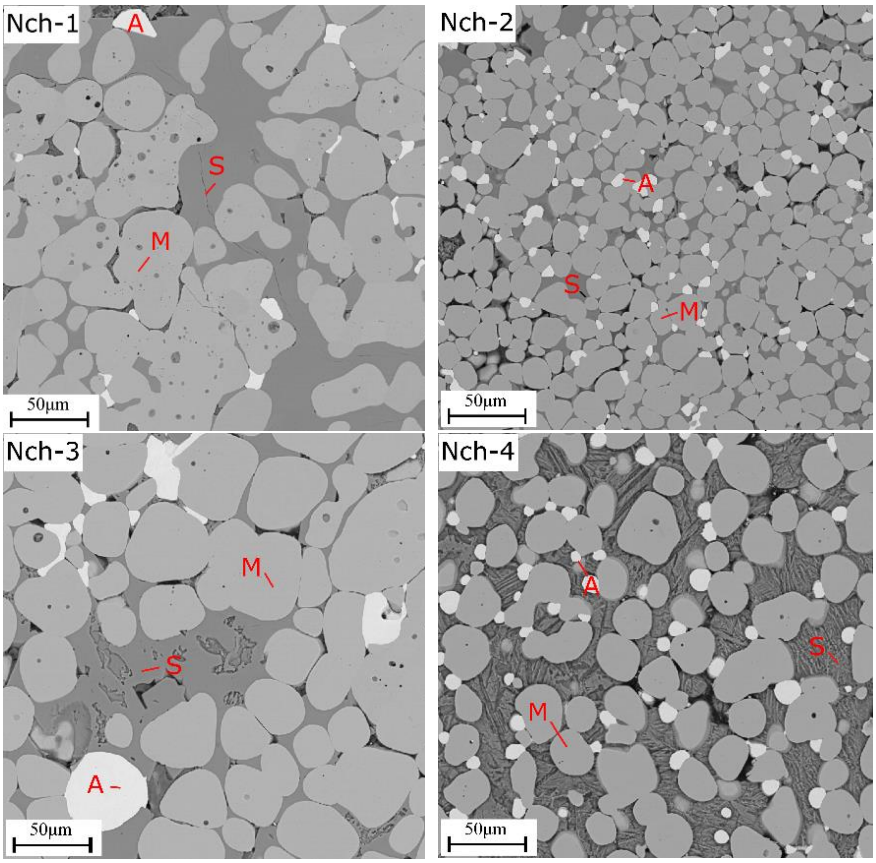

Figure 3.17: BSE images of Nchwaning slag samples Nch-1, Nch-2, Nch-3, and Nch-4 collected from positions on top of the coke with temperatures 1220 °C, 1270 °C, 1413 °C and 1505 °C, respectively. Legend: A = alloy, M= monoxide; S = slag matrix.

The microstructure of these slag samples consists of spherical manganosite (MnO) phases in co-existence with a grey slag matrix made up of mainly MnO, CaO and SiO_2. The grey slag matrix is believed to be liquid at high temperatures and the bright phase is the alloy produced. The composition of the alloy phase varies considerably as size increases, with the Mn/Fe ratios increasing with an increase in alloy particle size. The observed Mn/Fe ratios for the Nchwaning samples were on average approximately 0.04, 3.75 and 11.14 for the metal prills (<10µm), beads (10-100µm) and bulk phase (>100µm), respectively.

The micrographs for Nchwaning slag Nch-5 collected from positions 5 cm below the top of the coke bed with reference coke bed temperature at 1505 ℃ presented in Figure 3.18 show two distinct phases on higher magnification: a light grey phase and a dark grey slag matrix. MnO spheres have been completely dissolved and the light grey (LG) and dark grey (DG) phases have precipitated during cooling and a large region of MnO depleted slag was observed.

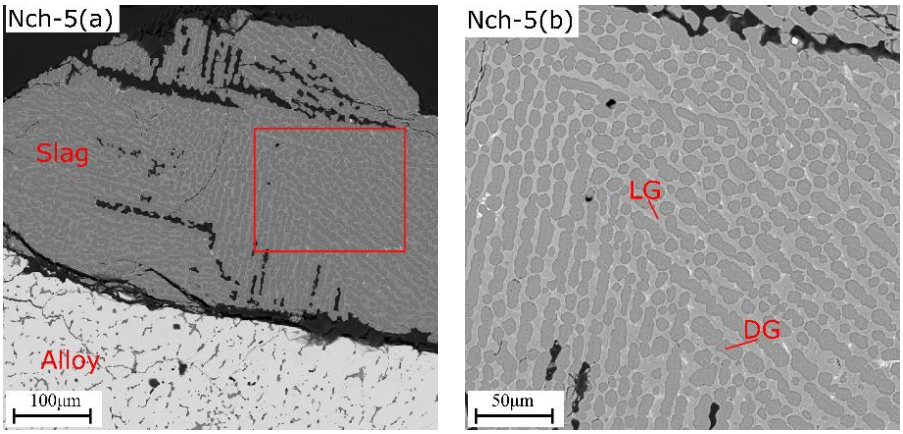

Figure 3.18: BSE images of Nchwaning slag Nch-5 (a) collected from positions 5cm below the top of the coke bed with reference coke bed temperature at 1505 ℃ and the area inside of the red rectangular line is higher magnification (b). Legend: A = alloy, LG = light grey phase and DG = dark grey slag matrix.

The compositions of the phases in these Nchwaning slag samples as measured in EPMA, are given in Table 3.12 and the liquid phase calculated based on area fraction and composition of the phases are shown in Table 3.13. The monoxide phase in Nchwaning contains up to 10 wt. % FeO and 2.73 wt. % MgO, which indicates that Nchwaning forms an (Mn,Mg,Fe)O monoxide solid solution. Slag formation and reduction of Nchwaning show that solid (Mn,Mg,Fe)O phase was present in the slag on top of the cokebed and the slag will hence not flow into the coke bed until the solid spherical monoxide phase is dissolved. The content of MnO in the liquid slag will be as high as 35 % MnO when the liquid is in equilibrium with solid monoxide phase. With complete dissolution of the solid monoxide phase in the basic Nchwaning slag, the MnO content in the liquid slag has reduced to approximately 17 wt. %.

Table 3.12: Average compositions of the phases experimentally observed from Nchwaning slags (Nch-1) – (Nch-4) from top of the coke bed and slag Nch-5 from 5cm below top of coke bed.

Identified phase	Sample name	Temperature (°C)	Wt Pct						Total
			MnO	SiO_2	Al_2O_3	MgO	CaO	FeO	
Monoxide	Nch-1	1220	89.4	0.16	0.04	0.44	0.72	7.29	98.1
	Nch-2	1270	84.5	0.12	0.06	0.55	1.52	10.2	97.0
	Nch-3	1413	86.1	0.05	0.10	0.50	1.40	4.40	92.6
	Nch-4	1505	83.1	0.4	0.20	2.73	3.06	8.09	97.6
Slag matrix	Nch-1	1220	35.2	28.5	0.06	0.63	29.0	1.35	94.7
	Nch-2	1270	31.9	29.5	0.02	0.30	33.0	1.47	96.2
	Nch-3	1413	33.9	30.1	0.11	0.46	29.6	0.90	95.1
	Nch-4	1505	22.1	34.4	0.26	9.63	34.1	0.09	101
Light grey (LG)	Nch-5	>1505	25.1	24.8	20.7	4.84	25.5	0.06	101
Dark grey (DG)	Nch-5	>1505	15.1	29.8	7.41	7.80	37.7	0.03	97.8

Table 3.13: Calculated liquid slag composition based on measured area fraction by ImageJ® and EPMA phase analysis for Nchwaning slags (Slags (Nch-1) – (Nch-4) were on top of the coke bed and Nch-5 is 5cm into the coke bed)

Slag sample		Nch-1	Nch-2	Nch-3	Nch-4	Nch-5
Temperature (°C)		1220	1270	1413	1505	>1505
% Area fraction	Monoxide/LG	63.6	71.0	82.7	50.7	19.3
	Slag matrix	36.4	29.0	17.3	49.3	80.7
Total MnO (wt pct)		69.7	69.3	74.6	49.4	17.1
Liquid composition	MnO	35.2	31.9	33.9	22.1	17.1
	FeO	1.35	1.47	0.90	0.89	0.03
	SiO_2	28.5	29.5	30.1	34.4	28.8
	Al_2O_3	0.06	0.02	0.11	0.26	9.98
	CaO	29.0	33.0	29.6	34.1	35.3
	MgO	0.63	0.30	0.46	9.63	7.21
	BaO	0.04	0.19	0.08	0.05	0.57
	TiO_2	0.01	0.01	0.01	0.06	0.13
	Total	94.8	96.4	95.2	101.5	99.1

3.3.1.3.Phase development and compositions for UMK ore

UMK samples UMK-1, UMK-2, UMK-3, UMK-4, and UMK-5 were from top of the cokebed and these were exposed to temperatures at 1180 °C, 1223 °C, 1226 °C, 1308 °C and 1367 °C, respectively. Backscattered micrographs for these UMK slags are shown in Figure 3.19.

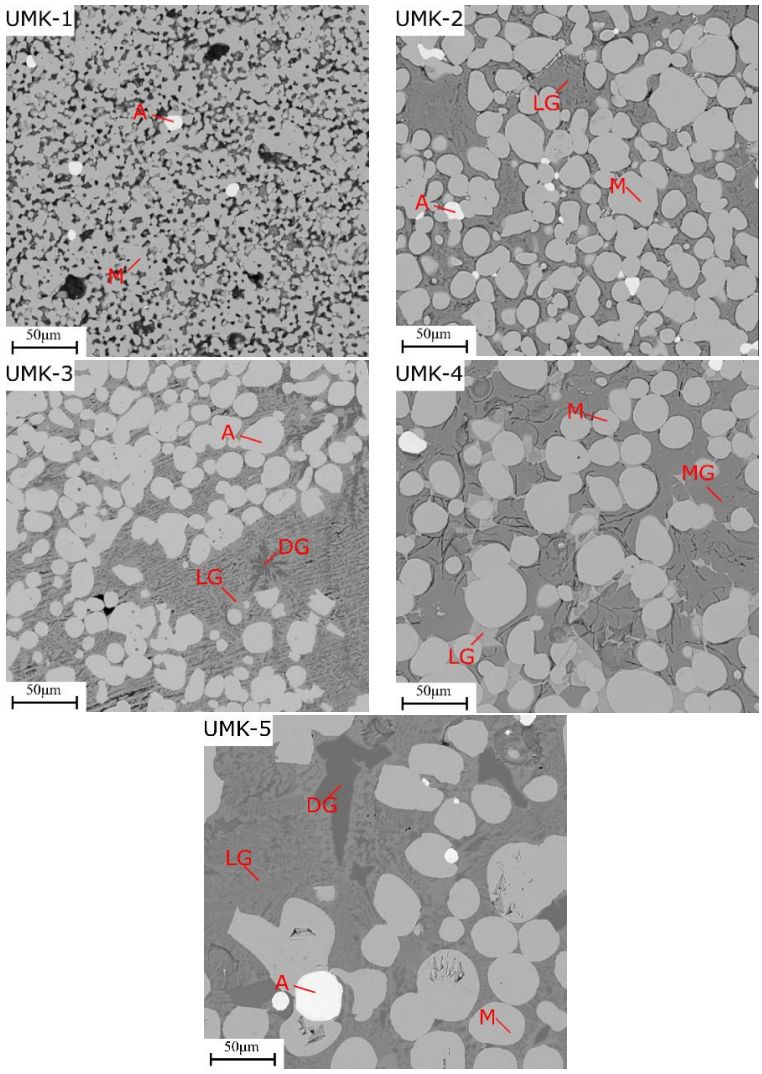

Figure 3.19: BSE images of UMK slag samples UMK-1, UMK-2, UMK-3, UMK-4, UMK-5, and UMK-6 collected from positions on top of the coke with temperatures 1156 °C, 1180 °C, 1223 °C, 1226 °C, 1308 °C and 1367 °C, respectively. Legend: A = alloy, M= monoxide; LG = light grey phase and DG = dark grey phase

The microstructure of slag sample UMK-1 shows a slag structure at temperatures below 1200 °C, were the sample is not melted and at the initial softening stages in the formation of the primary slags. Slag samples UMK-2 to UMK-5 show that at higher temperatures, spherical manganosite (MnO) phases is formed and is in co-existence with a light and dark grey slag matrix. The slag matrix is believed to be liquid at high temperatures and the bright phase is the alloy produced. The observed

Mn/Fe ratios for the UMK samples were generally low, on average approximately ranging between 0.02 to 0.06 for the metal prills (<10μm), which was mainly Fe in the alloy. In the UMK experiments no slag was observed at any position inside the coke and no bulk alloy was observed. This implies that this is a situation where there has been no significant melting and reduction of slag in the investigated temperature range. Hence, this shows that UMK will require temperatures as high as 1500 °C to achieve significant reduction and complete dissolution of monoxide phase in slag.

The compositions of the phases in these UMK slag samples as measured in EPMA, are given in Table 3.14 and the liquid phase calculated based on area fraction and composition of the phases are shown in Table 3.15. The monoxide phase in UMK-1 contains up to 17 wt. % FeO and 6 wt. % MgO, which indicates that UMK formed an (Mn,Mg,Fe)O monoxide solid solution. However, the level of FeO and MgO in monoxide phase in this sample was extremely high compared to the other samples. Slag formation and reduction of UMK show that solid (Mn,Mg,Fe)O phase will be present in the slag on top of the cokebed and the slag did not flow into the coke bed until the solid spherical monoxide phase was dissolved. In the UMK experiments, completely reduced slag was not observed inside the coke and all the slag remained on top of the cokebed, an indication that the temperatures were not high enough to promote significant monoxide dissolution and slag reduction. The content of MnO in the liquid slag will be on average at 25 % MnO when the liquid is in equilibrium with solid monoxide phase.

Table 3.14: Average compositions of the phases experimentally observed from UMK slags (UMK-1) – (UMK-5) from top of the coke bed.

Identified Phase	Sample ID	Temperature (°C)	wt. pct						Total
			MnO	SiO_2	Al_2O_3	MgO	CaO	FeO	
Manganosite	UMK-1	1180	72.1	0.01	0.11	5.95	6.18	17.0	101
	UMK-2	1223	94.5	0.15	0.10	2.78	2.03	1.24	100
	UMK-3	1266	96.8	0.16	0.59	1.12	0.40	1.32	100
	UMK-4	1308	90.5	0.12	0.23	1.63	2.13	3.65	101
	UMK-5	1367	98.3	0.05	1.06	0.67	0.32	0.43	101
LG phase	UMK-2	1223	14.7	32.6	0.14	0.68	47.7	0.26	96.1
	UMK-3	1266	27.8	26.0	26.5	0.52	18.3	0.39	99.6
	UMK-4	1308	26.5	19.7	26.9	1.63	23.1	3.65	99.1
	UMK-5	1367	37.4	15.9	40.8	0.49	5.08	0.13	99.8
DG phase	UMK-4	1308	22.2	32.8	0.28	1.42	38.5	0.52	95.8
	UMK-5	1367	23.0	0.22	75.7	0.74	0.07	0.12	99.8

Table 3.15: Calculated liquid slag composition based on measured area fraction by ImageJ® and EPMA phase analysis for UMK slags (Slags (UMK-2) – (UMK-5) were on top of the coke bed).

Slag sample		UMK-2	UMK-3	UMK-4	UMK-5
Temperature (°C)		1223	1266	1308	1367
% Area fraction	Monoxide	68.0	49.7	48.8	40.6
	LG/MG	32.0	36.2	13.0	39.9
	DG		14.1	38.2	19.5
Total MnO (wt pct)		69.0	62.1	56.1	59.3
Liquid composition	MnO	14.7	27.8	23.3	32.7
	FeO	0.26	0.39	0.69	0.13
	SiO_2	32.6	26.0	29.5	10.8
	Al_2O_3	0.14	26.5	7.01	52.3
	CaO	47.7	10.3	31.7	3.44
	MgO	0.68	0.52	1.47	0.58
	Total	96.1	99.6	94.1	99.6

3.3.1.4 Calculated equilibrium phases during reduction of Comilog, Nchwaning and UMK

The slag and metal in FeMn furnaces are not believed to be in chemical equilibrium with carbon. The path from unreduced primary slag to tapped metal and slag is however influenced by the equilibrium conditions, hence an evaluation of the equilibrium state at various temperatures are done. The calculated equilibrium phase distribution for the prereduced ore compositions of Comilog, Nchwaning and UMK (listed in Table 3.16) for temperatures 1100 °C to 1600 °C are shown in Figure 3.20(a-f).

Table 3.16: Calculated primary slag composition assuming prereduction of higher manganese and iron oxides to MnO and FeO

Charge	MnO	FeO	SiO_2	CaO	MgO	Al_2O_3	Total	Basicity
Com	83.2	4.70	4.20	0.50	0.10	7.30	100	0.10
Nch	67.4	14.9	8.18	8.80	7.17	1.07	100	0.91
UMK	59.8	9.86	8.50	16.8	3.69	1.29	100	2.10

*Basicity = $(CaO+MgO)/(SiO_2+Al_2O_3)$

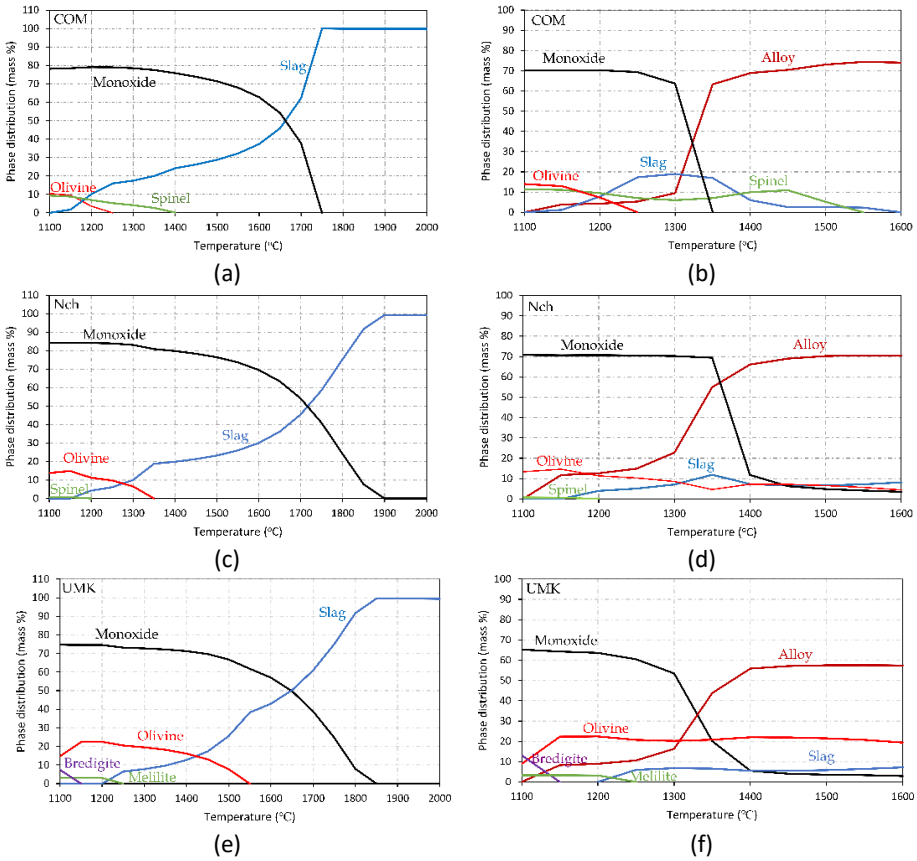

Figure 3.20: Equilibrium phase distribution with increasing temperature that shows: (a) Phases in primary Comilog slag, (b) Phases when Comilog is in equilibrium with solid carbon, (c) Phases in primary Nchwaning slag, (d) Phases when Nchwaning is in equilibrium with solid carbon, (e) Phases in primary UMK slag, & (d) Phases when UMK is in equilibrium with solid carbon

Figure 3.20(a) shows phase distribution in primary slag and Figure 3.20(b) shows the phase distribution upon heating and reduction for Comilog slag. In Figure 3.20(a), four phases namely, monoxide ((Mn,Fe,Mg)O), liquid slag, olivine ((Mn, Mg,Ca)$_2$SiO$_4$) and spinel (Mn,Mg)Al$_2$O$_4$) are shown to vary with increasing temperature in a non-reducing environment in the primary slag. The solid monoxide phase completely dissolves into liquid slag at about 1750 °C. Figure 3.20(b) shows the phase distribution during the carbothermic reduction of Comilog. At 1100 °C three major phases are observed namely, monoxide phase ((Mn,Fe,Mg)O), olivine ((Mn,Mg,Ca)$_2$SiO$_4$-predominantly tephroite at 89 wt pct Mn$_2$SiO$_4$), spinel (predominantly galaxite phase-MnAl$_2$O$_4$) and a liquid slag started to form at approximately 1150 °C. Alloy is formed during slag reduction and the solid monoxide phase completely dissolves into liquid slag at about 1350 °C.

Figure 3.20(c) and Figure 3.20(d) show the phase distribution with increase in temperature in the primary slag and under reducing environment (i.e., in the presence of solid carbon), respectively for Nchwaning slag. Figure 3.20(c) shows that a liquid slag is formed during heating of Nchwaning ore with corresponding dissolution of olivine ($(Mn,Mg,Ca)_2SiO_4$), spinel $(Mn,Mg)Al_2O_4$) and monoxide ((Mn,Fe,Mg)O). The monoxide phase completely dissolves in the liquid slag at about 1900 °C. However, when Nchwaning is in equilibrium with solid carbon (Figure 3.20(d)), the monoxide phase is present throughout the temperature range with much of its dissolution occurring up to 1450 °C. This monoxide phase is predominantly MnO in the temperature range 1100 °C to 1300 °C and the composition changes with more MgO dissolving in the monoxide solid solution as presented in Table 3.17.

The phase distribution with increase in temperature in the primary slag for UMK is shown in Figure 3.20(e). During heating, a liquid slag is formed with corresponding dissolution of four phases namely olivine ($(Mn,Fe,Mg,Ca)_2SiO_4$), bredigite ($Ca_7Mg(SiO_4)_4$, melilite ($Ca_2AlSi_2O_7$), and monoxide ((Mn,Fe,Mg)O). The monoxide phase completely dissolves at approximately 1850 °C. In a reducing environment, i.e., when UMK slag is in equilibrium with solid carbon, the monoxide phase is present throughout the temperature range as presented in Figure 3.20(f). The monoxide phase significantly dissolves in the temperature range 1200 °C to 1400 °C, which corresponds to the range were the distribution of alloy is increasing. The (Mn,Fe)O in the monoxide phase ((Mn,Mg,Fe)O) dissolves in the slag with subsequent increase in MgO and at 1400 °C the monoxide phase is predominantly MgO rich as presented in Table 3.17.

The monoxide phase in Nchwaning and UMK ores is predominantly ((Mn,Mg,Fe)O) during heating when not in coexistence with carbon reductant as presented in Table 3.17. In contrast, Comilog ore is characterized by very low contents of basic oxides and the monoxide is mostly (Mn,Fe)O solid solution. The monoxide phase during heating shows that prior to reduction, FeO is stabilized in the solid monoxide phase. Table 3.19 and Table 3.20 respectively show the chemical compositions of liquid slag and alloy formed during carbothermic smelting of prereduced Comilog, Nchwaning and UMK in the temperature range of 1100 °C to 1600 °C.

Table 3.17: Composition (wt. %) of the monoxide phase during heating of Comilog, Nchwaning and UMK (FactSage 8.1). (Note: No carbothermic reduction of slag)

Ore	Temperature	Monoxide phase					
	(℃)	MnO	Al_2O_3	MgO	CaO	FeO	Total
Comilog	1100	93.7	0.79	0.06	0.08	5.32	100
	1200	93.6	1.01	0.08	0.02	5.30	100
	1300	93.5	1.26	0.09	0.02	5.10	100
	1400	93.4	1.53	0.10	0.03	5.00	100
	1500	93.9	1.30	0.10	0.05	4.70	100
	1600	94.7	1.00	0.11	0.08	4.12	100
Nchwaning	1100	80.8	0.36	1.85	0.88	16.0	100
	1200	80.6	0.40	1.87	1.08	16.0	100
	1300	80.5	0.25	1.88	1.46	15.7	99.8
	1400	80.4	0.13	1.90	2.16	15.3	99.9
	1500	80.8	0.10	1.96	2.98	14.2	100
	1600	82.5	0.06	2.12	3.44	11.8	99.9
UMK	1100	79.6	0.16	4.31	2.81	13.2	100
	1200	79.2	0.31	4.80	2.64	13.1	100
	1300	78.8	0.36	4.86	3.22	12.8	100
	1400	78.7	0.28	4.88	3.84	12.3	100
	1500	78.9	0.16	4.98	4.96	11.0	100
	1600	78.7	0.10	5.30	6.30	8.60	99.0

Table 3.18: Composition (wt. %) of the monoxide phase during carbothermic reduction of Comilog, Nchwaning and UMK (FactSage 8.1)

Ore	Temperature	Monoxide phase					
	(℃)	MnO	Al_2O_3	MgO	CaO	FeO	Total
Comilog	1100	98.7	0.8	0.06	0.08	0.3	99.9
	1200	98.8	1.0	0.07	0.03	0.1	100
	1300	98.6	1.2	0.10	0.02	0.03	100
	1400	Monoxide is completely dissolved in liquid slag at 1350 ℃					
Nchwaning	1100	96.2	0.3	2.2	0.9	0.4	100
	1200	95.9	0.4	2.3	1.3	0.1	100
	1300	94.9	0.3	2.9	1.9	0.03	100
	1400	33.5	0.01	66.2	0.3	0.01	100
	1500	8.3	-	91.4	0.2	-	99.9
	1600	2.9	0.11	96.4	0.7	-	100
UMK	1100	91.4	0.2	4.5	3.6	0.4	100
	1200	90.9	0.3	5.6	3.1	0.1	100
	1300	89.0	0.3	6.5	4.1	0.03	99.9
	1400	36.9	0.01	61.8	1.4	0.01	100
	1500	8.8	0.2	90.7	0.5	-	100
	1600	3.0	0.1	96.2	0.8	-	100

Table 3.19: Calculated equilibrium composition (wt. %) of liquid slag phase in coexistence with monoxide phase and solid carbon for Comilog, Nchwaning and UMK reduction (FactSage 8.1)

Ore	Temperature (°C)	MnO	FeO	SiO_2	Al_2O_3	CaO	MgO	Total
				(Initial slag formation at 1150 °C)				
	1200	55.4	0.09	26.2	12.9	5.4	0.1	100
Comilog	1300	59.3	0.05	22.1	15.8	2.6	0.1	100
	1400	52.0	0.03	22.6	22.3	2.7	0.4	100
	1500	39.7	0.03	23.8	33.2	2.8	0.5	100
	1600	26.1	0.02	22.4	45.2	5.3	1.0	100
				(Initial slag formation at 1200 °C)				
	1200	28.2	0.04	27.2	12.1	31.6	0.9	100
Nchwaning	1300	29.1	0.01	27.3	9.8	32.5	1.2	99.9
	1400	13.2	<0.01	22.3	18.1	41.0	5.4	100
	1500	4.6	<0.01	20.8	20.2	47.9	6.6	100
	1600	1.1	<0.01	19.0	18.0	56.6	5.3	100
				(Initial slag formation at 1250 °C)				
	1250	23.8	0.03	21.6	18.2	35.2	1.2	100
UMK	1300	24.3	0.01	22.0	16.6	35.7	1.4	100
	1400	9.0	0.01	14.6	23.5	50.1	2.9	100
	1500	3.3	-	16.2	22.1	54.1	4.3	100
	1600	1.1	-	18.7	17.9	57.3	5.0	100

Table 3.20: Calculated equilibrium composition (wt. %) of the liquid alloy for the reduction of Comilog, Nchwaning and UMK slags (FactSage 8.1)

Ore	Temperature °C	Mn	Fe	Si	C	Mn/Fe
	1200	11.7	83.5	<0.01	4.8	0.14
	1300	55.4	38.3	<0.01	6.3	1.45
Comilog	1400	86.0	5.3	1.8	6.8	16.2
	1500	85.5	5.0	2.7	6.8	17.1
	1600	85.2	4.9	2.7	7.1	17.4
	1200	11.2	84.1	<0.01	4.8	0.13
	1300	51.9	41.9	<0.01	6.2	1.24
Nchwaning	1400	77.2	15.7	0.2	7.1	4.92
	1500	77.0	15.5	0.2	7.3	4.97
	1600	76.5	15.6	0.3	7.5	4.90
	1200	10.3	85.0	-	4.8	0.12
	1300	47.0	47.0	-	6.1	1.00
UMK	1400	79.1	13.7	0.02	7.2	5.77
	1500	79.2	13.3	0.03	7.3	5.95
	1600	78.7	13.3	0.3	7.6	5.92

Based on equilibrium calculations in FactSage, it can be summarized that during heating, the slag will consist of a liquid slag phase in coexistence with the solid monoxide phase from 1400 – 1600 °C for Comilog and Nchwaning ore. This will also

be the case for UMK ore, with the exemption of some additional olivine phase being present from 1400-1550 °C. The monoxide (MnO) phase will for UMK and Nchwaning ore also contain some MgO and FeO while for Comilog ore it will contain mainly MnO plus FeO. As the reduction proceeds, the solid monoxide will be dissolved in the liquid phase and additional solid olivine, or spinel phases may appear. The monoxide phase in Comilog will be mostly pure MnO and for Nchwaning and UMK ore it will be a solid solution of (Mn,Mg)O which becomes MgO enriched as reduction progresses. Initially, Fe is formed and as reduction progresses there is progression in alloy composition with increased levels of MnO dissolution and reduction in liquid slag. The alloy phase becomes subsequently enriched in Mn and C.

3.3.2 Q series: Slag reduction from TF1 furnace experiments

The TGA experiments in TF1 were conducted for the Comilog, Nchwaning and UMK charges to ascertain the extent of prereduction on the high temperature metal producing reaction i.e., MnO + C = Mn + CO and establish the extent of reduction of MnO from the primary slag. Results of mass loss during reduction and EPMA analyses are reported in this section.

3.3.2.1 Reduction behavior

The weight changes for Comilog, Nchwaning and UMK charge mixtures are compared following two different heating pathways as shown in Figure 3.21, Figure 3.22 and Figure 3.23, respectively. The first pathway is characterized by non-isothermal heating of the charge mixtures at 25 °C/min up to 1200 °C , holding time for 30 minutes at 1200 °C and further heating at 4.5 °C/min up to final temperatures of 1400, 1500 and1550 °C. Holding for 30 minutes was done to ensure complete prereduction of higher manganese and iron oxides. On the other hand, the second pathway follows the same temperature regime, but has no isothermal stage of holding time for 30 minutes at 1200 °C.

The weight loss curves in the different charge mixtures overlap each other which is an indication of high accuracy in weight loss measurements for different experiments of the same ore type. Under the experimental conditions investigated, the mass changes for the different charge mixtures were mainly divided into two stages. At temperatures up to 1200 °C, the weight loss was from prereduction reactions whereas at temperatures between 1200 and 1550 °C, the mass changes were from the MnO reduction stage.

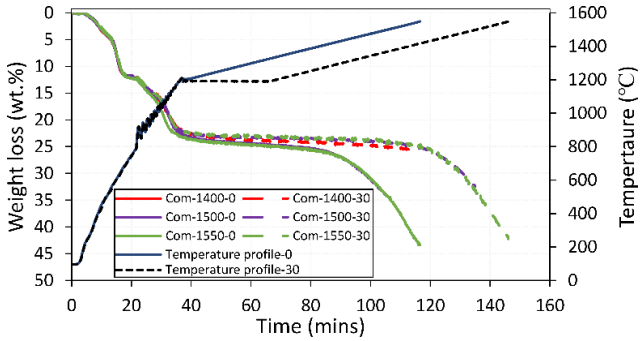

Figure 3.21: Comparison of weight loss behavior of Comilog charge mixture i.e., Q1-series, with (pathway 1) and without holding temperature at 1200 °C (pathway 2).

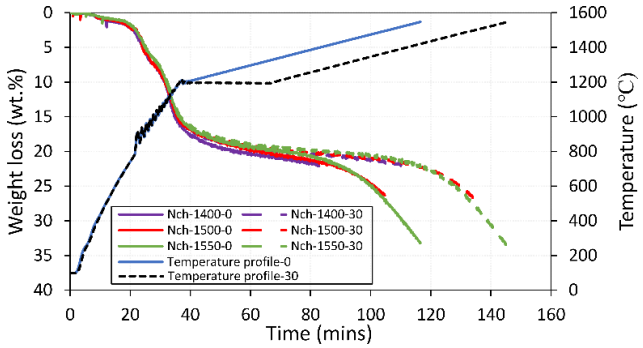

Figure 3.22: Comparison of weight loss behavior of Nchwaning charge mixture i.e., Q2-series, with (pathway 1) and without holding temperature at 1200 °C (pathway 2).

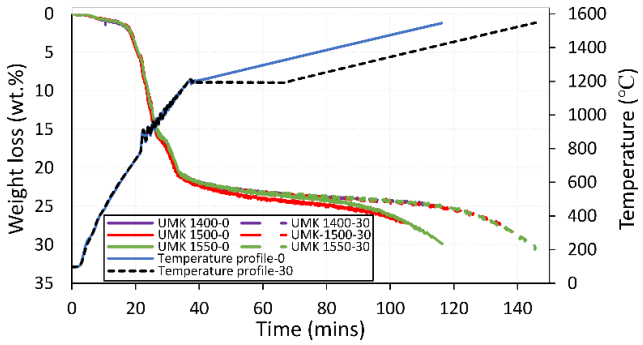

Figure 3.23: Comparison of weight loss behavior of UMK charge mixture i.e., Q3-series, with (pathway 1) and without holding temperature at 1200 °C (pathway 2).

Elimination of holding time at 1200 °C was used to create a lower prereduction extent and this was used to investigate effect of incomplete prereduction on the metal producing reaction. The mass loss for prereduction of Comilog, Nchwaning and UMK charges during heating up to 1200 °C show that holding ore samples temperature at 1200 °C for 30 minutes results in a higher weight loss i.e., complete prereduction, compared to not holding. The prereduction mass loss results with and without holding for 30 minutes at 1200 °C are presented in Table 3.21.

Table 3.21: Prereduction mass loss for Comilog, Nchwaning and UMK experiments with and without holding for 30 minutes at 1200 °C

Experiment	Starting Mass (g)	Prereduction mass loss (g)		Mass loss (%)
		30 mins holding at 1200 °C	No holding time at 1200 °C	
Com-1200-0	12		2.58	21.5
Com-1200-30	12	2.85		23.7
Nch-1200-0	12		1.77	14.8
Nch-1200-30	12	2.23		18.6
UMK-1200-0	12		2.62	21.9
UMK-1200-30	12	2.84		23.7

As presented in Table 3.21, the weight loss for Nchwaning ore during heating up to 1200 °C is significantly lower than UMK ore and Comilog ore. This is mainly because Nchwaning is an Mn_2O_3 based ore with significantly lower O/Mn ratio of 1.47 compared to 1.9 for Comilog and less carbonates compared to UMK. UMK has CO_2 content of about 16 % which is significantly higher than Nchwaning as presented in Table 3.1. Therefore, mass loss in UMK is close to that of Comilog even though it has a lower O/Mn ratio of 1.45. The different ore prereduction behaviors based on the ore characteristics, will be discussed in detail in section **Section 3.3.4**.

The weight loss in the MnO reduction stage i.e., between 1200 and 1550 °C is obtained by deducting the weight loss from prereduction from the total weight loss. The raw data for mass loss in the reduction stage was subject to Gaussian smoothing in Fityk and the data smoothing is illustrated in **Appendix A**. The weight loss in the MnO reduction stage is shown by Figure 3.24, Figure 3.25 and Figure 3.26, for Comilog, Nchwaning and UMK series, respectively.

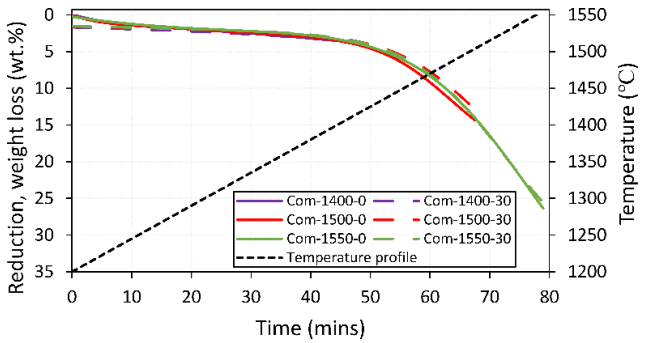

Figure 3.24: Weight loss curves during slag reduction for Comilog charge (Q1 series). The temperature profile is shown.

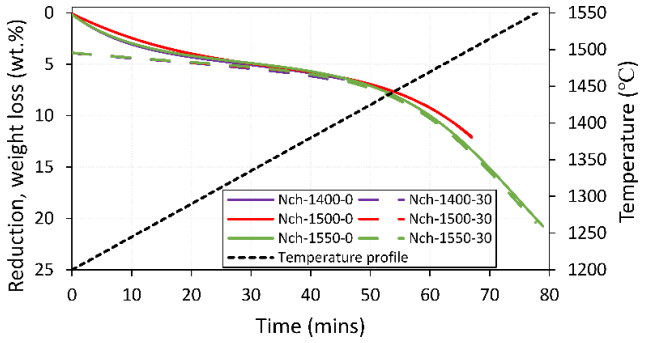

Figure 3.25: Weight loss curves during slag reduction for Nchwaning charge (Q2 series). The temperature profile is shown.

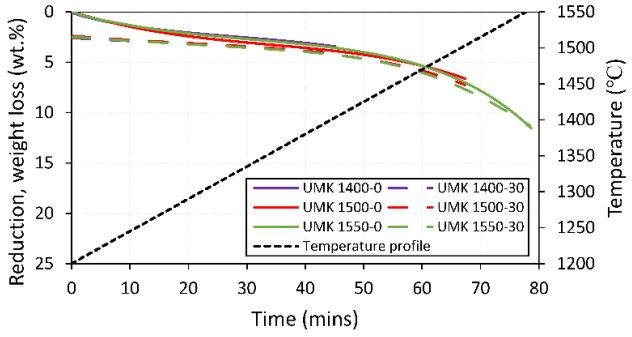

Figure 3.26: Weight loss curves during slag reduction for UMK charge (Q3 series). The temperature profile is shown.

In the MnO reduction stage i.e., between 1200 and 1550 °C, weight loss is seen to increase with increasing final temperatures. However, two important results are shown from the curves. Firstly, the overall weight loss in each experimental series is the same when comparing the two pathways in each charge mixture. Secondly, Comilog charge mixture has a greater weight loss followed by Nchwaning and lastly UMK charge mixtures when comparing the weight loss for the different charge

mixtures. This implies that Comilog will have a higher reduction extent followed by Nchwaning and lastly UMK. The weight loss at final temperatures of 1400, 1500 and 1550 °C in "Q1", "Q2" and "Q3" series experiments, is seen to be at the same level when comparing temperature profiles with or without holding for 30 mins 1200 °C in each experimental series. This is confirmed by the calculated slag compositions based on the TGA data from the reduction stage (i.e., 1200 to 1550 °C) and the chemical compositions of the ores. Details of the calculations are discussed in **Appendix B**. The calculated slag compositions are presented in Table 3.22. As an example, the reduction of Com-1550-30 i.e., after complete prereduction and Com-1550-0 i.e., after incomplete prereduction, shows that the composition of slag will have an MnO content of 39.9 wt.% and 37.4 wt.%, respectively. Hence the composition of the slags is quite similar with negligible variations. This implies that the end point during reduction is independent on whether the ores are completely prereduced or not when they approach the high temperature region. In general, incomplete prereduction has been observed to have no effect on the overall weight loss in the metal producing reduction. As such, a lower extent of prereduction has been concluded to have no effect on the metal formation reaction.

Table 3.22: Calculated final slag composition based on weight loss results (TGA data) at 1400, 1500 and 1550 °C.

Experiment		Slag component (wt. %)					
		MnO	SiO_2	Al_2O_3	CaO	MgO	Total
Comilog "Q1" series	Com-1400-0	84.2	5.92	9.66	0.17	0.11	100
	Com-1400-30	83.9	6.03	9.84	0.18	0.11	100
	Com-1500-0	77.6	8.38	13.7	0.25	0.16	100
	Com-1500-30	76.6	8.74	14.3	0.26	0.16	100
	Com-1550-0	37.4	23.4	38.1	0.68	0.44	100
	Com-1550-30	39.9	22.4	36.6	0.66	0.42	100
Nchwaning "Q2" series	Nch-1400-0	77.4	10.5	1.36	9.16	1.65	100
	Nch-1400-30	77.2	10.6	1.38	9.25	1.66	100
	Nch-1500-0	73.3	12.4	1.61	10.82	1.95	100
	Nch-1500-30	72.0	12.9	1.69	11.35	2.04	100
	Nch-1550-0	59.6	18.7	2.44	16.35	2.94	100
	Nch-1550-30	59.1	18.9	2.46	16.54	2.97	100
UMK "Q3" series	UMK-1400-0	65.4	9.72	1.47	19.2	4.22	100
	UMK-1400-30	64.5	9.96	1.51	19.7	4.33	100
	UMK-1500-0	60.3	11.1	1.69	22.0	4.84	100
	UMK-1500-30	59.8	11.3	1.71	22.3	4.89	100
	UMK-1550-0	53.3	13.1	1.99	25.9	5.69	100
	UMK-1550-30	51.5	13.6	2.06	26.9	5.91	100

The reduction rate for all the charges is calculated by differential weight loss curve with time. Prior to reduction rate calculations, the mass loss data from the reduction stage were subjected to exponential smoothing at 0.98 damping factor and subsequently, the smoothed and normalized data was used for reaction rate calculation. Figure 3.27, Figure 3.28, and Figure 3.29 shows a comparison of the reduction rate for the two reduction pathways in Comilog 'Q1' series, Nchwaning 'Q2' series and UMK 'Q3' series, respectively.

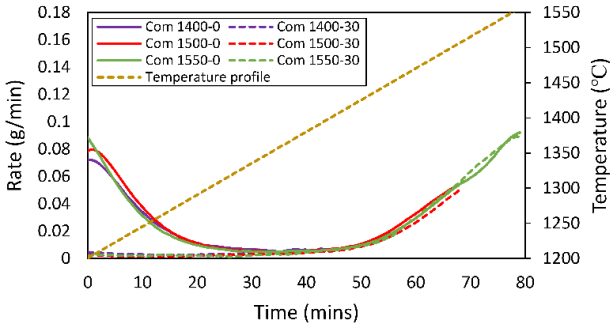

Figure 3.27: Calculated reduction rate and temperature profile, all as a function of time for Comilog 'Q1' series.

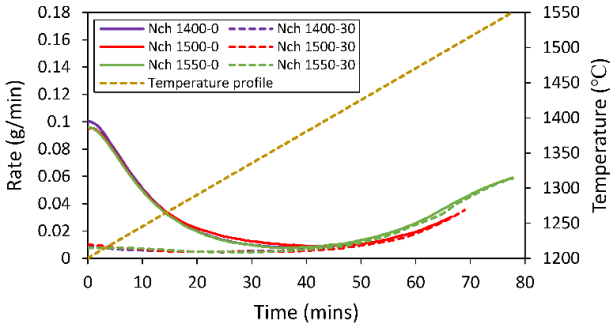

Figure 3.28: Calculated reduction rate and temperature profile, all as a function of time for Nchwaning 'Q2' series.

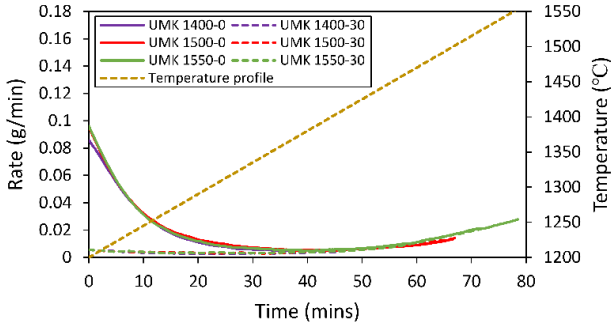

Figure 3.29: Calculated reduction rate and temperature profile, all as a function of time for Comilog 'Q1' series.

It can be seen from the rate curves that for completely reduced charges i.e., after holding for 30 minutes at 1200 °C, the reduction rate is constant for temperatures T<1400 °C. However, at T>1400 °C the reduction rate increases with increase in temperature. On the other hand, for experiments with lower prereduction extent i.e., experiments which were not held at 1200 °C, the reaction rate is high at 1200 °C and proceeds at decreasing rate until it levels up with reaction rate of completely prereduced charges. At temperature T>1400 °C the reduction rate increases following the same trend as the completely prereduced experimental series. This indicates that charges with a lower extent of prereduction will complete prereduction at a decreasing rate prior to the main MnO reduction reaction which proceeds from temperatures greater than 1400 °C.

Figure 3.30 shows a comparison of the reduction rate for the three different ores for experiments with final temperature at 1550 °C. The reduction rate curves are plotted on a different scale to clearly highlight the intrinsic differences in the reduction rate.

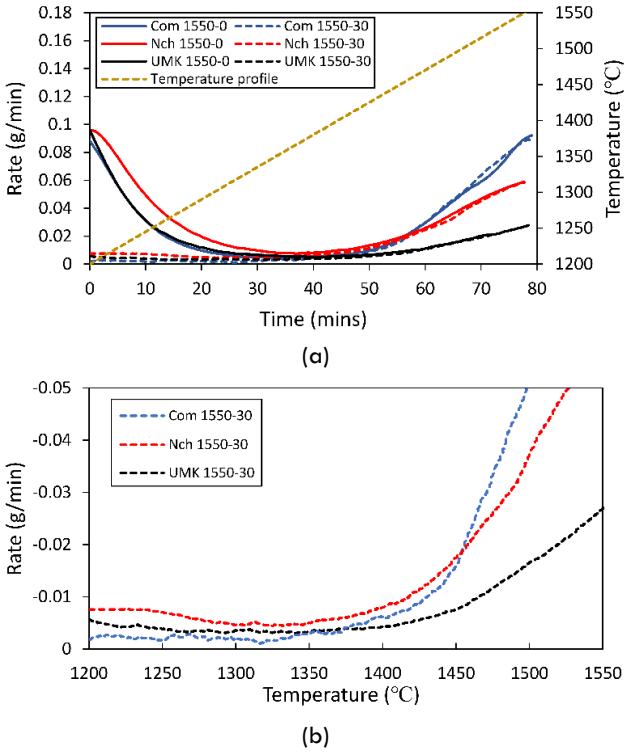

Figure 3.30: (a) Reduction rate comparison for Comilog, Nchwaning and UMK series experiments for experiment with final temperature at 1550 °C. Temperature profile is shown. (b) Reduction rate curves for completely prereduced Comilog, Nchwaning and UMK ores are shown on a different scale to indicate the differences in heating rate at T<1450 °C.

Figure 3.30(a) shows that at temperatures T<1450 °C, the reduction reaction for incompletely prereduced Nchwaning is seen to have a higher rate of reduction compared to Comilog and UMK charges. In addition, Nchwaning has a higher rate of reduction in completely prereduced charges (Figure 3.30 (b)) followed by UMK and lowest rate is observed in Comilog. With increase in temperature, the reduction rate of Comilog is seen to be higher than Nchwaning and UMK. The main result is that the slag reduction rate is higher for Nchwaning and UMK at low temperatures, whereas for Comilog the reduction rate is significantly higher at higher temperature.

3.3.2.2 Slag phase development

The slag phases from the TF1 experiments (Q series) were analysed in EPMA and the composition of the various phases are given in **Appendix C**. EPMA analyses were used to describe the phase development during reduction for the Comilog, Nchwaning and

UMK charges. Figure 3.31 shows the backscattered micrographs for slags in the Comilog 'Q1' series experiments.

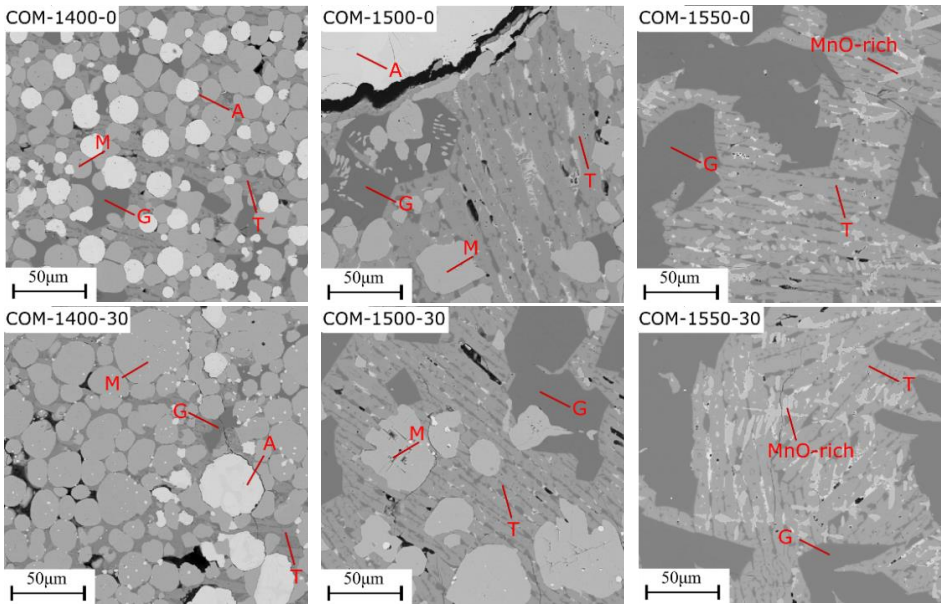

Figure 3.31: BSE images of Comilog slag samples in 'Q1' series experiments. Legend: A = alloy, M = monoxide; T = tephroite and G = galaxite.

Like IF75 results, the microstructure of Comilog slag samples contains spherical manganosite (MnO) phases in co-existence with a medium grey matrix which is tephroite ($2MnO{\cdot}SiO_2$) phase, a dark grey galaxite ($MnO{\cdot}Al_2O_3$) phase and bright alloy phase. The microstructure shows a decrease in solid monoxide phase with increasing temperature for samples from both complete and incompletely prereduced charges. Between 1400 and 1500 °C, the slag samples show presence of solid monoxide phase which implies that the reduction was relatively low. This correlates very well with low reduction as observed in the mass changes in Figure 3.24. At 1550 °C, solid monoxide has completely dissolved, and MnO-rich dendrites precipitated on cooling. This also is reflected in the significant weight loss observed from the weight loss curves (Figure 3.24). The corresponding calculated slag composition based on EPMA analyses for all charges in the Comilog 'Q1' series is shown in Table 3.23. The total MnO content in the slags are in general different than calculated composition from TGA data (Table 3.22). For example, at 1500 °C, EPMA analysis gives 51 – 53 wt.% MnO whereas TGA based calculations give approximately 37 – 40 wt.% MnO resulting in a difference of about 10 wt.%. The main reason for the discrepancy could

be due to inhomogeneity of the slag and as such the calculated compositions could not be fully representative of the whole slag matrix.

Table 3.23: Calculated liquid slag composition based on measured area fraction by ImageJ® and EPMA phase analysis for Comilog slags in 'Q1' series

*Slag sample ID		Com-1400-0	Com-1400-30	Com-1500-0	Com-1500-30	Com-1550-0	Com-1550-30
% Area fraction	Monoxide	55.2	65.5	26.7	27.7	5.4	6.90
	Tephroite	27.1	24.8	54.1	48.0	47.7	51.1
	Galaxite	17.7	9.70	19.2	24.3	46.9	42.0
Total MnO (wt pct)		77.2	84.3	67.0	65.8	51.0	53.2
Liquid composition	MnO	52.2	56.2	43.5	53.5	51.0	53.2
	FeO	1.02	0.22	0.13	0.16	0.14	0.15
	SiO_2	17.0	20.2	7.68	18.5	14.0	15.2
	Al_2O_3	22.5	17.0	41.0	19.7	26.0	23.5
	CaO	0.12	0.43	0.15	0.22	0.39	0.37
	MgO	0.29	0.19	0.57	0.38	0.82	0.80
	BaO	0.03	0.06	0.07	0.03	0.11	0.12
	TiO_2	0.29	0.37	0.36	0.39	0.48	0.51
	Total	93.4	94.6	93.4	92.9	92.9	94.0

*Ore type-temperature(℃)-holding time (mins) at 1200 ℃

Backscattered micrographs for Nchwaning 'Q2' series and UMK 'Q3' series are shown in Figure 3.32 and Figure 3.33, respectively. Their corresponding calculated slag composition are shown in Table 3.24 and Table 3.25, respectively. Common aspects of all the samples are that the microstructure of the slags consists of spherical monoxide phases in co-existence with a grey slag matrix which is believed to be liquid at high temperatures and the bright phase is the alloy produced. The monoxide phase in both Nchwaning and UMK samples, are quite significant in all samples and there is no clear variation of their concentration in the microstructures. However, for Nchwaning samples more significant alloy phases are observed compared to UMK. This indicates that more metal was produced in Nchwaning which shows that there was more slag reduction compared to UMK. This agrees with weight loss changes observed, where Nchwaning had a reduction weight about 21 wt.% compared to about 12 wt.% for UMK as seen in Figure 3.25 and Figure 3.26, respectively.

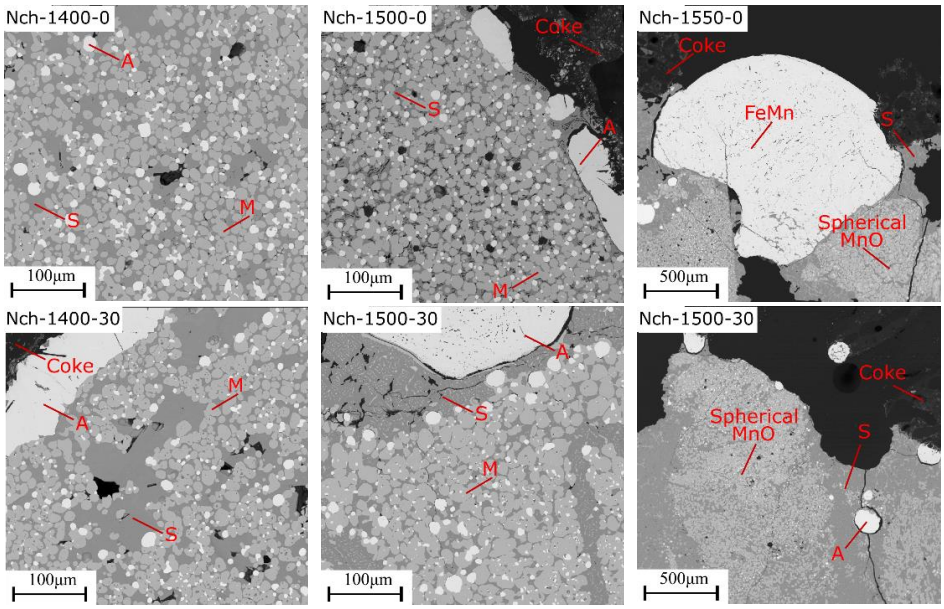

Figure 3.32: BSE images of Nchwaning slag samples in 'Q2' series experiments. Legend: A = alloy, M= monoxide; S = slag matrix.

Table 3.24: Calculated liquid slag composition based on measured area fraction by ImageJ® and EPMA phase analysis for Nchwaning slags in 'Q2' series

Slag sample ID		Nch-1400-0	Nch-1400-30	Nch-1500-0	Nch-1500-30	Nch-1550-0	Nch-1550-30
% Area fraction	Monoxide	62.2	53.7	66.6	60.7	46.1	41.4
	Slag matrix	37.8	46.3	33.4	39.3	53.9	58.6
Total MnO (wt pct)		60.3	69.0	71.6	71.4	54.4	50.2
Liquid composition	MnO	42.3	37.4	28.1	34.5	26.0	25.0
	FeO	0.3	0.5	0.5	0.5	0.6	0.1
	SiO_2	30.9	31.9	31.5	30.6	25.9	31.4
	Al_2O_3	0.1	0.2	0.5	0.1	10.1	0.7
	CaO	19.8	24.5	33.4	27.3	22.7	33.6
	MgO	1.3	1.9	1.7	1.3	2.0	4.0
	BaO	0.1	0.03	0.03	0.1	4.0	0.2
	TiO_2	0.03	0.01	0.03	0.04	0.7	0.1
	Total	94.8	96.5	95.7	94.5	91.9	95.0

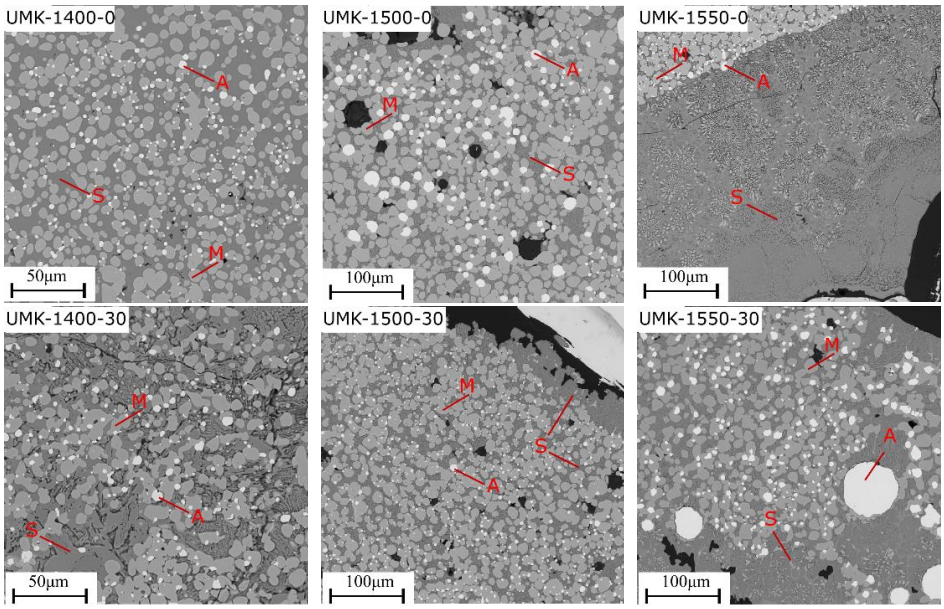

Figure 3.33: BSE images of UMK slag samples in 'Q3' series experiments. Legend: A = alloy, M= monoxide; S = slag matrix.

Table 3.25: Calculated liquid slag composition based on measured area fraction by ImageJ® and EPMA phase analysis for UMK slags in 'Q3' series

Slag sample ID		UMK-1400-0	UMK-1400-30	UMK-1500-0	UMK-1500-30	UMK-1550-0	UMK-1550-30
% Area fraction	Monoxide	48.0	46.9	65.1	60.8	45.0	49.5
	Slag matrix	52.0	53.1	34.9	39.1	55.0	50.5
Total MnO (wt pct)		57.2	51.9	66.2	60.1	55.0	52.2
Liquid composition	MnO	26.4	25.0	23.4	21.0	26.3	27.7
	FeO	0.4	0.4	0.8	0.5	0.1	0.1
	SiO_2	32.5	32.5	25.6	21.4	31.8	20.1
	Al_2O_3	0.1	0.03	15.8	22.6	0.5	17.2
	CaO	33.4	33.8	24.7	26.4	34.6	26.0
	MgO	3.7	4.9	1.4	1.7	2.7	1.5
	BaO	0.1	0.1	2.5	0.4	0.01	1.4
	TiO_2	0.03	0.02	0.5	0.6	0.1	0.6
	Total	96.7	96.8	94.7	94.5	95.8	94.6

The slag phase development as reflected in the microstructures for Comilog (Figure 3.31), Nchwaning (Figure 3.32) and UMK (Figure 3.33) charges have shown considerable differences in terms of reduction degrees for the three charges. The images shows that the slag contained a solid phase and liquid phase and show that the reduction process has not reached the liquidus slag composition in these experiments for both Nchwaning and UMK, only for Comilog charges. Considering that the initial MnO content in the primary slag were 84 wt.%, 73 wt.% and 64 wt.%, respectively for Comilog, Nchwaning and UMK charges, the reduction degree is seen

to be highest for Comilog followed by Nchwaning and lastly UMK. The slag compositions from Table 3.22, Table 3.23, Table 3.24 and Table 3.25, clearly show the different MnO reduction extents in the three charges. In addition, the degree of reduction in all the charges is independent of the extent of the prereduction.

3.3.3 R-series: Prereduction behavior in induction furnace

3.3.3.1 Variation of O/Mn ratio with temperature

The industrial furnace process was simulated in an induction furnace setup with temperatures on top of the cokebed held at 1200 °C, 1300 °C and 1400 °C for Comilog, Nchwaning and UMK ores. These ores were unmixed and mixed with coke on parallel studies. The variation of O/Mn ratio as a function of temperature, which indicates the extent of prereduction of Comilog, Nchwaning and UMK ores is shown in Figure 3.34. Temperature corresponds to the stable temperature measured at the level the reduced ore samples were excavated.

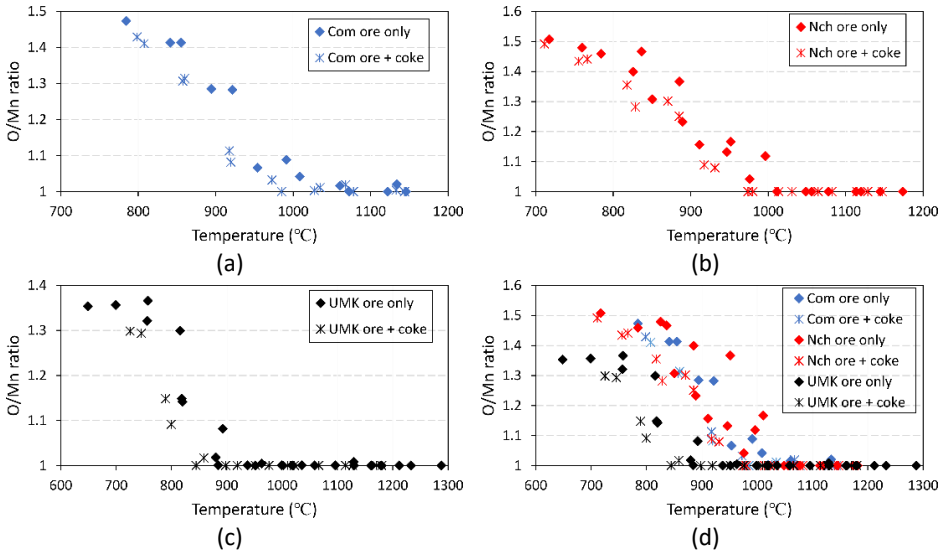

Figure 3.34: Variation of O/Mn ratio in manganese ores as a function of temperature for (a) Comilog ore, (b) Nchwaning ore, (c) UMK ore and (d) a comparison of the three ores.

The ores are completely prereduced when approaching the highest temperature zone of the furnace. That is, the O/Mn ratio decreases with increasing temperature following the vertical temperature gradient of the crucible. In a mixture consisting of 90 wt. % ore + 10 wt. % coke reductant, the O/Mn ratio is in general lower than the prereduction of ore only as can be seen in Figure 3.34 for the three

ores. This implies that addition of coke increases the extent of prereduction of manganese ores. Considering ores not mixed with coke, Figure 3.34(c) shows that UMK is prereduced completely i.e., reaches O/Mn ration equal to 1.0 at temperatures lower than both Nchwaning and Comilog. In comparison to Comilog and Nchwaning ores which reaches an O/Mn ratio of 1 within the same area at about 950 °C, UMK ore has an O/Mn ratio of 1 at approximately 100 °C lower temperature. As such, UMK ore shows the highest extent of prereduction compared to Comilog and Nchwaning ores.

3.3.3.2 Porosity development and carbonates decomposition

The porosity and the residual carbonate content (given as CO_2 content) all as a function of temperature for the excavated ores from the experiments are presented in Figure 3.35. Manganese ores are heterogeneous and hence variation in properties from particle to particle can be significant. Porosity is measured for single particles and as such, a large variation in porosity is expected.

The trendlines shown in Figure 3.35 were calculated using Lowess filter with a smoothing parameter of 0.35. It can be seen that ore porosity increases with increasing temperature during heating and reduction. The peak porosity of Comilog and Nchwaning during reduction is around 1000 °C, whereas for UMK it is at about 850 – 950 °C. In UMK ore (Figure 3.35(c)), the porosity is seen to decrease with increasing temperature beyond the temperature range where the porosity was highest. This decrease in porosity is mainly attributed to the sintering of the particles which was observed during the sample 'digouts', when approaching the high temperature regions greater than 1100 °C. There is no clear distinction on the effect on porosity when the ores are mixed with coke.

As shown in Figure 3.35(a), Comilog ore shows negligible CO_2 contents. This is so because Comilog ore does not contain carbonate minerals and the analyzed CO_2 could be from coke dust contaminating the ore particles. Carbonates in Nchwaning ore are also seen to decompose with increasing temperature up 900 °C with some outliers since the initial CO_2 content measured in Nchwaning ore was 4.45 wt. % as presented in Table 3.1. The high carbonate content in some particles at elevated temperatures, as seen in Figure 3.35(b) could be pockets of undecomposed carbonates resulting from ore heterogeneity since minerals are typically unevenly distributed. The decomposition of carbonates in UMK ore (Figure 3.35(c)) shows dependency on temperature with increasing temperature resulting in a decrease residual CO_2. The trend shows that carbonates in UMK ore decompose with increase in temperature up to 900 °C, after

which carbonate decomposition is complete. The rapid increase in porosity in UMK ore with increase in temperature is correlated to a decrease in residual CO_2 content. Hence, it is believed that the rapid increase in porosity in UMK is due to decomposition of carbonates leaving voids in the ore particles.

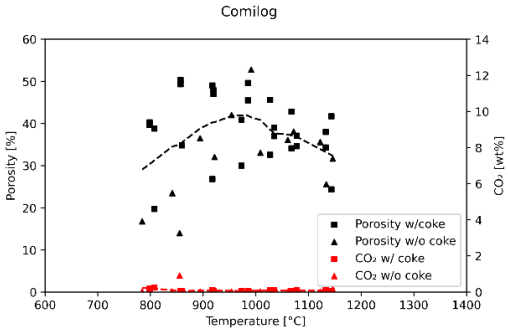

(a)

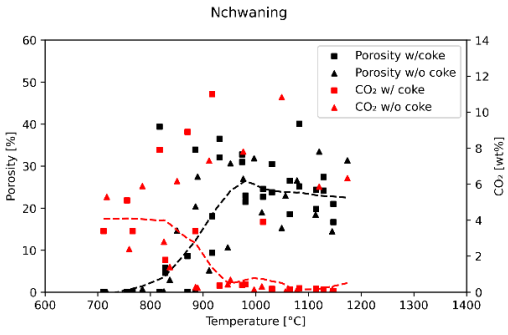

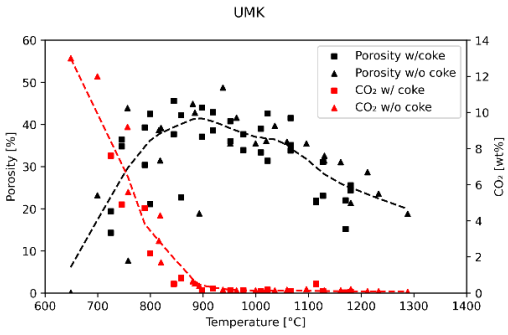

(c)

Figure 3.35: The development of porosity and decomposition of carbonates as a function of temperature for (a) Comilog, (b) Nchwaning and (c) UMK ores.

3.3.4. S-series: Manganese ore prereduction in CO/CO_2 atmosphere

3.3.4.1 Weight reduction behavior and change in O/Mn ratio

Comilog, Nchwaning and UMK ores with particles size range 10 – 12.5 mm were heated non-isothermally in 70/30 CO/CO_2 atmosphere at heating rates of 3, 6 and 9 °C/min with a target temperature of 1000 °C. The weight loss and the corresponding change in O/Mn ratio calculated through mass loss, all as a function of both temperature and time are shown in Figure 3.36. The three ores are differentiated by colour and the three heating rates are differentiated by dashed line patterns.

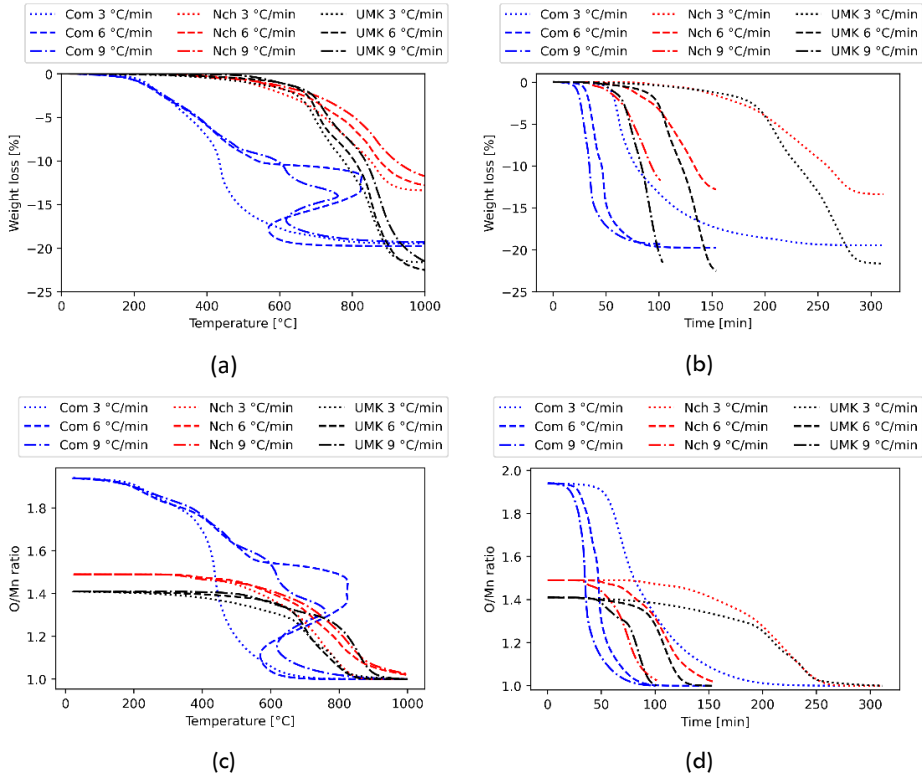

Figure 3.36: Weight loss (wt.%) as a function of (a) temperature and (b) time. O/Mn ratio as a function of (c) temperature and (d) time, all for Comilog, Nchwaning and UMK ores (10 to 12.5 mm particles). The TGA and calculated O/Mn curves are at heating rates of 3, 6 and 9 °C/min all at 70 % CO and 30 % CO_2.

Mass loss during prereduction increases with increase in temperature. Comilog ore which has a higher initial O/Mn ratio of 1.93, forms a "Z-shape" in the weight loss

vs temperature curve. This is due to exothermic reduction reactions, which causes the measured temperature to increase above the programmed temperature. Nchwaning and UMK are Mn_2O_3 based ores and their prereduction starts from an initial O/Mn ratio of 1.50 and 1.45, respectively. Figure 3.36(a) shows that UMK has the highest weight loss followed by Comilog and lastly, Nchwaning. As presented in Table 3.4, a greater part of the weight loss in UMK ore is from decomposition of carbonates, which is 4 times as large as the weight loss contribution from prereduction reactions. The weight loss in Comilog can be attributed to prereduction reactions and water evaporation as it contains higher manganese oxides MnO_2 and water content of about 3.8 wt. %. Nchwaning is an Mn_2O_3 ore, with lower carbonate content compared to UMK has weight loss contribution from prereduction and carbonate decomposition.

As seen in Figure 3.36, the very exothermic reactions observed when prereducing Comilog occurs very close to 500 °C at heating rates 6 °C/min and 9 °C/min. This exothermic peak rapidly increases the temperature close to or exceeding 800 °C. At a heating rate of 3 °C/min the exothermic peak is not significant due to better temperature control in the furnace. Low heating rate will give sufficient time for reduction of MnO_2 to Mn_2O_3, hence if all MnO_2 is reduced to Mn_2O_3 before 500 °C, the exothermic peak will not occur to the same extent as 6 and 9 °C/min[75]. Weight loss in Comilog starts at approximately 200 °C and Comilog has an O/Mn ratio very close to 1 at 800 °C. Between 400 and 600 °C it can be seen that the lower heating rate gives a lower O/Mn ratio at a given temperature. Nchwaning shows a clear distinction of the effect of heating rate on prereduction, with a lower heating rate of 3 °C/min giving rise to a higher extent of prereduction. The prereduction of Nchwaning commences at about 350 °C and the prereduction is complete by 1000 °C. On the other hand, the prereduction of UMK commences at slightly higher temperature at 500 °C compared to Nchwaning and is completely prereduced by 900 °C. The prereduction behavior of the three ores highlight that in a high and constant CO/CO_2 atmosphere Comilog ore will be prereduced to O/Mn ratio of 1 at lower temperatures compared to Nchwaning and UMK ores.

The chemical composition of reduced samples from these experiments heated up to 1000 °C are shown in Table 3.26.

Table 3.26: Chemical analysis of Comilog, Nchwaning and UMK samples exposed to non-isothermal reduction.

Ore	Temp. (°C)	Heating Rate (°C/min)	$Fe_{,tot}$	$Mn_{,tot}$	MnO_2	SiO_2	Al_2O_3	CaO	MgO	K_2O	CO_2	Ratio O/Mn
			(wt.%)									
Com	1000	3	2.28	66.5	3.79	2.97	5.13	0.11	0.12	1.05	0.11	1.04
	1000	6	3.00	64.0	5.22	3.30	6.82	0.10	0.12	1.00	0.10	1.05
	1000	9	2.99	65.2	5.64	3.91	5.15	0.11	0.04	0.97	0.11	1.05
Nch	1000	3	11.5	52.9	0.05	4.61	0.53	7.86	1.19	0.05	0.20	1.00
	1000	6	11.4	49.4	0.05	7.41	0.42	8.49	1.97	0.06	0.37	1.00
	1000	9	12.6	51.7	0.05	3.62	0.40	7.35	1.15	0.11	0.22	1.00
UMK	1000	3	14.1	41.4	0.05	7.17	0.49	16.1	3.20	0.15	0.11	1.00
	1000	6	10.0	42.3	0.05	6.82	0.53	19.7	3.56	0.11	0.22	1.00
	1000	9	10.9	42.0	0.05	6.95	0.29	17.9	3.35	0.08	0.29	1.00

As presented in Table 3.26, the O/Mn ratio was 1 in reduced Nchwaning and UMK ore samples. This is an indication that the ores are completely prereduced at this temperature. On the other hand, the O/Mn ratio in reduced Comilog samples lies between 1.04 and 1.05. Although the O/Mn ratio in reduced Comilog is slightly higher than 1, complete prereduction is believed to be obtained in these samples. This is so, considering that the recorded weight remains stable for a period between about 900 °C to 1000 °C. In addition, the variations could be due to uncertainty in analyses[138] and some oxidation in reduced Comilog ore[139].

3.3.4.2 Reduction rate and decomposition of carbonates

Figure 3.37 shows the reduction rate of the ores as a function of temperature for all the three heating rate scenarios. The reduction rates (wt. %/s) are calculated from change in weight per unit time. The rate of reaction varies with heating rate, with decreasing heating rate resulting in longer time at each temperature and lower reaction rate. As shown in Figure 3.37(a), the exothermic peak in Comilog reaches a higher temperature at a heating rate of 6 °C/min compared to 9 °C/min. This is an anomaly in the experiment as a higher exothermic peak is expected at a higher heating rate of 9 °C/min. For Nchwaning (Figure 3.37 (b)), the rate of reduction curves are characterized by the highest peak occurring at about 900 °C. At temperatures less than 900 °C, the lower peaks are less pronounced with decreasing heating rate. As shown in Figure 3.37(c), the prereduction of UMK ore is characterized by two distinctive peaks, the first one occurring at approximately 700 °C, and the second peak at a higher temperature i.e., 900 °C. The peaks in the prereduction of UMK ore reduce in size with decreasing heating rate, due to the longer time at each temperature.

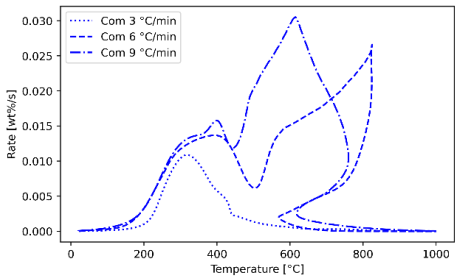

(a)

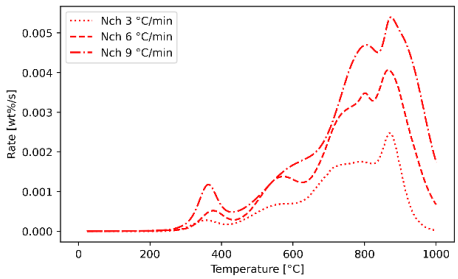

(b)

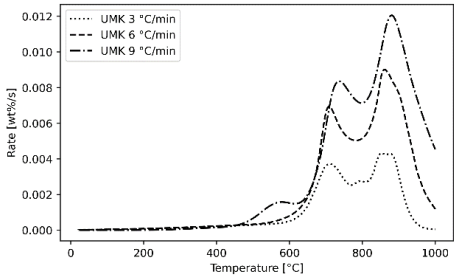

(c)

Figure 3.37: Variation of rate (wt. %/sec) with temperature for Comilog, Nchwaning and UMK ores (10 to 12.5 mm), heated at 3, 6 and 9 °C/min in a 70 wt.% CO and 30 wt.% CO_2 atmosphere.

The reactions occurring at the distinctive peaks in Nchwaning and UMK ore were evaluated by conducting non-isothermal experiments at 9 °C/min in 70/30 CO/CO_2 gas atmosphere, with final temperatures at the peak regions. The final temperatures were 700, 800 and 900 °C for UMK whereas for Nchwaning the experiment was ended at 900 °C. The chemical composition of the reduced samples from these experiments are shown in Table 3.27.

Table 3.27: Chemical analysis of Nchwaning heated up to 900 °C and UMK samples heated up to 700, 800 and 900 °C.

Ore	Temp. (°C)	Heating Rate (°C/min)	$Fe_{,tot}$	Mn, $_{tot}$	MnO_2	SiO_2	Al_2O_3	CaO	MgO	K_2O	CO_2	Ratio O/Mn
			(wt.%)									
Nch	900	9	9.69	49.4	6.55	4.10	0.57	9.06	1.92	0.10	2.4	1.08
UMK	700	9	5.08	36.4	16.4	6.79	0.47	16.0	3.11	0.19	13.0	1.29
	800	9	4.60	43.8	13.7	7.03	0.46	15.1	2.79	0.10	8.8	1.20
	900	9	13.1	39.7	0.05	6.55	0.37	16.3	3.65	0.13	1.4	1.00

Nchwaning and UMK ores have initial carbonate content measured as CO_2 at 4.5 wt. % and 15.9 wt.%, respectively (listed in Table 3.1). The chemical composition presented in Table 3.27, show significant decrease in carbonate content for

Nchwaning and UMK at the investigated temperatures. It can also be seen for UMK ore that between 700 °C and 800 °C, the O/Mn ratio ranges between 1.29 to 1.20, which implies that carbonates are decomposing in parallel to prereduction reactions. At 900 °C prereduction reactions in UMK are complete prior to complete decomposition of carbonates. The percentage of decomposed carbonates at each peak temperature from Nchwaning and UMK ore was calculated from initial values and the results are shown in Figure 3.38.

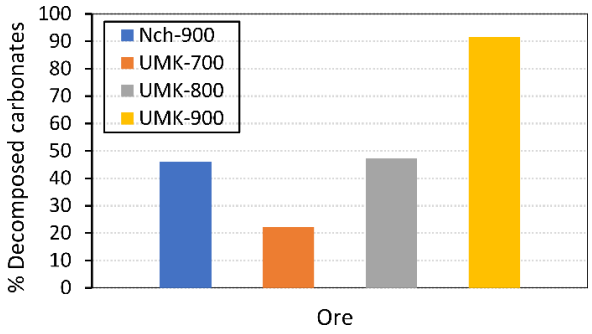

Figure 3.38: Fraction of carbonates decomposed in Nchwaning and UMK as a function of temperature. Legend: ore type-final temperature (°C) e.g., Nch-900.

3.4 Discussion

The previous section (**section 3.3**) presented the results from laboratory scale experiments. In a similar flow, the presented results will be analyzed and discussed in this section. The first segment discusses the phase development and reduction of slag as a function of temperature and in relation to position within the cokebed. The discussion in the second segment will focus on the effect of extent of prereduction on the slag reduction based on the TGA results from TF1 experiments. In the last segment, the discussion will be centered on prereduction behavior of Comilog, Nchwaning and UMK ores with solid carbon and in CO/CO_2 atmosphere.

3.4.1 Reduction of MnO from slag

3.4.1.1 Overview

The reaction system in ferromanganese production involves five phases namely, liquid slag with solid MnO, metal, carbon, and gas. To give an overview of the slag reduction

in ferromanganese production, a simplified illustration of the slag-cokebed system shown in Figure 3.39 will be considered.

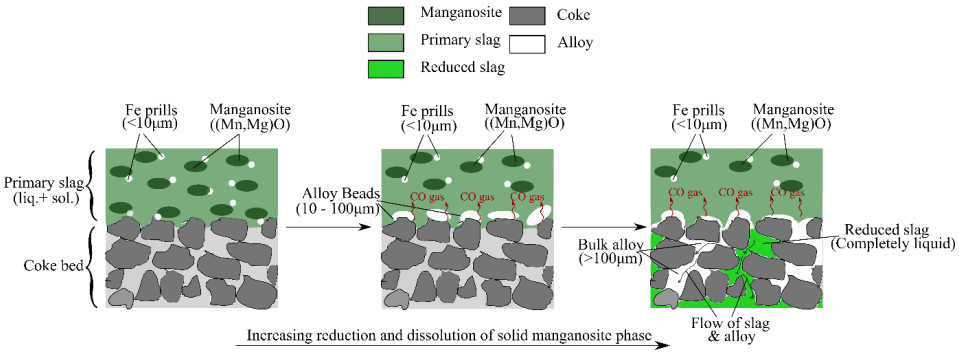

Figure 3.39: A schematic illustration of the interactions in the slag-coke bed system

The presented schematic is stepwise for clarity even though the process is continuous. As seen in the phase development in Comilog, Nchwaning and UMK ores (**Section 3.3.1.1 – 3**), the initial slag formed is mainly liquid + solid monoxide phase. The initial alloy form Fe prills mainly located in areas outside and adjacent to the solid monoxide phase. This indicates that Fe is formed at the transition from prereduction zone to cokebed zone at about 1200 °C when the ore is softened prior to melting and slag reduction in coke bed. The alloy droplets increase in size as well as wt % Mn and wt. % C. This is due to an increased proximity to reductant carbon, where it is reasonable to consider MnO reduction to be highly significant at the slag/coke interface. At equilibrium, the activity of MnO is equal in the solid monoxide phase and liquid phase. Therefore, the activity of MnO remains high in the presence of solid monoxide. On the other hand, metallic iron lowers the Mn activity in the reaction system to increase reduction of MnO at the slag/coke interface and the Mn is added to the iron metal prills, thus increasing the wt. % Mn. The presence of solid monoxide phase will make the slag highly viscous. However, reduction occurs on top of the coke bed with an increased dissolution of monoxide in slag rendering the slag fluid enough to trickle down the coke bed. Not much reduction occurs inside the coke bed area due to the lower MnO activity which emanates from complete dissolution of solid monoxide phase. As such, the slag will be tapped at a composition close to the liquidus compositions.

3.4.1.2 Monoxide phase development and its dissolution in slag

The solid monoxides and liquid slag phase are of great importance in the manganese smelting process[140]. During the production of ferromanganese, the coexistence of a solid phase and a liquid slag phase is important to explain the high MnO activity in the slag as well as affect the viscosity of the slag. As such, a special focus is placed on the development of the monoxide phase.

The phase change from solid to liquid is dependent on temperature and chemical composition of the prereduced ore. As the ore is heated, the original phases in the ore will change into a solid monoxide phase and a liquid phase according to the ore composition. Experimentally, the fraction of solid monoxide phase on top of the cokebed in Comilog was observed to considerably decrease during reduction. On top of the cokebed a liquid slag is in coexistence with solid MnO phase in the temperature range 1217 °C – 1410 °C, and 5 cm below the top of the cokebed i.e., at 1410 °C slag was observed to be completely liquid. This shows that liquid slag from Comilog flows into the cokebed at temperatures close to 1410 °C. This is slightly higher than the temperature for complete dissolution of monoxide phase i.e., 1350 °C based on equilibrium calculations from FactSage. Based on the same analysis, Nchwaning slag is observed at 5 cm inside the cokebed at the higher temperature of 1505 °C compared to Comilog. In UMK, a liquid slag is in coexistence with solid MnO phase on top of the cokebed in the temperature range 1223 °C – 1367 °C. No complete dissolution of monoxide phase was observed as the temperature was low and therefore no sufficient reduction of the liquid slag occurred. It is envisaged that UMK will require temperatures higher than 1500 °C to achieve sufficient reduction of slag and dissolution of monoxide phase. . According to the thermodynamics, the UMK ore should be reduced in the same area as the Comilog and Nchwaning ore, and the lack of reduction is hence determined by the kinetics. As the extent of solid MnO phase is larger in the UMK ore, the primary slag will be more viscous, and hence this will have reduced the reduction rate. This is in agreement with results by Oslø[141], where a higher basicity in the ore reduces the reduction rate in the two phase area of solid MnO and a liquid phase.

From the thermodynamic analysis of the phase development in the primary slag presented in Figure 3.20, Comilog is seen to have a higher primary liquid slag formation per unit temperature compared to both Nchwaning and UMK. During heating, the monoxide phase in Comilog dissolves in liquid at 1750 °C, which is lower

than 1900 °C for Nchwaning and 1850 °C for UMK as presented in Figure 3.20. This is dependent on the total Mn content and the basicity of the ore.

The initial slag formation temperature during carbothermic reduction is lower for Comilog at 1150 °C than that for Nchwaning and UMK at 1200 °C and 1250 °C, respectively. However, the dissolution of the monoxide solid solution is dependent on the composition of the ore and charge mixture as previously reported[21], [93], [95]. Comilog ore forms a monoxide solution which is purely MnO since the ore has negligible MgO content. This is seen in monoxide phase compositions from EPMA (Table 3.10) which are in close agreement with those calculated in FactSage (Table 3.17). As temperature increases and reduction in the liquid slag proceeds, the solid MnO phase in Comilog completely dissolves in the liquid slag at 1350 °C at equilibrium conditions as shown in Figure 3.20(b).

In contrast to Comilog, the monoxide solution phase in Nchwaning and UMK did not dissolve completely in liquid slag as shown in Figure 3.20 (d) and Figure 3.20 (f), respectively. The monoxide phase chemistry in Nchwaning and UMK ores are different from Comilog ore, as they form a (Mn,Mg,Fe)O monoxide solid solution phase. This (Mn,Mg,Fe)O solid solution becomes enriched in MgO with increasing temperature and dissolution in liquid slag as presented in Table 3.17. Based on EPMA analysis of the monoxide phase in Nchwaning and UMK slag samples, the monoxide phase in Nchwaning and UMK exhibit MgO enrichment, however not to the same values thermodynamically predicted in FactSage 8.3. In addition, the composition of the monoxide phase in Nchwaning and UMK shows significantly higher FeO contents compared to predicted values in FactSage 8.3. In the induction furnace experimental setup CO gas flows are low due to limited metal producing reactions and the ore material is not mixed with carbon reductant. As such higher iron oxides are reduced to FeO instead of Fe and FeO becomes stabilized in the monoxide solid solution. This could be a probable explanation for the inconsistency between experimental values and FactSage based equilibrium calculations. Contrastingly, previous studies [21], [95], [142] on manganese ores mixed with carbon which were conducted in a relatively high and constant CO gas flow have shown the solid monoxide phase to be pure MnO or (Mn,Mg)O solid solution.

Based on monoxide phase dissolution into slag, Comilog is expected to be fluid enough to percolate through the coke bed at temperatures around 1400 °C. These temperatures are low when compared to Nchwaning and UMK which have a considerable quantity of solid monoxide spheres. Equilibrium calculations for the UMK

slags shows that there is formation of high melting point silicates which are predominantly Ca_2SiO_4, Mg_2SiO_4 and Mn_2SiO_4. However, these have not been observed experimentally from EPMA analysis of UMK slags. These silicates make the slag highly viscous and with dissolution of MnO in liquid during reduction, the silicates remain solid thus making the slag highly viscous. This implies that Nchwaning and UMK ores needs higher temperature to behave as a fluid compared to Comilog due to a higher amount of basic oxides, and hence a higher quantity of solid monoxide spheres. The dissolution and slag reduction behaviour of Comilog, Nchwaning and UMK ores agrees with findings in earlier works[97], [98], [102], [103], where materials with higher acid oxides (e.g. Comilog ore) melt and reduce at a lower temperature than materials with higher basic oxides (e.g. Nchwaning and UMK).

The composition of the monoxide phase in both the induction furnace experiments and TGA experiments are compared to the equilibrium composition all as a function of temperature as shown in Figure 3.40 for Comilog ore, Figure 3.41 for Nchwaning ore and lastly Figure 3.42 for UMK ore.

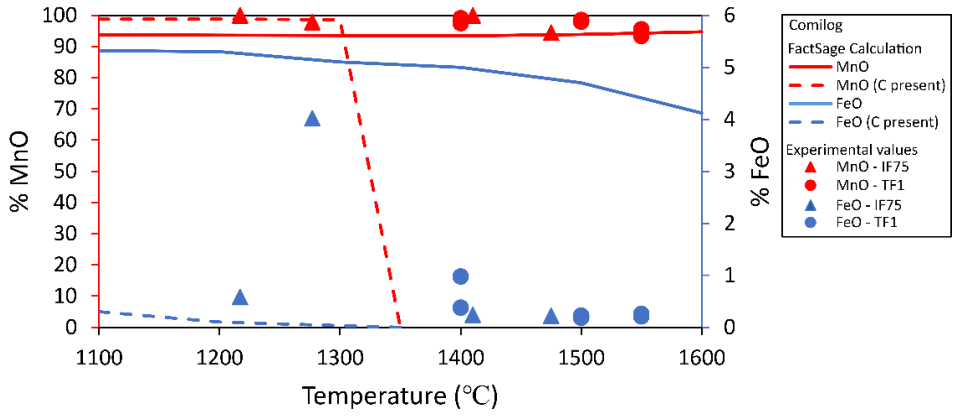

Figure 3.40: Composition of the monoxide phase as a function of temperature in Comilog ore. Experimental measured values from EPMA analysis are shown for both IF75 and TF1 experiments.

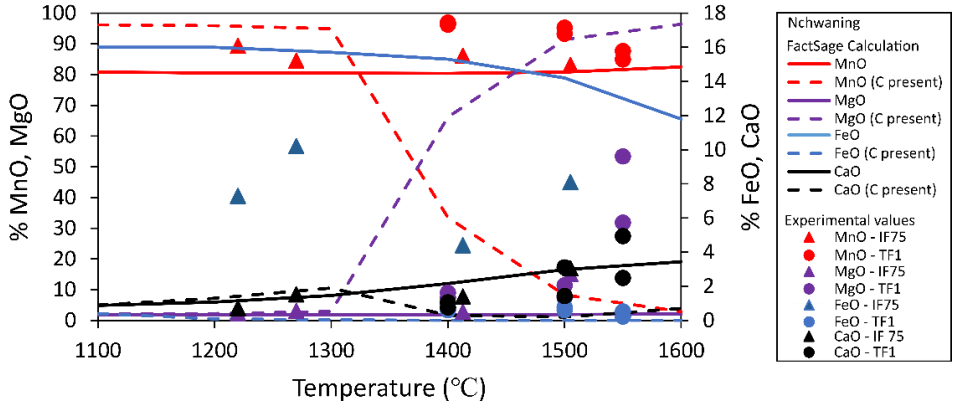

Figure 3.41: Composition of the monoxide phase as a function of temperature in Nchwaning ore. Experimental measured values from EPMA analysis are shown for both IF75 and TF1 experiments.

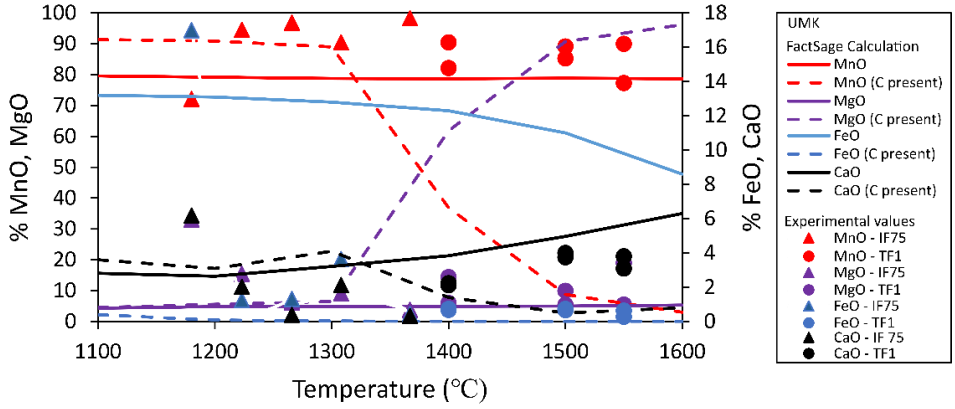

Figure 3.42: Composition of the monoxide phase as a function of temperature in UMK ore. Experimental measured values from EPMA analysis are shown for both IF75 and TF1 experiments.

As presented in Figure 3.40, FactSage based equilibrium calculation of Comilog shows that in the absence of carbon, the monoxide phase is (Mn,Fe)O solid solution with approximately 5 wt.% FeO which decreases to 4 wt.% with increasing temperature. FeO is seen to be of low concentration below 1 wt.% in the presence of carbon and is completely reduced below 1300 °C. This implies that during reduction the monoxide phase is purely MnO and this is confirmed by experimental values were the monoxide composition shows mostly MnO and less than 1 wt.% FeO as analysed in EPMA in both IF75 and TF1 experiments, except for about 4wt.% FeO at

approximately 1280 °C in IF75. Hence, the monoxide phase in Comilog reduction was confirmed to be predominantly pure MnO.

Based on equilibrium calculations in FactSage, Figure 3.41 and Figure 3.42 shows that, in the absence of carbon, the monoxide phase in both Nchwaning and UMK, respectively is a (Ca,Mn,Fe)O solid solution. The differences in the monoxide composition of these ores are that UMK ore has relatively high content of CaO and MgO and relatively lower FeO content compared to Nchwaning ore. In the presence of carbon reductant, the monoxide phase in both Nchwaning and UMK becomes enriched in MgO with subsequent lowering of CaO and MnO at temperatures greater than 1300 °C. All FeO is reduced below 1200 °C. However, experimentally, the monoxide in Nchwaning have a higher FeO content in the monoxide compared to UMK as can be seen in the data for IF75 experiments. This is expected as Nchwaning ore has a higher Fe content at 9 wt.% compared to 4.7 wt.% in UMK. The MgO enrichment of monoxide phase is observed experimentally in both Nchwaning and UMK ore but not to the same extent as predicted by equilibrium calculations in FactSage. Equilibrium calculations in FactSage has been used as tool to describe the monoxide phase composition and its dissolution in the liquid slag for the three ores. This is so because the path from unreduced primary slag to tapped metal and slag will be influenced by equilibrium conditions. However, the slag and metal in FeMn furnaces are not believed to be in chemical equilibrium.

3.4.1.3 Slag reduction path

The composition of the liquid slag in coexistence with the solid monoxide phase and after complete dissolution for Comilog, Nchwaning and UMK have been presented in Table 3.11, Table 3.13 and Table 3.15, respectively. Before the reduction commences, the primary slags show a liquid slag in co-existence with solid MnO. In the temperature range 1410 °C to 1475 °C, the reduction of the primary slag from Comilog ore was observed to take place from about 85 wt. % MnO in the presence of two stable phases, manganosite + liquid slag down to the liquidus composition of about 63 wt % MnO. Thereafter, the further reduction goes through the liquid phase down to the final composition of about 45 – 52 wt. % MnO (Table 3.11). This means that the Comilog slag reaches liquidus composition close to 1475 °C. A similar mechanism is also observed for the reduction of the primary Nchwaning slag. At temperatures from 1413 °C to 1505 °C, the reduction of the primary slag from Nchwaning ore will take place from about 74 wt. % MnO in the presence of two stable phases, manganosite + liquid

slag, down to the liquidus composition of about 34 wt. % MnO. Further reduction takes through the liquid phase down to the final composition of about 22 – 17 wt. % MnO at 1505 °C. As such the slag from Nchwaning ore will not reach a completely liquid slag at temperatures below 1505 °C during the reduction in the presence of two stable phases, manganosite + liquid. The relatively small difference between the MnO content at liquidus composition and the content in the final slag inside the coke bed is an indication that significant reduction occurs on top of the coke bed and the MnO content in the final slag is close to the liquidus composition. Typical slag tapping temperatures from industrial SAF have been reported at 1450 °C to 1500 °C[2]. FactSage based calculation of the content of MnO in the liquidus composition at 1500 °C for the reduced Comilog ore was 39.7 wt. % and 14.4 wt. % for Nchwaning which is in close agreement with industrial data[2]. Similarly, the reduction of UMK primary slag will commence from about 70 wt. % MnO in the presence of two stable phases, manganosite + liquid slag and based on equilibrium calculations the final slag composition will contain about 9.0 wt. % MnO at 1500 °C.

The liquidus compositions are highly dependent on the basicity of the slag. The basicities for Comilog, Nchwaning and UMK were 0.1, 0.9 and 2.1, respectively. As shown in Figure 3.43, basic ores i.e., Nchwaning and UMK ores, were observed to have a lower MnO content in the liquid slag phase compared to an acidic Comilog ore which is consistent with previous findings [2], [95]. A liquid slag phase on top of the coke bed which coexist with the solid monoxide was observed to have a higher MnO content than calculated liquidus composition for both Comilog and Nchwaning slags. This shows that the experimental system was not at equilibrium. Some inconsistencies are observed in UMK ore as well, which are attributed to the heterogeneity of manganese ores. It is important to note that FactSage equilibrium calculation results cannot account for the heterogeneity of the ores. The MnO content in the liquid slag phase for Comilog and Nchwaning slags inside coke bed is slightly lower than slags on top of the coke bed which shows that much of the reduction occurs on top of the coke bed. The discrepancies between EPMA determined and calculated phases and compositions exist, since the concentration of chemical species are calculated under the assumption that compounds react to reach a state of equilibrium which is hardly ever achieved.

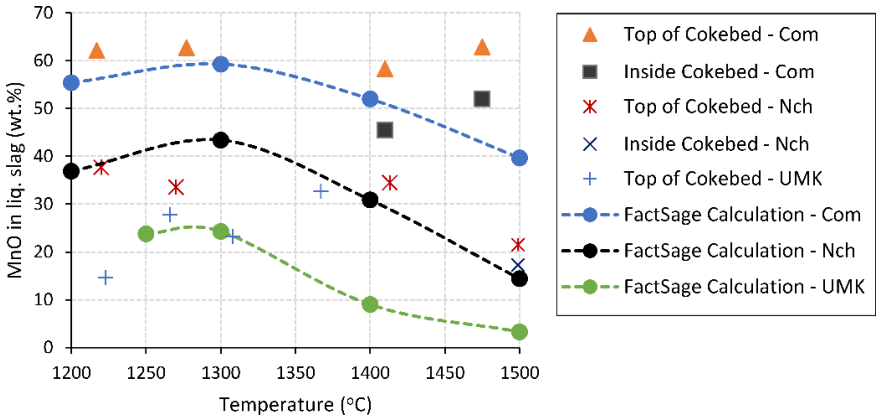

Figure 3.43: Calculated equilibrium content of MnO versus temperature for the liquid phase in the presence of carbon. Experimental MnO contents versus temperature in the liquid phase relative to their position within the coke bed zone are indicated.

The equilibrium composition of the alloy phase formed during carbothermic reduction of Comilog, Nchwaning and UMK slags presented in Table 3.20 is highly dependent on temperature. The alloy phase is mainly Fe at the start of the reduction and becomes enriched in manganese with increase in temperature and further reduction of dissolved MnO. In addition to temperature, metallization has been shown to vary considerably with size of alloy droplets, with the Mn/Fe ratios increasing with increase in alloy particle size. Metallization begins with metallic iron nucleation adjacent to the solid monoxide spheres within the liquid slag as shown in micrographs for Comilog, Nchwaning and UMK (i.e., Figure 3.15, Figure 3.17 and Figure 3.19, respectively).

3.4.1.4 Effect of extent of prereduction on slag reduction

In TF1 experiments (**section 3.3.2**), holding time for 30 minutes has been used as an experimental parameter to create different prereduction extents prior to the main metal producing reaction i.e., MnO + C = Mn + CO. This ensures complete prereduction when samples were held at 1200 ℃ for 30 minutes and vice versa when no holding time was used. Analysis of the reduction extents as expressed by the final weight loss and MnO content in the final slag has shown that the end point is independent of the prereduction extent. As presented in the reduction curves, it is seen that prereduction will complete at a decreasing reduction rate in the low temperature range 1200 – 1400 ℃. Thereafter, the reduction rate increases with temperature following the same reduction rate similar to completely prereduced charge. This

implies that the metal producing reaction is not affected by the extent of prereduction. Hence, ore prereduction completes first before the final metal formation reaction at higher temperatures.

The TGA data and the corresponding rate curves showed considerable differences between the different charges. Comparing the weight loss curves (i.e., Figure 3.24, Figure 3.25 and Figure 3.26) shows that Nchwaning will have a higher weight loss followed by UMK and lastly Comilog at temperatures T<1400 °C. At this temperature the reduction rate is however very slow for all three ores. With increase in temperature up to 1550 °C, Comilog shows the highest weight loss followed by Nchwaning and lastly UMK. As such, the reduction rate is higher for Nchwaning and UMK at low temperatures, whereas for Comilog the reduction rate is significantly higher at higher temperature. Similar observations are shown in the calculated reduction rate curves versus temperature presented in Figure 3.30(b). The findings are reasonably consistent with previous studies by Xiang et al.,[95] and Ngoy et al., [143], though this study exhibits lower mass loss due to reduction for similar investigated temperatures.

The higher reduction rates at temperatures T<1400 °C for Nchwaning and UMK compared to Comilog are mainly due to high Fe concentration in these ores. Safarian *et al.*,[109] studied the kinetics and mechanism of the simultaneous carbothermic reduction of FeO and MnO from high carbon ferromanganese slag at 1600 °C. In their work, they evaluated the reduction rates by sampling at different reaction times and analyzing the chemical composition of the reaction products. They found that the rate of reduction of FeO was initially fast followed by a slower rate and the rate of MnO reduction is slow in the fast FeO reduction stage and starts to increase with increasing temperature. As such, since Nchwaning has a higher Fe content followed by UMK and lastly Comilog, it is believed that higher rate of reduction in the low temperature region is because of the Fe concentration.

The primary constituents of the slag after complete prereduction are mainly MnO, SiO_2, Al_2O_3, CaO and MgO. Comilog ore contains very little CaO and MgO and the slag formed during the reduction process is very acidic. However, the slag is basic for Nchwaning and UMK ores as they contain significant amounts of CaO and MgO. The backscattered micrographs have shown that the slag structure is a two-phase component of solid + liquid, which increases in liquid with dissolution of solid MnO. Compared to Comilog (Figure 3.31), the micrographs show that reduction process in Nchwaning (Figure 3.32) and UMK (Figure 3.33) has not reached liquidus

slag compositions. As the extent of solid MnO phase is larger in the UMK ore, the primary slag will be more viscous, and hence this will have reduced the reduction rate. This is in agreement with Olsøs[141] results, where a higher basicity in the ore reduces the reduction rate in the two phase area of solid MnO and a liquid phase.

The variation in reduction between the two basic ores i.e., Nchwaning and UMK can be explained using the liquidus relations for MnO-SiO_2-CaO calculated in FactSage 8.3 with the 'FToxid databases' as presented in Figure 3.44. The other basic oxides e.g., MgO have been reported to behave similarly to CaO and the Al_2O_3 content in Nchwaning and UMK are in general very low and insignificant, hence the slag phase relations can describe the slags from these ores.

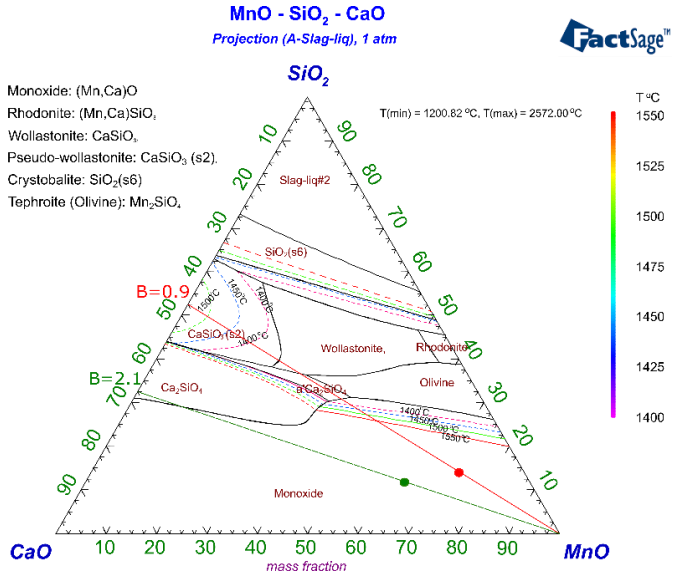

Figure 3.44: Calculated liquidus relations for the MnO-SiO_2-CaO slag system calculated in FactSage 8.3. The starting composition after prereduction are represented by red and green dots and the subsequent reduction paths are represented by red and green lines with basicities indicated for Nchwaning and UMK, respectively.

As illustrated in Figure 3.44, the red and green lines represent the reduction path for Nchwaning and UMK and the dots represents the starting composition after prereduction. Considering Nchwaning with a basicity of 0.9, the reduction proceeds along the reduction path with subsequent decrease in solid MnO phase. Between 1400 and 1550 °C the liquidus composition in coexistence with the solid monoxide will be 44 - 51wt.% MnO and if temperature is 1500 °C reduction will proceed in the liquid phase down to approximately 6 wt.% MnO. In contrast, the total MnO content from the experiment (Table 3.24) at 1550 °C was about 50 wt.% when the liquidus is about

26 wt.% MnO. The experimental values are not in agreement with predicted values from FactSage and this indicates that equilibrium has not been reached in Nchwaning experiments. On the other hand, reduction of UMK charge with a basicity of 2.1 as indicated in Figure 3.44, cannot reach the complete liquid zone as reduction proceeds along the basicity line. UMK with its higher basicity, will have a higher viscosity because of the presence of two stable phases manganosite + liquid slag. Because of the low reduction rate observed, UMK will end with higher MnO content, and this will be one of the reasons why UMK ore must be mixed with more acid ores. Typically in industrial ferromanganese production the ores are blended to achieve a desired basicity area around 0.4 to 1[2].

3.4.2 Prereduction behavior of Manganese ores

Prereduction of manganese ores is influenced by CO concentration in the reducing gas atmosphere. The CO content in the reducing gas atmosphere is generated from metal producing reaction (reaction (1.8)) and Boudouard reaction (reaction (1.7)) i.e., gasification of solid carbon. Reactions (1.7) and (1.8) are shown below for easy readability.

$$C + CO_2(g) = CO(g), \qquad \Delta H^0_{298} = +172 \text{ kJ/mol.} \tag{1.7}$$

$$MnO_{(l)} + C_{(s)} = Mn_{(l)} + CO_{(g)} \qquad \Delta H^0_{298} = +258.7 \text{ kJ/mol} \tag{1.8}$$

Several studies[42], [64], [65], [67], [73] have reported an increased reduction rate of manganese ores with increasing CO concentration in the CO/CO_2 atmosphere. In the induction furnace setup (R series experiments), the amount of slag produced for subsequent reduction to alloy was low. Hence, there was no significant metal producing reactions occurring in this setup. As such, low CO concentration which can be utilized for prereduction of higher manganese oxides is produced from metal producing reaction. Results from the prereduction of manganese ores in the induction furnace have shown that UMK ore has the highest extent of prereduction compared to Comilog and Nchwaning. In comparison to Nchwaning, the higher extent of prereduction in UMK is mainly because UMK contains a higher CO_2 content as shown in Table 3.1, and will release more CO_2 during heating which oxidizes C thereby producing CO for prereduction of higher manganese oxides. Most of the carbonates in UMK were observed to decompose up to 900 °C which correlates well with the temperature region where UMK has an O/Mn ratio of 1 i.e., complete prereduction. The increased porosity in UMK ore with decomposition of carbonates is expected to

increase the surface area for the solid - gas prereduction reactions as well as the reduction rate. In as much as the porosity levels appear to be within the same range as for UMK, the lower extent of prereduction in Comilog is attributed to CO deficiency in the reducing gas atmosphere. Since Comilog is not a carbonate ore, the lack of CO is due to the less CO_2 produced that can react according to the Boudouard reaction and generate CO.

Kor[68] studied the thermal decomposition of Mn_2O_3 and the reduction of Mn_3O_4 by C at 900 to 1200 °C and found that the overall rate of reduction by solid carbon was determined by the oxidation of the carbon by CO_2. In addition, the gasification of carbon was found to be catalyzed by Mn_3O_4. In this work, the increased extent of prereduction for ores mixed with solid carbon (i.e., 90 wt. % ore + 10 wt. % coke) is due to increased oxidation of C by CO_2 in the presence of coke, thereby increasing the rate of reduction by CO.

The prereduction of higher manganese oxides is generally fast in CO containing atmospheres[68] and in this work, a stable 70/30 CO/CO_2 atmosphere was supplied in a TGA furnace to establish differences in the prereduction characteristics of Comilog, Nchwaning and UMK ores (S series experiments). The weight change during the experiments corresponds to prereduction reactions i.e., the removal of oxygen from higher manganese oxides and iron oxides, evaporation of water and decomposition of carbonates. Therefore, isolation of the effects of the individual reaction components to the total weight loss is difficult. In this work a combination of experimental weight loss verification based on expected weight loss from chemical of ores and establishing contributions from different components from the rate curves were utilized. Fityk[135], a general purpose model fitting software was utilized in decomposing rate curves into separate contributions and verified with expected weight loss.

The overall weight loss in Comilog emanates from prereduction reactions and water evaporation. The TGA curves for Comilog have a total weight loss of 19.6 wt. % at 6 °C/min which is above the 18.4 wt. % calculated from the chemical composition of the ore. The discrepancy between the experimental and the calculated weight loss is believed to be due to water content in ore composition being underestimated. The water content in Comilog in this work has been estimated to be 3.8 wt. %, however in several other studies by Tangstad *et al.*,[57], Ngoy[134] and Larssen[75], the chemically bound moisture in Comilog has been estimated to be approximately 5 wt. %. Figure 3.45 shows a plot of the contribution of water evaporation and prereduction

reactions to the overall rate of weight loss, at different heating rates with the temperature profiles indicated on the secondary axis.

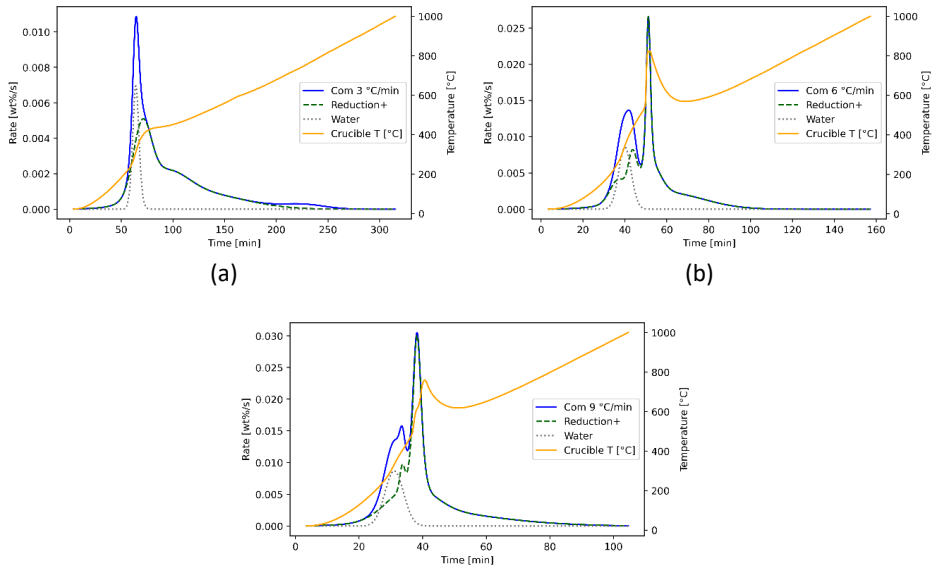

Figure 3.45: Contribution of water evaporation and prereduction reactions to the overall rate of prereduction for Comilog ore heated at (a) 3 °C/min, (b) 6 °C/min and 9 °C/min in a 70/30 CO/CO_2 atmosphere.

Larssen[75] conducted quantitative XRD of Comilog samples reduced at a heating rate of 6 °C/min and established the mechanism of prereduction of Comilog. As shown in Figure 3.46, the reduction of MnO_2 in Comilog which is initiated at about 200 °C follows a stepwise reduction MnO_2- to a combination of Mn_2O_3, Mn_3O_4 and MnO in the initial stages. At 550 °C, a rapid increase in reaction rate accompanied by a large exothermic temperature peak was observed and found to be the rapid removal of any MnO_2 remaining at this temperature. This implies that the faster the heating rate the greater the amount of MnO_2 remaining at 550 °C, which can result in exothermic temperature peak. As such, it can be observed from this work (Figure 3.45(a)), that there is no exothermic temperature peak at 550 °C, which implies that all MnO_2 has been reduced prior to 550 °C, at a heating rate of 3 °C/min. In addition, it can be seen in Figure 3.45(a) that the water evaporation happens at the same time as the main reduction rate peak at a heating rate of 3 °C/min. At heating rates of 3, 6 and 9 /min, integration of the water evaporation curves gives total weight of 3.24, 3.88 and 3.84 wt. % respectively. The values are within the same region as the 3.8

wt. % chemically bound water in Comilog ore. Water evaporation occurs between 200 – 300 °C, which is agreement with evaporation temperature range previously reported by Larssen[75]. The reduction reaction can be seen to start at low temperatures at 6 and 9 °C/min and the crucible temperature increases following the exothermic reactions. However, the main bulk of the reduction reactions occur after water evaporation is complete, resulting in a very exothermic peak which is characteristic for Comilog ore[48], [65], [144], [145].

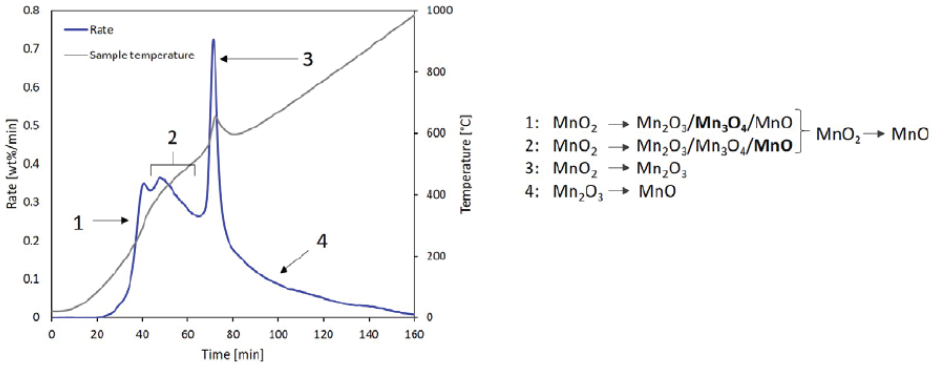

Figure 3.46: Reaction steps during non-isothermal (6 °C/min) reduction of Comilog ore (11.2 - 15.0 mm) in 50/50 CO/CO_2 [75].

TGA data for Nchwaning ore highlighted that a lower heating rate gives the highest mass loss, mainly because of an increased residence time per temperature as evidenced by a total weight loss of 13.4, 12.8 and 11.7 wt. % at 3, 6 and 9 °C/min, respectively. The total weight loss is not the same eventhough chemical analysis results in Table 3.26 show that Nchwaning ore has been reduced to MnO in the three heating rates. This is believed to be due to variations in extent of decomposition of carbonates at different heating rates with more carbonates decomposition at lower heating rates and thus higher weight loss. The overall weight loss in Nchwaning is due to prereduction reactions and decomposition of carbonates. Figure 3.47 shows the contribution of these constituents to the overall weight loss in Nchwaning at different heating rates.

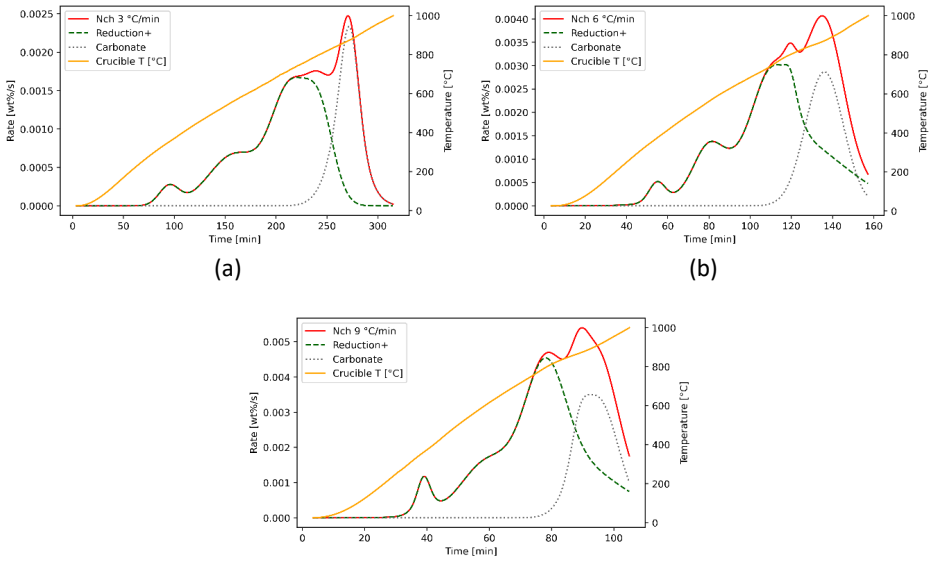

Figure 3.47: Contribution of various ore constituents to the overall rate of prereduction for Nchwaning ore heated at (a) 3 °C/min, (b) 6 °C/min and 9 °C/min in a 70/30 CO/CO_2 atmosphere.

An endothermic dip at 900 °C in the sample temperature profiles shown in Figure 3.47 corresponds to the peak region for weight loss due to carbonate decomposition. The decomposition of carbonates in Nchwaning ore are expected to contribute with 4.45 wt. % mass loss to the overall weight loss. At heating rates of 3, 6, 9 °C/min, the integration of the carbonate decomposition rate curves gives a total weight loss of 4.21, 3.91 and 3.47 wt. %, respectively. Analysis of the contributions of both prereduction reactions and decomposition of carbonates shows that at the endothermic dip at 900 °C, decomposition of carbonates in Nchwaning dominates in the overall rate of weight loss compared to prereduction reaction. This is more pronounced at 3 °C/min, were the prereduction reactions are almost complete when rate of decomposition of carbonates is at the peak. However, with increasing heating rate remaining prereduction reactions and decomposition of carbonates occur simultaneously.

In UMK ore, weight loss is a combination of decomposition of carbonates and prereduction reactions. In contrast to Nchwaning ore, decomposition of carbonates in UMK ore is a two step-process as presented in Figure 3.48.

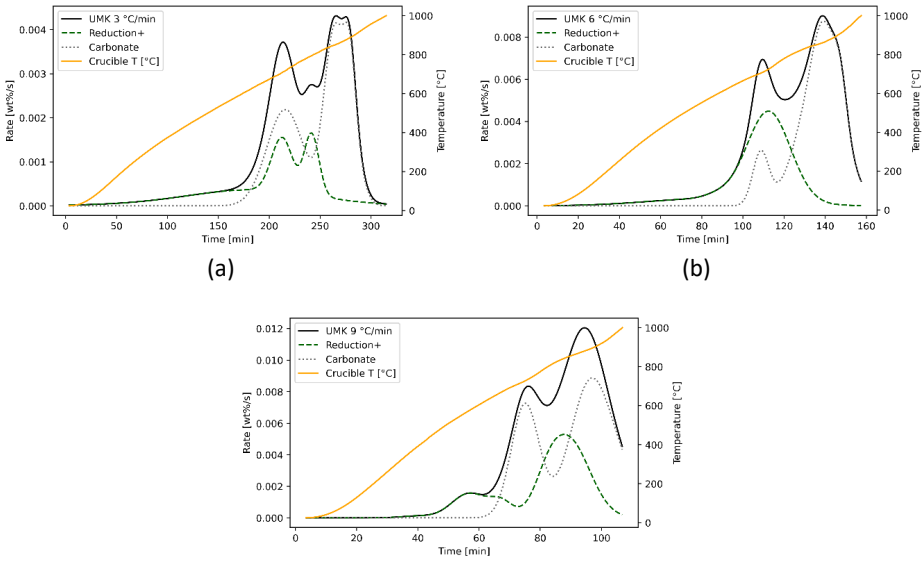

Figure 3.48: Contribution of prereduction reactions and decomposition of carbonates to the overall rate of prereduction for UMK ore heated at (a) 3 °C/min, (b) 6 °C/min and 9 °C/min in a 70/30 CO/CO_2 atmosphere.

Temperature profile as a function of time shown by the secondary axis has two endothermic dips in sample temperature at 700 °C and 900 °C. At 700 °C, the height of the peak decreases with increasing heating rate and is due to both decomposition of carbonates and prereduction reactions. For UMK experiments ending at 700 °C, it has been shown that approximately 20 wt. % carbonates decomposed at a heating rate of 9 °C/min, and the O/Mn ratio of the reduced sample was 1.29 which means that reduction reactions and carbonate decomposition occurred simultaneously up to this temperature. Heating rate seems not to affect the height of the second peak at 900 °C. It has been shown (Figure 3.38) that approximately 90 wt. % of carbonates in UMK at 9 °C/min were decomposed at 900 °C and the prereduction reactions are completed as the O/Mn ratio was 1 in the analysed reduced samples. This is not the case in Figure 3.48(c), where UMK ore still has some reduction of MnOx to MnO remaining at 900 °C when the heating rate is 9 °C/min and is believed to be a discrepancy in the analysis of the contributions as illustrated in the curves. However, complete prereduction at 900 °C is supported by the curves at 3 and 6 °C/min (i.e., Figure 3.48(a) and (b)), where prereduction reactions are complete when carbonates are still decomposing at a decreasing rate. The carbonates in UMK ore are assumed to be dolomitic based on the chemical composition in Table

3.1. This agrees with recent mineralogical investigations[146], [147] by XRD in which UMK ore was observed to contain various carbonate minerals containing manganese i.e., kutnohorite (Ca,Mn,Mg,Fe)CO_3 and manganese-free carbonates calcite ($CaCO_3$) and dolomite ((Ca,Mg)CO_3). Sukhomlinov and Tangstad[146] carried a SEM characterization of UMK ore were it was found that the main carbonate phases were enriched in Ca and Mg, detected at concentrations up to 28 wt.% and 4.5 wt.%, respectively. Several studies [64], [148], [149] have shown that the decomposition of carbonates is highly dependent on temperature and CO_2 content in the reducing atmosphere, with increasing temperature and lowering the partial pressure of CO_2 resulting in a greater extent of decomposition. Rat'Ko *et al.*,[149] and Gunasekaran and Anbalagan[148] have shown that the decomposition of dolomite is a two-step process with temperature zones dependent on mineral type surrounding the carbonate. Gunasekaran and Anbalagan[148] identified two decomposition peaks at 777.8 °C and 834 °C to be decomposition of dolomite and calcite in a N_2 gas atmosphere. The first peak was found to begin at 687 °C and ending at 781 °C whilst the second peak began at 781°C and ends at 916 °C. This fits very well with the two endothermic peaks in the rate of weight loss in UMK ore which are attributed to be decarbonation of dolomite and reduction reactions for the first peak and mainly decarbonization of calcite in the second peak. From the chemical composition of UMK ore, prereduction reactions are expected to contribute 5 wt. % to the overall weight loss whereas decomposition of carbonates contributes about 16 wt. %. Integration of the rate curves of the carbonate contribution in Figure 3.48 gives a total weight loss of 14.7, 14.0 and 13.8 wt. % at heating rates of 3, 6 and 9 °C/min, respectively. The values are within reasonable region of the expected total weight loss from decomposition of carbonates and the variations could be due to ore heterogeneity and uncertainty in chemical analysis.

Results of manganese ore prereduction in 70/30 CO/CO_2 atmosphere has shown that there are some discrepancies on the level of prereduction when comparing chemical analyses and weight loss data. Based on the TGA data (Figure 3.36) and reduction rate curves (Figure 3.45), Comilog is seen to be fully prereduced at 1000 °C for all heating rates. However, chemical analyses presented in Table 3.26 shows that the reduction in Comilog was incomplete at 1000 °C. For Nchwaning, weight loss (Figure 3.36) and reduction rate curves (Figure 3.47) show that Nchwaning is completely reduced at 3 °C/min and reduction is incomplete at 6 and 9 °C/min. In UMK, weight loss (Figure 3.47) and reduction rate curves (Figure 3.48) show incomplete reduction at 9 °C/min and complete reduction at 3 and 6 °C/min. On the

other hand, chemical analyses (Table 3.26) show that both Nchwaning and UMK are completely reduced at all heating rates. Recent work by Bao *et al.*,[138] has shown that the chemical analysis underestimates the O/Mn ratio when Fe is present as Fe_3O_4 or FeO. Comilog ore has very low Fe content compared to Nchwaning and UMK ore and as such, it is believed that the chemical analyses underestimate the O/Mn ratio in Nchwaning and UMK. On the other hand, ore reoxidation investigations by Schanche have shown occurrence of reoxidation in Comilog ore samples reduced in CO/CO_2 atmosphere. Reoxidation was not observed in Nchwaning ore were significant quantities of FeO was observed and forms an (Mn,Fe)O solid solution which stabilized MnO against reoxidation. This is also believed to occur in UMK since it contains relatively high Fe content. Reduction degree of Comilog samples reduced at temperatures up to 455 °C in CO/CO_2 atmosphere were seen to have an O/Mn ratio close to the average composition of Mn_3O_4 after reoxidation. In another study, Teguri *et al.*,[32] investigated reoxidation of manganese ore which had previously been reduced with solid carbon in a rotary kiln in the temperature range 1000 – 1150 °C. The reduced ore was found to reoxidize from MnO to Mn_3O_4 rapidly above 600 °C while limited oxidation was observed in the temperature range 300 – 500 °C. Therefore, it is plausible to assume that MnO in reduced Comilog samples may oxidize in air giving a higher O/Mn ratio in chemical analyses when in actual fact the ore had been completely reduced. Therefore, the minor variations between chemical analysis in this work are concluded to be mainly due underestimation of O/Mn ratio emanating from high Fe content in Nchwaning and UMK or overestimation of O/Mn ratio because of reoxidation in air for Comilog.

3.5 Summary

Data from TGA showed that the extent of ore prereduction will not have any effect on the metal producing reaction i.e., MnO + C = Mn + CO. Any remaining prereduction will be completed in the low temperature range 1200 – 1400 °C prior to the metal producing reaction.

Phase development in Comilog, Nchwaning and UMK ores is dependent on temperature and composition of the ore. The evolution of slags from these ores, showed that the initial slag formed is mainly liquid + solid monoxide phase and slag reduction will occur on top of the coke bed with an increased dissolution of monoxide in slag rendering the slag fluid enough to trickle down the coke bed. The coexistence of a solid phase and a liquid slag phase explains the high MnO activity in the slag as well

as its effect on viscosity of the slag. Therefore, low reduction extent will occur inside the coke bed area due to the lower MnO activity which emanates from complete dissolution of solid monoxide phase. Hence, the slag will be tapped at a composition close to the liquidus compositions.

The monoxide phase chemistry in Comilog is pure MnO which completely dissolves in liquid slag whereas Nchwaning and UMK ores form a (Mn,Mg,Fe)O monoxide solid solution phase which becomes enriched in MgO with increasing temperature. The dissolution and slag reduction behaviour of Comilog, Nchwaning and UMK ores showed that ores with higher acid oxides (i.e., Comilog ore) melt and reduce at a lower temperature than materials with higher basic oxides (i.e., Nchwaning and UMK). UMK, with its higher basicity, was found to have a higher extent of monoxide phase compared to Nchwaning and Comilog, and will hence have a higher viscosity because of the presence of two stable phases manganosite + liquid slag. Because of the low reduction rate observed, UMK will end with higher MnO content, and this will be one of the reasons why UMK ore must be mixed with more acid ores.

The prereduction of ores mixed with solid carbon i.e., coke in the induction furnace improved the extent of prereduction. The decomposition of carbonates leads to better prereduction due to the CO produced in the Boudouard reaction. Hence, UMK ore was found to have a better prereduction compared to Nchwaning which is low in carbonates and Comilog which is known to have a higher CO reactivity at similar CO contents. However, Comilog is seen to have a higher extent of prereduction in stable CO/CO_2 atmosphere followed by UMK and lastly Nchwaning.

Analysis of the rate curves from TGA shows that decomposition of carbonates in UMK is a two-step process with peak temperatures at 700 and 900 °C whereas for Nchwaning it is a single step with peak temperature at 900 °C. The first endothermic peak in UMK is a combination of decomposition of carbonates and prereduction reactions whereas the second peak is mainly carbonate decomposition and O/Mn ratio is 1.0 showing that prereduction of higher manganese oxides is complete prior to second decomposition reaction. For Nchwaning, the endothermic peak is mainly decomposition of carbonates and prereduction reaction is almost complete with an O/Mn ratio of 1.08.

Chapter 4

4 Pilot Scale Furnace

4.1 Introduction

The main goal of this thesis has been to increase knowledge concerning the utilization of pretreated manganese ores in ferromanganese production. In this chapter eight pilot experiments, where ferromanganese was produced from untreated and pretreated manganese ores, are presented. The pretreated ores had been preheated in air or preheated as a mixture of ore plus coke in a rotary kiln. The goal of these pilot experiments was to demonstrate the effect of pretreated ores on furnace performance. One of the goals was to generate data from pilot experiments which can be utilized to assess and map the changes in the process energy consumption and carbon footprint.

Pilot experiments are characterized by several work tasks such as, preparation and manual feeding of charge materials into the furnace, furnace operation i.e., control of furnace electrical parameters, furnace tapping, measurement of furnace off gas and post experimental work. As such, team collaboration between researchers from SINTEF and NTNU was key to the successful execution of the experiments. Details of the experiments conducted and furnace operation parameters such as electrical parameters and off gas measurements are reported in the experimental section. In addition, post experimental work i.e., methods describing the digout of the prereduction zone and excavation of the coke bed zone of the pilot furnace are described. The main contribution of the PhD study was on post experimental work. The main findings from the post-experimental investigations i.e., quantification and composition development of the tapped products, compositional and phase analysis of samples from digout of the prereduction zone and excavation of the coke bed zone are also described. Results of the inner structure and reactions in the furnace based on untreated and pretreated ores are discussed.

4.2 Experimental

4.2.1 Raw Materials and charge mixtures

Eight pilot experiments were conducted with charge mixtures containing untreated, preheated and prereduced ores at NTNU/SINTEF. All the raw materials were received from external partners. The ores used in the different experiments are commercially used in industry and these were Comilog, Nchwaning, UMK, and Kudumane ores. Pretreatment was done on Comilog and Nchwaning ores and the pretreated ores were either preheated or prereduced by Eramet Ideas. The ores were preheated in a rotary kiln in air or prereduced by mixing ore and coal. The targeted temperature for both the calcined ore and prereduced ore during pretreatment was around 700 – 800 °C [28]. The ores were pretreated by Eramet Ideas and shipped to Norway for use in pilot scale experiments[28].

The untreated, preheated and prereduced ores materials were chemically analysed by SINTEF Norlab using X-ray fluorescence while the MnO_2 amount was obtained by titration for ore and sinter. Eltra (combustion-IR) was used to determine amount of carbon, which was recalculated to CO_2. The untreated, preheated and prereduced ores has different oxygen levels i.e., O/Mn ratio, and Figure 4.1 shows the different oxygen levels of the ores utilized in the experiments. It can be seen in Figure 4.1, that untreated Comilog has an oxygen level of 1.98 and after pretreatment the oxygen level was lowered to 1.59 and 1.50 for the preheated and prereduced Comilog ore, respectively. For Nchwaning ore, the untreated ore has an oxygen level of 1.51 and after pretreatment in a rotary kiln the oxygen levels were 1.52 and 1.38 for preheated and prereduced Nchwaning ores, respectively. UMK and Kudumane ores have similar compositions and O/Mn ratios. In addition to ores, sinter was also used in the experiments and Table 4.1 shows the detailed chemical composition of all the ores, sinter and coke used in the experiments. The chemical composition shows that carbonates in Nchwaning were not decomposed after pretreatment and the high CO_2 (analysed as C) in all prereduced ores is expected to come from contamination from the coal which was utilized for the prereduction of the ores. The species in the prereduced ores should hence be about 10 % higher than given in Table 4.1.

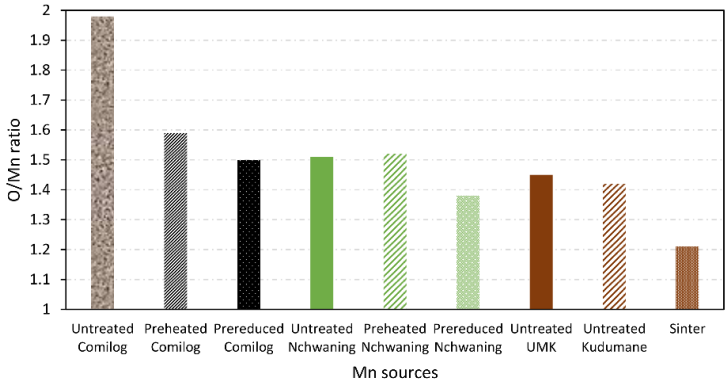

Figure 4.1: O/Mn ratio for different manganese sources

Table 4.1: Chemical composition of ores and sinter for pilot experiments. (Analysed by SINTEF Norlab). (Note: Com = Comilog, Nch = Nchwaning, Kud = Kudumane and UMK = United Manganese of Kalahari)

Wt. pct	Untreated				Preheated		Prereduced		Sinter	Coke
	Com	Nch	UMK	Kud	Com	Nch	Com	Nch		
MnO_2	79.6	38.2	26.4	25.0	51.8	38.3	43.1	29.2	19.3	
$Mn_{,tot}$	51.2	47.3	37.0	37.5	55.1	46.2	54.4	48.4	57.5	
$Fe_{,tot}$	2.9	8.94	3.86	4.47	3.03	9.35	3.15	8.77	3.89	
SiO_2	3.3	5.47	5.59	5.43	4.93	5.36	4.45	5.29	6.41	5.05
Al_2O_3	5.8	0.76	0.38	0.39	6.55	0.68	6.39	0.54	7.38	3.31
K_2O	0.7	0.10	0.25	-	1.18	0.10	1.13	0.06	0.78	0.27
CaO	0.4	5.94	16.1	16.5	0.35	7.19	0.18	5.87	0.12	0.34
MgO	0.1	1.30	2.98	2.17	0.22	2.22	0.22	1.30	0.04	0.21
BaO	-	0.35	0.02		0.26	0.30	0.24	0.35	-	0.03
P	0.1	0.03	0.03	0.02	0.11	0.03	0.13	0.03	0.09	-
S	-	0.05	0.02	-	0.02	0.11	0.06	0.14	-	0.52
LOI 950	12.8	4.92	16.8	16.0	4.83	4.08	7.49	5.55	-	-
CO_2	-	4.10	16.1	15.8	0.22	3.0	13	12	-	-
Fix C	-	-	-		-	-	-	-	-	88.4
O/Mn	1.98	1.51	1.45	1.42	1.59	1.52	1.50	1.38	1.21	-

The ores were used in combination with other raw materials such as sinter, flux, and coke as charge mixtures. The raw materials were in the size range 5 – 25 mm. The calculation of the charge mix relied on a set of assumptions and aimed at a targeted metal and slag composition out of the furnace. The following assumptions were made:

(i) Oxides such as SiO_2, MgO, Al_2O_3, TiO_2, CaO and BaO will go to the slag phase.

(ii) The tapped slag is assumed to contain 30 % MnO except for Mintek mix were it was assumed 20 % MnO in slag. This is assumed to be achieved

with a basicity of 0-5 – 0.8 for the 30 % MnO and a basicity larger than 0.9 for the 20 % MnO.

(iii) Fe and P will end up in the metal phase.

(iv) The carbon requirement was calculated by assuming that the degree of pre-reduction was 0 %. This implies that it is assumed that the final reduction step Mn_3O_4 to MnO proceeds in the active region of the Boudouard reaction.

Table 4.2 shows a summary of the planned calculated experimental charge mix parameters for all pilot experiments.

Table 4.2: Targeted slag basicity, slag/alloy ratio and chemical composition of slag and alloy products. (Note: Com = Comilog, Nch = Nchwaning, UMK = United Manganese of Kalahari, and Mint = Mintek mix)

		Untreated				Preheated		Prereduced	
	wt. %	Com	Nch	UMK	Mint	Com	Nch	Com	Nch
Slag	MnO	30.0	30.0	30.0	20.0	30.0	30.0	30.0	30.0
	SiO_2	17.2	26.3	24.0	37.7	17.7	26.3	17.5	29.0
	Al_2O_3	27.2	11.3	13.8	2.80	26.5	10.8	26.9	8.5
	CaO	23.3	25.0	24.4	32.2	23.3	23.6	23.0	24.9
	MgO	0.40	5.4	5.80	5.40	0.50	7.3	0.50	5.50
	Rest	2.00	2.00	2.00	2.00	2.00	2.00	2.00	2.00
	B*	0.53	0.81	0.80	0.93	0.54	0.84	0.53	0.81
Alloy	Mn	85.5	76.6	83.7	80.1	85.4	77.7	85.4	78.0
	Fe	6.20	16.4	9.20	12.8	6.2	15.2	6.3	14.8
	Si	1.30	-	0.10	0.10	1.4	0.10	1.4	0.20
	C	7.00	7.00	7.00	7.00	7.00	7.00	7.00	7.00
	P	0.17	0.01	0.11	0.05	0.17	0.08	0.17	0.07
Slag/Alloy	ratio	0.48	0.37	0.66	1.33	0.51	0.45	0.49	0.38

B* = $(CaO + MgO)/(SiO_2 + Al_2O_3)$

The calculated charge mixture in the Comilog and Nchwaning series are shown in Table 4.3 and Table 4.4, respectively. The charge mixture were batches of 30kg each and the total number of batches which translates to the total amount of charged materials in each pilot experiment are indicated. Comilog ore is a highly reactive ore with an O/Mn ratio around 1.98 and in order to achieve a stable operation, sinter of oxygen level 1.21 was added to the charge mixture to lower the O/Mn ratio to around 1.5 for the untreated Comilog ore charge mix. In addition, sinter and lime were added in all charge mixtures with the purpose of controlling the basicity which was mainly targeted at 0.5. Nchwaning is a high basicity ore and as such basicity was controlled by addition of acid sinter and no burnt lime was added in the charge mix as shown in Table 4.4. The charge mixtures for pilot experiments conducted with

untreated UMK and Mintek mix are shown in Table 4.5. UMK and Kudumane are highly basic ores, and these two ores are blended with quartz to achieve a desired basicity of 0.93 in the Mintek experiment.

Table 4.3: Charge blend for each pilot experiment in the Comilog series (Each batch had a total weight of 30kg)

Raw Materials	Pilot experiment charge blend (%)		
	Untreated	Preheated	Prereduced
Ore	29.3	29.0	29.6
Sinter	46.0	45.5	46.5
Coke	16.0	16.2	14.8
Lime	8.7	9.23	9.10
Total	100	100	100
O/Mn	1.51	1.36	1.32
Total batches	21	19	29.5

Table 4.4: Charge blend for each pilot experiment in the Nchwaning series (Each batch had a total weight of 30kg)

Raw Materials	Pilot experiment charge blend (%)		
	Untreated	Preheated	Prereduced
Ore	66.5	66.7	75.3
Sinter	15.6	15.7	7.00
Coke	17.9	17.7	17.7
Total	100	100	100
O/Mn	1.45	1.46	1.37
Total batches	25	25	15

Table 4.5: Charge blend for the UMK and Mintek mix pilot experiments (Each batch had a total weight of 30kg)

Raw Materials	Pilot experiment charge blend (%)	
	Untreated UMK	Untreated Mintek mix
UMK Ore	47.0	46.3
Kudumane Ore	-	29.3
Sinter	36.0	-
Quartz	-	9.67
Coke	17.0	14.7
Total	100	100
O/Mn	1.35	1.44
Total batches	22	28

4.2.2 Pilot Furnace description and operation

Pilot-plant smelting test-works have been conducted at SINTEF/NTNU in a 400 kVA electric furnace operated in AC mode. Figure 4.2 and Figure 4.3 show the sketch of the pilot-scale furnace set-up and a photograph of the pilot-scale furnace in operation, respectively.

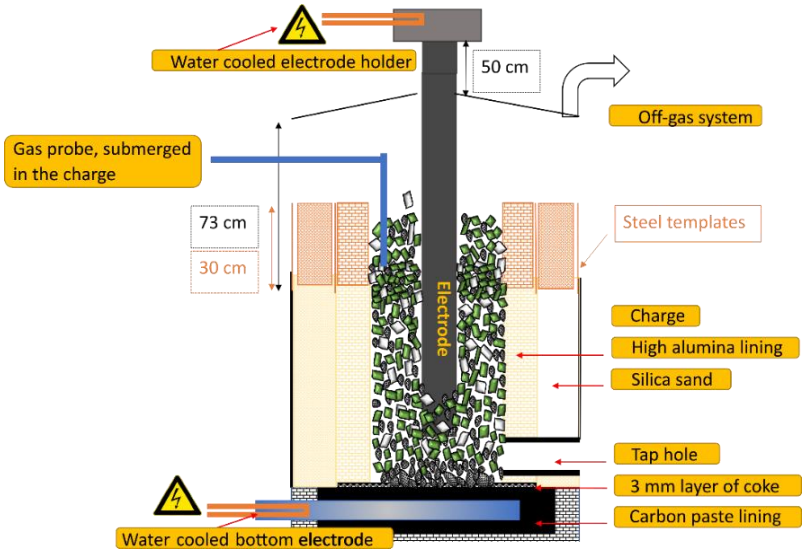

Figure 4.2: Schematic drawing of the pilot furnace

Figure 4.3: A photograph of the pilot furnace in operation

The furnace consists of an outer steel shell with a bottom and a top electrode. Both the top and bottom electrodes are water cooled. A lining is built inside the steel shell and a 150 mm graphite electrode is used as the top electrode located in the centre of the furnace. The inner diameter of the furnace shell is typically around 450 mm. The gap between the high alumina inner lining, and the outer steel shell is filled with quartz sand. The inner lining is approximately 100 mm thick and lasts for one smelting experiment.

During pilot runs, the furnace was initially charged with a 10 kg coke bed placed at the bottom of the furnace and the top-electrode was lowered into the coke bed. The furnace was then preheated for 150 kWh before the tap hole was plugged and around 180 to 200 kg of premixed raw materials was charged in 30 kg batches into the furnace up to the rim. This charge level was kept constant throughout the experiment by manual charging. The electrode height was slowly increased until it was held at constant position of 20 cm above the bottom of the furnace during all experiments. Control of the furnace operation is mainly centred on keeping the electrode position constant and adjusting the current to achieve the desired effect. The first tap was done when the furnace had been supplied with 150 kWh after the initial charging. Further, the furnace was tapped every 80 kWh of electrical energy consumed. Typically, the tapping time from opening to closing the furnace tap hole was within 2 minutes. The furnace was shut down 40 kWh after the last tapping and then it was cooled down for approximately 72 hours before it was excavated. During the experimental run, electrical parameters such as resistance, power, voltage, and current are continuously recorded. In general, the electrical parameters and the number of taps varied for the different experiments conducted with different charge mixtures as will be discussed later. The amount of metal and the slag from each tapping was measured and samples analyzed using XRF at SINTEF Norlab.

A Micro Gas Chromatography (micro-GC) off-gas sampling system was used to measure the composition of the off-gas with the sampling line located vertically 100 mm under the top of the charge surface and 75 mm horizontally from the electrode as shown in Figure 4.2. The process off-gas composition was continuously measured throughout the pilot experiments to quantify CO, CO_2, H_2, O_2, N_2, and CH_4. Temperature in the upper part of the furnace i.e., the prereduction zone was measured by placing thermocouples at 100mm interval distances from the top of the charge starting at the gas sampling position up to a total furnace depth of 500mm. The thermocouples were shielded by an alumina cap and steel pipe. It was noted that the temperatures recorded were continuously rising during the entire experiment without

substantive stable temperatures recorded. This could have been due to the slower heat transfers from charge to thermocouple during the experiments. As such, the temperature measurements are reported elsewhere.

4.2.3 Electrical parameters

The furnace resistance and electrode tip position during operation of untreated, preheated and prereduced Comilog experiments is shown in Figure 4.4. In general, it can be seen that the furnace resistance increases as the electrode tip position is increased. Untreated and preheated Comilog experiments had a more rapid increase in the electrode tip position compared to the prereduced Comilog experiment. The electrode was raised to 20 cm prior to the first tapping for untreated and preheated Comilog experiments whereas for prereduced Comilog it reached 20 cm after the first tapping. The initial stages of increasing the height of electrode tip are very variable in all the experiments. The furnace resistance in all the experiments stabilizes over time, with highest resistance in untreated Comilog experiment, followed by preheated Comilog and lowest for prereduced Comilog experiment. All the furnace experiments in the Comilog series were tapped a total of 12 times. It can also be seen that the furnace resistance increases for short time intervals during tapping. The increase in electrical resistivity is expected mainly due to the fact that tapping removes the slag and alloy that kept the electrical conductivity of the coke bed high. Hence, conductivity in the cokebed drops and resistivity increases. After first 4 tappings, the furnace resistances were measured in the ranges 6 – 8 mΩ, 5 – 6mΩ and 4 – 6mΩ for untreated, preheated and prereduced Comilog experiments, respectively. Compared to previous pilot scale experiments, they are all in a low area, indicating good operation.

Power, voltage and current as a function of time is shown in Figure 4.5, Figure 4.6 and Figure 4.7, respectively, for the untreated, preheated and prereduced Comilog experiments. As seen in Figure 4.5 for the untreated Comilog pilot experiment, the power fluctuated between 140 – 180 kW in the first half of the experiment but was stabilized in the last half, averaging around 160kW. The preheated Comilog pilot experiment had power in the range 140 – 180 kW for the first 4 tappings and had also average power about 160kW in the last 8 tappings as shown in Figure 4.6. In general power for the prereduced Comilog pilot was lowest compared to pilot experiments with untreated and preheated Comilog charge mixtures. It can be seen in Figure 4.7 that the power ranged from 100 – 160 kW. In

most stable period from tap 3 to the end of the experiment it was in the range 100 – 140 kW.

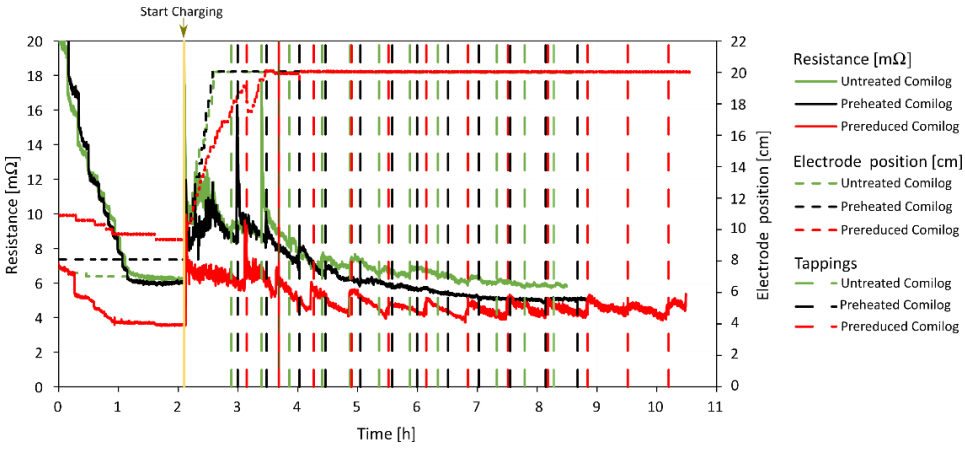

Figure 4.4: Electrode tip position and resistance as a function of time in the untreated, preheated and prereduced Comilog experiments. Start of charging and the tappings thereafter are indicated for each experiment.

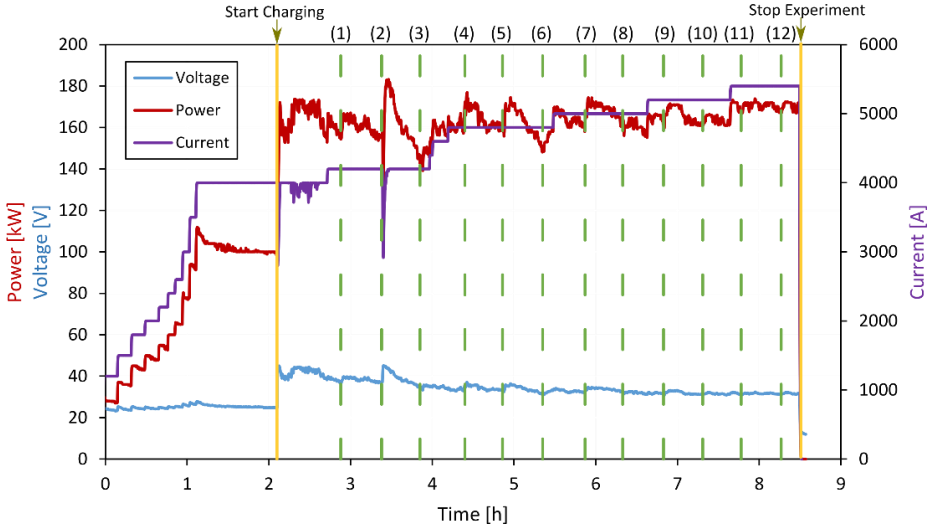

Figure 4.5: Voltage, power and current as function of time in the untreated Comilog experiment

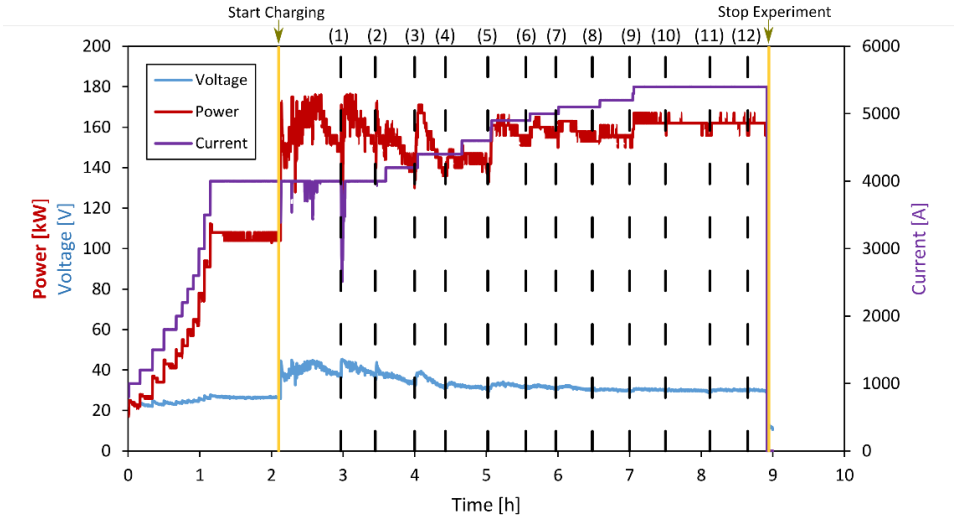

Figure 4.6: Voltage, power and current in the preheated Comilog experiment

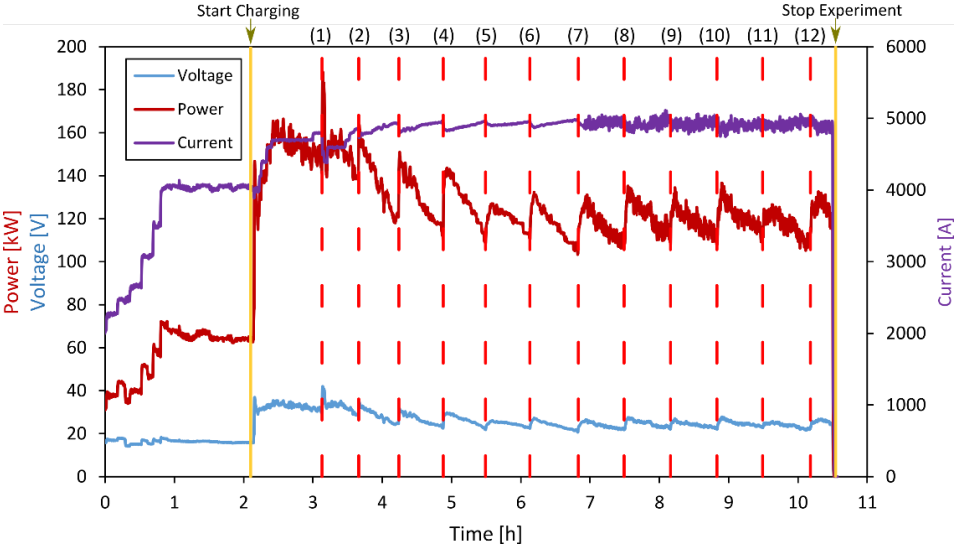

Figure 4.7: Voltage, power and current in the prereduced Comilog experiment

Figure 4.8 shows the furnace resistance and electrode tip position during pilot experiments in the Nchwaning series. A constant electrode height of 20 cm was reached prior to the first tap for both preheated and prereduced Nchwaning pilot

experiments with a more rapid increase in preheated Nchwaning. Untreated Nchwaning pilot reached 20 cm after the first tap. Similarly, to Comilog series, the furnace resistance is high and unstable during the period of electrode height adjustment. The furnace resistance is generally high for untreated Nchwaning and is more stable in the last half of the experiment ranging 6 – 8 mΩ. The furnace resistance in preheated Nchwaning is lower than untreated Nchwaning experiment and is normally around 4 mΩ and rises to 8 mΩ after each tapping in the last 4 tappings. The total number of tappings were 12, 7 and 5 respectively for the untreated, preheated and prereduced Nchwaning experiments. Furnace resistance for the prereduced Nchwaning experiment gradually decreased over time and the most stable period was not reached as the experiment was stopped earlier than normal mainly due to difficulties in tapping the furnace.

Power, voltage and current as a function of time for the untreated, preheated and prereduced Nchwaning experiments is shown in Figure 4.9, Figure 4.10 and Figure 4.11, respectively. The power in untreated Nchwaning experiment (Figure 4.9) is stable in the last part of the experiment, averaging around 150kW. As seen in Figure 4.10, the power is most stable between tapings 4 – 6, ranging between 100 – 140 kW in the preheated Nchwaning experiment. Power gradually decreased over time for the prereduced Nchwaning experiment which had the least number of tappings as shown in Figure 4.11.

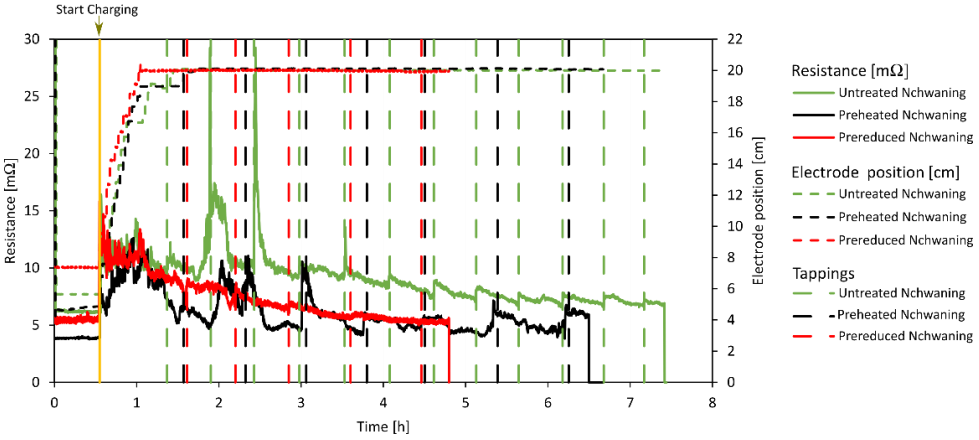

Figure 4.8: Electrode tip position and resistance as a function of time in the untreated, preheated and prereduced Nchwaning experiments. Start of charging for all the experiments are indicated.

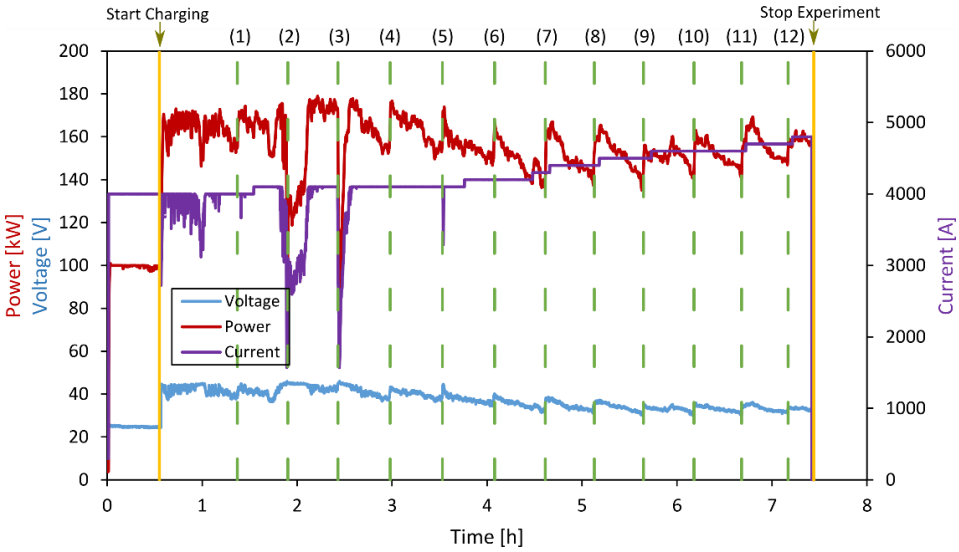

Figure 4.9: Voltage, power and current as function of time in the untreated Nchwaning experiment

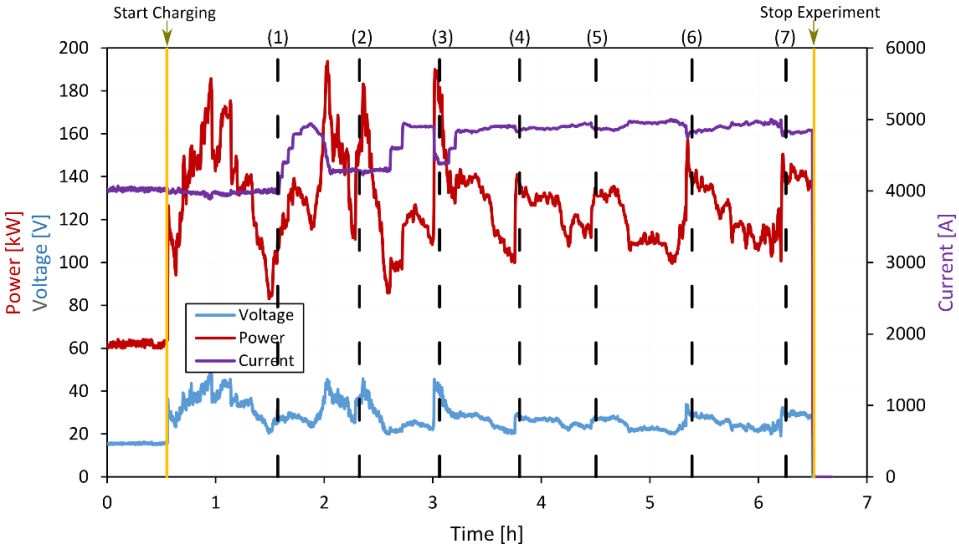

Figure 4.10: Voltage, power and current as function of time in the preheated Nchwaning experiment.

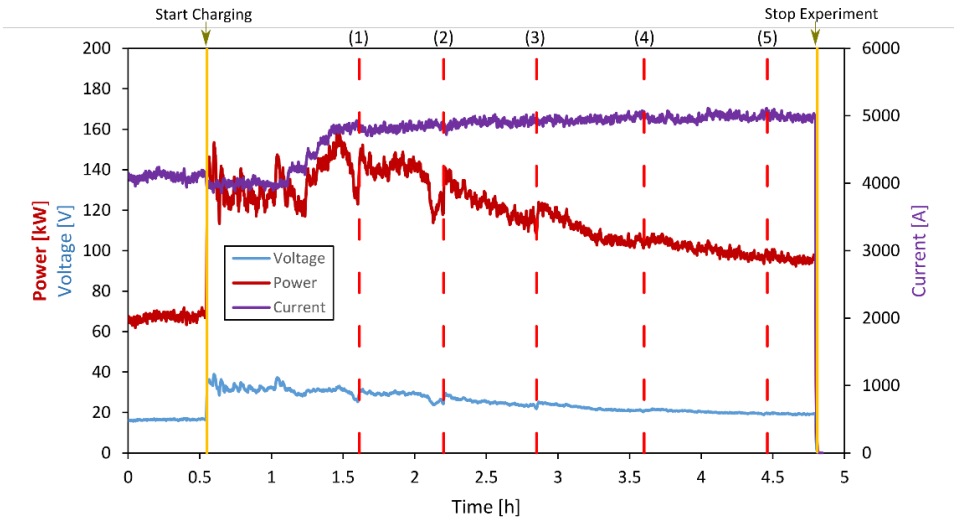

Figure 4.11: Voltage, power and current as function of time in the prereduced Nchwaning experiment

Furnace resistance and electrode position for the untreated UMK experiment is shown in Figure 4.12. Power, voltage and current as a function of time for the UMK experiment is also presented in Figure 4.13. Similarly, to all other experiments conducted in this work, the electrode height position was raised and maintained at 20cm. The furnace resistance gradually decreases from tap 2, after the initial unstable period of electrode height adjustment. The power is more stable in the last 4 tappings ranging between 165 and 180 kW. In comparison to untreated UMK, the electrode height adjustment was slower in untreated Mintek mix reaching 20 cm after 4 tapings as presented in Figure 4.14. However, the furnace resistance is more stable in untreated Mintek mix (7 mΩ - 9 mΩ) compared to UMK experiment. The stable resistance is observed from tap 7 to 12, with corresponding power fluctuating between 140 and 160 kW. Similar to all other experiments there exists interval increases in electrical resistivity and power during taping intervals which is due loss of conductivity from removal of slag and alloy.

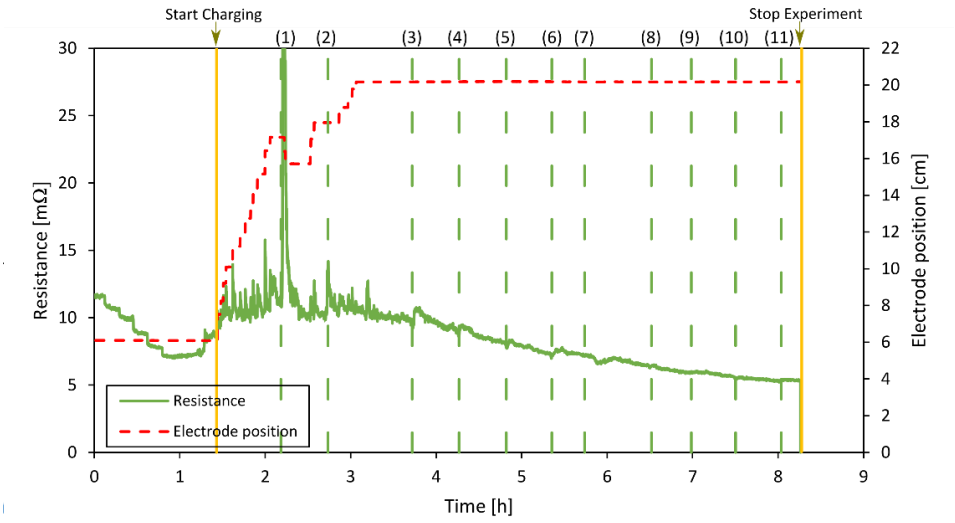

Figure 4.12: Electrode tip position and resistance as a function of time in the untreated UMK experiment. Start of charging, end of experiment and tappings (in brackets) for all the experiment are indicated.

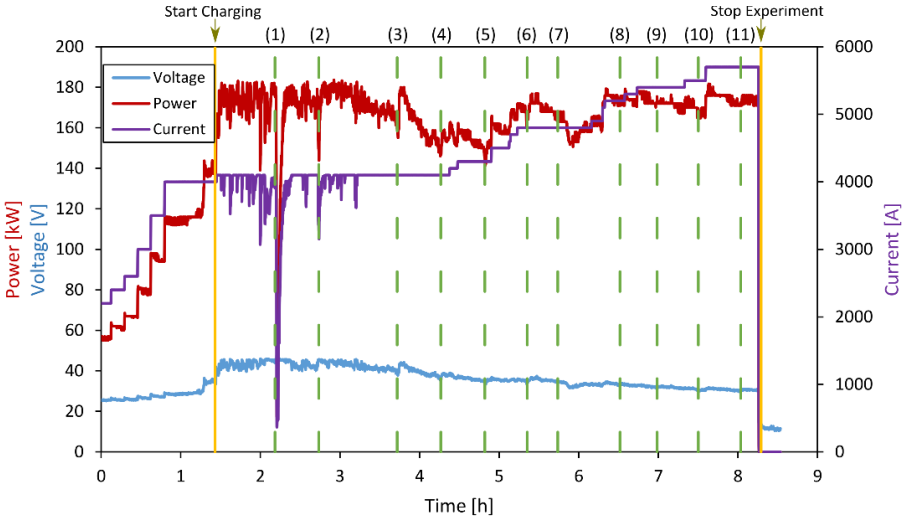

Figure 4.13: Voltage, power and current as function of time in the untreated UMK experiment. Tappings are shown in brackets.

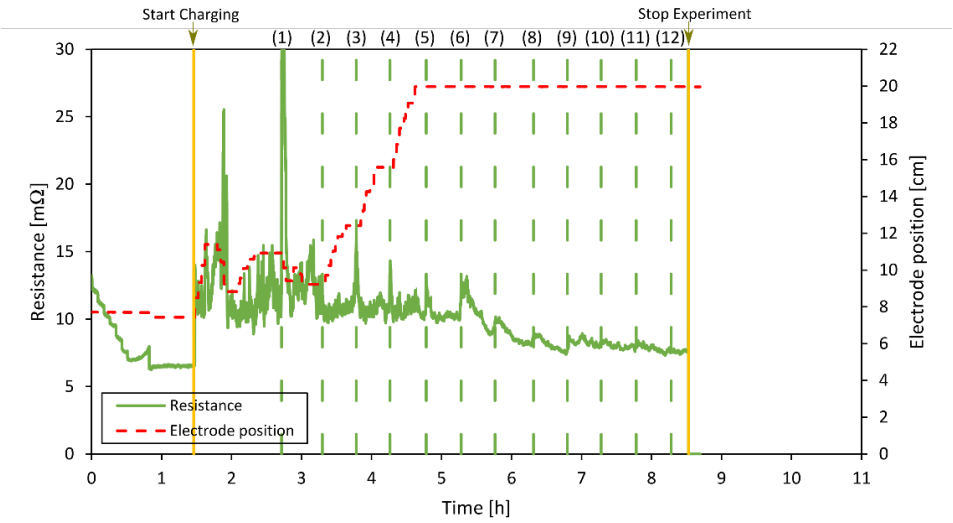

Figure 4.14: Electrode tip position and resistance as a function of time in the untreated Mintek mix experiment. Start of charging, end of experiment and tappings (in brackets) for the experiment are indicated.

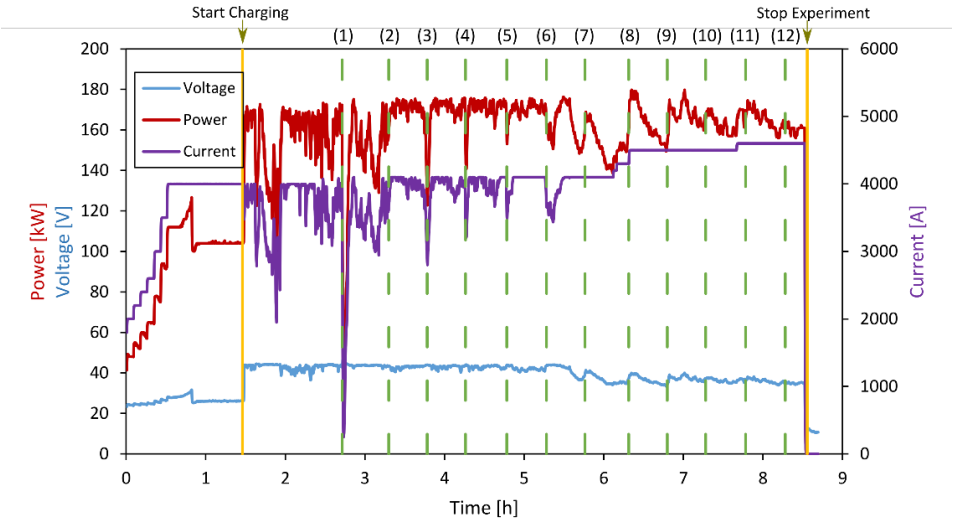

Figure 4.15: Voltage, power and current as function of time in the untreated Mintek mix experiment. Tappings are shown in brackets.

4.2.4 Off-gas measurements

Off-gas measurement using a micro-GC sampling system is based on gas chromatography Thermal Conductivity Detector (TCD) principle and can detect air, hydrogen, carbon monoxide, carbon dioxide, nitrogen, sulfur dioxide, inorganic gases, and many other compounds[150]. The TCD is based on the principle of thermal conductivity which depends upon the composition of the off-gas. The process off-gas is continuously collected at the sampling point located 100 mm under the top of the charge surface and 75 mm from the electrode as shown in Figure 4.2. An inert carrier gas transfers the furnace off-gas sample components into a measuring channel and a second channel serves as a reference channel where only pure carrier gas flows as shown in Figure 4.16. The carrier gas is both used to transfer the sample through a column and into the TCD detector, and as a reference gas. Located on both channels (Wheatstone bridge) are electrically heated resistance wires. The thermal conductivity between the column effluent flow (furnace off-gas sample components in carrier gas) and the reference flow of carrier gas is different and this produces a voltage signal proportional to this difference. The signal is proportional to the concentration of the sample components. The process off-gas was continuously measured throughout the pilot experiments to quantify CO, CO_2, H_2, O_2, N_2, and CH_4 contents. However, in this work only measured CO and CO_2 composition are reported as they are the main constituents.

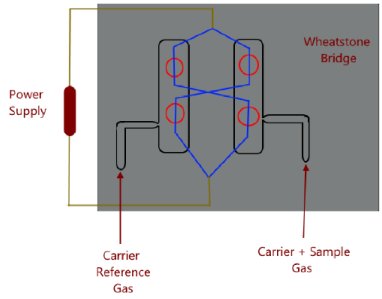

Figure 4.16: Micro-GC Thermal Conductivity Detector (TCD) principle[150].

Figure 4.17 and Figure 4.18 respectively show the CO and CO_2 concentrations in pilot experiments conducted with untreated, preheated and prereduced Comilog ore. The off-gas concentrations are compared from the start of the experiments i.e., from the point the gas sampling point is immersed in the charge mixture and their end points are different based on the total time conducted in each pilot experiment. Charge mixture with prereduced Comilog ore had the highest CO

concentrations during the experimental runs, followed by charge mixture with preheated Comilog and lastly, untreated Comilog ore with the lowest observed CO concentration. The opposite trend is observed for CO_2 concentrations. This is mainly due to the higher oxygen in untreated Comilog ore followed by preheated Comilog and prereduced Comilog. It was also however be due to the extent of the Boudouard reaction as will be discussed later.

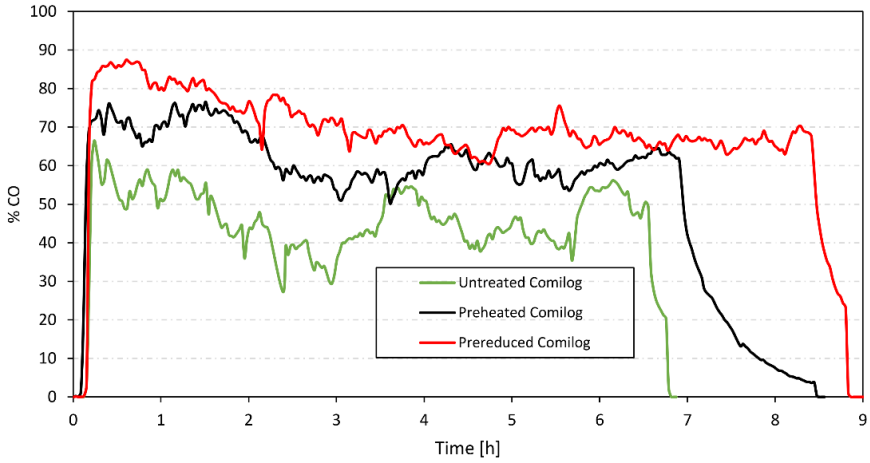

Figure 4.17: CO concentration in the offgas measured from pilot experiments in the Comilog series

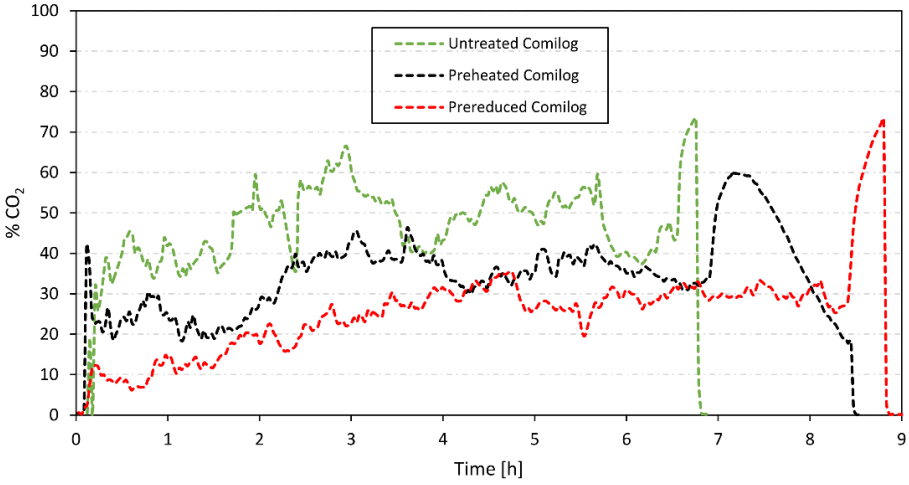

Figure 4.18: CO_2 concentration in the offgas measured from pilot experiments in the Comilog series

The CO and CO_2 concentrations in pilot experiments conducted with untreated, preheated and prereduced Nchwaning ore are presented in Figure 4.19 and Figure 4.20, respectively. The prereduced Nchwaning experiment had a higher concentration of CO in the first 2 hours of the experiment and gradually decreased thereafter. This experiment was characterized by difficulties in tapping as could be seen in the section on electrical parameters. The CO concentrations in the untreated Nchwaning and preheated Nchwaning experiment can be seen to be at the same level in the last 100 minutes of the experiment. This is in-line with insignificant changes in oxygen level of the ore after pretreatment as presented in Figure 4.1. The last 100 minutes is considered to reflect the stable operation and stable off-gas conditions. This period is used during the analysis of the furnace as these would have been the conditions prior to furnace shut down. The untreated Nchwaning had a period between 4th and 5th hour were no off-gas composition was measured. This was a result of clogging and hence cleaning of the micro-GC equipment. An opposite trend can be seen for CO_2 concentrations in Figure 4.20.

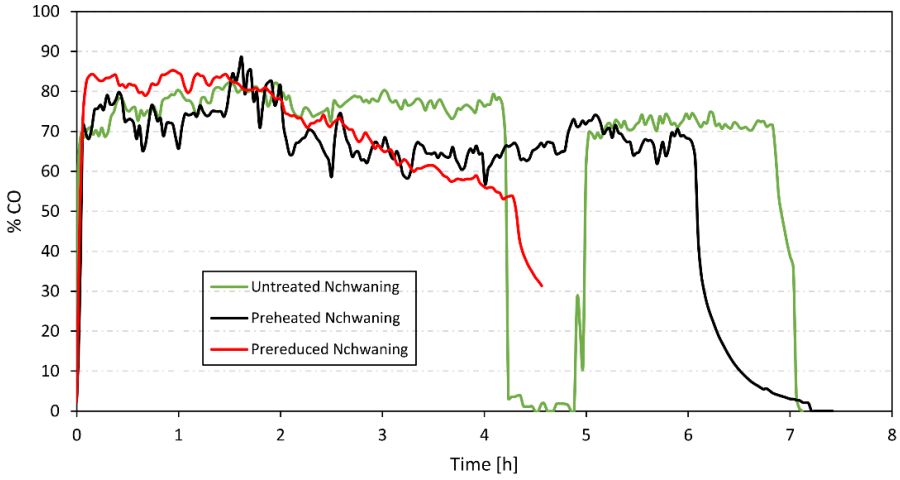

Figure 4.19: CO concentration in the offgas measured from pilot experiments in the Nchwaning series.

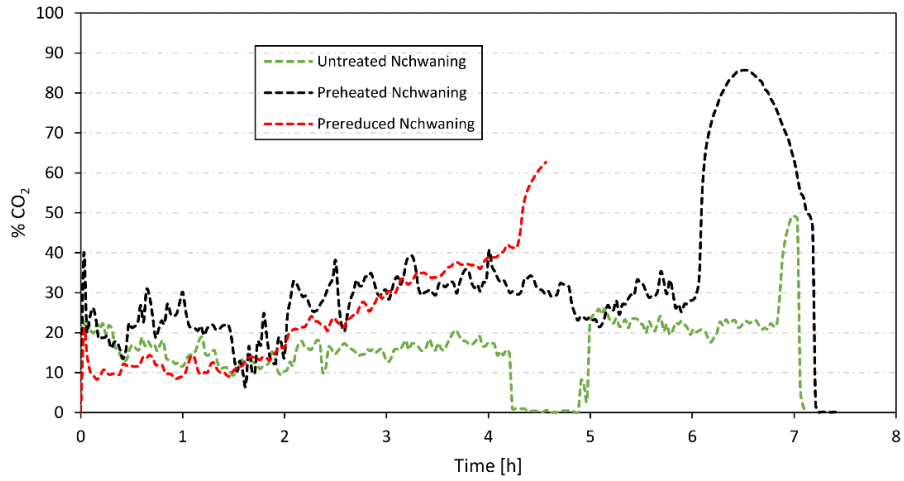

Figure 4.20: CO_2 concentration in the offgas measured from pilot experiments in the Nchwaning series.

The CO and CO_2 concentrations for pilot experiments with UMK and Mintek charge mixtures are compared and presented in Figure 4.21 and Figure 4.22. In the first 5 hours of both experiments, the trend for CO concentrations in untreated UMK is higher than that for untreated Mintek mix. However, in the last segment the CO concentrations are within the same region.

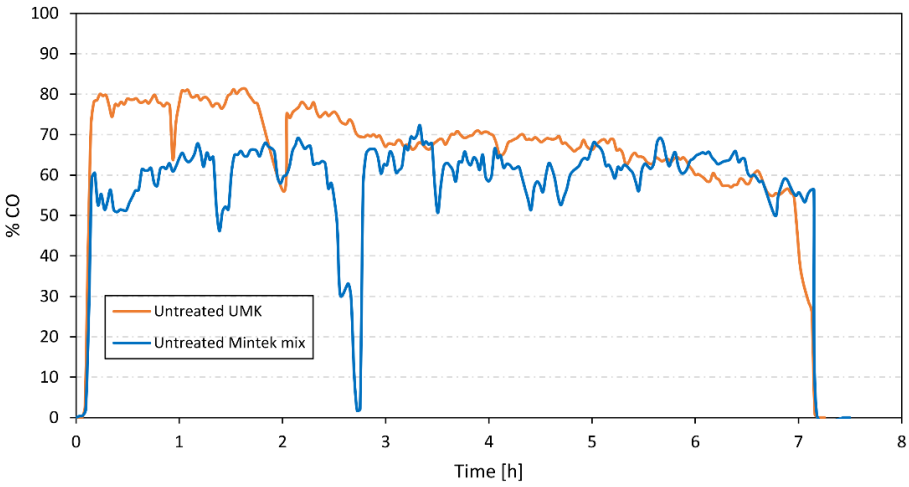

Figure 4.21: CO concentration in the offgas measured from untreated UMK and Mintek mix pilot experiments.

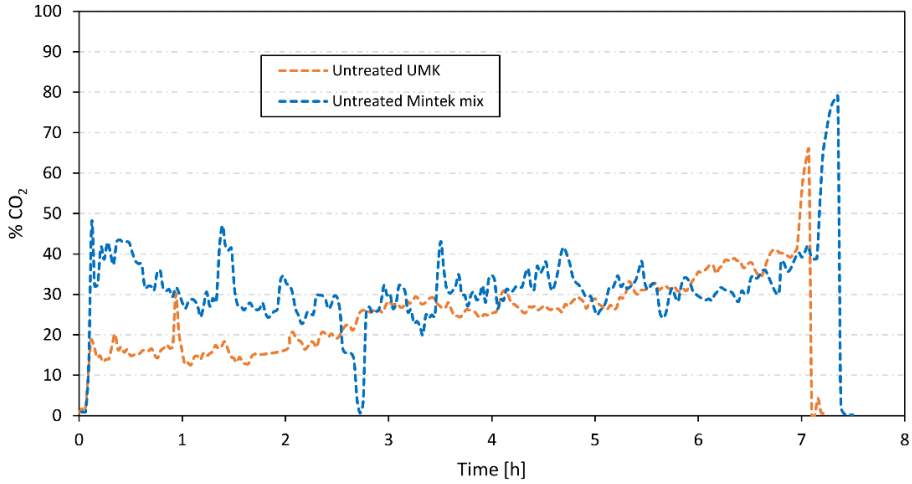

Figure 4.22: CO_2 concentration in the offgas measured from untreated UMK and Mintek mix pilot experiments

4.2.5 Post Experimental Work

Upon completing the pilot experiments, the furnace was allowed to cool down for 72 hours before excavation. The furnace excavation for the HCFeMn pilot experiment was divided based on the two zones of the furnace namely the prereduction zone and the coke bed zone.

4.2.5.1 Dig out of prereduction zone

The top part of the furnace i.e., the prereduction zone was composed of loose solid charge materials and this zone was excavated by manually digging out the materials. The schematic illustration of the furnace digout is shown in Figure 4.23.

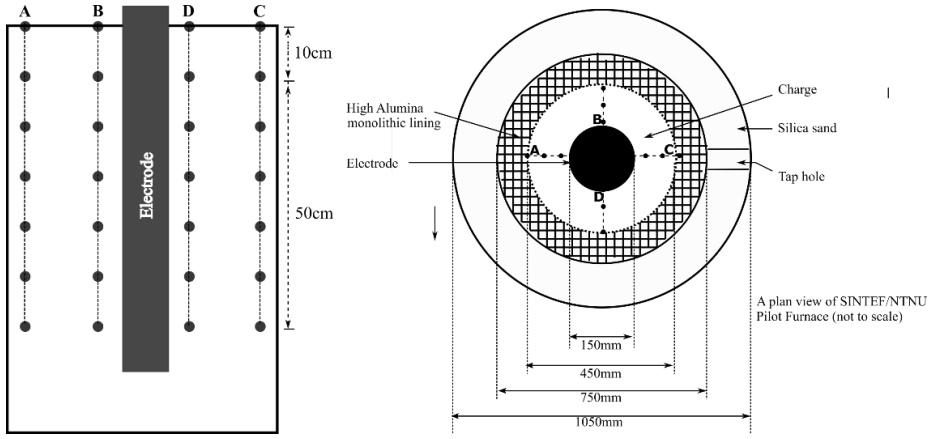

(a)

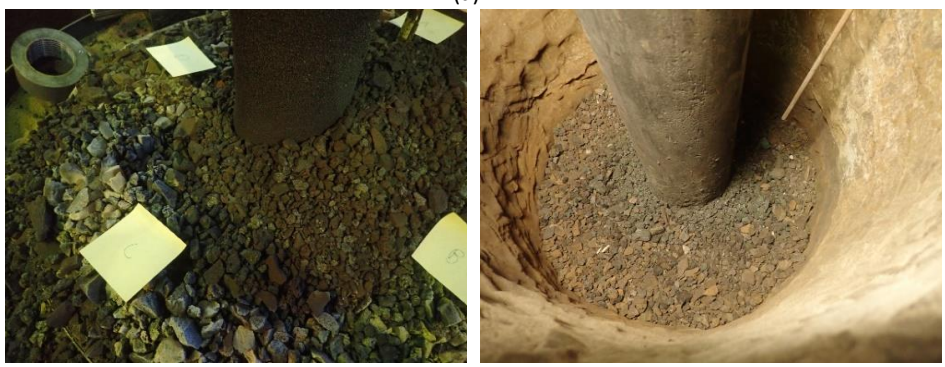

(b) (c)

Figure 4.23: (a) A schematic illustration of the sampling regions during the furnace digout and a plan view of the SINTEF/NTNU Pilot furnace. (b) Photographs of furnace top prior to dig-out & (b) interior of the furnace and top of cokebed after complete digout of the prereduction zone.

The original charge mixtures were 5 – 25mm particles, however, due to ore decrepitation during operation, samples in the range approximately 3 – 25 mm were excavated. Finer particles were not considered as most of the finer particles percolated through the loosely packed charge towards the high temperature zone, and as such they were considered not to be representative of the position. The 3 – 25 mm particles were taken from two regions close to the electrodes (i.e., positions B and D) and two regions close to the lining (i.e., positions A and C). Vertically, the samples were taken at 100mm interval distances from the top of the furnace to a depth of 600mm, as illustrated in Figure 4.23. The sampling positions were selected with a rationale that samples would exhibit differences in prereduction depending on the position of the sample in relation to the electrode (i.e., adjacent the electrode and towards the wall of the furnace) and depending on the level of the sample in relation

to the top of the furnace. This variation in material flow and extent of reduction for materials adjacent the electrode and at regions further away from the electrode has been previously reported for industrial furnaces [130].

Approximately 500 – 1200g samples were sampled at each position and level. The samples were later separated into three categories, namely, coke, sinter, and ore for further investigations. The ore samples from the furnace digouts were analysed by SINTEF Norlab using X-ray fluorescence while the oxygen content related to the manganese oxides, given as MnO_2 amount was obtained by titration. The obtained results were used to calculate the oxygen level of the ore samples determined as the O/Mn ratio.

4.2.5.2 Excavation of the cokebed zone

Charge materials were observed to be sintered at a depth of 600mm and this represents the second part of the process i.e., the coke bed zone. After complete removal of the reacted materials from the prereduction zone, the remaining cokebed zone was filled with epoxy. After 72 hours of epoxy hardening, the sand between the inner lining and the outer shell of the furnace, as shown in Figure 4.2 was removed. Subsequently, the electrode was cut, and the epoxy hardened, and inner part of furnace could be excavated. The excavation of the furnaces was done in two ways, due to practical reasons. The first method was that a vertical cross section of 8cm thickness was cut in the middle of the furnace as shown in Figure 4.24. This was used to describe different zones of the furnace and samples were core drilled from the cross section. The samples were analysed in EPMA.

Figure 4.24 shows an example of furnace cross-section excavated from the untreated UMK charge mix pilot experiment. Different regions of the excavated cokebed can be viewed. Approximately, 10cm from the top of the excavation adjacent the electrode and extending towards the furnace lining, a region with sintered particles was observed. Regions below and close to the tip of the electrode were mainly filled with coke, below which a slag enriched region was observed. In addition, regions of partially molten charge were observed to extend from sides of the electrodes as illustrated in the diagram. At the very bottom, untapped alloy and the tap hole region could be seen. The drilling of the samples was mainly at 5cm interval distance going down the electrode from regions adjacent the electrode and regions 10cm parallel to electrode height. However, due to the ragged nature of the excavations, samples could not be collected. Then the sampling was strategically shifted to accessible near regions.

The excavation procedure was later improved by drilling cores down the depth of the excavated cokebed at positions shown in Figure 4.25. From the cores, samples were cut at 5cm interval distances from the top of the furnace cokebed, and the samples were later analysed in EPMA. This method of core drilling throughout the depth of the cokebed was applied to the experiments for prereduced Comilog ore and prereduced Nchwaning ore.

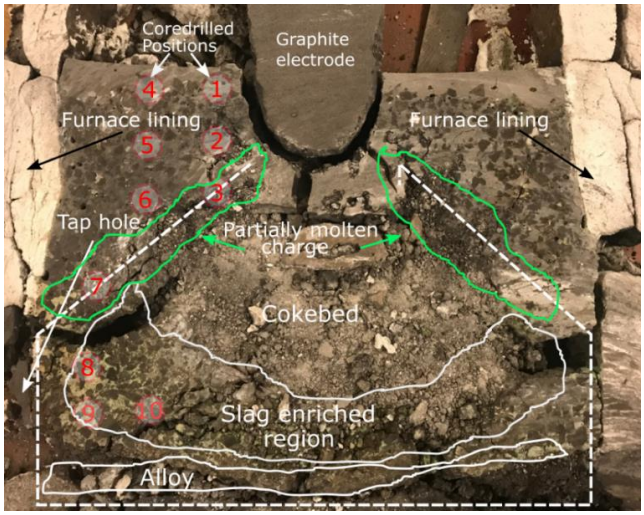

Figure 4.24: Cross - section of the interior part of the cokebed zone

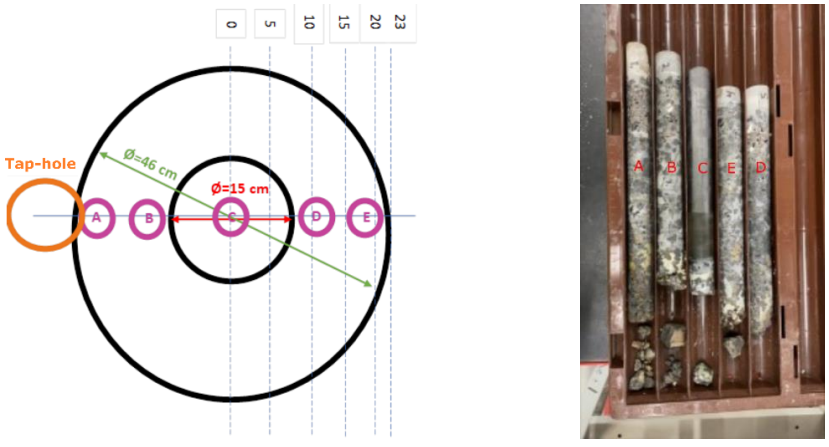

(a) (b)

Figure 4.25: (a) Schematic showing core drilling of excavated cokebed furnace interior. (b) Cores from the drilling.

4.3 Results

The results from pilot experimental work for the different charge mixtures are presented in this section. The tapped slag and alloy, and their respective analyses are presented. In addition, the main results from the digout of the prereduction zone and excavation of the cokebed zone of the pilot furnace are reported. The findings are reported for all the experiments following the order of Comilog series, Nchwaning series, and lastly, UMK and Mintek mix series. In this way the results are compared for untreated, preheated and prereduced mix for Comilog and Nchwaning ore, while the Mintek and UMK ores were not pretreated.

4.3.1 Comilog Series

4.3.1.1 Analyses of tapped slag and alloy

As previously mentioned in the experimental section, the pilot furnace is charged in batches and is periodically tapped every 80 kWh. The tapped slag and alloy, were separated at the end of the experiment, weighed, and analyzed. Table 4.6 shows the weight of slag and alloy at each tap for the experiments with untreated, preheated and prereduced Comilog.

Table 4.6: Weight of tapped slag and alloy for the experiments with untreated, preheated and prereduced Comilog charge mixtures

Tap #	Untreated Comilog			Preheated Comilog			Prereduced Comilog		
	Slag (kg)	Alloy (kg)	S/A ratio	Slag (kg)	Alloy (kg)	S/A ratio	Slag (kg)	Alloy (kg)	S/A ratio
1	-	9.33	0.00	13.5	15.4	0.88	22.1	18.9	1.17
2	27.6	18.2	1.52	9.61	13.6	0.71	8.88	15.4	0.58
3	8.31	10.1	0.82	8.24	13.0	0.63	11.7	17.9	0.65
4	8.59	14.4	0.60	6.60	10.6	0.62	12.8	18.5	0.69
5	8.13	14.2	0.57	8.37	12.0	0.70	12.9	18.5	0.70
6	9.36	15.4	0.61	6.97	11.5	0.61	11.7	20.1	0.58
7	9.66	14.5	0.67	3.73	8.89	0.42	8.47	19.0	0.44
8	7.48	14.5	0.52	6.32	11.9	0.53	9.61	19.1	0.50
9	6.38	12.9	0.50	3.03	7.03	0.43	8.39	19.6	0.43
10	6.22	11.3	0.55	8.91	10.4	0.86	9.37	20.0	0.47
11	4.32	11.2	0.39	4.56	9.00	0.51	11.0	20.0	0.55
12	6.06	12.5	0.48	3.75	9.00	0.42	7.93	19.7	0.40
Total	**102.1**	**158.4**	**0.64**	**83.6**	**132.2**	**0.63**	**134.9**	**226.6**	**0.60**
Tapping 7-12	40.1	76.9	0.52	30.3	56.2	0.54	54.8	117.4	0.47

The prereduced Comilog experiment gave the highest total weights of slag and alloy, followed by untreated Comilog and lastly, preheated Comilog as presented in Table 4.6. The slag/alloy ratios for the three pilot experiments are compared as presented in Figure 4.26. In each experiment, the planned slag/alloy ratio is compared to the slag/alloy ratios of the whole experiment (i.e., tapping 1-12), the second half of the experiment (i.e., tapping 7-12) and the calculated slag/alloy ratios. The calculated slag/alloy ratios were determined by mass balance in HSC Chemistry software as will be discussed in the mass and energy balance section (**Chapter 5**).

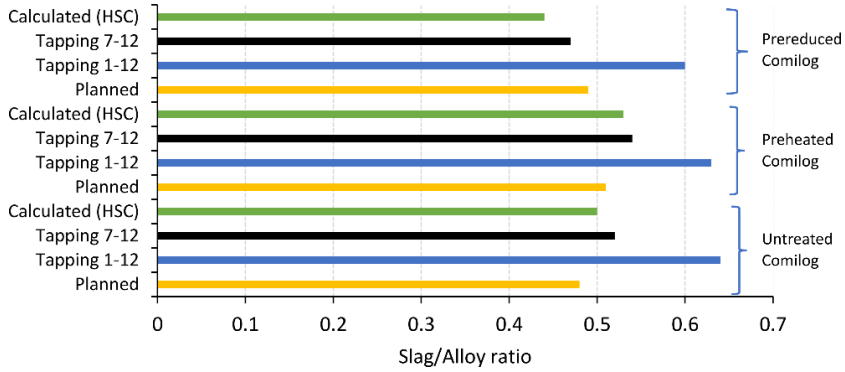

Figure 4.26: Comparison of the slag/alloy ratios for the whole experiments and tappings 7 to 12 with values from HSC mass balance calculation and the planned slag/alloy ratio in the untreated, preheated and prereduced Comilog experiments.

As expected, the process is unstable in the beginning and experimental slag/alloy ratios in each tapping are significantly higher as shown in Table 4.6. It can be seen that experimental slag/alloy ratios (i.e., tapping 1-12) for untreated and preheated Comilog are at the same region and higher than slag/alloy ratio in prereduced Comilog experiment. The same trend is observed for both the calculated and slag/alloy ratios for tapping 7-12. The slag/alloy ratios in tapping 7-12 in all experiments indicate a stable operation as they are close to the calculated values by mass balance. As presented in Table 4.6, the productivity is highest for prereduced Comilog experiment, followed by preheated Comilog and lastly untreated Comilog.

Figure 4.27 is an illustration of the variation of the slag and alloy composition with tapping number for the experiments in the Comilog series. Table 4.7, Table 4.8 and Table 4.9 show the slag compositions for the untreated, preheated and prereduced Comilog experiments. Target MnO content in the slag in the Comilog series experiments was 30 %. In all the experiments, the MnO content starts at high concentration and decreases with increasing tapping number. The first tapping in

untreated Comilog experiment was only alloy and from tapping 2 a slag with 53 % was tapped. The MnO content decreased to 34 % in tapping 4. Between tapping 7 and 12, the MnO content in slag was lower and fluctuating with an average 26.6 % MnO. The unreduceable oxides increase from tapping 2 to 4 and are stable between tapping 4 and 12. The average content of CaO, MgO, SiO_2 and Al_2O_3 components in slag between tapping 7 and 12 is 23.0 %, 0.99 %, 20.8 % and 25.7 %, respectively. The Al_2O_3/SiO_2 ratio increases signficantly from 1.1 in tapping 1 to 1.35 in tapping 12, this could indicate that there is some dissolution of Al_2O_3 from the Al_2O_3 based furnace lining during the experiment. It can be seen in Table 4.7 that the slag basicity is constant with an average basicity of 0.51. This basicity is close to 0.53 calculated from input material.

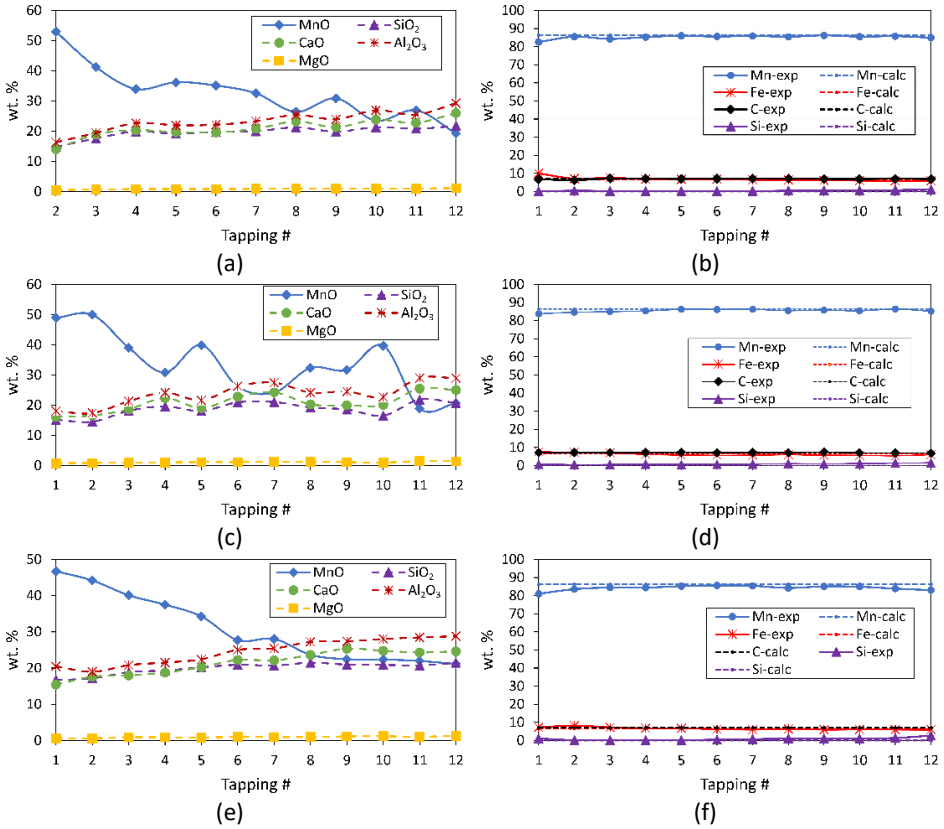

Figure 4.27: Variation of slag and alloy composition with tapping number for Comilog series experiments. Untreated Comilog (a & b), preheated Comilog (c & d) and prereduced Comilog (e & f).

As shown in Figure 4.27(c), the MnO content in the preheated Comilog experiment starts from 48.9 % and decreases to 30.8 % MnO in tapping 4. In the second half of the experiments i.e., tappings 7 to 12, the MnO content is fluctuating and unstable. In the same manner, the unreduceable oxides CaO, MgO, SiO_2 and Al_2O_3 are also fluctuating, decreasing and increasing in the same direction. As such, the basicity remains within the region of 0.52 +/-0.03, which is close to the planned 0.54. The Al_2O_3/SiO_2 ratio in the first for tapping is about 1.2 and increases to 1.4 in the last tapping, which is quite similar to observations from untreated Comilog experiment. The average MnO content between tapping 7 to 12 is 27.9 %.

Table 4.7: Measured slag composition for untreated Comilog experiment

Tap#	Slag Component (wt%)										
	Al_2O_3	BaO	CaO	K_2O	MgO	Fe	SiO_2	TiO_2	MnO	$Total$	$Basicity$
1											
2	16.3	0.60	14.0	0.14	0.46	0.74	14.8	0.02	53.0	100.0	0.46
3	19.4	0.66	18.9	0.28	0.67	0.67	17.6	0.02	41.2	99.4	0.53
4	22.7	0.75	20.3	0.26	0.79	0.60	19.9	0.03	34.0	99.3	0.50
5	22.0	0.75	19.6	0.20	0.82	0.67	19.1	0.03	36.2	99.4	0.50
6	22.1	0.75	19.6	0.23	0.82	0.64	19.7	0.03	35.1	99.0	0.49
7	23.3	0.78	20.8	0.22	0.85	0.77	19.9	0.05	32.5	99.2	0.50
8	25.4	0.85	23.2	0.21	0.96	0.60	21.2	0.07	26.4	98.8	0.52
9	24.0	0.81	21.3	0.21	1.00	1.07	19.8	0.08	30.8	99.1	0.51
10	26.9	0.86	23.8	0.18	1.00	0.60	21.3	0.10	23.5	98.1	0.51
11	25.4	0.84	22.8	0.20	0.99	0.76	20.8	0.08	26.9	98.7	0.51
12	29.3	0.92	26.0	0.27	1.13	0.73	21.7	0.02	19.2	99.3	0.53
Av. (7-12)	25.7	0.84	23.0	0.22	0.99	0.76	20.8	0.07	26.6	98.9	0.51

*Basicity, $B = \frac{CaO+MgO}{Al_2O_3+SiO_2}$

Table 4.8: Measured slag composition for preheated Comilog experiment

Tap#	Slag Component (wt%)										
	Al_2O_3	BaO	CaO	K_2O	MgO	Fe	SiO_2	TiO_2	MnO	$Total$	$Basicity$
1	18.0	0.65	16.1	0.08	0.77	0.58	15.2	0.02	48.9	100.3	0.51
2	17.4	0.63	16.6	0.08	0.83	1.06	14.5	0.02	50.0	101.0	0.55
3	21.3	0.73	18.6	0.17	0.97	0.63	18.1	0.02	39.1	99.6	0.50
4	24.1	0.77	22.4	0.12	1.03	0.63	19.6	0.07	30.8	99.5	0.53
5	21.6	0.74	19.1	0.15	1.14	1.55	18.1	0.05	39.9	102.3	0.51
6	26.3	0.87	22.8	0.15	1.13	0.75	21.0	0.07	26.1	99.1	0.51
7	27.4	0.87	24.3	0.24	1.32	0.81	21.0	0.07	24.2	100.2	0.53
8	24.2	0.78	20.3	0.28	1.18	0.80	19.3	0.10	32.3	99.2	0.49
9	24.5	0.76	20.0	1.13	1.12	0.89	18.6	0.12	31.7	98.8	0.49
10	22.7	0.72	20.1	0.74	0.98	1.89	16.5	0.13	39.7	103.4	0.54
11	29.0	0.91	25.5	0.45	1.46	0.70	21.9	0.17	18.9	99.0	0.53
12	28.9	0.88	25.0	0.52	1.39	0.87	20.7	0.17	20.6	99.1	0.53
Av. (7-12)	26.1	0.82	22.5	0.56	1.24	0.99	19.7	0.13	27.9	99.9	0.52

*Basicity, $B = \frac{CaO+MgO}{Al_2O_3+SiO_2}$

Table 4.9: Measured slag composition for prereduced Comilog experiment

Tap#	Slag Component (wt%)										
	Al_2O_3	BaO	CaO	K_2O	MgO	Fe	SiO_2	TiO_2	MnO	$Total$	$Basicity$
1	20.5	0.63	15.4	0.09	0.65	0.66	16.7	0.46	46.7	101.8	0.43
2	19.0	0.65	17.6	0.11	0.61	0.74	17.2	0.47	44.2	100.5	0.50
3	20.8	0.7	18.0	0.24	0.9	0.72	18.9	0.5	40.1	100.8	0.48
4	21.5	0.73	18.8	0.35	0.87	0.78	19.3	0.51	37.5	100.4	0.48
5	22.4	0.74	20.3	0.37	0.84	0.73	20.2	0.52	34.3	100.3	0.50
6	25.0	0.85	22.3	0.41	0.98	0.65	20.9	0.49	27.7	99.3	0.51
7	25.4	0.86	22.1	0.4	0.93	0.8	20.7	0.46	28.1	99.7	0.50
8	27.2	0.92	23.6	0.39	0.96	0.69	21.5	0.43	23.7	99.4	0.51
9	27.4	0.89	25.4	0.32	1.13	0.84	21.0	0.39	22.5	99.7	0.55
10	28.0	0.92	24.8	0.36	1.17	0.79	20.9	0.38	22.4	99.7	0.53
11	28.5	0.96	24.3	0.41	1.06	0.7	20.7	0.37	22.0	99.0	0.52
12	28.8	0.94	24.6	0.37	1.23	0.81	21.5	0.38	21.1	99.8	0.51
Av. (7-12)	27.6	0.92	24.1	0.38	1.08	0.77	21.1	0.40	23.3	99.6	0.52

*Basicity, $B = \frac{CaO+MgO}{Al_2O_3+SiO_2}$

Figure 4.27 (d) shows that the MnO content in prereduced Comilog experiment starts from 46.7 % and decreases until 27.7 % MnO in tapping 6. The period tapping 7 to 12 is on average at 23.3% MnO and is stable compared to tapping 1 to 6. It can also be seen that the unreducible oxides CaO, MgO, SiO_2 and Al_2O_3 gradually increases with tapping due to the lower MnO content. There is a potential dissolution of Al_2O_3 from the furnace lining as previously observed in the untreated and preheated Comilog experiment. This is mainly due to increase in Al_2O_3/SiO_2 ratio in slag. Prereduced Comilog shows a more stable operation between tapping 7-12, compared to untreated and preheated Comilog experiments. This fits very well with the MnO content and slag/alloy ratio which is lowest in prereduced Comilog experiment.

The alloy composition in the Comilog series experiment is in general close to the targeted composition from tapping 4 to 12 as shown in Figure 4.27(b), (d) and (f). The measured alloy compositions for each tapping and experimental average are compared to the planned alloy composition in Table 4.10 for untreated and preheated Comilog. Table 4.11 show the alloy composition measured and the calculated values for prereduced Comilog experiment. It can be summarized that the alloy compositions in all the experiments are within the same region with minor variations.

Table 4.10: Alloy composition for untreated and preheated Comilog experiments

Tap	Untreated Comilog						Preheated Comilog				
#	Mn	Fe	Si	C	Tot		Mn	Fe	Si	C	Tot
1	82.6	10.0	0.2	6.8	99.5		83.8	7.6	0.8	7.1	99.3
2	85.5	7.1	0.4	6.2	99.2		84.6	7.3	0.5	7.2	99.6
3	84.3	7.6	0.3	7.2	99.3		84.9	7.0	0.6	7.1	99.6
4	85.3	6.8	0.2	7.1	99.4		85.3	6.1	0.7	7.1	99.3
5	86.0	6.7	0.2	7.0	99.8		86.2	5.8	0.6	7.3	99.8
6	85.6	6.7	0.1	7.1	99.6		86.2	5.6	0.7	7.1	99.5
7	86.0	6.5	0.2	7.0	99.7		86.2	5.7	0.7	7.2	99.8
8	85.5	6.4	0.4	7.1	99.4		85.5	5.9	1.0	7.1	99.5
9	86.2	6.2	0.5	7.0	99.8		85.8	5.7	0.9	7.5	99.8
10	85.5	6.0	0.7	6.9	99.1		85.4	5.6	1.1	7.0	99.1
11	85.8	5.9	0.7	7.1	99.4		86.4	5.4	1.3	7.0	100
12	85.0	5.9	1.2	6.9	99.0		85.2	6.0	1.5	6.8	99.5
Exp. avg	82.6	6.8	0.4	6.9	99.5	Exp. avg	85.5	6.1	0.9	7.1	99.6
Avg. Tap 7 - 12	85.7	6.1	0.6	7.0	99.4	Avg. Tap 7 - 12	85.8	5.7	1.1	7.1	99.6

Table 4.11: Alloy composition for prereduced Comilog experiments

Tap	Prereduced Comilog				
#	Mn	Fe	Si	C	Tot
1	81.1	7.2	1.1	7.0	96.4
2	83.6	8.2	0.2	7.0	98.9
3	84.5	7.2	0.2	7.0	98.9
4	84.4	6.8	0.3	7.0	98.5
5	85.2	6.7	0.2	7.0	99.2
6	85.7	6.3	0.5	7.0	99.4
7	85.4	6.0	0.7	7.0	99.2
8	84.3	6.3	1.0	7.0	98.6
9	85.1	6.0	1.0	7.0	99.2
10	84.9	6.1	1.1	7.0	99.2
11	83.9	6.1	1.4	7.0	98.3
12	83.0	6.0	2.7	7.0	98.7
Exp. avg	84.3	6.6	0.9	7.0	98.7
Avg. Tap 7 - 12	84.4	6.1	1.3	7.0	98.9

4.3.1.2 Composition of prereduced samples

Prereduced samples were excavated by digging out samples in the prereduction zone from two regions close to the electrodes and two regions close to the wall of the furnace as has been described in section 4.2.5.1 of the post experimental work. The raw materials in the burden were observed to be loosely sintered during the digout of the prereduction zone down to a depth of about 60cm from the top of the furnace in all experiments. The detailed chemical composition of the samples from the digout of prereduction zone of all pilot experiments are presented in **Appendix D**, indicating the oxygen level in the ore as x in MnO_x. The two MnO_x values on the same level, and same distance from the electrode, for each region were averaged. Figure 4.28 shows the oxidation level of manganese (i.e., x in MnO_x) in regions close to the electrode (B

& D) and furnace lining (A & C) for untreated, preheated and prereduced Comilog experiments. In addition, the trends based on averages are indicated.

The initial MnO_x values for untreated, preheated and prereduced Comilog were 1.98, 1.59 and 1.50, respectively. It can be seen that there is a greater extent of prereduction adjacent the electrode compared to ore materials in regions adjacent the furnace lining in all the three experiments. This is an indication of prevailing high temperature conditions for ore materials close to the electrode. In order to get an overview of the overall prereduction extent in the pilot furnace, it was assumed that the ore reduction followed a material distribution of 70% and 30% for material close to the electrode and furnace wall, respectively. A comparison of the variation of MnO_x for the three ores is as shown in Figure 4.28(d). The prereduction of untreated Comilog starts at a higher MnO_x on top of the charge material compared to preheated and prereduced Comilog ores. As prereduction proceeds, the MnO_x in all ores are within the same values at a depth of 40cm and proceeds with the same extent until the materials reaches the lowest MnO_x at 60cm depth. There are not any significant differences between the prereduction trend for preheated and prereduced Comilog ore.

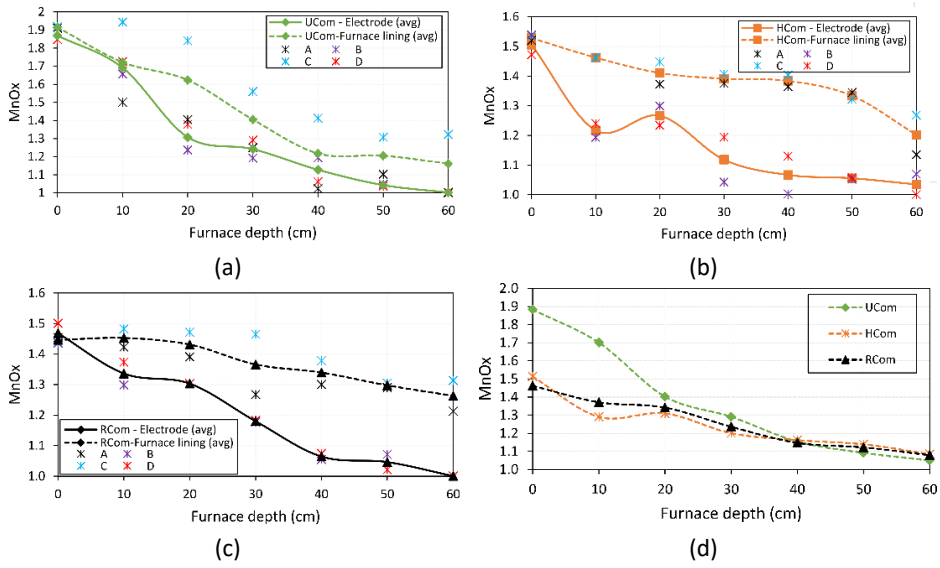

Figure 4.28: MnO_x as a function of depth from the top of charge material. (a) Untreated Comilog (UCom), (b) Preheated Comilog (HCom), (c) Prereduced Comilog (RCom) & (d) Comparison of MnO_x vs depth for the three experiments assuming a 70/30 Electrode/Furnace ratio of flow material in each experiment.

4.3.1.3 Composition of excavated samples from the cokebed zone

As described in section 4.2.5.2, different regions were observed from excavated plates. Typical regions are unmelted charge, partially molten charge, coke enriched region, slag enriched region and alloy region within the excavated plates. In this section, sketches of different points from which samples were core drilled will be illustrated. Samples were core drilled from the cross-sections of the coke bed zone of untreated, preheated and prereduced Comilog excavations as illustrated in Figure 4.29.

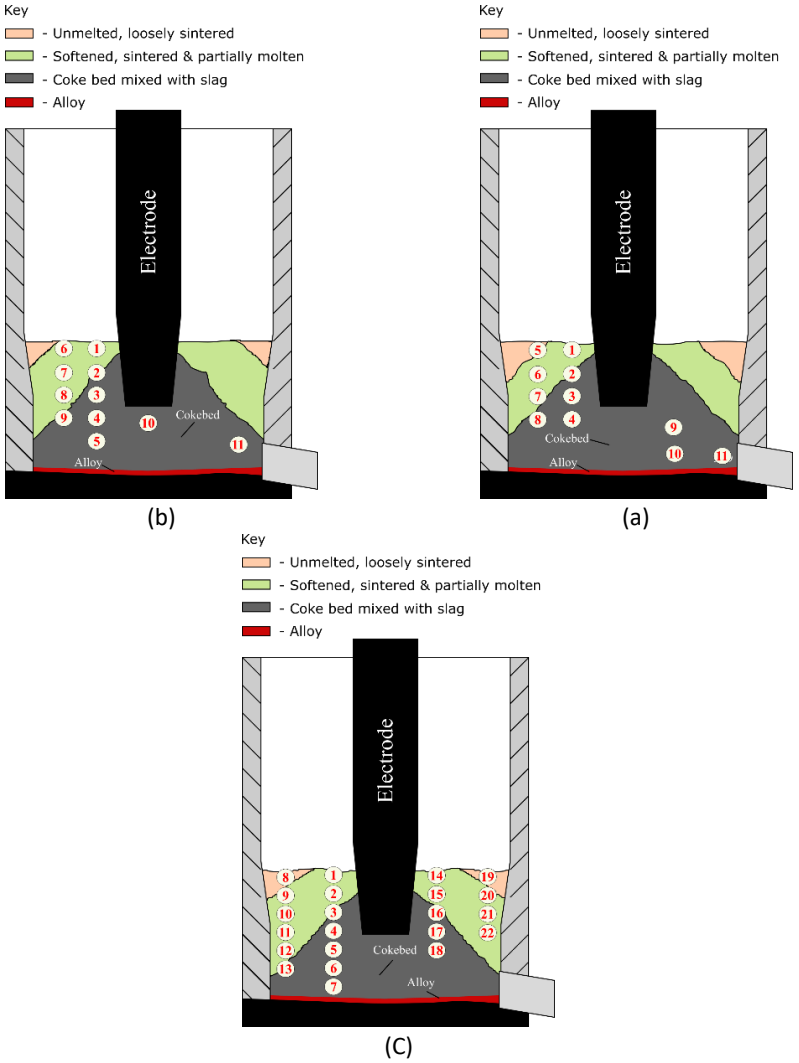

Figure 4.29: Sample positions in the cross-section of cokebed in Comilog series experiments. (a) Untreated Comilog samples 1-11 (named UC1-UC11), (b) preheated Comilog samples 1-11 (named HC1-HC11), & prereduced Comilog samples 1-22 (named RC1-RC22)

In cokebed cross-sections from untreated and preheated Comilog, samples were generally excavated vertically from top of the cross-sections, at 5cm from the electrode and 10cm from the electrode, with other samples core drilled at selected points inside the cokebed. For prereduced Comilog experiment, vertical cores at 5cm and 10cm distances from the electrode were drilled and samples taken at 5cm interval distances in each core. The samples are named into three categories namely; UC1-11 for the untreated Comilog samples, HC1-12 for the preheated Comilog samples and RC1-22 for the prereduced Comilog samples. The cokebed size and shape was observed to be similar in Comilog series. The region with partially molten material was observed to be slightly larger in the prereduced Comilog experiment compared to untreated and preheated Comilog experiments.

Figure 4.30 shows the backscattered micrographs of samples UC1 – 5, from excavation of cokebed from untreated Comilog experiment. The samples are from 5cm vertical distance adjacent the electrode. Microstructure of these samples show a variety of phases as observed using backscattered electron images. These samples were close to the electrode were temperature conditions are expected to be generally high, and it can be seen from the micrographs that the phases are mostly a liquid slag and alloy in all the samples. This implies that there is more dissolution of the solid monoxide phase and reduction of liquid slag in this region. The slag phase is composed mostly of dark and light grey phase regions. The dark grey matrix is rich in SiO_2, CaO and Al_2O_3, whereas the light grey matrix is mainly composed of MnO, SiO_2 and CaO. In contrast, Figure 4.31 shows samples UC 6 – 9 taken from 10cm distance from the electrode, typically composed of four phases namely FeMn alloy, solid MnO and a slag matrix composed of dark and light grey regions. The presence of solid MnO in these samples imply that there is less reduction and dissolution of MnO in liquid slag compared to samples from 5 cm adjacent the electrode. Samples UC-10 and UC-11, show a reduced slag phase which had been completely liquid at high temperatures and the dendrites in UC-11 had precipitated during solidification. The composition of each of the phases were found by three-point analysis in EPMA. The composition of liquid slag and the total MnO considering area fraction of solid MnO were found based on area fraction analysis in ImageJ®. The slag composition results are presented in Table 4.12 for selected samples.

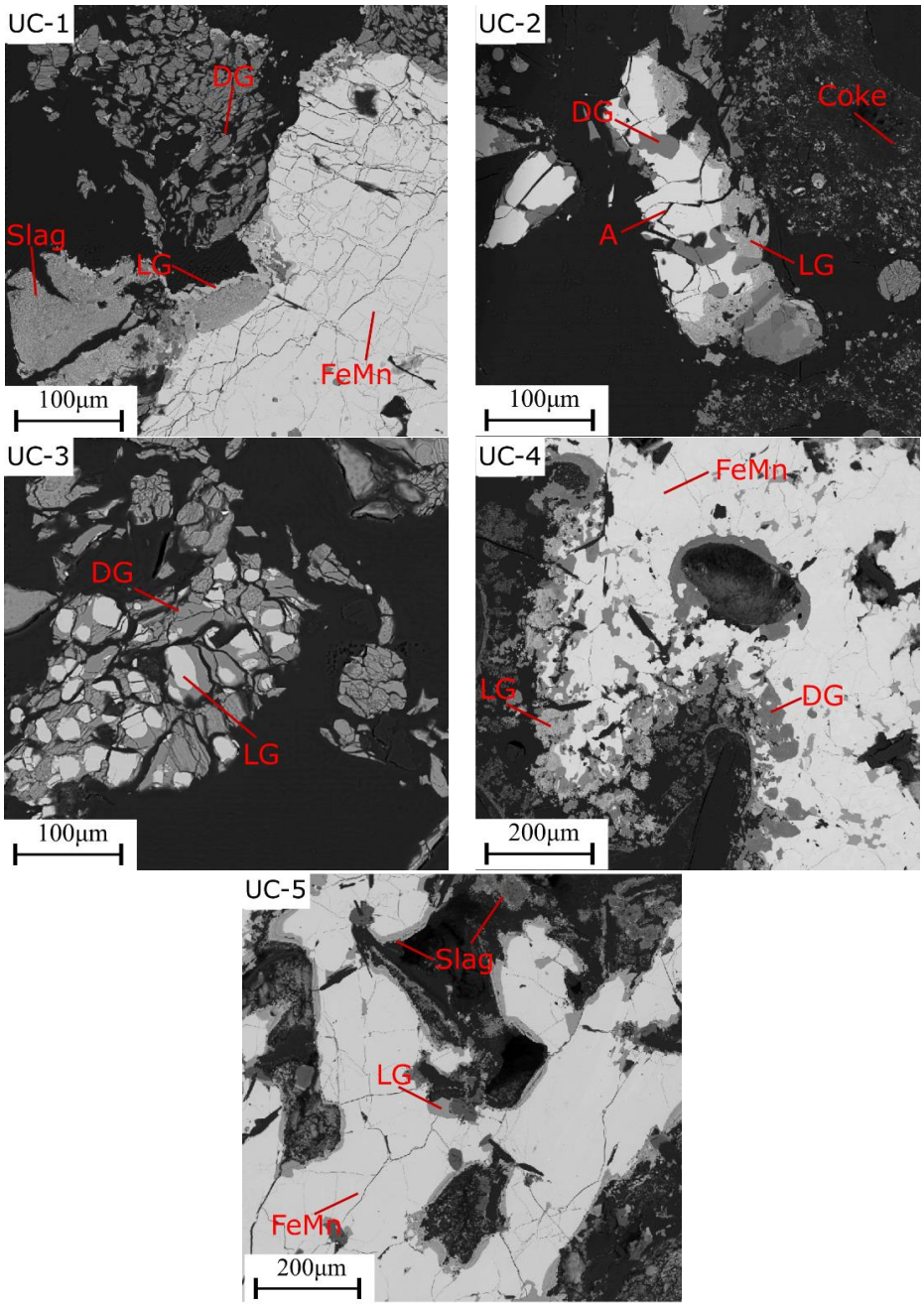

Figure 4.30: Backscattered electron micrographs of untreated Comilog samples UC-1, UC-2, UC-3, UC-4, and UC-5 collected from positions 5cm vertically adjacent the electrode. Legend: DG = dark grey phase; LG = light grey phase.

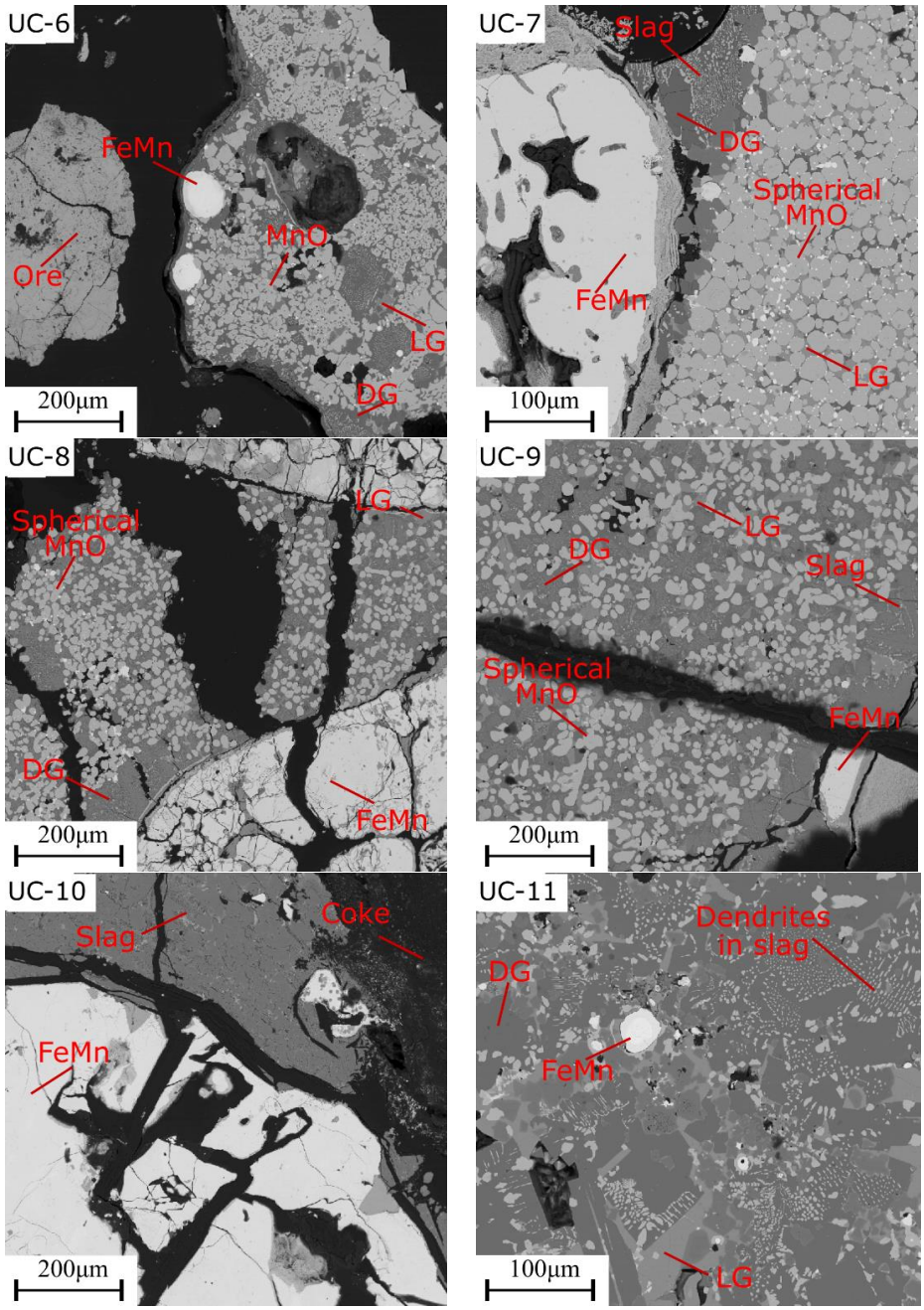

Figure 4.31: Backscattered electron micrographs of untreated Comilog samples UC-6, UC-7, UC-8, and UC-9 collected from positions 10cm vertically adjacent the electrode. Samples UC-10 and UC-11 are from below the tip of the electrode and close to the taphole, respectively. Legend: DG = dark grey phase; LG = light grey phase.

Table 4.12: Calculated liquid slag composition based on measured area fraction by ImageJ® and EPMA phase analysis for samples from untreated Comilog experiment.

Sample		UC2	UC3	UC4	UC6	UC7	UC8	UC9	UC10	UC11
Area fraction (%)	Monoxide	-	-	-	51.2	69.7	42.0	39.8	-	6.50
	LG phase	66.9	29.9	35.1	48.8	15.7	56.5	23.6	-	34.2
	DG phase	33.1	70.1	64.8	4.42	14.6	1.50	37.7	100	59.3
Total MnO (wt. pct)		57.5	31.3	51.5	78.7	87.0	60.1	47.9	0.03	22.5
Liquid slag	MnO	57.5	31.3	51.5	56.7	57.0	33.2	16.3	0.03	22.5
	FeO	2.65	0.06	4.23	0.32	0.28	0.06	0.03	-	0.07
	SiO_2	19.0	2.69	32.2	28.7	28.4	29.0	23.0	-	17.4
	Al_2O_3	2.41	32.6	1.70	0.43	0.47	1.31	21.0	61.1	30.3
	CaO	0.83	28.4	0.05	13.4	13.2	32.7	34.0	32.6	26.0
	MgO	0.01	0.64	0.01	1.24	1.23	0.80	0.88	0.01	0.96
	BaO	0.09	0.14	0.42	0.03	0.02	0.09	0.09	2.17	0.09
	TiO_2	0.01	0.11	0.02	0.18	0.20	0.44	0.23	0.12	0.15
	Total	86.2	96.0	94.4	101.0	100	97.6	95.6	96.1	97.5
	Basicity	0.01	0.82	0.002	0.50	0.50	1.11	0.79	0.53	0.56

As presented in Table 4.12, samples UC1 and UC5 are not included as they were mostly alloy and hence no slag regions could be used to estimate liquid slag composition. Samples UC2 – UC4 were completely liquid with no solid MnO and contained between 31.3 to 57.5 % MnO in liquid slag. Samples UC6 to UC9 show a trend of decreasing fraction of solid MnO phase. The total MnO content is 78.7 % MnO in UC6 whereas the liquid slag contains 57 % MnO which is similar to % MnO in liquid slag for UC7. The CaO content in liquid slag is higher for UC8 and UC9 compared to UC6 and UC7. This shows that there is an increased dissolution of lime into the slag phase when approaching the high temperature regions of the cokebed, resulting in lower %MnO in liquid slag. Sample UC10 was mostly composed of Al_2O_3 and CaO. The composition of sample UC11 which was close to the tap hole had a 22.5 % MnO content in liquid slag which is quite close to 19.2 % MnO in slag from the last tapping measured by XRF as shown in Table 4.7. It can be seen that the basicity of this sample i.e., 0.56 is the close to 0.53 found in the tapped slag.

Figure 4.32 shows the backscattered micrographs of samples HC1 – 4 from 5cm vertical distance adjacent the electrode excavated from the preheated Comilog experiment. Backscattered micrographs for samples HC5 – 11 are shown in Figure 4.33. Samples HC5 – 8 were from 10 cm adjacent the electrode and samples HC9 – 11 were from selected positions close to the tap hole. Backscattered micrograph for HC1 consists of FeMn alloy, solid MnO and a slag matrix composed of dark and light grey regions. The slag phases in HC2-4 do not contain any solid MnO phase and the micrographs show mostly alloy phase. Sample HC5 is mostly a softened ore particles were no solid MnO and liquid slag matrix are formed. The microstructure of sample

HC6 and HC7 consists of spherical manganosite (MnO) phases in co-existence with a light and dark grey slag matrix and the smallest brightest particles are metal drops. The slag in micrographs from HC8 – 11 are considered completely liquid at high temperatures and the solid MnO observed in HC11 precipitated during cooling. The composition of liquid slag and the total MnO in samples were found by EPMA and evaluation area fraction all the phases. Details of the liquid slag composition presented in Table 4.13.

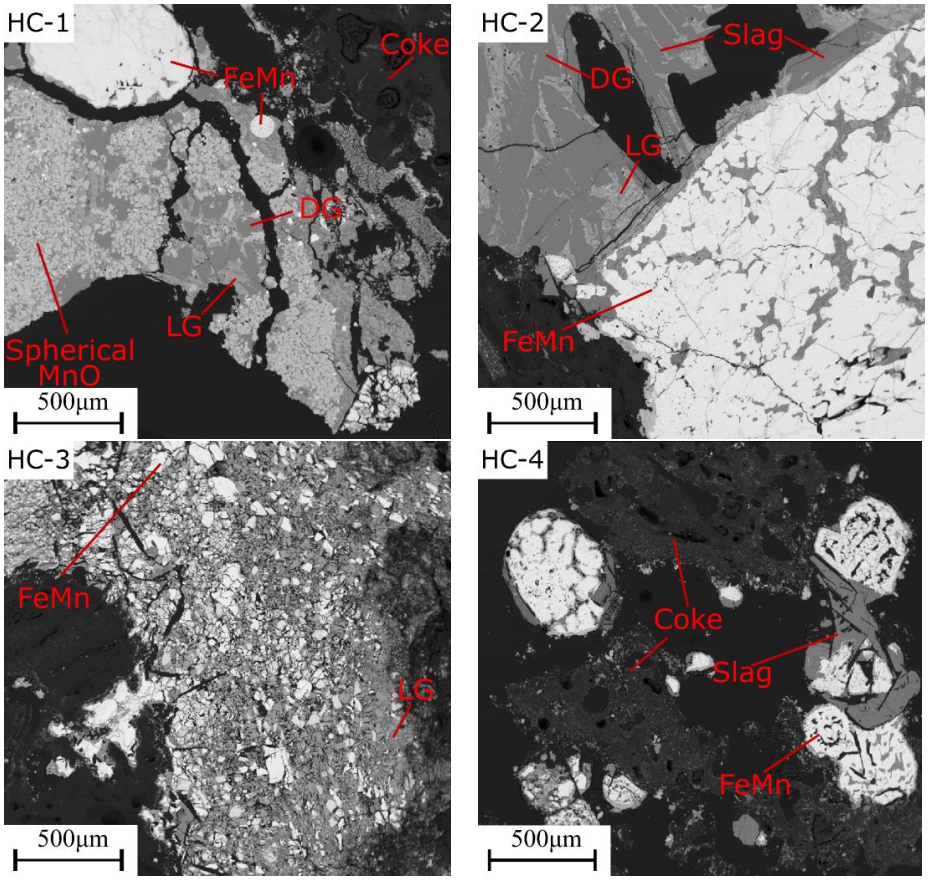

Figure 4.32: Backscattered electron micrographs of preheated Comilog samples HC-1, HC-2, HC-3, and HC-4 from positions 5cm vertically adjacent the electrode. Legend: DG = dark grey phase; LG = light grey phase.

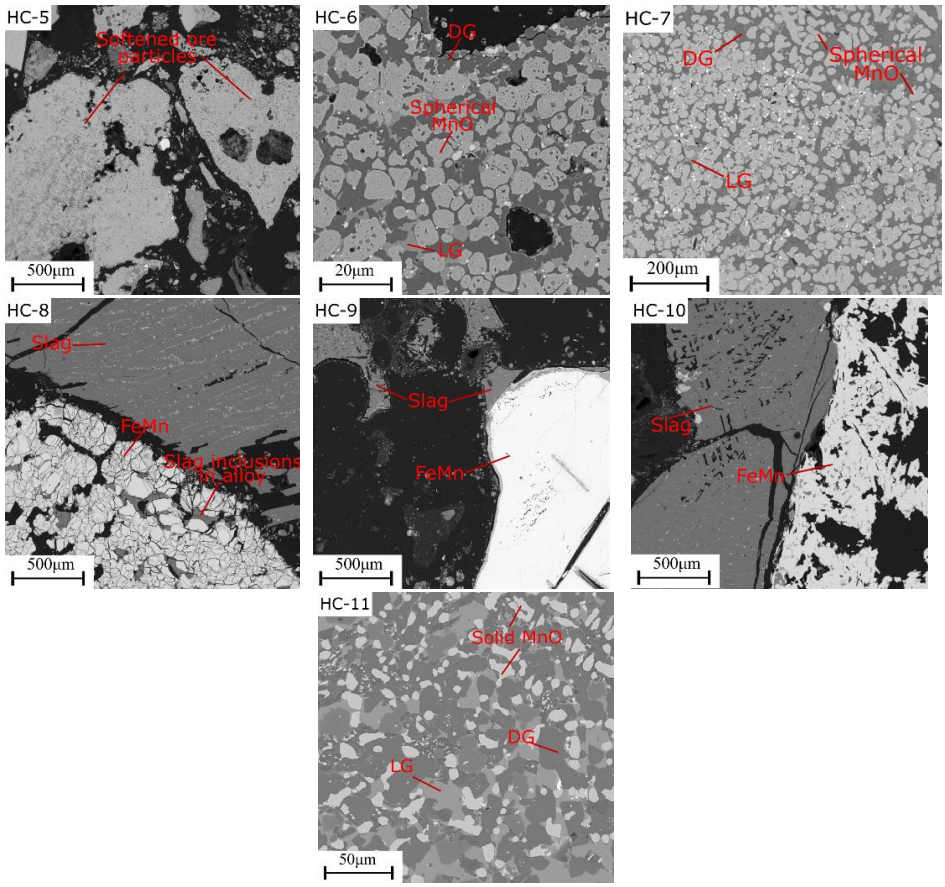

Figure 4.33: Backscattered electron micrographs of preheated Comilog samples HC-5, HC-6, HC-7, and HC-8 collected from positions 10cm vertically adjacent the electrode. Samples HC-9, HC-10 and HC-11 are from positions inside the cokebed and close to the taphole.

Table 4.13: Calculated liquid slag composition based on measured area fraction by ImageJ® and EPMA phase analysis for samples from preheated Comilog experiment

Sample		HC1	HC2	HC3	HC4	HC6	HC7	HC8	HC9	HC10	HC11
Area fraction (%)	Monoxide	38.8	-	-	-	45.1	51.9	-	-	-	17.1
	LG phase	36.2	26.7	100	33.8	15.6	23.9	24.5	-	-	37.5
	DG phase	25.0	73.4	-	66.2	39.4	24.2	75.5	100	-	45.4
Total MnO (wt. pct)		69.2	11.9	35.9	1.06	55.1	61.6	9.50	0.50		33.4
Liquid slag	MnO	51.3	11.9	35.9	1.06	21.2	23.4	9.50	0.50	3.23	22.4
	FeO	0.17	0.03	0.22	0.02	0.29	0.15	0.05	-	-	0.08
	SiO_2	17.3	22.6	56.1	13.0	35.0	25.6	28.4	5.53	16.4	17.3
	Al_2O_3	25.8	32.4	0.24	52.9	23.8	19.1	32.2	55.8	42.1	25.2
	CaO	4.86	30.6	1.08	32.2	0.73	30.7	21.9	35.0	32.7	22.3
	MgO	0.90	0.47	0.02	0.01	0.05	0.96	0.90	-	1.15	0.74
	Total	100.4	99.0	100.4	99.2	100.9	100	96.0	96.8	95.8	99.2
	Basicity	0.13	0.57	0.02	0.49	0.01	0.71	0.38	0.57	0.58	0.54

The backscattered micrographs for samples RC1 – 7 and RC8 – 13 from prereduced Comilog experiment are shown in Figure 4.34 and Figure 4.35, respectively. Samples RC1 – 7 are from 5cm vertically adjacent the electrode. The microstructure of RC1 and RC2 consists of spherical manganosite (MnO) phases in co-existence with a light and dark grey slag matrix and the smallest brightest particles are metal prills. RC3 is an alloy phase composed of some slag inclusions. The slags in RC4 – 6 have been completely liquid at high temperature with dendrites precipitating on cooling. The backscattered micrograph for RC7 is an alloy phase consisting of light and dark grey regions. The light grey regions are rich in Si with a composition of 87.5 % Mn, 8.45 % Fe, 4.72 %Si and 4.51 % C as measured in EPMA WDS. The composition of the dark grey areas was 87.5 % Mn, 5.01 % Fe and 5.85 % C.

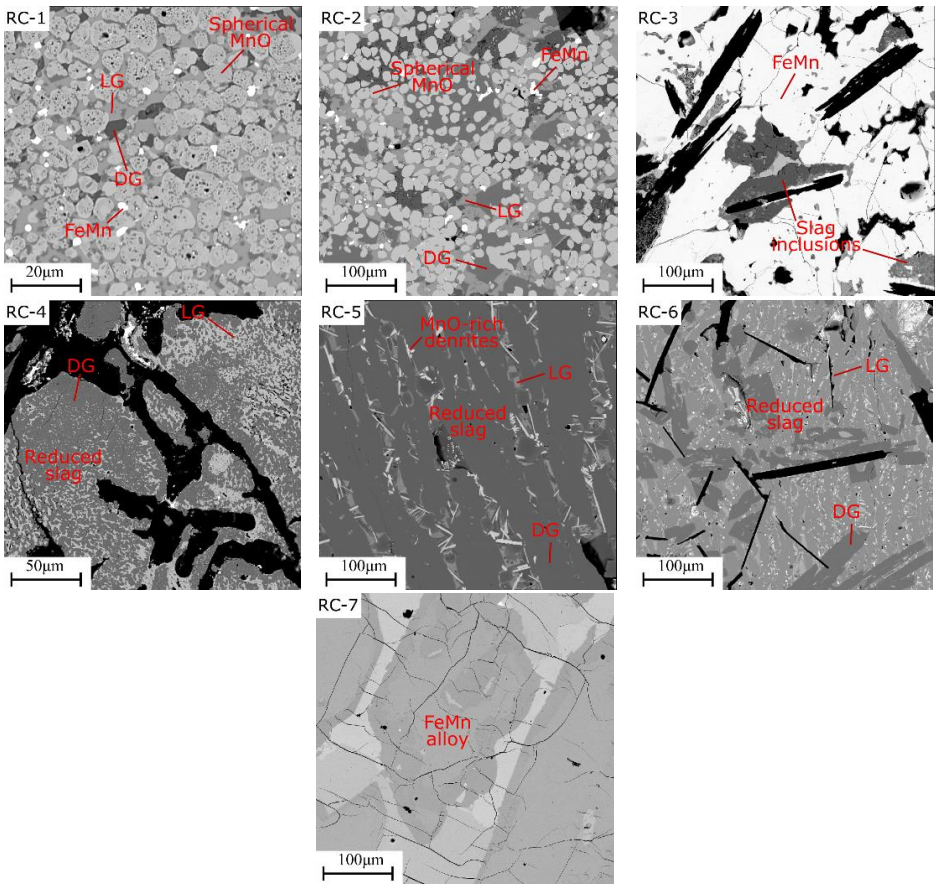

Figure 4.34: Backscattered electron micrographs of prereduced Comilog samples RC-1 to RC-7 from positions 5cm vertically adjacent the electrode. Legend: DG = dark grey phase; LG = light grey phase.

Samples RC8 and RC9 are mostly sinter consisting of MnO rich phase with sharp edges, light grey phase (Mn_2SiO_4) and medium grey phase rich in MnO and Al_2O_3. The microstructure of RC10 and RC11 consists of mostly solid MnO phase in co-existence with a slag matrix. The total MnO content in samples RC8 – 11 varies widely between 63.5 % to 80%. The slag in RC12 and RC13 has been completely liquid at high temperature and the MnO content is at 33.6 and 32 % MnO, respectively whereas the basicities of these slags is significantly different as presented in Table 4.14.

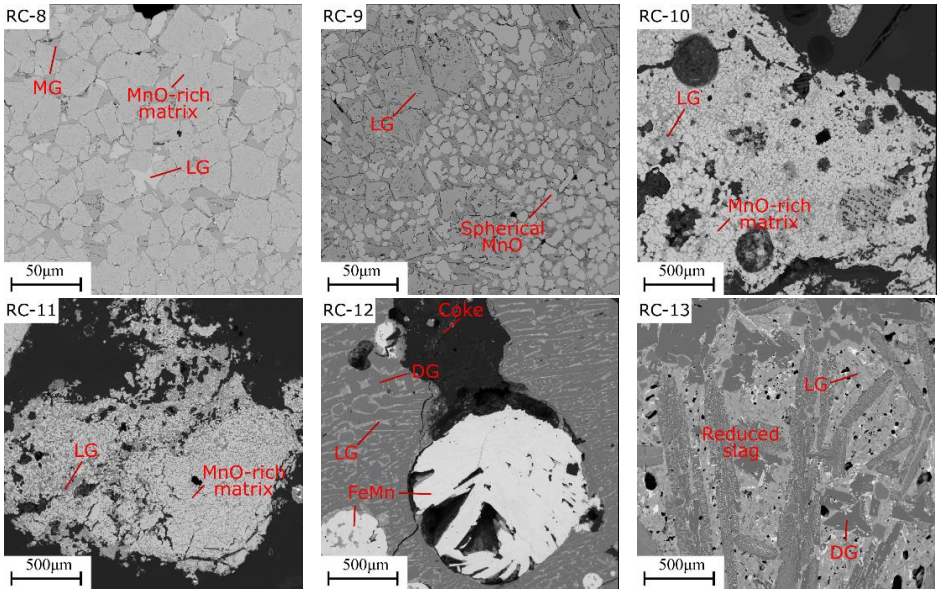

Figure 4.35: Backscattered electron micrographs of prereduced Comilog samples RC-8 to RC-13 from positions 10cm vertically adjacent the electrode. Legend: DG = dark grey phase; MG = medium grey phase & LG = light grey phase.

Table 4.14: Calculated liquid slag composition based on measured area fraction by ImageJ® and EPMA phase analysis for samples from prereduced Comilog experiment

Sample		RC1	RC2	RC4	RC5	RC6	RC12	RC13
Area fraction (%)	Monoxide	56.7	46.8	-	-	-	-	12.3
	LG phase	28.2	22.0	44.6	18.1	68.9	22.6	44.1
	DG phase	0.15	32.3	55.4	81.2	31.1	77.4	43.6
Total MnO (wt. pct)		82.2	76.7	28.5	5.65	3.85	33.6	32.0
Liquid slag	MnO	59.5	40.6	28.5	5.65	3.85	33.6	32.0
	FeO	1.28	0.15	0.16	0.02	0.02	0.07	0.08
	SiO_2	17.5	19.3	32.7	23.1	17.7	5.16	16.5
	Al_2O_3	21.2	29.2	18.2	34.2	47.9	50.0	24.1
	CaO	0.25	4.04	2.25	35.6	26.4	2.05	22.6
	MgO	0.15	0.18	-	0.13	0.39	4.61	0.56
	Total	100	99.3	97.7	99.0	99.7	96.1	95.9
	Basicity	0.01	0.09	0.04	0.60	0.41	0.12	0.57

4.3.2. Nchwaning series

4.3.2.1 Analyses of tapped slag and alloy

Table 4.15 shows the weight of slag and alloy at each tapping for the experiments with untreated, preheated and prereduced Nchwaning. In all the experiments in the Nchwaning series, the initial tapping was after 150kWh of energy input. The energy input inbetween tappings from tapping 1 to 12 in untreated Nchwaning experiment was after every 80 kWh. Due to challenges with tapping the furnace in the preheated Nchwaning experiment, this pilot experiment was tapped on average after every of 103 kWh of energy input from the first tapping. As such this resulted in 7 tappings within the entire duration of the pilot experiment. As can be seen in Table 4.15, the pilot experiment with prereduced Nchwaning had the lowest number of taps with only 5 taps, which were at 80kWh energy input intervals from the first tap.

In contrast to prereduced Nchwaning experiment, the first taps in untreated and preheated Nchwaning were very low in the total weight, with mostly alloy tapped. The untreated Nchwaning experiment gave a total of 90.1 kg and 198.7 kg of slag and alloy, respectively. The slag/alloy ratio for the whole experiment was 0.45. The slag/alloy ratio for the whole preheated Nchwaning experiment was 0.33 for total slag and alloy weight of 64.0 kg and 195.1 kg, respectively. The prereduced Nchwaning experiment had a total slag and alloy weight of 24.5 kg and 71.6 kg, respectively. The slag/alloy ratio was 0.35 and this experiment was stopped after 5 taps due to difficulties in tapping the furnace.

Table 4.15: Weight of tapped slag and alloy for the experiments with untreated, preheated and prereduced Nchwaning charge mixtures.

Tap #	Untreated Nchwaning			Preheated Nchwaning			Prereduced Nchwaning		
	Slag (kg)	Alloy (kg)	S/A ratio	Slag (kg)	Alloy (kg)	S/A ratio	Slag (kg)	Alloy (kg)	S/A ratio
1	0.72	11.8	0.06	0.91	13.8	0.07	5.33	21.0	0.25
2	2.46	15.8	0.16	0.85	28.6	0.03	6.86	20.7	0.33
3	20.9	24.3	0.86	24.5	28.3	0.87	6.1	14.8	0.41
4	0.32	16.0	0.02	7.37	28.7	0.26	3.16	11.0	0.29
5	17.8	25.1	0.71	9.23	27.9	0.33	3.32	4.14	0.80
6	5.08	16.7	0.30	10.2	33.7	0.30			
7	8.96	16.8	0.53	10.9	34.1	0.32			
8	6.71	13.3	0.51						
9	8.20	17.6	0.47						
10	7.52	13.7	0.55						
11	6.45	14.6	0.44						
12	5.00	13.0	0.39						
Total	**90.1**	**198.7**	**0.45**	**64.0**	**195.1**	**0.33**	**24.8**	**71.6**	**0.35**

The planned slag/alloy ratio and HSC based calculated ratios in each experiment are compared to slag/alloy ratios of the entire experiments and slag/alloy ratios in tappings 7-12 for untreated Nchwaning, tappings 4-7 for preheated Nchwaning and tappings 2-5 for prereduced Nchwaning experiment as shown in Figure 4.36. It can be seen that the planned slag/alloy ratio for untreated Nchwaning experiment was lower than the experimental as well as the last 6 tappings. In this experiment, the HSC calculated slag/alloy ratio is lower than experimental values. In the preheated Nchwaning experiment, the whole experiment and last 4 tappings had lower slag/alloy ratios compared to the planned values and HSC values. For the prereduced Nchwaning experiment, the slag/alloy ratios for tappings 2-5 are higher when compared to values from HSC and the planned slag/alloy ratio.

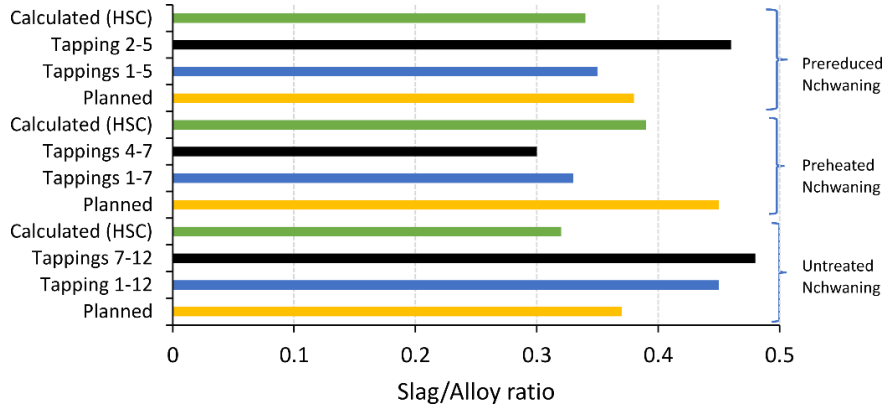

Figure 4.36: Comparison of experimental slag/alloy ratios with values from HSC mass balance calculation and the planned slag/alloy ratio in the untreated, preheated and prereduced Nchwaning experiments.

The variation of the slag and alloy composition with tapping number for the experiments in the Nchwaning series is as shown in Figure 4.37. The detailed compositions for the untreated, preheated and prereduced Nchwaning experiments are shown in Table 4.16, Table 4.17 and Table 4.18, respectively. In all the experiments, the MnO content starts at high concentration and decreases with increasing tapping number. It can be seen that no stable period was reached in all the experiments. As shown in Figure 4.37(a), the MnO content in the untreated Nchwaning experiment starts from 58.0 % and decreases with no stable composition reached until 21.1 % MnO in the last tapping. The average MnO content in the last tappings 7-12 is 27.4 %, which is slightly lower than the planned 30 % MnO in slag. The unreduceable oxides of CaO, MgO, SiO_2 and Al_2O_3 slightly increase from first tappings and are relatively stable in the last 6 tappings at 25.1 %, 6.15 %, 24.8 %

and 10.8 %, respectively. The basicity values are also shown in Table 4.16, and the basicity values are close to 0.9 for tapping 7 to 12. The basicity is relatively stable between 0.87 and 0.9 and higher than the planned 0.81. This could possibly explain the relatively lower MnO content in the slag than planned. Figure 4.37(b) shows that from tapping 2, the alloy composition is stable and close to the planned composition.

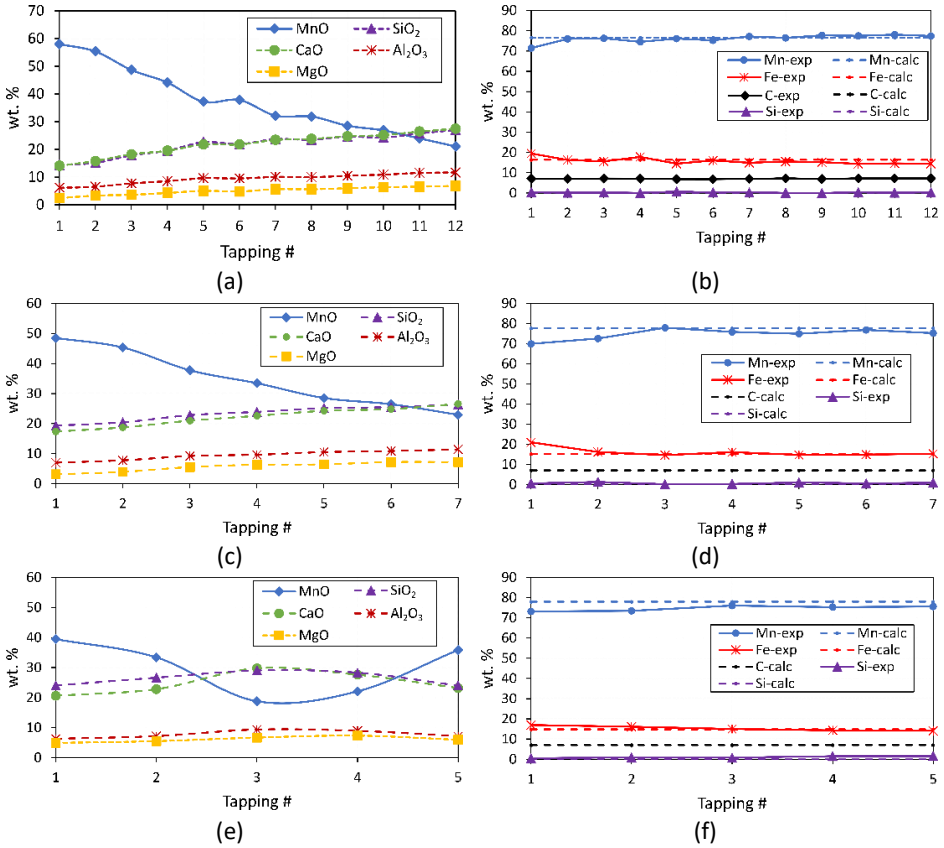

Figure 4.37: Variation of slag and alloy composition with tapping number for Comilog series experiments. Untreated Nchwaning (a & b), preheated Nchwaning (c & d) and prereduced Nchwaning (e & f).

Figure 4.37(c) shows that the MnO content in preheated Nchwaning experiment starts from 48.5 % and decreases with no stable composition reached until 22.9 % MnO in the last tapping. The targeted basicity from raw materials input in this experiment was 0.84 and as can be seen in Table 4.17, the basicity for tappings 4 to 7 is stable and on average at 0.87 and increases to 0.9 in the last tapping. The average MnO content in the period where basicity is stable i.e., tapping 4 to 7, is 27.8 % which is closer to the planned 30 % MnO. In the same period, the unreduceable oxides of CaO, MgO, SiO_2 and Al_2O_3 are on average considerably

stable at 24.6 %, 6.79 %, 25.2 % and 10.9 %, respectively. The development of alloy composition as shown in Figure 4.37(d) shows that composition of alloy is stable from tapping 3 to 7 and is close to the planned composition.

Table 4.16: Measured slag composition for untreated Nchwaning experiment

Tap#	Slag Component (wt%)										
	Al_2O_3	BaO	CaO	K_2O	MgO	Fe	SiO_2	TiO_2	MnO	$Total$	$Basicity$
1	6.11	0.89	14.1	0.01	2.43	5.96	14.4	0.19	58.0	102	0.81
2	6.52	0.98	15.8	0.01	3.28	3.11	15.1	0.19	55.3	100	0.88
3	7.70	1.12	18.2	0.01	3.62	2.50	17.8	0.23	48.6	99.9	0.85
4	8.51	1.19	19.5	0.02	4.26	1.98	19.5	0.24	44.1	99.3	0.85
5	9.59	1.29	21.8	0.04	5.01	0.90	22.6	0.28	37.2	98.6	0.83
6	9.49	1.27	21.8	0.01	4.79	1.17	21.9	0.28	37.8	98.5	0.85
7	10.1	1.41	23.4	0.04	5.62	1.03	23.7	0.28	32.2	97.7	0.86
8	9.96	1.40	23.8	0.02	5.61	1.04	23.5	0.28	31.9	97.4	0.88
9	10.5	1.46	24.7	0.05	5.95	1.03	24.6	0.30	28.5	97.1	0.87
10	10.9	1.42	25.1	0.10	6.35	1.82	24.2	0.27	26.8	97.0	0.90
11	11.5	1.40	26.4	0.02	6.53	1.40	25.8	0.28	24.0	99.3	0.88
12	11.6	1.42	27.4	0.03	6.82	1.60	27.0	026	21.1	97.2	0.89
Av. Tapping 7-12	10.8	1.42	25.1	0.04	6.15	1.32	24.8	4.57	27.4	97.6	0.88

*Basicity, $B = \frac{CaO+MgO}{Al_2O_3+SiO_2}$

Table 4.17: Measured slag composition for preheated Nchwaning experiment

Tap#	Slag Component (wt%)										
	Al_2O_3	BaO	CaO	K_2O	MgO	Fe	SiO_2	TiO_2	MnO	$Total$	$Basicity$
1	7.00	1.07	17.3	0.06	3.13	4.04	19.3	0.21	48.5	100.6	0.78
2	7.78	1.11	18.7	0.05	3.93	1.33	20.4	0.24	45.3	98.8	0.80
3	9.22	1.19	21.0	0.05	5.54	0.93	22.8	0.28	37.8	98.8	0.83
4	9.65	1.23	22.6	0.05	6.32	1.32	23.9	0.29	33.4	98.8	0.86
5	10.5	1.35	24.3	0.09	6.44	0.92	25.2	0.29	28.5	97.6	0.86
6	11.9	1.38	24.8	0.11	7.20	1.21	25.5	0.27	26.4	98.8	0.86
7	11.4	1.52	26.6	0.10	7.20	1.03	26.3	0.24	22.9	97.3	0.90
Av. Tapping 4-7	10.9	1.37	24.6	0.09	6.79	1.12	25.2	0.27	27.8	98.1	0.87

*Basicity, $B = \frac{CaO+MgO}{Al_2O_3+SiO_2}$

Table 4.18: Measured slag composition for prereduced Nchwaning experiment

Tap#	Slag Component (wt%)										
	Al_2O_3	BaO	CaO	K_2O	MgO	Fe	SiO_2	TiO_2	MnO	$Total$	$Basicity$
1	6.31	1.12	20.6	0.03	4.94	1.78	24.1	0.19	39.5	98.6	0.84
2	7.20	1.17	22.8	0.04	5.52	1.42	26.6	0.21	33.4	98.4	0.84
3	9.40	1.47	29.8	0.04	6.71	1.78	29.1	0.14	18.8	97.2	0.95
4	8.97	1.40	27.6	0.04	7.35	2.43	28.3	0.14	22.1	98.3	0.94
5	7.16	1.23	23.2	0.04	6.00	4.91	24.0	0.12	35.8	103	0.94
Av. Tapping 2-5	8.18	1.32	25.9	0.04	6.40	2.64	27.0	0.15	27.5	99.1	0.92

*Basicity, $B = \frac{CaO+MgO}{Al_2O_3+SiO_2}$

The prereduced Nchwaning pilot experiment was characterized by difficulties in tapping the furnace. It can also be seen in Figure 4.37(d) that the development of

the slag composition is highly unstable as the MnO content starts from 39.5 % and drops to 18.8 % in tapping 3 and increases to 35.8 % in the last tapping. The lower MnO content in tapping 3 corresponds to a significantly high basicity of 0.95. Considering the last 4 tappings in this experiment, the average MnO is 27.5 % against a target of 30 % calculated from raw materials. The highest content of CaO and SiO_2 are at tapping 3 and the other unreduceable oxides slightly increase up to tapping 3 and decrease thereafter. The alloy composition is lower than the expected composition for all tappings, as can be seen in Figure 4.37(e).

A detailed comparison of the alloy composition measured and the calculated values in untreated and preheated Nchwaning experiments are shown in Table 4.19. For the prereduced Nchwaning experiment, the alloy compositions are shown in Table 4.20.

Table 4.19: Alloy composition for untreated and preheated Nchwaning experiments

Tap	Untreated Nchwaning						Preheated Nchwaning				
#	Mn	Fe	Si	C	Tot		Mn	Fe	Si	C*calc	Tot
1	71.5	19.5	0.4	7.1	98.4		69.9	21.0	0.6	7.0	98.5
2	76.0	16.3	0.2	6.9	99.4		72.6	16.1	1.3	7.0	97.0
3	76.3	15.6	0.2	7.2	99.3		77.9	14.6	0.2	7.0	99.7
4	74.5	17.8	0.1	7.1	99.5		75.9	16.1	0.2	7.0	99.2
5	76.1	14.5	0.7	6.8	98.2		75.0	14.7	1.0	7.0	97.6
6	75.3	16.1	0.3	6.9	98.6		76.8	14.9	0.5	7.0	99.2
7	77.2	14.9	0.3	6.9	99.3		75.2	15.2	0.8	7.0	98.3
8	76.5	15.5	0.1	7.3	99.4						
9	77.7	15.2	-	6.9	99.9						
10	77.5	14.4	0.3	7.2	99.5						
11	78.1	14.6	0.2	7.2	100.1						
12	77.4	14.5	0.3	7.3	99.4						
Exp. avg	76.2	15.7	0.26	7.06	99.2	Exp. avg	74.8	16.1	0.65	7.00	98.5
Avg. Tap 2 - 12	76.6	15.4	0.25	7.07	99.3	Avg. Tap 4 - 7	76.2	15.1	0.54	7.00	98.8

Table 4.20: Alloy composition for prereduced Nchwaning experiment

Tap #	1	2	3	4	5	Exp. avg	Avg. Tap 2 - 5
Mn	73.2	73.5	71.1	75.3	75.6	74.7	75.1
Fe	17.0	16.2	15.0	14.3	14.1	15.3	14.9
Si	0.5	0.9	0.9	1.5	1.6	1.1	1.2
C*calc	7.0	7.0	7.0	7.0	7.0	7.0	7.0
Total	97.7	97.5	98.9	98.1	98.3	98.1	98.2

4.3.2.2 Composition of prereduced samples

Figure 4.38 shows the variation of oxidation level of manganese (i.e., x in MnO_x) in regions close to the electrode (B & D) and furnace lining (A & C) for untreated,

preheated and prereduced Nchwaning experiments. In addition, the trends based on averages are indicated.

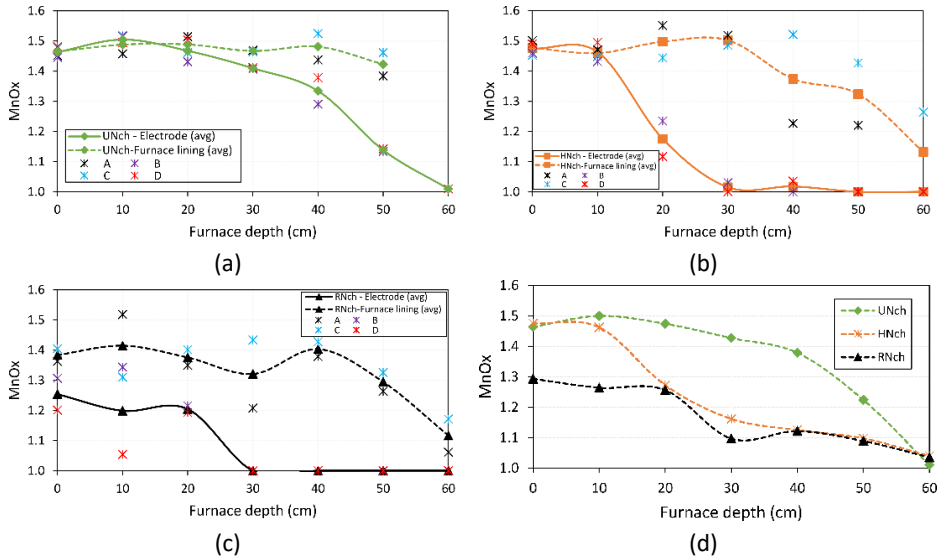

Figure 4.38: MnO_x as a function of depth from the top of charge material. (a) Untreated Nchwaning (UNch), (b) Preheated Nchwaning (HNch), (c) Prereduced Nchwaning (RNch) & (d) Comparison of MnO_x vs depth for the three experiments assuming a 70/30 Electrode/Furnace ratio of flow material in each experiment.

The initial MnO_x values of untreated, preheated and prereduced Nchwaning were 1.51, 1.52 and 1.38, respectively. It can be seen from Figure 4.38, that the MnO_x values adjacent the furnace lining are lower than those adjacent the electrode in all furnace digouts. This is mainly because of high temperature conditions adjacent the electrode, resulting in faster prereduction and flow of materials. A comparison of Figure 4.38 (a) and (b), shows that the MnO_x adjacent the electrode in preheated Nchwaning reaches an MnO_x of 1 at a depth of 30cm whereas, for untreated Nchwaning it reaches an MnO_x of 1 at a depth of 60cm. This implies that preheated Nchwaning will have a greater extent of prereduction than untreated Nchwaning. Likewise, prereduced Nchwaning also shows an MnO_x of 1 at 30cm depth. The MnOx values adjacent the furnace lining, indicate that the pretreated ores will reach a similar MnO_x approximately equal to 1.1 at 60cm depth. On the other end the untreated Nchwaning could only be excavated up to 50cm depth, due to practical limitations during the digout.

A comparison of the prereduction extent for the three ores assuming a 70/30 electrode/furnace prereduction ratio is illustrated in Figure 4.38(d). Overally, the prereduction of preheated and prereduced Nchwaning is significantly faster than

untreated Nchwaning. Prereduced Nchwaning will start at a lower MnO_x value compared to preheated Nchwaning. However, at a depth of 20cm, the two pretreated ore types will considerably follow a similar extent of prereduction with some minor variations. Approaching the highest temperature zone i.e., at a depth of 60 cm, all the ores will have a similar MnO_x approximately equal to 1.

4.3.2.3 Composition of excavated samples from the cokebed zone

In Nchwaning series experiments, samples were excavated by core drilling cokebed cross-sections for untreated and preheated Nchwaning experiments, whereas, for the prereduced Nchwaning cokebed, two vertical cores at 5cm and 10cm distances from the electrode were drilled. Samples for EPMA analysis were then taken at 5cm interval distances from the top in each core. The samples are named into three categories namely, UN-1 – UN-10 for the untreated Nchwaning samples, HN-1 – HN-11 for the preheated Nchwaning samples and RN-1 – RN-9 for the prereduced Nchwaning samples. Figure 4.39 shows sketches illustrating relative positions where samples were taken from the cokebed of each experiment in the Nchwaning series.

The micrographs in Figure 4.40, shows the phase development where the solid monoxide phase is in co-existence with liquid slag as in sample UN-1. The monoxide phase in UN-1 is an (Mn,Mg)O solid solution with about 2.2% MgO. Samples UN-2 and UN-3 contain alloy phase surrounded by edgy phases which are mostly MnO. These phases appear to have not melted and the samples are considered not representative since they are in a region close to the electrode and on top of the cokebed where particles typically contain a liquid slag. Sample UN-4 is a reduced liquid slag from a position inside the cokebed. The sample contains 27.6 % MnO and a basicity of 0.83 as presented in Table 4.21.

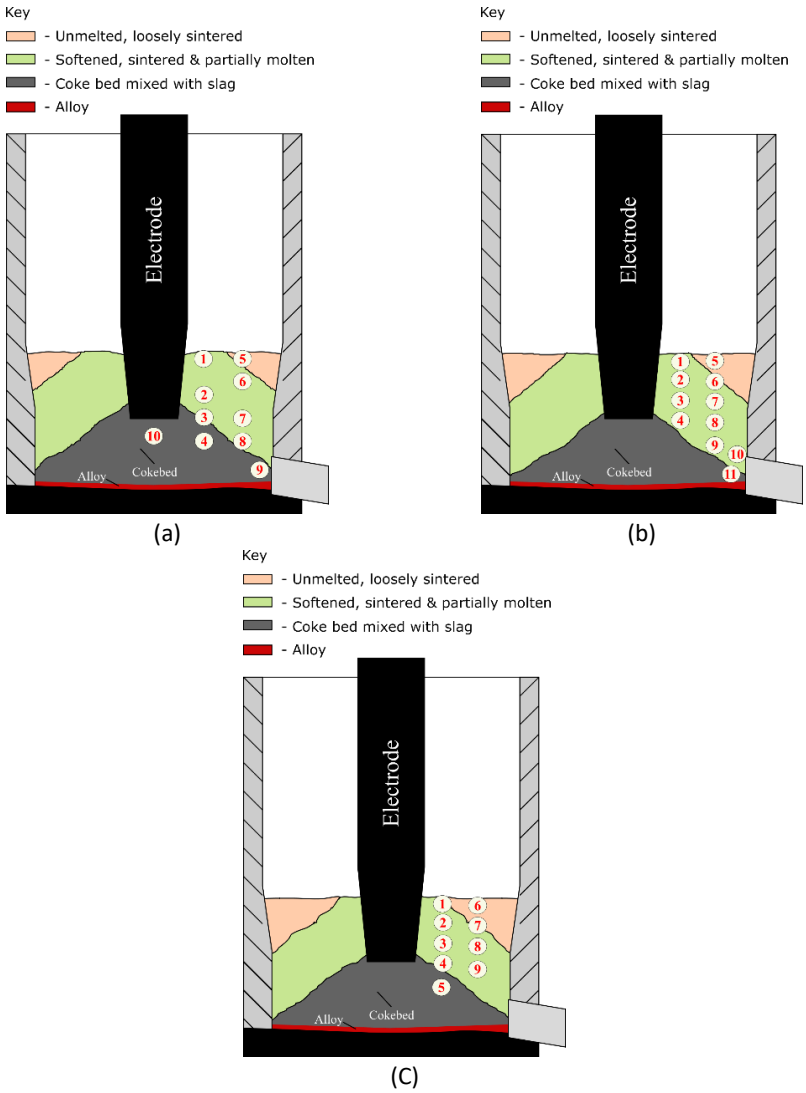

Figure 4.39: Sampling positions in the cross-section of cokebed in Nchwaning series experiments. (a) Untreated Nchwaning samples 1-10 (named UN1-UN10), (b) preheated Nchwaning samples 1-11 (named HN1-HN11), & prereduced Nchwaning samples 1-9 (named RN1-RN9).

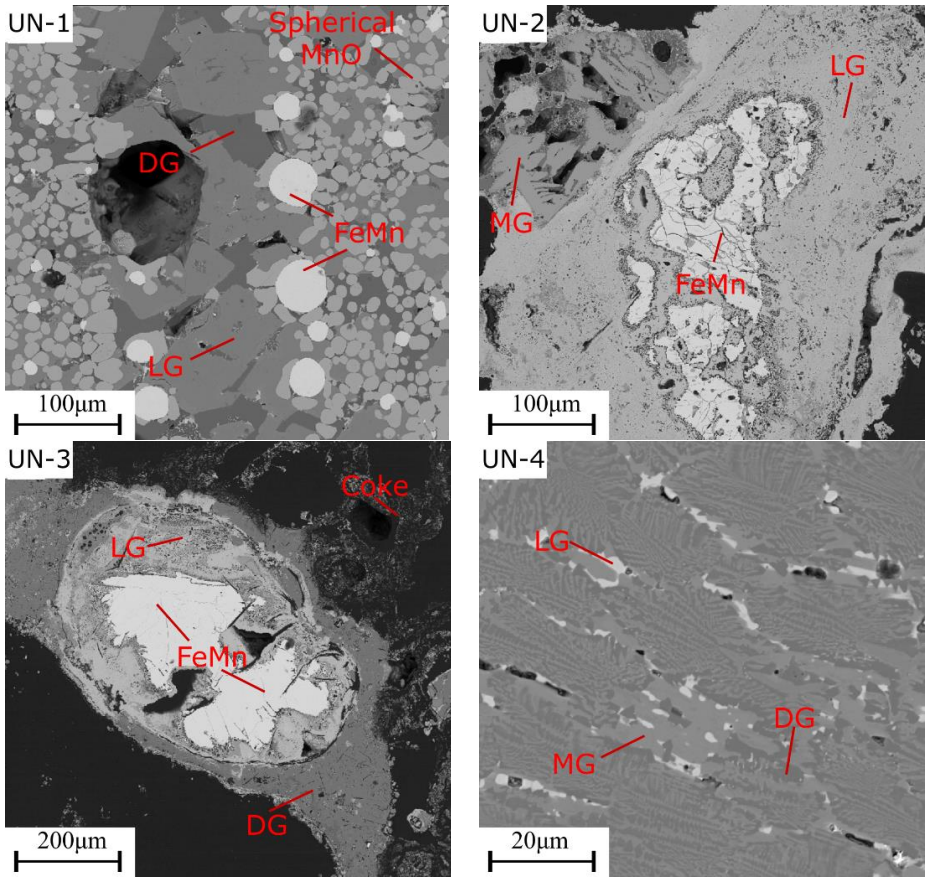

Figure 4.40:Backscattered electron micrographs of untreated Nchwaning samples UN-1 – UN-5 collected from positions 5cm vertically adjacent the electrode. Legend: DG = dark grey phase; MG = medium grey phase & LG = light grey phase.

Samples UN-5 to UN-8 are from a region on top of the cokebed and they can be seen to be composed of a liquid slag in co-existence with solid monoxide phase. The monoxide phase is fully formed when approaching the high temperature regions of the cokebed. In addition, the monoxide phase is an (Mn,Mg)O solution with %MgO ranging between 3.9 to 16 % which increases when approaching top of the cokebed. The MnO content in the liquid phase varies for samples UN6 to UN8 as does the basicities in these samples. Sample UN9 located close to the furnace tap hole is seen to have an MnO content in the liquid phase and basicity close to the tapped slag. The final tapped slag in the untreated Nchwaning experiment had a basicity of 0.89 and 21.1 % MnO.

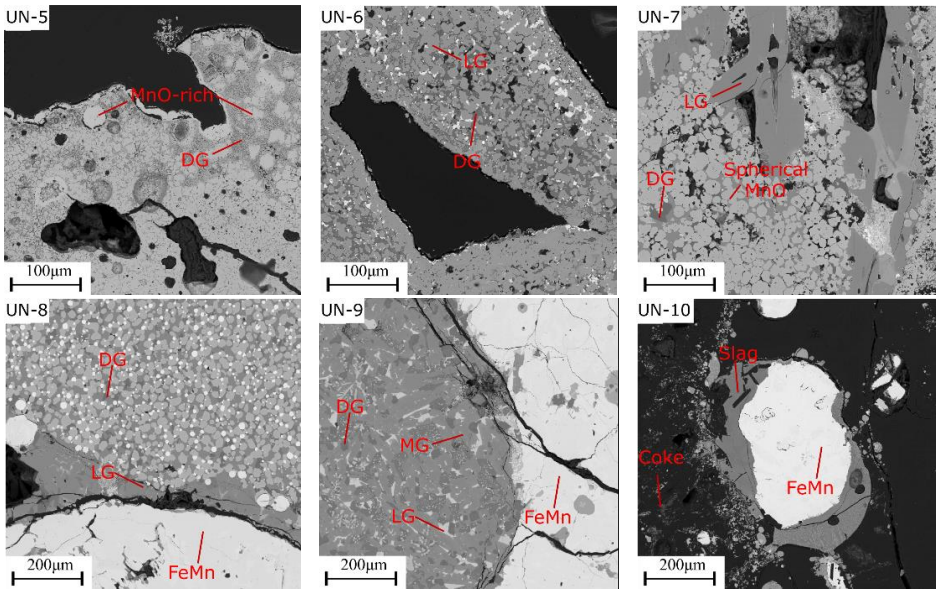

Figure 4.41: Backscattered electron micrographs of untreated Nchwaning samples UN-5 – UN-8 from positions 10cm vertically adjacent the electrode. Samples UN-9 and UN-10 are from close to the taphole and below the tip of the electrode, respectively.

Table 4.21: Calculated liquid slag composition based on measured area fraction by ImageJ® and EPMA phase analysis for samples from untreated Nchwaning experiment

Sample		UN1	UN4	UN6	UN7	UN8	UN9
Area fraction (%)	Monoxide	40.2	-	65.3	43.0	48.5	-
	LG phase	40.4	3.4	6.58	13.3	38.0	16.5
	MG phase	-	59.5	28.2	43.8	-	58.1
	DG phase	19.4	37.1	-	-	13.5	25.3
Total MnO (wt. pct)		53.0	27.6	56.6	47.4	60.3	24.2
Liquid slag	MnO	23.4	27.6	23.9	20.8	30.4	24.2
	FeO	-	0.01	0.36	-	0.30	-
	SiO_2	28.3	30.6	32.6	33.8	25.3	28.3
	Al_2O_3	9.80	8.50	-	4.95	16.3	9.56
	CaO	32.3	31.4	30.9	26.7	20.5	31.1
	MgO	1.12	0.98	9.53	9.20	9.90	3.54
	Total	94.9	99.1	97.3	95.5	103	96.8
	Basicity	0.88	0.83	1.24	0.93	0.73	0.91

The micrographs for samples HN-1 to HN-4 close to the electrode in the preheated Nchwaning experiment are shown in Figure 4.42. The samples show a liquid slag matrix in co-existence with solid monoxide phase with increasing degree of formation of spherical MnO when approaching the top of the cokebed. These samples except for HN2, show a trend of decreasing total MnO content as presented in Table 4.22. The MnO content in the liquid phase in these samples varies.

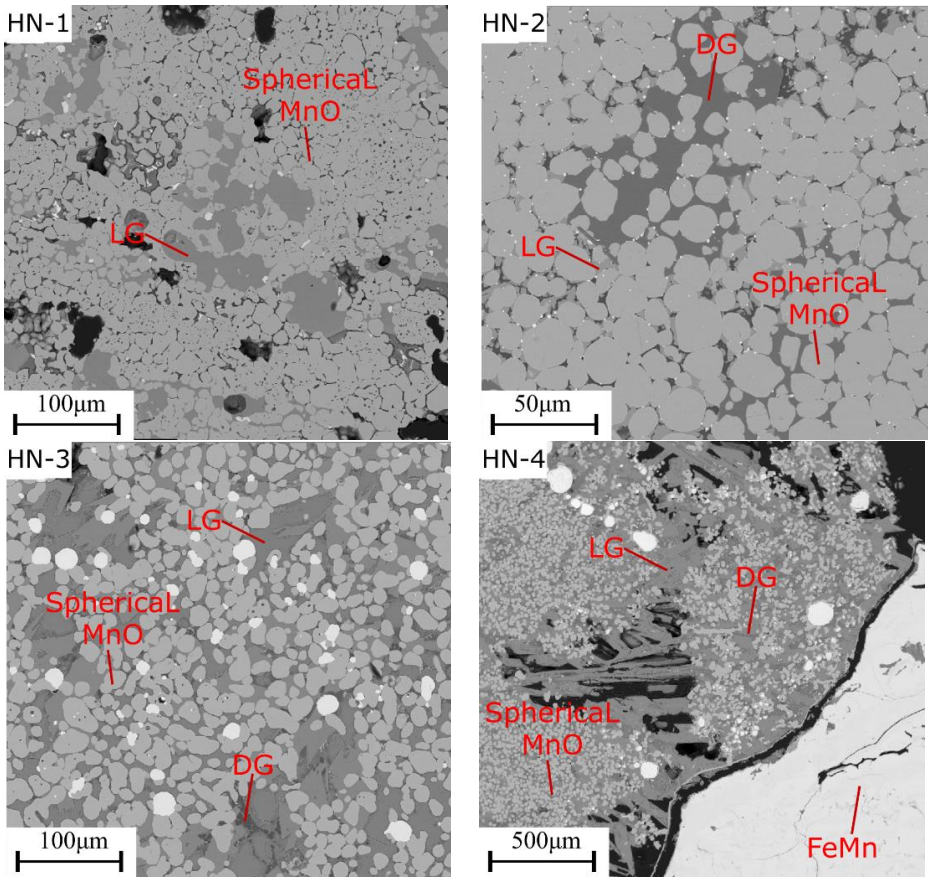

Figure 4.42:Backscattered electron micrographs of preheated Nchwaning samples HN-1 – HN-4 collected from positions 5cm vertically adjacent the electrode. Legend: DG = dark grey phase & LG = light grey phase

As can be seen in Figure 4.43, samples HN-6 – HN-10 from the top of the cokebed contains solid MnO in a liquid phase matrix. Moving from top of the cokebed to inside the cokebed, sample HN-11 is a completely reduced liquid slag with 30.3 % MnO. This indicates that in the two-phase region, the slag is highly viscous and will flow into the cokebed after complete dissolution of solid MnO. The MnO content in the liquid phase varies and the basicity in samples HN-6 to HN-11 varies between 0.91 and 1.07 as presented in Table 4.22. A comparison of the microstructure of samples 5 cm and 10cm from the electrode did not show clear indications that there was more reduction close to the electrode. However, in all the samples the fraction of the liquid phase increases when approaching top of the coke bed as can be seen in Table 4.22.

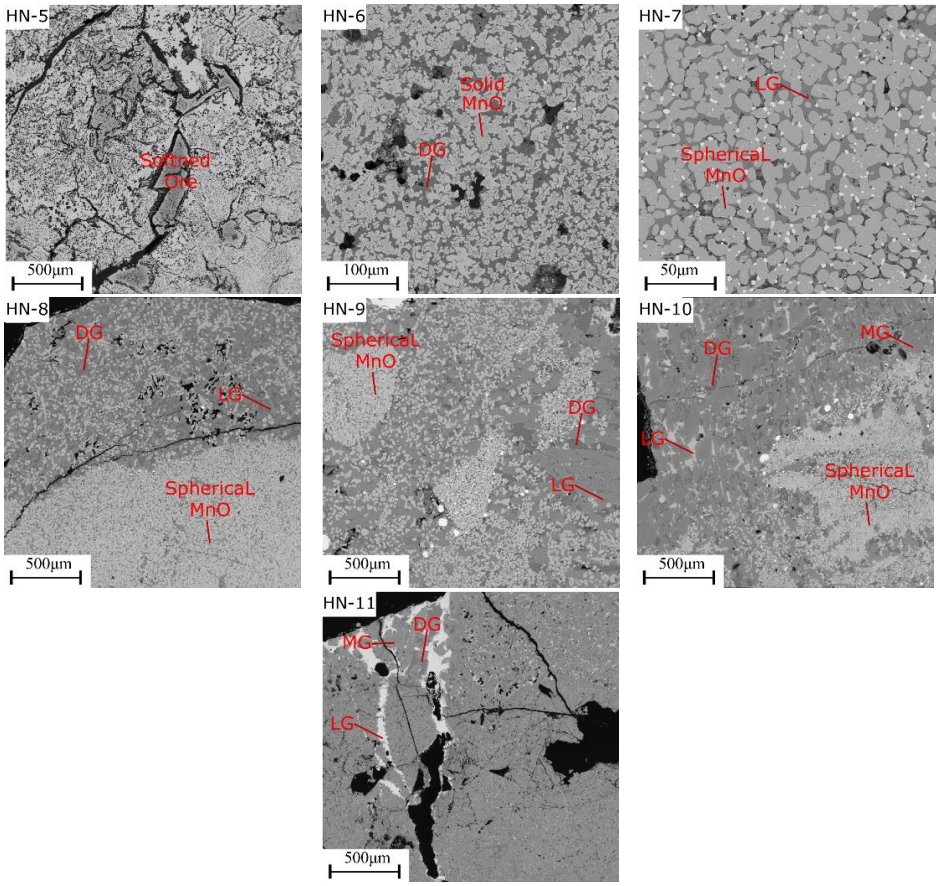

Figure 4.43: Backscattered electron micrographs of preheated Nchwaning samples HN-5 – HN-8 from positions 10cm vertically adjacent the electrode. Samples HN-9 – HN-11 are from close to the taphole.

Table 4.22:Calculated liquid slag composition based on measured area fraction by ImageJ® and EPMA phase analysis for samples from preheated Nchwaning experiment

Sample		HN1	HN2	HN3	HN4	HN6	HN7	HN8	HN9	HN10	HC11
Area fraction (%)	Monoxide	79.1	76.3	54.7	43.5	63.0	78.5	48.1	36.5	30.9	-
	LG phase	20.9	9.9	43.4	41.8	-	21.5	36.7	50.2	59.4	6.77
	MG phase	-	-	-	-	-	-	-	-	-	81.0
	DG phase	-	13.8	1.87	14.7	37.0	-	15.2	13.3	9.70	11.3
Total MnO (wt. pct)		83.4	89.1	65.9	54.1	62.5	83.4	56.1	49.8	47.6	30.3
Liquid slag	MnO	48.3	56.0	31.5	23.7	16.1	33.4	21.8	24.0	25.8	30.3
	FeO	1.53	0.82	0.43	0.06	1.05	0.40	0.11	0.04	0.10	0.07
	SiO_2	31.1	8.77	31.4	30.0	27.0	31.6	30.8	30.7	31.4	30.7
	Al_2O_3	-	35.7	2.00	8.81	30.9	0.06	9.09	7.20	5.20	4.92
	CaO	17.6	0.58	30.7	32.0	22.0	33.6	32.1	32.4	30.7	28.9
	MgO	0.86	0.22	1.84	3.65	0.09	0.31	5.20	4.20	5.80	3.41
	Total	99.4	102	98.1	98.0	102	99.4	99.1	98.6	98.9	98.2
	Basicity	0.59	0.02	0.98	0.92	0.38	1.07	0.93	0.96	1.00	0.91

The backscattered micrographs for samples from 5cm adjacent the electrode in the prereduced Nchwaning experiment are shown in Figure 4.44. It can be seen that RN1 contains a FeMn alloy and completely reduced slag and has been probably held-up in a region high-up from top of cokebed and thus obstructed to flow into the cokebed. The MnO content in the liquid phase for RN2 and RN3 is quite similar as presented in Table 4.23 and the monoxide phase contains 2 -3 % MgO. Sample RN-4 is mostly alloy and the slag is mostly composed of CaO, Al_2O_3 and SiO_2. Sample RN-5 is a completely reduced slag found inside the cokebed and is significant low in MnO content with 7.61 % MnO.

Table 4.23: Calculated liquid slag composition based on measured area fraction by ImageJ® and EPMA phase analysis for samples from prereduced Nchwaning experiment

Sample		RN1	RN2	RN3	RN4	RN5	RN8	RN9
Area fraction (%)	Monoxide		52.3	65.5	-	-	78.6	54.4
	LG phase		10.5	7.51	50.6	13.1	15.6	36.6
	MG phase		-	-	49.4	7.90	-	-
	DG phase		37.2	27.0	-	79.0	5.80	9.00
Total MnO (wt. pct)		11.5	65.9	72.9	0.98	7.61	64.7	64.6
Liquid slag	MnO	11.5	30.5	30.1	0.98	7.61	37.9	28.4
	FeO	0.04	0.31	0.29	0.02	0.02	1.05	0.22
	SiO_2	14.3	30.5	30.0	16.3	35.2	45.4	34.4
	Al_2O_3	22.1	4.73	5.51	19.3	11.6	8.15	6.88
	CaO	45.4	26.6	26.9	59.9	36.5	0.84	28.0
	MgO	0.19	2.11	2.48	0.30	7.06	0.16	1.32
	Total	93.5	97.0	95.0	96.8	98.0	98.6	101.1
	Basicity	1.25	0.82	0.84	1.69	0.93	0.02	0.71

Figure 4.45 shows the micrographs of samples from 10cm distance adjacent the electrode for prereduced Nchwaning experiment. All the samples were from positions above top of the cokebed. The microstructure for RN-6 and RN-7 indicated that the samples were mostly solid ore particles which had no molten regions. Sample RN-8 is mostly sinter consisting of MnO rich phase with sharp edges. The liquid phase in this samples contains 37.9 % MnO. Sample RN-9 has the typical appearance of the slag found on top of the cokebed. The solid monoxide phase contains about 1.5 %MgO and is in co-existence with a liquid slag with 28.4 % MnO. Most of the samples from the prereduced Nchwaning experiment were from regions above top of the cokebed due to practical limitations encountered during the excavation.

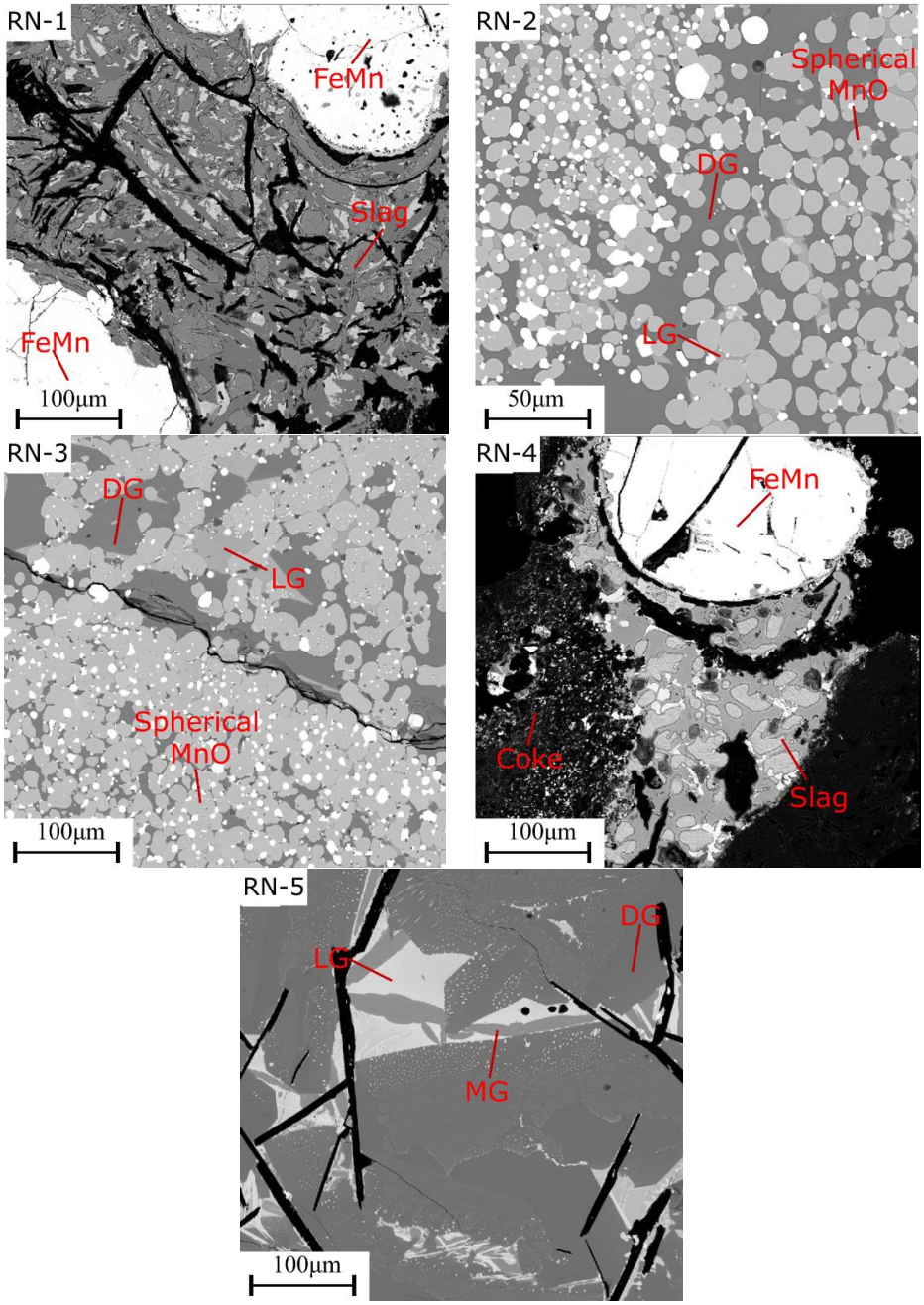

Figure 4.44: Backscattered electron micrographs of prereduced Nchwaning samples RN-1 to RN-5 from positions 5cm vertically adjacent the electrode. Legend: DG = dark grey phase; MG = medium grey phase & LG = light grey phase.

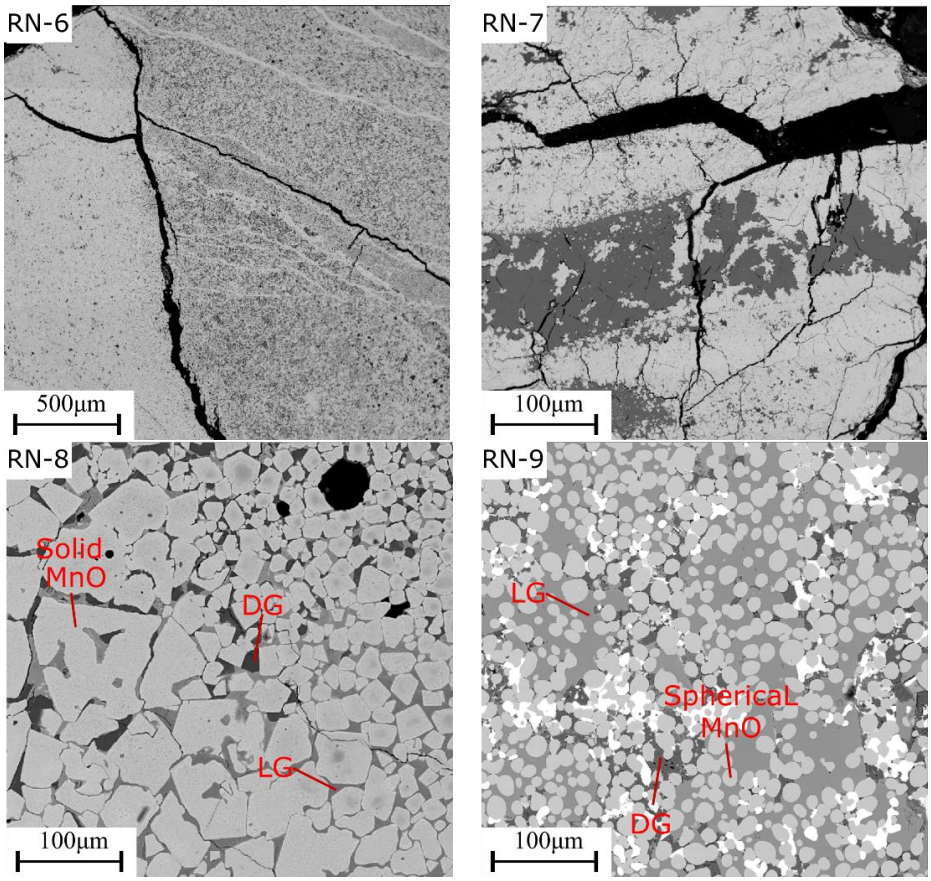

Figure 4.45: Backscattered electron micrographs of prereduced Nchwaning samples RN-6 – RN-9 from positions 10cm vertically adjacent the electrode.

4.3.3. UMK and Mintek mix

4.3.3.1 Analyses of tapped slag and alloy

In the UMK and Mintek mix experiments, the initial tapping was after 150kWh of energy input and the subsequent tappings were after every 80 kwh, resulting in a total of 12 tappings in each experiment. The weight of slag and alloy at each tapping for the UMK and Mintek mix experiments are as shown in Table 4.24. The planned slag/alloy ratio is compared to the entire experimental slag/alloy ratios and the slag/alloy ratios in the last half tappings for the UMK and Mintek mix experiments are illustrated in Figure 4.46.

Table 4.24: Weight of tapped slag and alloy for the experiments with untreated, preheated and prereduced Nchwaning charge mixtures

Tap #	UMK			Mintek mix		
	Slag (kg)	Alloy (kg)	S/A ratio	Slag (kg)	Alloy (kg)	S/A ratio
1	15.4	17.1	0.90	27.7	24.3	1.14
2	9.82	12.8	0.77	15.6	13.1	1.19
3	10.5	13.2	0.80	13.7	9.63	1.43
4	10.1	14.5	0.70	17.5	13.4	1.31
5	8.97	14.6	0.62	17.1	13.1	1.31
6	7.88	12.7	0.62	14.7	14.8	0.99
7	8.90	11.7	0.76	12.5	12.5	1.00
8	8.61	12.2	0.71	7.84	8.63	0.91
9	4.62	11.1	0.42	8.77	7.91	1.11
10	4.69	7.04	0.67	7.96	11.4	0.70
11	4.03	1.58	2.55	10.2	10.3	0.99
12	3.55	9.49	0.37	8.45	9.85	0.86
Total	**97.1**	**137.9**	**0.70**	**162.0**	**148.9**	**1.09**
Tapping 7-12	**34.4**	**53.1**	**0.65**	**55.7**	**60.6**	**0.92**

As shown in Table 4.24, the untreated UMK experiment gave a total of 97.1 kg and 137.9 kg of slag and alloy, respectively. The slag/alloy ratio for the whole experiment was 0.7. The planned slag/alloy ratio was 0.66 and is close to 0.65 considered for tappings 7 to 12. However, these values are higher than slag/alloy ratio determined from mass balance calculations in HSC Chemistry software as can be seen in Figure 4.46. A total of 162 kg and 148.9 kg of slag and alloy, respectively were obtained for the Mintek mix experiment. The experimental slag/alloy ratio was 1.09 and the average for tappings 7 to 12 was 0.92. These were generally lower than the 1.33 slag/alloy ratio planned as can be seen from Figure 4.46. The HSC mass balance slag/alloy ratio in untreated mix is same as the slag/alloy ratios for tapping 7-12, which indicate that the experiment was highly stable.

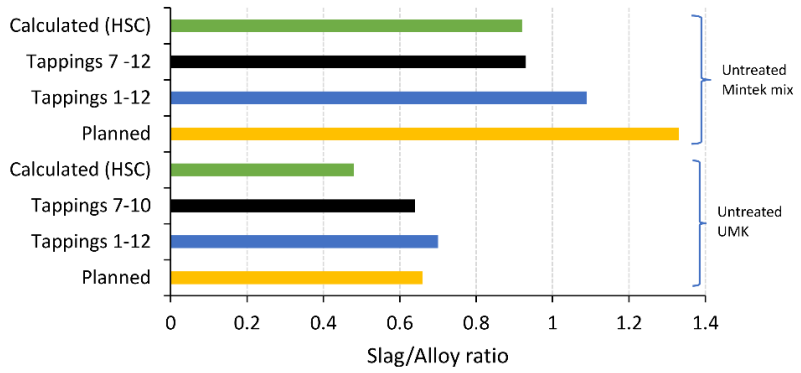

Figure 4.46: Slag/alloy ratios in whole experiment, tappings in the last half of the experiment and planned theoretical slag/alloy ratio in the untreated UMK and Mintek mix experiments.

The development of the slag and alloy composition with tapping number for the experiments in the UMK and Mintek mix experiments is as shown in Figure 4.47. The detailed slag compositions for the untreated UMK and Mintek mix experiments are shown in Table 4.25 and Table 4.26 respectively. The stable period in both experiments is within tappings 7 to 12.

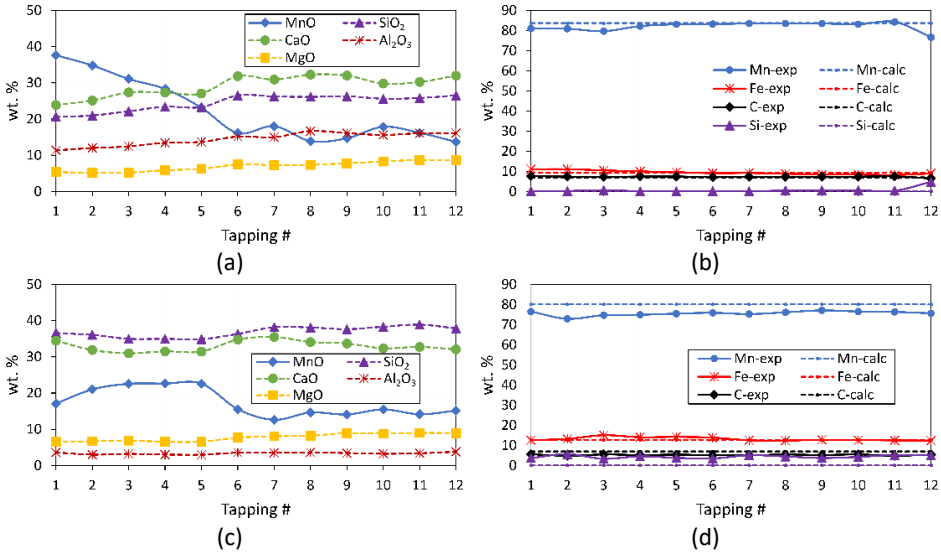

Figure 4.47: Variation of slag and alloy composition with tapping number for untreated UMK and Mintek mix experiments. Untreated UMK (a & b) and Mintek mix (c & d).

Table 4.25: Measured slag composition for untreated UMK experiment

Tap#	Slag Component (wt%)										
	Al_2O_3	BaO	CaO	K_2O	MgO	Fe	SiO_2	TiO_2	MnO	$Total$	$Basicit$
1	11.4	0.45	23.9	0.04	5.37	0.72	20.6	0.28	37.6	100.4	0.92
2	12.0	0.46	25.1	0.04	5.17	0.89	21.0	0.27	34.8	99.7	0.92
3	12.4	0.49	27.4	0.03	5.24	0.78	22.2	0.29	31.1	99.9	0.94
4	13.4	0.52	27.3	0.03	5.85	0.69	23.4	0.32	28.3	99.9	0.90
5	13.7	0.52	27.1	0.06	6.25	0.63	23.3	0.32	23.1	95.0	0.90
6	15.2	0.56	31.8	0.04	7.47	0.66	26.5	0.32	16.1	98.7	0.94
7	15.0	0.59	30.9	0.05	7.27	0.72	26.3	0.33	18.0	99.1	0.93
8	16.7	0.58	32.3	0.14	7.37	0.95	26.1	0.27	13.9	98.3	0.93
9	16.1	0.58	32.0	0.06	7.77	0.67	26.3	0.29	14.7	98.5	0.94
10	15.6	0.57	29.8	0.08	8.31	0.69	25.6	0.30	17.9	98.8	0.92
11	16.1	0.59	30.2	0.10	8.70	0.72	25.8	0.30	16.2	98.8	0.93
12	16.1	0.60	32.0	0.11	8.65	0.92	26.5	0.28	13.7	98.9	0.95
Av. Tapping 7-12	15.9	0.59	31.2	0.09	8.01	0.78	26.1	0.30	15.7	98.7	0.93

*Basicity, $B = \frac{CaO+MgO}{Al_2O_3+SiO_2}$

Table 4.26: Measured slag composition for untreated Mintek mix experiment

Tap#	Slag Component (wt%)										
	Al_2O_3	BaO	CaO	K_2O	MgO	Fe	SiO_2	TiO_2	MnO	$Total$	$Basicity$
1	3.58	0.13	34.5	0.15	6.56	0.98	36.6	0.03	17.1	99.6	1.03
2	3.01	0.12	31.9	0.19	6.67	0.75	36.1	0.03	21.0	99.7	0.99
3	3.20	0.13	31.0	0.15	6.90	0.83	35.0	0.03	22.6	99.8	1.00
4	3.02	0.13	31.5	0.18	6.55	0.84	35.0	0.03	22.6	99.8	1.01
5	2.98	0.12	31.5	0.18	6.58	0.84	34.9	0.03	22.6	99.7	1.01
6	3.54	0.14	34.8	0.08	7.69	0.77	36.3	0.03	15.6	98.9	1.07
7	3.52	0.14	35.5	0.08	8.06	0.71	38.2	0.03	12.6	98.8	1.05
8	3.60	0.14	34.1	0.12	8.24	0.74	38.1	0.03	14.6	99.7	1.02
9	3.44	0.13	33.7	0.15	8.93	0.71	37.7	0.03	14.1	98.8	1.04
10	3.24	0.12	32.4	0.24	8.81	0.92	38.3	0.04	15.5	99.5	0.99
11	3.37	0.13	32.8	0.26	8.99	0.77	38.9	0.03	14.2	99.3	0.99
12	3.80	0.14	32.1	0.30	8.94	0.86	37.9	0.03	15.1	99.1	0.99
Av. Tapping 7-12	3.50	0.13	33.4	0.19	8.66	0.79	38.2	0.03	14.4	99.2	1.01

*Basicity, $B = \frac{CaO+MgO}{Al_2O_3+SiO_2}$

The planned MnO content based on raw materials input was 30 % and 20 % respectively for the untreated UMK and Mintek mix experiments. As shown in Figure 4.47(a), the MnO content in the untreated UMK experiment started from 37.6 % and decreased until the MnO content stabilizes between tap 7 to 12. The average MnO content between tapping 7 and 12 was 15.7 % MnO when the average MnO content for the entire experiment is 22.1 %. The unreduceable oxides of CaO, MgO, SiO_2 and Al_2O_3 are seen to be stable from tap 7 to 12 and on average at 31.2 %, 8.01 %, 26.1 % and 15.9 %, respectively. The UMK experiment had a target basicity of 0.8 and as presented in Table 4.25, the basicity was mostly stable throughout the experiment, and this ideally expected since the oxides used to calculate basicity are unreducible. The average basicity in tappings 7-12 for the UMK experiment was 0.93, which is higher than planned. This could indicate that the analysis of input raw materials could be slightly off, and the higher basicity could be probable reason for a lower MnO content than planned.

The development of MnO content in Mintek mix experiment shows mainly two stable regions. From Figure 4.47(c), the MnO content is high and stable from tapping 2 to 5, on average at 22.2 % MnO. Thereafter, it decreases until tapping 7 where its stable up to tapping 12. The average MnO content between tapping 7 to 12 is 14.4 %, which is lower than the targeted 20 % MnO in slag. The average MnO content for the whole experiment is 17.3%. The basicity is high and stable on average at 1.01 for tappings 7 – 12 against a targeted slag basicity of 0.93. Hence, the MnO content is lower than planned. The unreduceable oxides of CaO, MgO, SiO_2 and Al_2O_3 are stable in the two periods.

The alloy composition for the UMK experiment was close to the targeted composition from tapping 4 to 11 as shown in Figure 4.47(b). For Mintek mix (Figure 4.47(d)), the alloy composition is generally stable from tapping 3 to 12, with a Mn content lower than the theoretical. Table 4.27 shows a detailed comparison of the alloy composition measured and the calculated values for both the untreated UMK and Mintek mix experiment.

Table 4.27: Alloy composition for untreated UMK and Mintek mix experiments

Tap	Untreated UMK						Untreated Mintek mix				
#	Mn	Fe	Si	C	Tot		Mn	Fe	Si	C	Tot
1	81.0	11.1	0.08	7.68	99.9		76.5	12.6	3.69	5.59	98.4
2	80.9	11.1	0.23	7.39	99.6		72.9	13.2	5.66	4.87	96.7
3	79.7	10.5	0.70	7.28	98.2		74.7	15.1	3.36	5.49	98.6
4	82.2	10.0	0.10	7.42	99.7		74.9	14.1	4.57	5.22	98.8
5	83.1	9.60	0.07	7.45	100.2		75.5	14.2	3.81	5.40	98.9
6	83.2	9.10	0.21	7.16	99.7		75.9	13.9	3.49	5.15	98.4
7	83.5	9.20	0.13	7.36	100.2		75.3	12.5	5.10	5.11	98.0
8	83.5	8.80	0.44	7.30	100.0		76.2	12.4	4.49	5.46	98.5
9	83.5	8.50	0.52	7.37	99.9		77.1	12.8	3.74	5.24	98.8
10	83.1	8.40	0.57	7.37	99.4		76.5	12.6	4.27	5.49	98.9
11	84.3	8.20	0.37	7.49	100.4		76.4	12.5	5.25	4.87	99.0
12	76.7	8.90	4.80	6.46	96.9		75.7	12.4	5.04	5.37	98.4
Exp. avg	82.1	9.45	0.69	7.31	99.5	Exp. avg	75.6	13.2	4.37	5.27	98.5
Avg. Tap 4 - 11	83.3	8.98	0.30	7.37	99.9	Avg. Tap 3 - 12	75.8	13.2	4.31	5.28	98.7

4.3.3.2 Composition of prereduced samples

Figure 4.48 shows the variation of oxidation level of manganese (i.e., x in MnOx) as a function of furnace depth on regions close to the electrode (B & D) and furnace lining (A & C) for untreated UMK and Mintek mix experiments. The two MnO_x values on the same level, and same distance from the electrode, for each region were averaged and the trends based on averages are indicated. Similarly, to all other pilot experiments in this work, the extent of prereduction is greater adjacent the electrode compared to close to the furnace lining in all experiments. MnO_x adjacent the electrode in untreated UMK experiment is approximately close to 1.0 from 30cm down to 60cm and close to the furnace lining, the MnO_x is close to 1.1 at 60cm. For the Mintek mix, UMK ore was mixed with Kudumane ore and hence during furnace digout these ores could not be distinguish. As such, the MnO_x measured could be from either of the two ores. A comparison of the two experiments as illustrated in Figure 4.48(c), shows that untreated UMK has a higher extent of prereduction compared to Mintek mix from top of furnace up to a depth of approximately 40cm, whereas some variations were noticed between 40 to 60 cm depth.

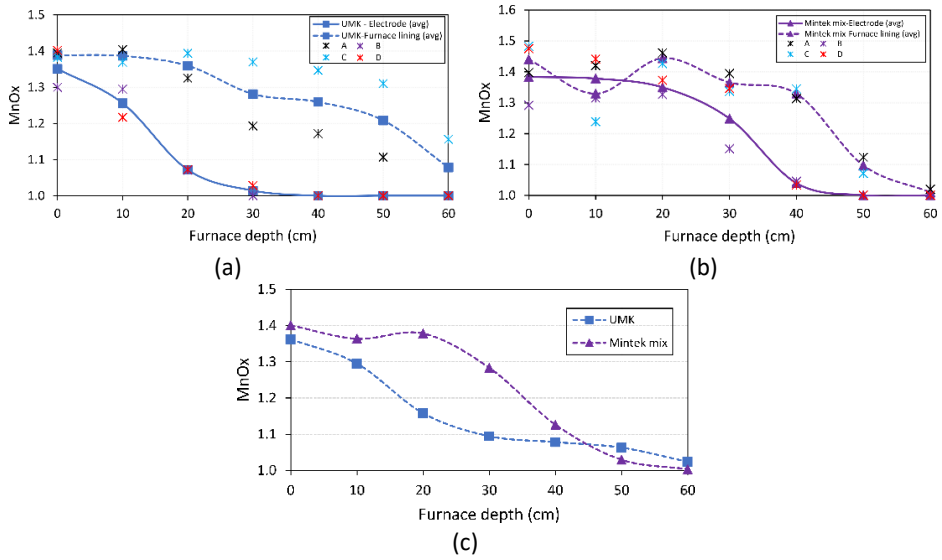

Figure 4.48: MnO_x as a function of depth from the top of charge material. (a) Untreated Mintek, (b) untreated Mintek & (c) comparison of MnO_x vs depth for the two experiments assuming a 70/30 Electrode/Furnace ratio of flow material in each experiment.

UMK and Kudumane ores are rich in carbonates with about 16 % carbonate content. The corresponding residual carbonate content (given as CO_2 content) as a function of furnace depth for the UMK and Mintek mix experiments is as shown in Figure 4.49.

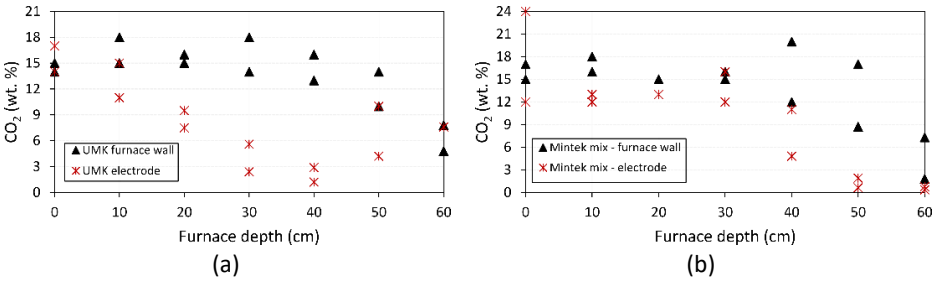

Figure 4.49: Decomposition of carbonates during prereduction as a function of furnace depth for (a) UMK and (b) Mintek mix experiments.

Decomposition of carbonates is temperature dependent, and there is greater extent of decomposition of carbonates for samples adjacent the electrode compared to samples adjacent the furnace lining for UMK experiment (Figure 4.49(a)). This is expected as there exist a temperature gradient with high temperature conditions prevailing adjacent the electrode compared to furnace wall. The carbonates are decomposed when approaching the high temperature zone with increasing furnace depth and most carbonates adjacent furnace electrode are decomposed at a depth

of approximately 40cm. From 40cm to 60 cm there was a trend of increasing carbonate content in the ore particles close to the electrode. It could be the case that the ore particles were contaminated with carbon fines generated from disintegration of coke particles as the charge mixture descends to the bottom of the prereduction zone. Similarly, for the Mintek mix (Figure 4.49(b)), most of the carbonates decompose when approaching the high temperature zone with a relatively greater extent adjacent the electrode compared to the furnace wall.

4.3.3.3 Composition of excavated samples from the cokebed zone

Figure 4.50 shows sketches illustrating sampling positions from the cokebed of untreated UMK and Mintek mix experiments. The samples are named UMK-1 – UMK-8 for the untreated UMK samples and MN-1 – MN-10 for the untreated Mintek mix samples. The backscattered micrographs for samples at 5cm and 10cm horizontal distances from the electrode are shown in Figure 4.51 and Figure 4.52, respectively. The calculated liquid slag compositions for these samples are shown in Table 4.28. It can be seen that UMK-1 shows a slag at the stage of initial formation of solid MnO and the slag in UMK-2 has been completely liquid at high temperatures. Samples UMK-3 and UMK-4 are mostly FeMn alloy, an indication of high reduction potential close to the electrode. The calculated amount of total MnO is approximately 70 % in the presence of solid MnO, as shown for UMK-5 and decreases to 14.3 % in a completely liquid slag i.e., UMK-8. The MnO content in UMK-8 slag is close to 13.7 % MnO in the last tapped slag measured by XRF (i.e., Table 4.25).

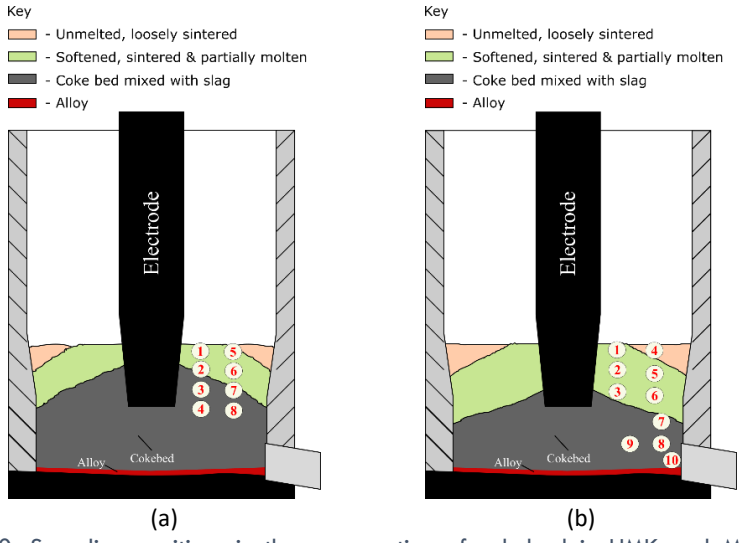

Figure 4.50: Sampling positions in the cross-section of cokebed in UMK and Mintek mix experiments. (a) Untreated UMK samples 1-8 (named UMK1-UMK8) & (b) untreated Mintek mix samples 1-10 (named MN1-MN10).

Table 4.28: Calculated liquid slag composition based on measured area fraction by ImageJ® and EPMA phase analysis for samples from untreated UMK experiment

Sample		UMK2	UMK5	UMK6	UMK8
Area fraction (%)	Monoxide	-	64.7	-	-
	LG phase	71.2	35.3	-	7.30
	MG phase	17.9	-	-	15.6
	DG phase	10.9	-	-	77.1
Total MnO (wt. pct)		23.2	69.2	26.4	14.3
Liquid slag	MnO	23.2	21.4	26.4	14.3
	FeO	-	0.3	0.10	-
	SiO_2	33.1	27.3	17.9	28.3
	Al_2O_3	14.7	11.9	27.4	15.2
	CaO	18.2	36.5	27.6	34.3
	MgO	2.84	2.00	1.00	7.44
	Total	94.6	99.4	100.6	101.4
	Basicity	0.44	0.98	0.63	0.96

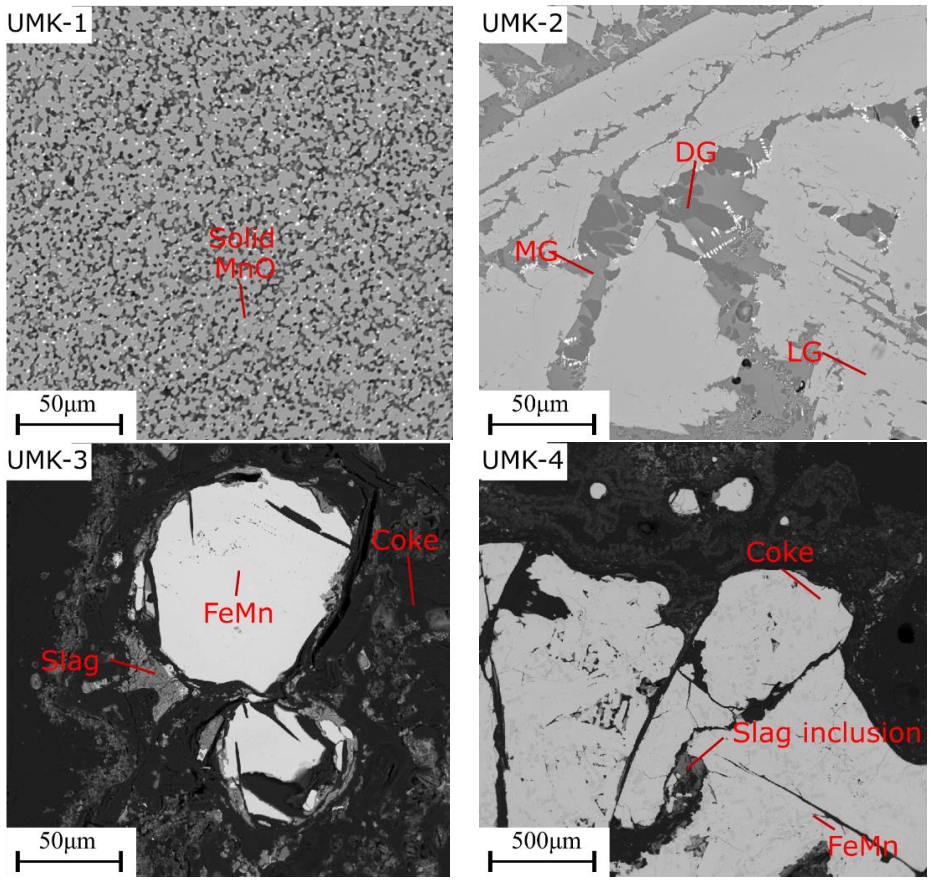

Figure 4.51: Backscattered electron micrographs of untreated UMK samples UMK-1 – UMK-4 taken from positions 5cm vertically adjacent the electrode. Legend: DG = dark grey phase, MG = medium grey phase & LG = light grey phase.

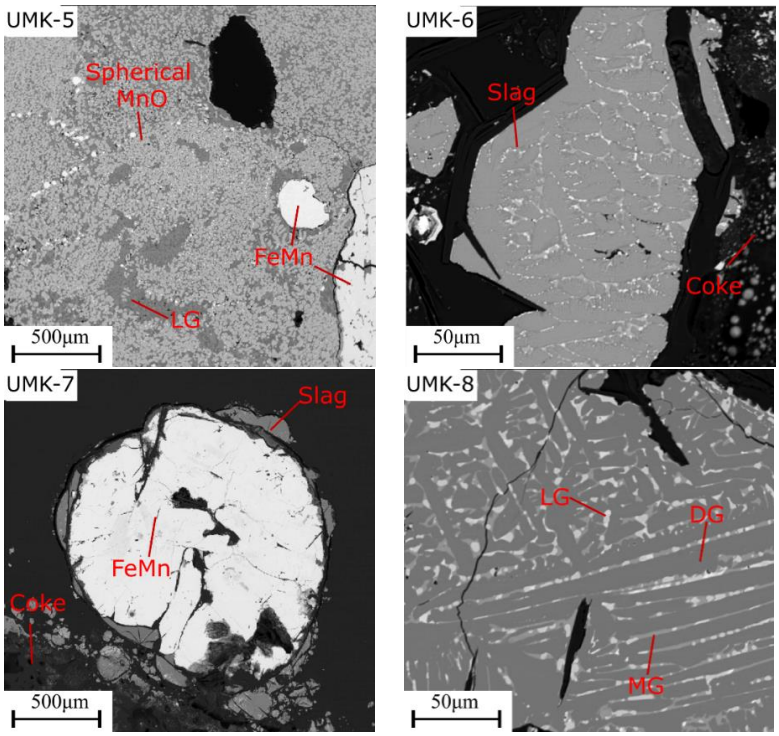

Figure 4.52: Backscattered electron micrographs of untreated UMK samples UMK-5 – UMK-8 from positions 10cm vertically adjacent the electrode.

Figure 4.53 shows the microstructure of slags MN-1 to MN-6 which are from regions on top of the cokebed in the Mintek mix excavations. Samples MN-1, MN-5 and MN-6 have appearance of the slag found on the top of the cokebed with spherical MnO in co-existence with a matrix of dark and light grey phases. The solid monoxide phase is an (Mn,Mg)O solid solution with about 4.2 %, 25 % and 22.3 % MgO in samples MN-1, MN-5, and MN-6, respectively. This shows that the monoxide slag phase becomes enriched in MgO with increased dissolution of MnO in liquid slag when approaching top of the cokebed. Subsequently, the total MnO content in these samples decreases from 55.5 % to 31.2 % as shown in Table 4.29. Samples MN-2 and MN-3 are mostly coke with CaO-rich regions.

The micrographs in Figure 4.54 show samples MN-7 to MN-10, which are composed of mainly an alloy and a reduced slag. The MnO content in these samples ranges between 5.3 to 16.3% as presented in Table 4.29. Sample MN-10 was taken from close to the taphole and it can be seen that the MnO content in this sample is close to the 15.1 % MnO in the last tap measured by XRF. However, the basicity in this sample is lower than the 0.99 from the tapped slag.

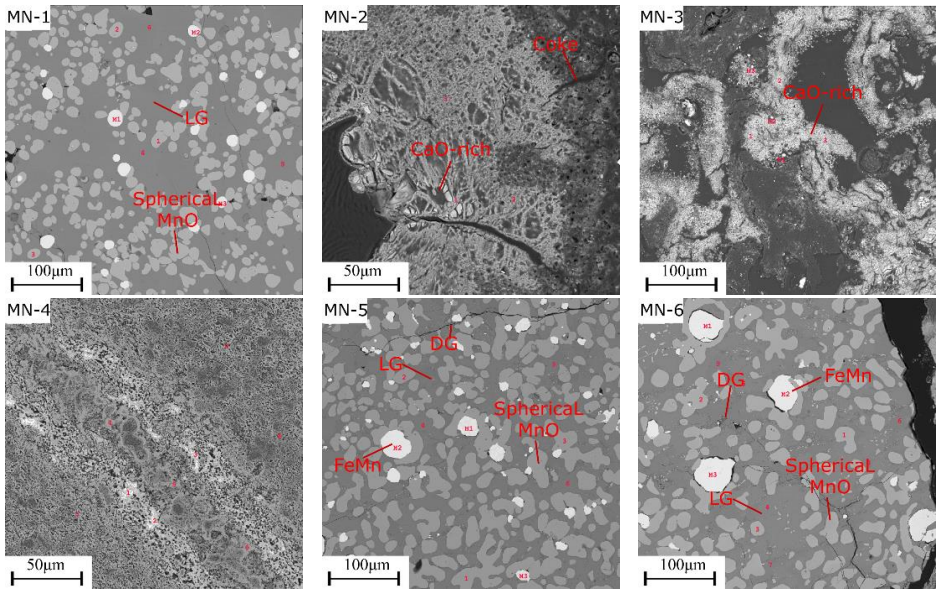

Figure 4.53:Backscattered electron micrographs of Mintek mix samples MN-1 – MN-6. Samples MN-1 – Mn-3 and MN-4 – MN-6 were collected respectively from positions 5cm and 10cm vertically adjacent the electrode. Legend: DG = dark grey phase & LG = light grey phase.

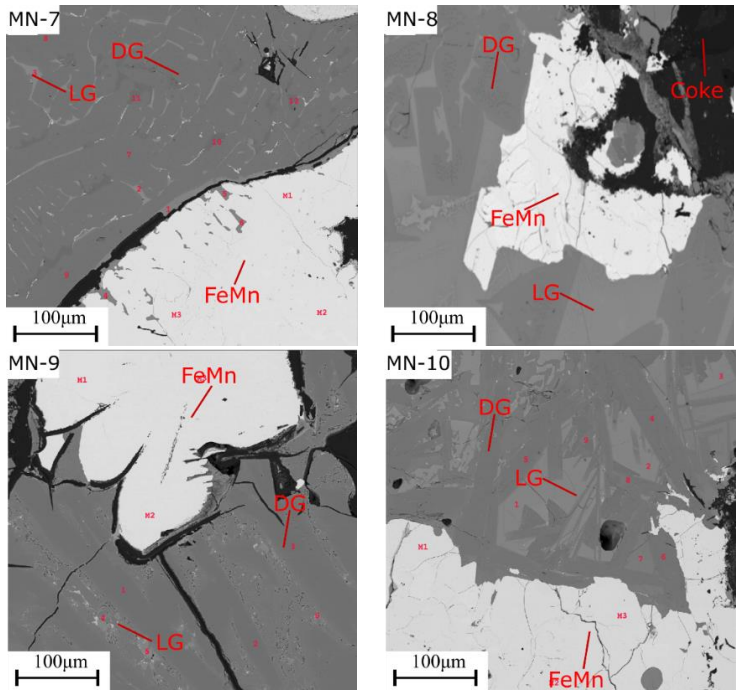

Figure 4.54: Backscattered electron micrographs of Mintek mix samples MN-7 – MN-10 from positions inside the cokebed close to the taphole.

Table 4.29: Calculated liquid slag composition based on measured area fraction by ImageJ® and EPMA phase analysis for samples from Mintek mix experiment

Sample		MN1	MN5	MN6	MN7	MN8	MN9	MN10
Area fraction (%)	Monoxide	34.8	48.5	35.7	-	-	-	-
	LG phase	62.3	51.5	55.3	10.3	44.8	36.8	28.9
	MG phase	-	-	-	86.8	-	-	-
	DG phase	-	-	8.93	2.82	55.2	63.2	71.1
Total MnO (wt. pct)		55.5	39.2	31.23	6.07	16.3	5.25	15.7
Liquid slag	MnO	34.5	5.60	5.85	6.07	16.3	5.25	15.7
	FeO	0.15	0.04	0.06	0.10	-	0.05	0.09
	SiO_2	32.8	33.5	33.3	42.6	35.6	37.5	44.9
	Al_2O_3	0.07	0.48	0.22	3.66	5.24	4.24	3.86
	CaO	28.0	52.2	53.5	35.3	28.5	43.3	31.5
	MgO	4.57	6.35	4.60	10.6	5.16	4.95	1.61
	Total	100	98.2	97.6	98.6	91.7	95.6	97.8
	Basicity	0.99	1.73	1.73	0.99	0.82	1.16	0.68

4.4 Discussion

4.4.1 Prereduction in pilot furnace

During pilot furnace operation, exothermic reactions are dominating in the prereduction zone and endothermic reactions i.e., melting and reduction of oxides are dominating in the cokebed zone. Sparta *et al.*,[151] have shown through furnace modelling that approximately a third of the ohmic power distribution is concentrated on the tip of the electrode and as such, high temperatures are concentrated at the tip of the electrode. Therefore, it is expected that regions around the electrode will have high temperature prevailing conditions compared to regions adjacent the furnace lining. Analysis of the digout samples from the prereduction zone has shown that the oxygen level in manganese ores, measured as MnO_x, will decrease with increasing furnace depth i.e., when approaching the high temperature zone of the furnace. The variation of MnO_x has shown that in general the extent of prereduction is higher adjacent the electrode compared to regions adjacent the furnace lining as shown in Figure 4.55. This is expected as there exist a temperature gradient in the prereduction zone with high prevailing temperature conditions adjacent the electrode compared to the furnace lining.

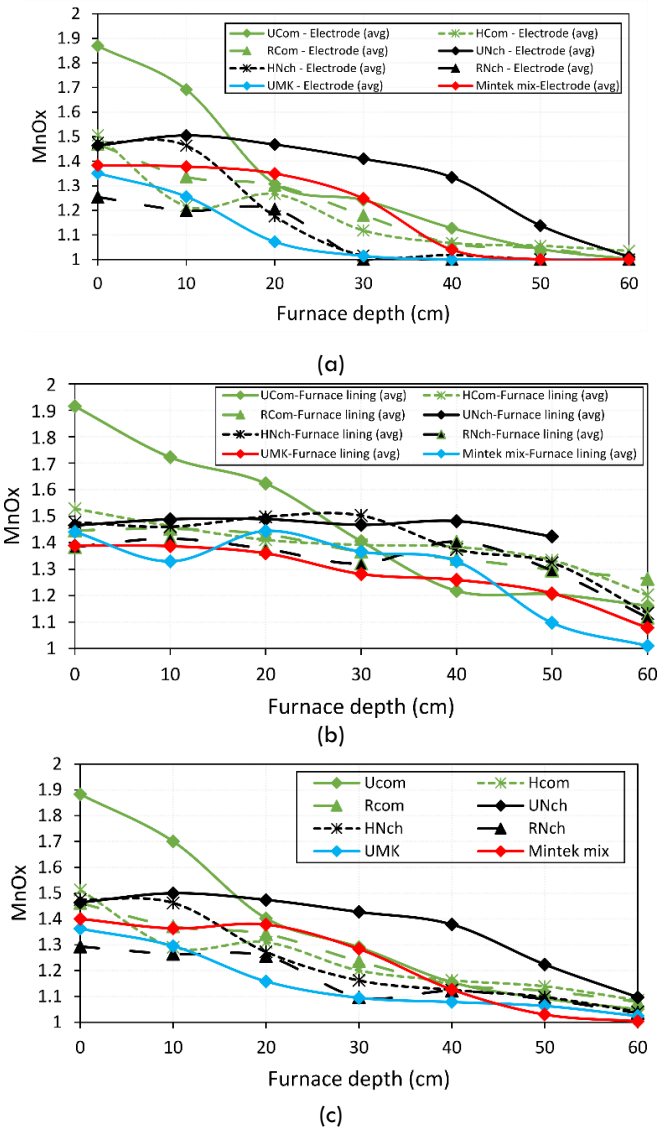

Figure 4.55: Comparison of MnO_x from digout of the prereduction zone of pilot experiments. (a) MnOx adjacent electrode, (b) MnO_x adjacent furnace lining and (c) Variation of MnOx with depth at an electrode/furnace wall material distribution ratio of 70/30.

In the laboratory scale induction furnace experiments, UMK has been seen to have a higher extent of prereduction followed by Comilog and lastly Nchwaning. The extent of prereduction is defined as a measure of how much oxygen is left to be removed from higher manganese oxides until an MnO_x of 1 is reached. The higher extent of prereduction in IF75 for UMK has been attributed to increased surface area due to porosity increase with increasing temperature, decomposition of carbonates

and gasification of C according to Boudouard reaction. The gasification of C generated more CO required for prereduction of manganese oxide. However, a similar trend is observed in pilot furnace. In contrast to the prereduction in induction furnace (IF75), there is significant metal producing reactions in the pilot furnace and as such a high and stable flow of reducing gas. Hence, it will be expected that Comilog will have a higher extent of prereduction compared to the other ores. As has been observed in lab scale TGA furnace, Comilog had a higher extent of prereduction when approaching the high temperature region, in a stable 70/30 CO/CO_2 gas atmosphere. In the pilot experiments the temperature profile of the prereduction zone is not known and there exists an uncertainty of how much prereduction varies from the different pilot experiments.

The furnace was shutdown 40kWh after the last tapping and the chemical reactions in the cokebed area were expected to stop within minutes of shutdown since metal producing reactions in the cokebed are highly endothermic[142]. After furnace shutdown, the furnace took over 48 hours to completely cool down and it is believed that the slow cooling prior to excavation might have enhanced some prereduction since these reactions are mostly exothermic. Hence it is uncertain how much prereduction occurs after furnace shutdown. However, as observed in the gas analysis, the offgas composition decreased rapidly once the furnace is shut down. Hence, it is believed that to a greater degree, the measured MnO_x closely represent the state of the prereduction zone during furnace operation.

It can be seen in Figure 4.55(c) that pretreatment of Comilog ore will reduce the initial MnO_x level in the prereduction zone. This will have an effect of increasing concentration of CO in the offgas composition since the proportion of oxygen available for prereduction will be lowered. An opposite trend is observed for CO_2 as illustrated in Figure 4.56. However, when approaching the high temperature zone, it can be seen that at a depth of about 40cm, the prereduction in Comilog ore series will be at the same level. For Nchwaning series, the initial MnO_x is at the same region for untreated and preheated Nchwaning ore. However, with increasing furnace depth, preheated Nchwaning ore shows a higher extent of prereduction when compared to untreated Nchwaning as presented in Figure 4.55(c). However, there isn't a big difference in the offgas composition as well as the degree of prereduction and energy consumption as will be discussed in the next chapter on mass and energy balance. Hence, it is believed that preheating Nchwaning ore has no significant effect of degree of prereduction as will be discussed later. Prereduced Nchwaning ore will have the same reduction profile as preheated Nchwaning ore at depth of 30cm, however, this

experiment was very unstable and hence the extent of prereduction cannot fully describe the effect on prereduction. Carbonates in UMK have been shown to decompose with greater degree adjacent the electrode compared to the furnace lining as presented in Figure 4.49. The higher CO concentration in UMK and Mintek (Figure 4.56) mix experiments when compared to untreated Comilog experiment corresponds to a lower degree of prereduction. This is seen from mass and energy balance calculations as will be discussed in the next chapter.

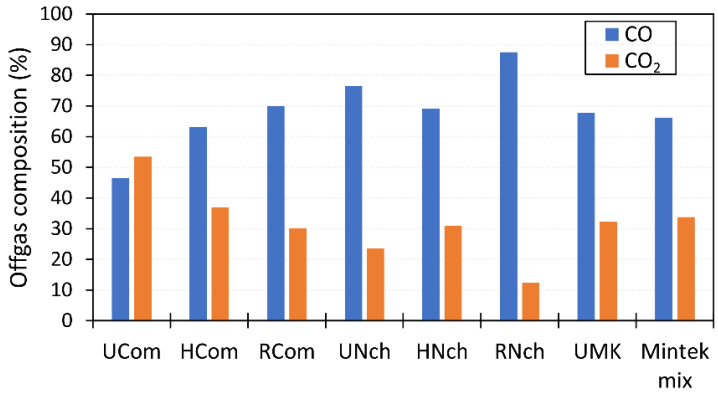

Figure 4.56: Average CO and CO_2 concentration in the offgas measured in the last 100 minutes for all pilot experiments.

4.4.2 Furnace interior and cokebed relations

The interior of the furnace in the Comilog series, Nchwaning series and UMK and Mintek series experiments are presented in Figure 4.57, Figure 4.58 and Figure 4.59, respectively. The variation of the O/Mn ratio i.e., MnOx in the prereduction zone are shown for each experiment. In the cokebed region of each experiment, there exists regions with unmelted material, the primary slag region, a cokebed and an alloy layer at the bottom. The primary slag in all experiments which exists on top of the cokebed is mainly characterized by solid monoxide phase plus liquid slag. Some of the excavations show alloy in the primary slag region (e.g., untreated Comilog experiment) and liquid slag without solid MnO (e.g., untreated Nchwaning). These are believed to be out layers, possibly emanating from slag boils. In the cokebed region, the slag is completely liquid. This shows that reduction of the primary slag will occur on top of the coke bed with an increased dissolution of monoxide in slag rendering the slag fluid enough to trickle down the coke bed. This agrees with laboratory results in this work and previous pilot studies[119], [120], [142].

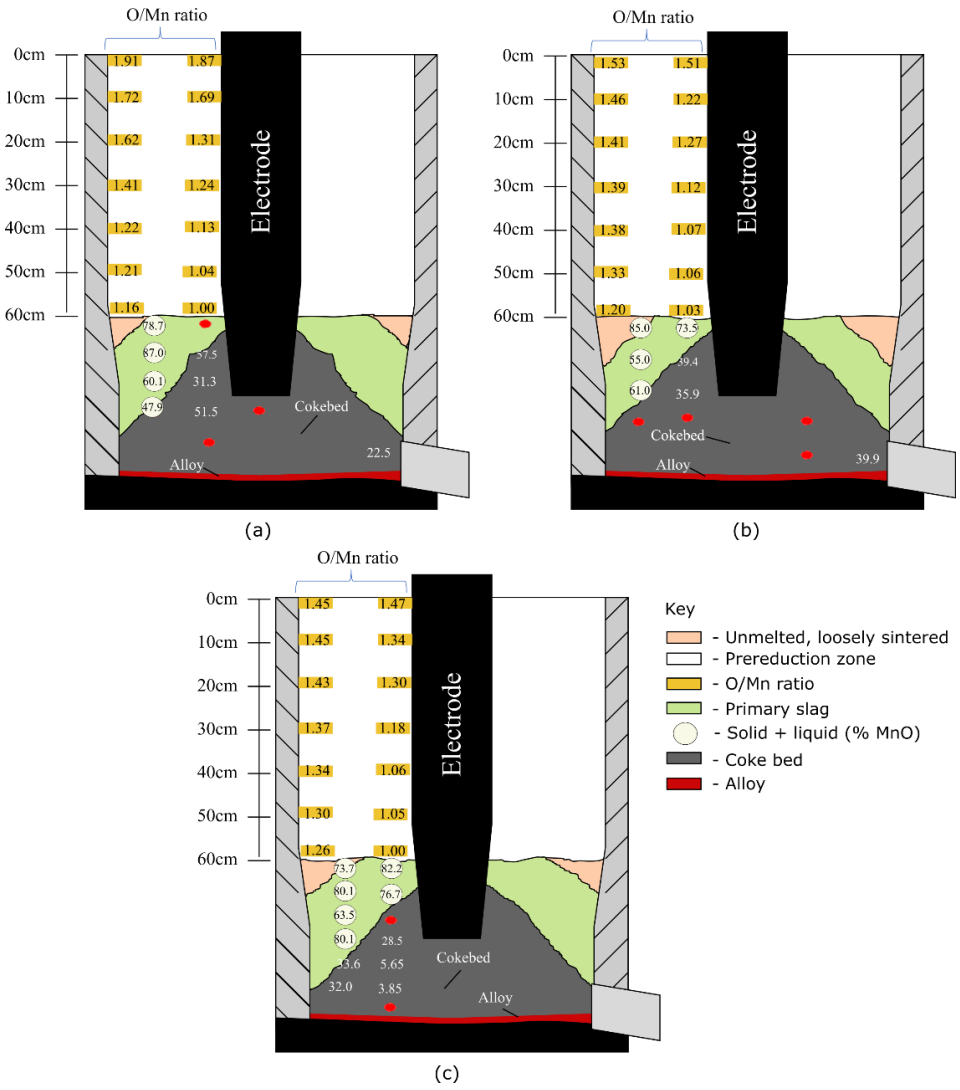

Figure 4.57: Schematic illustration of the interior of the furnace showing the O/Mn ratio (prereduction zone) and wt.% MnO in slag (cokebed zone) in (a) untreated Comilog experiment, (b) preheated Comilog experiment and (c) prereduced Comilog experiment.

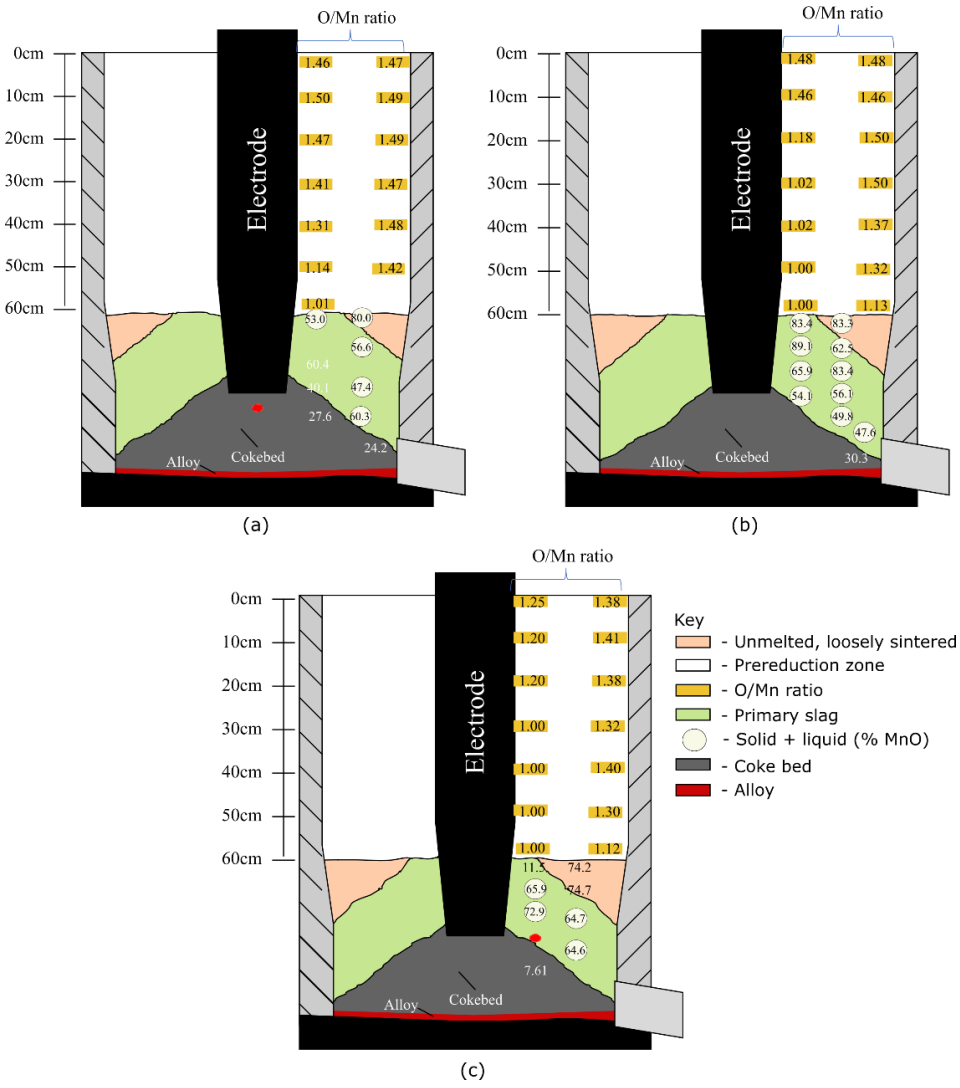

Figure 4.58: Schematic illustration of the interior of the furnace showing the O/Mn ratio (prereduction zone) and wt.% MnO in slag (cokebed zone) in (a) untreated Nchwaning experiment, (b) preheated Nchwaning experiment and (c) prereduced Nchwaning experiment

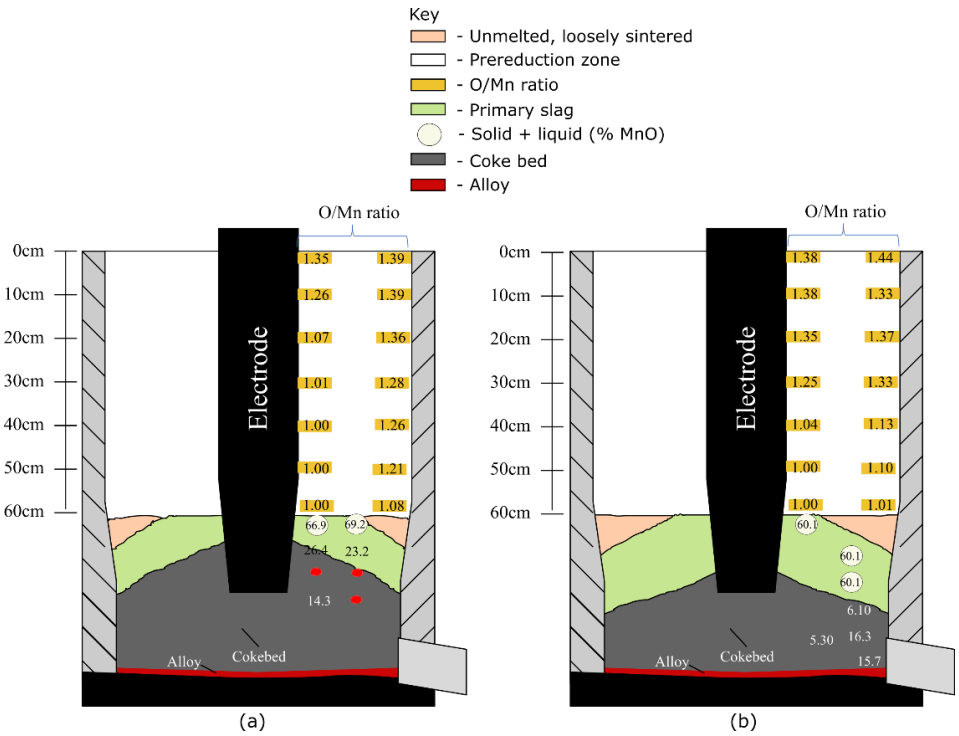

Figure 4.59: Schematic illustration of the interior of the furnace showing the O/Mn ratio (prereduction zone) and wt.% MnO in slag (cokebed zone) in (a) untreated UMK experiment and (b) untreated Mintek mix experiment.

The geometry and size of the cokebed in each experimental series were similar, but with minor variations. It can be observed in Figure 4.57, that the size and shape of the cokebed is similar for untreated, pretreated and prereduced Comilog experiments. This is however expected, as the slag chemistry of the charge materials, electrode position and subsequent furnace load, were similar across the three experiments. In comparison to the high cokebed in Comilog series, Nchwaning series experiments gave a low and wide cokebed. It has been shown by mass and energy balances (Table 5.3 and Table 5.4) that the degree of prereduction in Nchwaning series experiments is lower than Comilog series experiments. A lower degree of prereduction is expected to give high carbon consumption and low coke bed. UMK and Mintek series experiments with intermediate level of degree of prereduction when compared to the Comilog and Nchwaning series will hence give a cokebed large than the Nchwaning series as can be seen in Figure 4.59. The Mintek mix experiment gave a low cokebed when compared to UMK experiment. It is believed to be related to

probable higher cokebed temperature conditions in Mintek mix when compared to UMK experiments. In addition, the alloy from Mintek mix experiment had very high % Si content and is believed to be reduction of SiO_2 at high temperature. Considering that the Mintek experiment had the highest basicity at 1.0, it is expected that the activity coefficient of SiO_2 in slag will be low and subsequently the level of Si in alloy is expected to be very low. Hence high Si in alloy correlates well with high temperature conditions.

The Al_2O_3/SiO_2 ratio for the tapped slag ranged from 1.22 to 1.3, the MgO/CaO ratios were 0.04 to 0.05 and the basicity was about 0.5 in the Comilog series experiments. Therefore, a ternary phase diagram with Al_2O_3/SiO_2 at 1.3 and MgO/CaO at 0.05 calculated in FactSage was used to represent the MnO-SiO_2-Al_2O_3-CaO-MgO slag system of the tapped slags as shown in Figure 4.60.

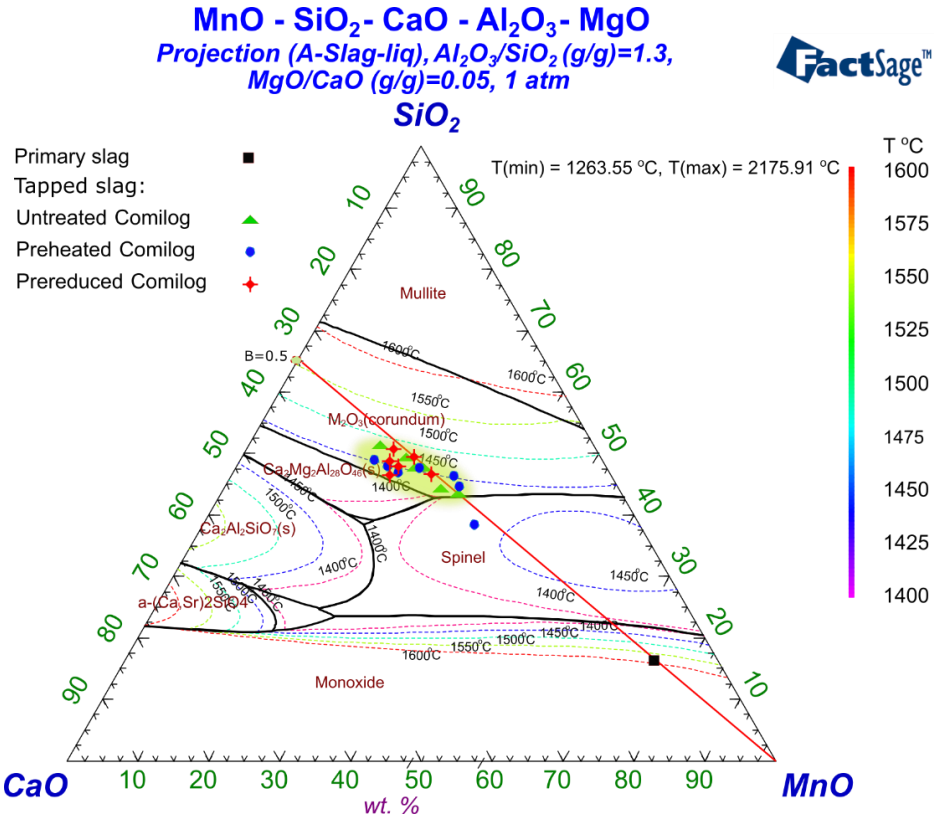

Figure 4.60: Ternary phase diagram representing the MnO-SiO_2-Al_2O_3-CaO-MgO slag system with Al_2O_3/SiO_2 at 1.3 and MgO/CaO at 0.05 calculated in FactSage 8.3.

The charge mix parameters i.e., basicity $(CaO+MgO)/(SiO_2+Al_2O_3)$ and Al_2O_3/SiO_2 ratio are quite similar for untreated, preheated and prereduced sources for a similar ore type and these will not change during reduction. As can be seen in Figure 4.60, the reduction of the primary slags in the Comilog series experiments will start in the two phase area solid monoxide + liquid and will follow the basicity line until final tapped slag with composition within the same area for untreated, preheated and prereduced Comilog charges. This shows that pretreatment will not have any effect on the metal producing reactions in the high temperature zone. This agrees with findings from laboratory experiments in this work. Similar trends are also observed for untreated and preheated Nchwaning experiments.

Chapter 5

5 Mass and Energy Considerations

5.1 Introduction

The purpose of this chapter is to give an overview of the effect of pretreatment of manganese ores on the carbon and energy footprint in FeMn alloy production. The specific carbon (kg C/t alloy) and energy consumption (kWh/t alloy) per metric tonne of alloy production are critical parameters in ferromanganese production as they are key drivers in terms of cost of production. These are related to quantities and chemical compositions of charge raw materials, tapped slag and alloy. In addition, they are closely connected to the CO/CO_2 ratio in the furnace offgas, and as such the total CO_2 emissions.

In the pilot experiments conducted, various charge mixtures with pretreated and untreated manganese ores have been used to produce ferromanganese. Slag and alloy from the pilot experiments were analyzed and quantified. In addition, the CO/CO_2 composition of the offgas was measured. In this section, results from material balance calculations and the resulting specific energy and carbon consumptions from using charge mixtures with pretreated and untreated manganese ores will be presented. Energy and carbon consumption will be discussed based on accounting mass and energy balances for the pilot experiments which are calculated in HSC Chemistry version 10.0.4.3.

5.2 Data from Pilot experiments

Operational data from the pilot experiments was used to calculate the material and energy balance. This data includes weights of raw materials input and the chemical composition of raw materials and tapped slag and alloy as well as measured CO/CO_2 composition in the offgas. The weights of tapped products are not used in the calculation as they are not highly accurate mainly because the furnace may not be emptied at every tapping and there exists entrapment of metal in slag and vice versa. The weight of alloy and slag will be calculated mainly based on weight of input raw materials, MnO content in slag, Si in alloy and assuming that all Fe in raw materials will report to alloy phase and unreducible oxides i.e., mainly CaO, MgO and Al_2O_3

enter the slag phase. The chemical composition of input raw materials and charge blends have been previously presented (**Chapter 4**) in Table 4.1, Table 4.3, Table 4.4 and Table 4.5. The average chemical composition of the tapped slag and alloy in the second half of each experiment is presented in Table 5.1. The measured range of CO/CO_2 composition in the offgas are summarized in Table 5.2. The offgas composition used was from the stable period 100 minutes prior to furnace shutdown, except for reduced Nchwaning were it was considered in the first 100 minutes. This was because the offgas in the reduced Nchwaning experiment was unstable and kept on decreasing during the experiment as was shown in Figure 4.19 and Figure 4.20.

Table 5.1: Composition of tapped slag and alloy from the pilot experiments. (UCom = untreated Comilog ore, HCom = preheated Comilog ore, RCom = prereduced Comilog ore, UNch = Untreated Nchwaning ore, HNCh = preheated Nchwaning ore and RNch = prereduced Nchwaning ore).

Charge mix	Slag composition					Alloy composition				
	MnO	SiO_2	Al_2O_3	CaO	MgO	Mn	Fe	Si	C	Mn/Fe
UCom	27.1	21.2	26.3	23.5	1.9	85.7	6.1	0.6	7.0	14.0
HCom	28.4	20.0	26.6	22.9	2.1	85.8	6.0	1.1	7.1	15.0
RCom	23.8	21.5	28.1	24.6	2.0	84.4	6.1	1.3	7.0	13.9
UNch	27.4	24.8	10.8	26.5	6.2	77.4	14.9	0.2	7.1	5.2
HNch	27.8	25.2	10.9	26.0	6.8	75.7	15.2	0.6	7.0	5.0
RNch	27.5	27.0	8.2	27.2	6.4	75.1	14.9	1.2	7.0	5.0
UMK	15.7	26.1	15.9	31.2	8.0	83.6	8.6	0.4	7.4	9.7
Mintek mix	14.4	38.2	3.5	33.4	8.7	76.2	12.5	4.7	5.3	6.1

Table 5.2: Measured range of CO/CO_2 in the offgas in the stable period 100 minutes prior to furnace shutdown and the calculated $CO_2/(CO_2 + CO)$ (*Note: Only CO/CO_2 for RNch was from first 100 minutes)

Charge mix	Off-gas component (%)		Calculated $CO_2/(CO_2+CO)$
	CO	CO_2	(Maximum – minimum)
UCom	35 – 55	65 – 45	0.65 – 0.45
HCom	53 – 65	47 – 35	0.47 – 0.35
RCom	62 – 70	38 – 30	0.38 – 0.30
UNch	68 – 75	32 – 25	0.32 – 0.25
HNch	62 – 75	38 – 25	0.38 – 0.25
RNch	78 – 85	22 – 15	0.22 – 0.15
UMK	55 – 70	45 – 30	0.45 – 0.30
Mintek mix	50 – 70	50 – 30	0.50 – 0.30

As presented in Table 5.2, untreated Comilog charge mixture gave the highest CO_2 concentrations during the experimental runs, followed by charge mixture with preheated Comilog and lastly, prereduced Comilog with the lowest observed CO_2

concentration. The opposite trend was observed for CO concentrations. In the Nchwaning series, the preheated Nchwaning experiment had slightly higher CO_2 concentration compared to untreated and prereduced Nchwaning experiments with prereduced Nchwaning having the lowest CO_2 concentrations. For the untreated UMK and Mintek mix experiments, the offgas compositions are within a similar range.

5.3 Mass and energy calculations

The material balance per 100 kg input material, calculated using the heat and material balance module in HSC Chemistry version 10.0.4.3[6] are presented in **Appendix F**, for all the pilot experiments. In mass balance calculations, the MnO in tapped slag was fixed according to MnO content in slag presented in Table 5.1. The Mn in the alloy was obtained by the difference between the total Mn from the charge mixture and the one reported in the slag as MnO. The carbon content in the alloy was saturated and fixed at 7% in the alloy, whilst the total input of Fe was considered to report to the alloy phase. The unreducible oxides reported to the slag phase and SiO_2 was calculated by balancing the amount of Si input from the charge mixture and Si reported in the alloy phase. In calculating the energy balance, raw materials input temperatures were assumed to be 25 °C whereas, slag and alloy were tapped at 1500 °C and the off gas was assumed to be 200 °C. The mixing enthalpies in slag and alloy as well as the enthalpy of dissolution of carbon are not considered in the balance. The relationship between the specific carbon consumption, the $CO_2/(CO_2+CO)$ ratio and energy consumption to produce 1 tonne of HCFeMn alloy was established based on calculations from 0 to 100 degree of prereduction. The degree of prereduction has been previously defined by Tangstad[142] as a measure of the extent of the gas reduction of higher manganese oxides, which is reflected in the $CO_2/(CO_2+CO)$ ratio of the off-gas and is inversely related to the coke and energy consumption. The degree of prereduction is defined to be 100% when all the Mn_3O_4 from the reduction of higher manganese oxides is reduced at low temperatures before the Boudouard reaction is activated. If all CO_2 from the reduction of Mn_3O_4 is consumed by the Boudouard reaction, the degree of prereduction is 0%.

The relationship between the specific carbon consumption, the off-gas $CO_2/(CO_2+CO)$ ratio and energy consumption to produce 1 tonne of HCFeMn alloy for the three different pilot-scale scenarios in the Comilog series are shown in Figure 5.1. Figure 5.1 shows that as the CO content of the off-gas increases, the energy consumption due to the Boudouard reaction increases. The main conclusion is that for a fixed charge the lower CO_2 to ($CO + CO_2$) ratio in the off-gas indicates higher CO_2 consumed in the Boudouard reaction and consequently higher carbon and energy

consumption as has been observed previously[7], [12], [13]. The minimum and maximum carbon consumption for the three pilot scale tests with untreated, preheated and prereduced Comilog were within the same range, because the chemistry of the slags and alloys tapped presented in Table 5.1 were similar with insignificant variations.

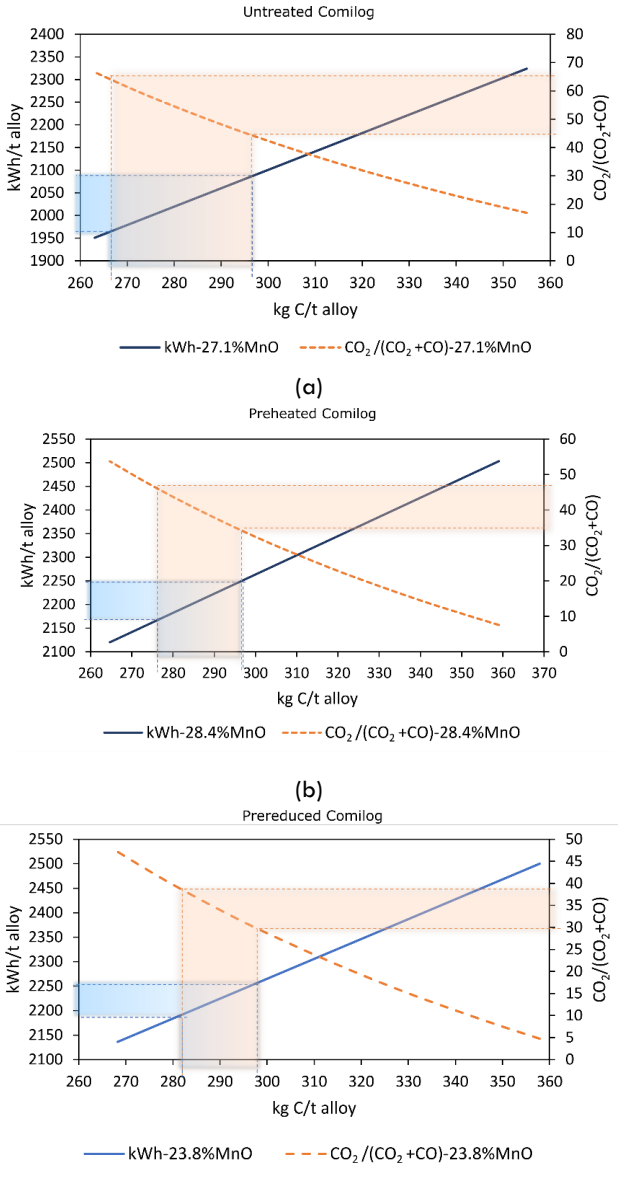

Figure 5.1: The relationship between energy consumption, $CO_2/(CO_2+CO)$ ratio and carbon consumption for production of 1 tonne of alloy using charge mixtures with (a) untreated Comilog (b) preheated Comilog and (c) prereduced Comilog ore.

Based on the composition range of the measured furnace off-gas from the Comilog series experiments, differences in carbon consumption are observed as illustrated in Figure 5.1. Untreated Comilog has a wide range of carbon consumption and this decreases for preheated and prereduced Comilog. The narrowing of the range of carbon consumption as is reflected in off-gas composition shows that the process was more stable for pretreated Comilog in comparison to untreated. The energy consumption when using untreated Comilog, ranging from 1960 to 2090 kWh is lower compared to preheated Comilog (2160 to 2250 kWh) and prereduced Comilog (2190 to 2255 kWh). If the prereduction reactions commences in the prereduction zone of the SAF, higher manganese oxides will reduce to lower manganese oxides from MnO_2 to Mn_2O_3 to MnO_3O_4 to MnO in addition to reduction of iron oxides. The reduction of these reactions is exothermic. Pretreatment of Comilog ore through preheating and prereduction lowers the O/Mn ratio of the ores and as such, this will eliminate a part of exothermic reactions resulting in increased energy consumption in the SAF. Average CO/CO_2 composition of the offgas, metal and slag chemistry, and the subsequent carbon and energy consumption for untreated, preheated and prereduced Comilog experiments are compared as presented in Table 5.3. The degree of prereduction is estimated as illustrated in **Appendix E**.

Table 5.3: Comparison between results of untreated, preheated and prereduced Comilog experiments. (NB: UCom – untreated Comilog, HCom – preheated Comilog and RCom – prereduced Comilog)

Parameter	UCom	HCom	RCom
Total kg C/t alloy	283	291	298
Stoichiometric fixed kg C/t alloy	263	265	268
Energy consumption kWh/t alloy	2017	2226	2250
Slag/Alloy ratio	0.50	0.53	0.44
% Mn recovery	89.1	88.0	91.4
Average Offgas CO/CO_2	47/53	63/37	70/30
Degree of prereduction (%)	78	72	64
Alloy composition (%)			
Mn	86.0	85.6	85.6
Fe	6.4	6.9	6.1
Si	0.6	0.4	1.3
C	7.0	7.0	7.0
Slag composition(%)			
MnO	27.1	28.4	23.8
SiO_2	19.2	18.4	19.1
Al_2O_3	26.4	26.0	28.7
CaO	22.0	23.8	25.0
MgO	2.2	0.6	-
Basicity $(CaO+MgO)/(Al_2O_3+SiO_2)$	0.53	0.55	0.52

*Stoichiometric fixed carbon = Carbon consumed in the high temperature zone

Figure 5.2 shows the relationship between the specific carbon consumption, the off-gas $CO_2/(CO_2+CO)$ ratio and energy consumption to produce 1 tonne of HCFeMn alloy for the three different pilot-scale scenarios in the Nchwaning series.

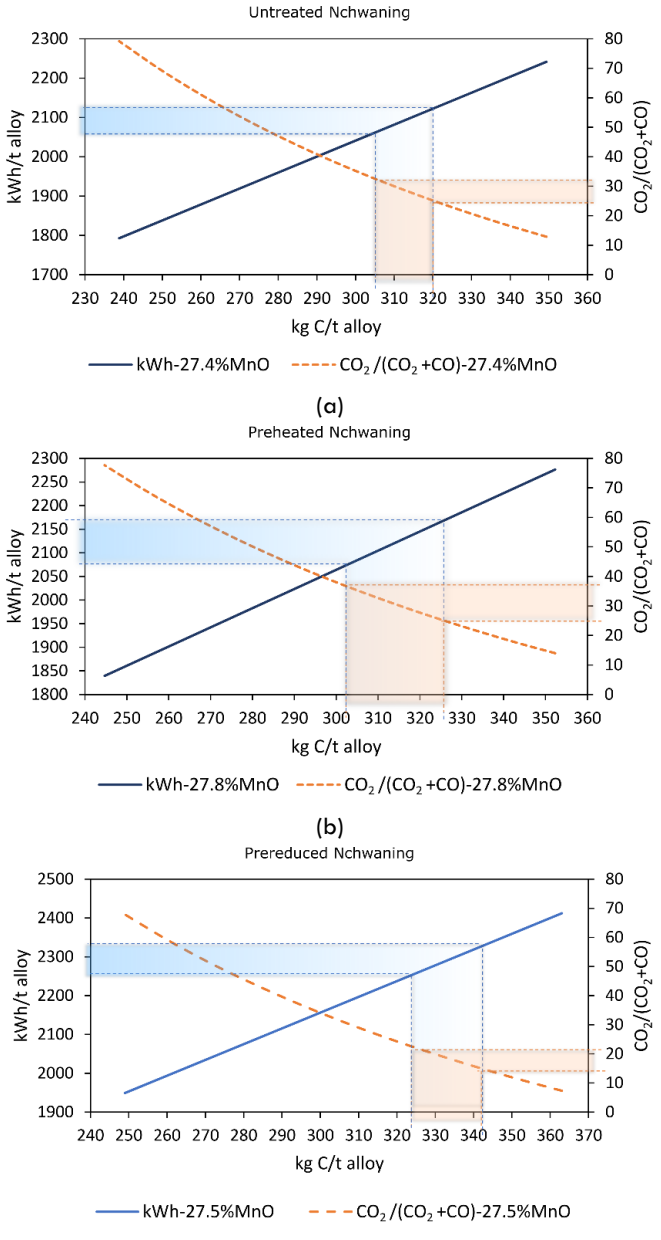

Figure 5.2: The relationship between energy consumption, $CO_2/(CO_2+CO)$ ratio and carbon consumption for production of 1 tonne of alloy using charge mixtures with (a) untreated Nchwaning (b) preheated Nchwaning and (c) prereduced Nchwaning ore.

The Nchwaning series (Figure 5.2) shows that untreated and pretreated Nchwaning charge mixtures show energy and carbon consumption within the same area i.e., ranging between 2080 – 2160 kWh/t alloy. This can also be observed for the carbon consumption ranging between 305 – 325 kg C/t alloy. This is expected and agrees with the oxygen level i.e., MnO_x values which was observed to remain at the same level after preheating Nchwaning. The MnO_x of untreated Nchwaning was at 1.5 and after preheating it slightly increased to 1.52 as shown in Figure 4.1. As such, this was considered to be an insignificant change. For Nchwaning ore, it can be seen that preheated Nchwaning ore does not show a more stable operation compared to untreated Nchwaning, as has been observed in the Comilog series. Prereduced Nchwaning has the highest energy and carbon consumption. However, the offgas composition used for the calculation was from the initial stages of the experiment and the process was very unstable throughout the experiment, hence the data used does not reflect the precise energy and carbon consumption. The average parameters for the Nchwaning series are presented in Table 5.4.

Table 5.4: Comparison between results of untreated, preheated and prereduced Nchwaning experiments. (NB: UNch – untreated Nchwaning, HNch – preheated Nchwaning and RNch – prereduced Nchwaning)

Parameter	UNch	HNch	RNch
Total kg C/t alloy	318	313	340
Stoichiometric fixed kg C/t alloy	239	245	249
Energy consumption kWh/t alloy	2110	2120	2315
Slag/Alloy ratio	0.32	0.39	0.34
% Mn recovery	91.8	90.3	91.3
Average Offgas CO/CO_2	74/26	69/31	88/12
Degree of prereduction (%)	30	37	20
Alloy composition (%)			
Mn	76.4	77.4	77.1
Fe	16.4	14.9	14.7
Si	0.2	0.6	1.2
C	7.0	7.0	7.0
Slag composition(%)			
MnO	27.4	27.8	27.5
SiO_2	26.6	26.3	26.1
Al_2O_3	12.6	12.4	9.0
CaO	26.5	23.0	31.7
MgO	5.6	9.2	5.8
Basicity $(CaO+MgO)/(Al_2O_3+SiO_2)$	0.87	0.83	1.07

Figure 5.3 show the relationship between the specific carbon consumption, the off-gas $CO_2/(CO_2+CO)$ ratio and energy consumption to produce 1 tonne of HCFeMn alloy for the UMK and Mintek mix experiments. The subsequent average parameters

for the stable period are presented in Table 5.5. It can be seen that the carbon and energy consumption in Mintek mix are at a higher level compared to UMK. This is mainly because the Mintek mix is a blend of mainly two carbonate ores i.e., UMK and Kudumane and as such the fraction carbonates in the charge mix is higher at 22.3 % compared to 11.9 % in UMK charge mix. Hence, this is expected to give a higher energy and carbon consumption compared to the UMK experiment. This is attributed to carbonate decomposition and Boudouard reaction which are energy demanding and consumes carbon. As presented in Table 5.5, the degree of prereduction in Mintek mix is lower than UMK and this reflects energy and carbon consumption from Boudoard and decomposition of carbonates. On the other hand, the minimum stoichiometric carbon requirements are higher in Mintek mix, compared to UMK. This is fixed per alloy composition, and it can be seen that the alloy from Mintek mix has significantly higher Si content compared to UMK and hence the carbon consumption is higher due to reduction of SiO_2.

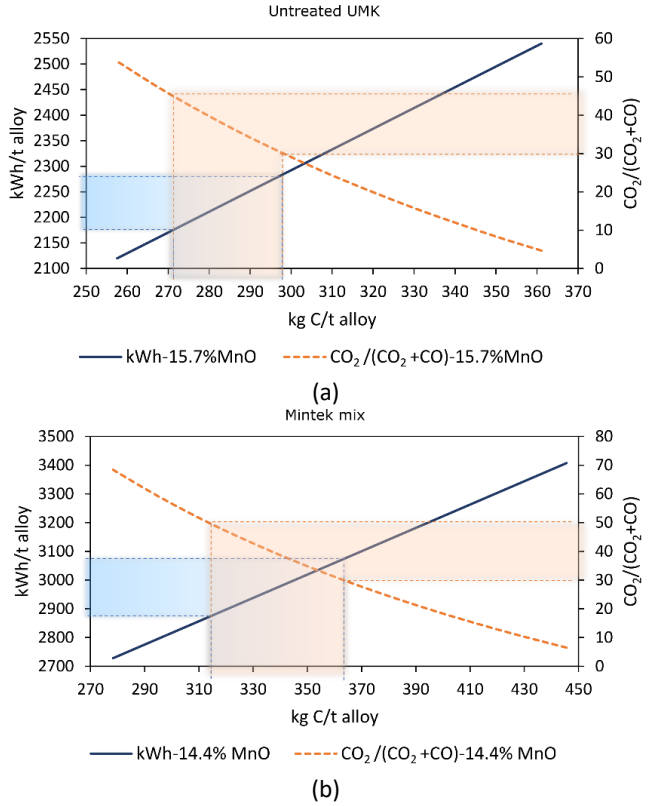

Figure 5.3: The relationship between energy consumption, $CO_2/(CO_2+CO)$ ratio and carbon consumption for production of 1 tonne of alloy using charge mixtures with (a) untreated UMK and (b) Mintek mix

Table 5.5: Comparison between results of untreated UMK and Mintek mix experiments.

Parameter	UMK	Mintek mix
Total kg C/t alloy	294.7	353.0
Stoichiometric fixed kg C/t alloy	257.6	278.3
Energy consumption kWh/t alloy	2277.8	3027.6
Slag/Alloy ratio	0.48	0.92
% Mn recovery	93.5	88.4
Average Offgas CO/CO_2	68/32	66/34
Degree of prereduction (%)	63	54
Alloy composition (%)		
Mn	84.1	77.1
Fe	8.5	11.2
Si	0.4	4.7
C	7.0	7.0
Slag composition(%)		
MnO	15.7	14.4
SiO_2	27.8	34.6
Al_2O_3	17.3	3.5
CaO	31.2	40.6
MgO	6.8	6.7
Basicity $(CaO+MgO)/(Al_2O_3+SiO_2)$	0.84	1.2

5.4 Comparison of carbon and energy consumption in different scenarios.

The calculations for experiments with untreated ores are considered the base case and differences were observed when compared to experiments with pretreated ores. The minimum i.e., stoichiometric carbon and total carbon consumption in all the experiments were calculated by the raw materials in and the slag and metal composition out. The stoichiometric carbon consumption refers to the carbon consumed in the high temperature cokebed zone, and the total carbon consumption refers to stoichiometric carbon plus additional carbon consumed in the prereduction zone. The total carbon consumption in the experiments is estimated based on the degree of prereduction which is reflected by the $CO_2/(CO_2+CO)$ offgas ratio. Figure 5.4 show the stoichiometric and total carbon consumption based on the degree of prereduction which is reflected in the offgas composition.

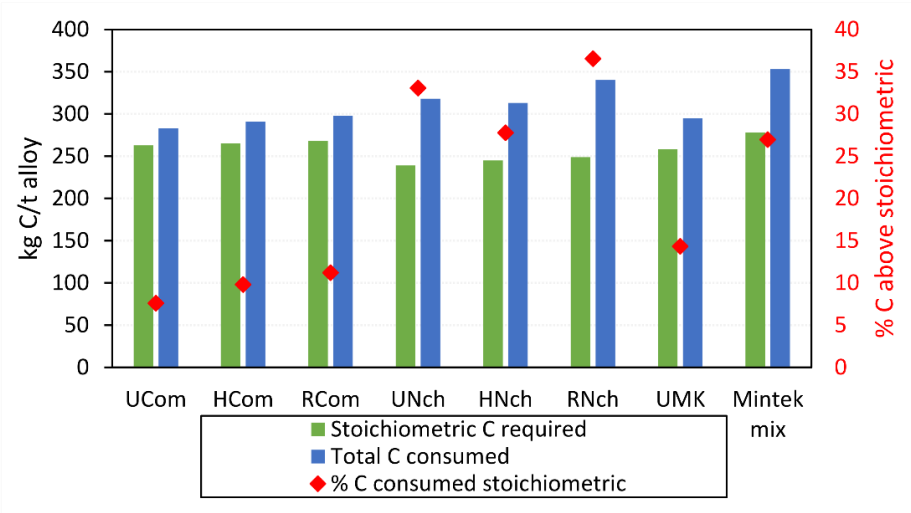

Figure 5.4: Minimum stoichiometric and total carbon consumption. The percentage of carbon above the minimum stoichiometric is shown on the vertical secondary axis for each experiment.

As can be seen in Figure 5.4, the stoichiometric carbon consumption for the untreated, preheated and prereduced Comilog ore are at the same level. This is mainly because there are no considerable differences in the alloy composition in the three experiments. This is also the same for the Nchwaning series. In comparison to all experiments, the stoichiometric carbon requirements are highest in Comilog series, followed by Mintek mix, UMK and lastly Nchwaning series. The trend is in direct correlation with the alloy composition in these experiments. The additional carbon above the stoichiometric carbon requirements is due to conditions in the prereduction zone. The total carbon consumption in the Comilog series is seen to be generally within the same region. Untreated and preheated Nchwaning show total carbon consumption within the same region whereas in prereduced Nchwaning, the total carbon consumption is higher than preheated and untreated Nchwaning. However, this experiment was very unstable and as such does not fully reflect the effect of prereduction of Nchwaning ore. Lastly, for the UMK and Mintek mix experiment, the carbon consumption is highest for the Mintek mix. This is attributed to significantly high level of carbonates in the charge mixture and as indicated by the degree of prereduction which is lower (Table 5.5), the carbon consumption is higher as expected. The total carbon consumption is above the respective stoichiometric fixed amount by 8 – 36 % for the experiments as can be seen in Figure 5.4. This is closer to the 10 – 30 % more carbon above the stoichiometric carbon as has been previously reported by Swamy *et al.*,[12] for industrial operations. Ishak and Tangstad [17], previously showed that for industrial furnaces the degree of prereduction varies between 10 to

40 % and can be as high as 50 to 60 % in very good periods. In this work, the degree of prereduction was in the range 64 – 78 % for the Comilog series as presented in Table 5.3. For Nchwaning series, it ranged 20 – 37 % as presented Table 5.4. Lastly for UMK and Mintek mix, the degree of prereduction is 64 and 53, respectively as presented in Table 5.5. As such, the degree of prereduction was generally high for Comilog series, followed by UMK and Mintek mix and lastly Nchwaning experiments. This agrees with findings from laboratory experiments in this work where Comilog is seen to have a higher extent of prereduction in stable CO/CO_2 atmosphere followed by UMK and lastly Nchwaning and correlates with previous findings by Ishak and Tangstad [17].

The energy balance was initially calculated with input temperatures of charge materials at 25 °C, offgas temperature at 200 °C and lastly the slag and alloy temperature at 1500 °C. To evaluate the benefit of charging hot pretreated charge blends, calculations were done assuming that the ores are pretreated in a separate unit and fed into the furnace at 600 °C. The calculation was made using the same degree of prereduction obtained when the blends were charged at 25 °C for the preheated and prereduced Comilog and Nchwaning experiments. The offgas was assumed to exit the furnace at 400 °C whilst the slag and alloy are tapped at 1500 °C. The energy comparison of the different scenarios is as shown in Figure 5.5.

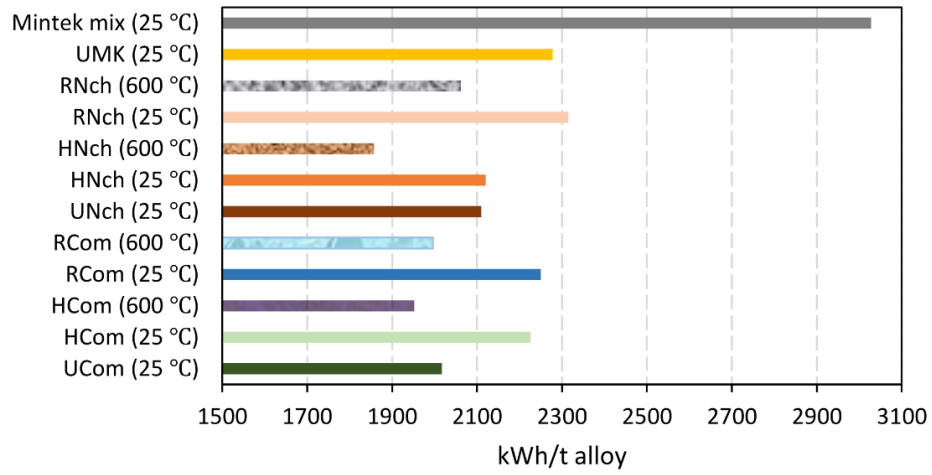

Figure 5.5: Energy consumption per ton of alloy for ore blends with untreated, preheated and prereduced ores, with input temperatures at 25 °C and 600 °C.

Energy requirement differences in the experiments were significant and dependent on the charge mixture. Carbonates in the burden have been reported to

have a double effect, first requiring energy on the decomposition of carbonates and secondly, to increase energy and coke consumption according to Boudouard reaction [7] . As such, it can be seen that for experiments with untreated ores, Mintek mix which contains UMK ore, a Mamatwan type-ore, which is enriched in Mn-bearing carbonates and Kudumane another carbonate ore, would exhibit the highest energy consumption. This is followed by UMK experiment followed by experiment with Nchwaning ore which contains less carbonates compared to UMK and Kudumane. Nchwaning mix was shown to have a higher carbon consumption, 318 kg C/t alloy compared to 295 kg C/t alloy for UMK mix and this is attributed to a lower degree of prereduction of 30 % in untreated Nchwaning. On the other hand, the energy consumption in UMK mix is higher than Nchwaning mainly due to higher amount of carbonates in UMK mix. This can also be due to the slag/alloy ratio; Nchwaning charge mixture had a lower S/A ratio of 0.32 compared to 0.48 for UMK charge mixture, which means there is less slag produced from untreated Nchwaning charge mixture and ultimately a lower kWh/t alloy. An increases in S/A ratio by about 0.1 has been reported to increase energy consumption by about 60 – 70 kWh/t alloy produced [2].

In both Comilog series and Nchwaning series, the energy consumption in using untreated charge mixtures is lower compared to charge blends with preheated and prereduced manganese ores, when considering charging the furnace at 25 °C. If the prereduction reactions commences in the prereduction zone of the SAF, higher manganese oxides will reduce to lower manganese oxides from MnO_2 to Mn_2O_3 to MnO_3O_4 to MnO in addition to reduction of iron oxides. The reduction of these reactions is exothermic. Therefore, pretreatment of Comilog ore through preheating and prereduction lowers the O/Mn ratio of the ores and as such, this will eliminate a part of exothermic reactions resulting in increased energy consumption in the SAF. However, the effect is not observed for preheated Nchwaning since there is minimal change in MnO_x when Nchwaning is preheated. As shown in Figure 5.5, pretreatment of Comilog ore and charging it hot into the furnace will significantly decrease the energy consumption by about 250 – 300 kWh in the SAF. The observed trend are in close agreement with previous reported calculations of different pretreatment scenarios[25]. However, sustainable energy sources should be used in preheating the ore in a separate unit in order to achieve reduced overall energy consumption for the ferromanganese process. In addition, pretreatment of carbonate ores is envisaged to lower the carbon and energy requirements which emanates from decomposition of carbonates and Boudouard reaction. This has not been investigated in this work. However, from small scale experiments approximately 50 % of carbonates have been found to have decomposed at 800 °C. Therefore, there is potential on reduction of

energy and carbon for carbonate ores if the pretreatment is done in a separate unit prior to charging the SAF.

5.5 Summary

The effect of pretreatment of manganese ores on carbon and energy consumption was investigated in this work. Pilot-scale experiments have been conducted at in a 440 kVA AC electric furnace using different feed mixtures of untreated manganese ore, manganese ore preheated in air and manganese ore prereduced with solid carbon. Energy and carbon consumption of a HCFeMn furnace were performed for untreated and pretreated Comilog based on pilot experimental data. Energy consumption and carbon requirements were quite significant, and the main conclusions can be summarized as follows:

- The minimum stoichiometric reductant required to produce ferromanganese is dependent on the composition of the alloy being produced. This is fixed for a given metal composition and was calculated from the metal composition that was determined by mass balance based on the slag composition from experiments. This carbon is consumed for the reduction of MnO and SiO_2 to Mn and Si in metal, respectively and carbon dissolution in the metal. This was found to be within similar values for the Comilog series and Nchwaning series experiments. This is due to the closeness of the composition of the tapped measured alloy and slag from the pilot runs in each series. In the Mintek mix experiments it was higher than UMK experiments due to high SiO_2 reduction in Mintek mix.

- Preheated and prereduced Comilog experiments show more stable operation compared to untreated Comilog experiment. As such pretreatment in Comilog series gives a stable operation. However, for Nchwaning ore, ore preheating does not show stable operation.

- For a fixed charge the lower CO_2 to ($CO + CO_2$) ratio in the offgas indicates higher CO_2 consumed in the Boudouard reaction and consequently higher carbon and energy consumption. Offgas measurements in the Comilog series show that the use of untreated Comilog ore leads to considerably lower CO/CO_2 off-gas composition compared to pretreated Comilog ores, largely related to the high oxygen level of Comilog ore. For untreated and preheated Nchwaning there was no significant differences in the offgas composition.

- The degree of prereduction is generally high for Comilog series, followed by UMK and Mintek mix and lastly Nchwaning experiments. As such Comilog will have the lowest carbon and energy consumption. The degree of prereduction in UMK was significantly higher compared to Nchwaning series experiments, hence the total carbon consumption was lower for UMK. Carbonates will have a double effect consuming both energy on decomposition and energy by Boudouard reaction and as such Mintek mix had the highest energy and carbon consumption.

- Due to the higher amount of exothermic reactions, the untreated Comilog ore will give lower energy consumption compared to pretreated ore if added cold in the SAF. However, charging hot pretreated ore will result in lowering of the energy consumption in SAF by 300kWh/ton alloy. Prereduced Comilog did not have any significant difference from preheated Comilog with regards to energy and carbon consumption owing to insignificant change in oxygen level when Comilog is prereduced with solid carbon. The degree of prereduction in the Comilog series is in the same area within the uncertainties of the experiment. This gives the same carbon consumption and hence the overall CO_2 emissions.

Chapter 6

6 Conclusions and Further work

Laboratory scale experiments simulating industrial ferromanganese furnace process were conducted to investigate the prereduction characteristics of Comilog, Nchwaning and UMK ore. In addition, the effect of varying extent of prereduction on the metal producing reaction was investigated. Pilot scale experiments were conducted with various charge mixtures containing untreated and pretreated manganese ores. The reactions and inner structure of the pilot furnace were investigated through digout of the prereduction zone and excavation of the cokebed zone. Based on the experimental data, mass and energy balance calculations were done using HSC Chemistry software to establish the effect of ore pretreatment on furnace operation. Key findings from the work are summarized.

TGA rate curves showed that decomposition of carbonates in UMK was a two-step process with peak temperatures at 700 and 900 °C. The first endothermic peak in UMK is a combination of decomposition of carbonates and prereduction reactions whereas the second peak is mainly carbonate decomposition and O/Mn ratio is 1.0 showing that prereduction of higher manganese oxides is complete prior to second decomposition reaction. In addition to prereduction reactions, Nchwaning is also characterized by an endothermic step which is decomposition of carbonates at 900 °C. Comilog was observed to have a higher extent of prereduction in a stable CO/CO_2 gas atmosphere.

Varying the extent of ore prereduction will not have any effect on the metal producing reaction i.e., $MnO + C = Mn + CO$. This was in agreement with findings from pilot experiments, were pretreatment of manganese ores was seen to have no effect on the metal producing reaction. The charge mix parameters i.e., basicity $(CaO+MgO)/(SiO_2+Al_2O_3)$ and Al_2O_3/SiO_2 ratio are quite similar for untreated, preheated and prereduced sources for a similar ore type and these will not change during reduction. Hence, the final slag for example in untreated, pretreated and prereduced Comilog ores, will be tapped at compositions which are in the same region in the stable period of the furnace operation.

Phase development in untreated and pretreated charge mixtures of Comilog, Nchwaning, UMK and Kudumane ores, which is dependent on temperature and composition of the ore, showed that the initial slag formed is mainly liquid + solid monoxide phase and slag reduction will occur on top of the coke bed with an increased dissolution of monoxide in slag rendering the slag fluid enough to trickle down the coke bed. The coexistence of a solid phase and a liquid slag phase explains the high MnO activity in the slag. Therefore, low reduction extent will occur inside the coke bed area due to the lower MnO activity which emanates from complete dissolution of solid monoxide phase.

The geometry of the cokebed was seen to be similar for untreated and pretreated manganese ore charge blends. This was considered to be correlated to the degree of prereduction which remains within the same region within the experimental variations. The furnace offgas composition, mass, and energy calculations showed a more stable operation in preheated and prereduced Comilog experiments compared to untreated Comilog experiment. As such pretreatment in Comilog series gives a stable operation. However, for Nchwaning ore, ore preheating does not show stable operation. For a fixed charge the lower CO_2 to ($CO + CO_2$) ratio in the offgas indicates higher CO_2 consumed in the Boudouard reaction and consequently higher carbon and energy consumption. Offgas measurements in the Comilog series show that the use of untreated Comilog ore leads to considerably lower CO/CO_2 off-gas composition compared to pretreated Comilog ores, largely related to the high oxygen level of Comilog ore. For untreated and preheated Nchwaning there was no significant differences in the offgas composition. The degree of prereduction is generally high for Comilog series, followed by UMK and Mintek mix and lastly Nchwaning experiments. As such Comilog will have the lowest carbon and energy consumption. The degree of prereduction in UMK was significantly higher compared to Nchwaning series experiments, hence the total carbon consumption was lower for UMK. Carbonates will have a double effect consuming both energy on decomposition and energy by Boudouard reaction and as such Mintek mix had the highest energy and carbon consumption.

Untreated Comilog ore will give lower energy consumption compared to pretreated ore if added cold in the SAF. This is so because a higher proportion of exothermic reactions will be eliminated as a result of lowering the oxygen level in the ore. However, charging hot pretreated ore will result in lowering of the energy consumption in SAF by 250 – 300 kWh/ton alloy. Prereduced Comilog did not have any significant difference from preheated Comilog with regards to energy and carbon

consumption owing to insignificant change in oxygen level when Comilog is prereduced with solid carbon. The degree of prereduction in the Comilog series is in the same area within the uncertainties of the experiment. This gives the same carbon consumption and hence the overall CO_2 emissions.

Further work

In as much as a large amount of work has been considered in this thesis, there are still some aspects that are not clear, and some work remains to be done. Some recommendations for future work can be pointed out.

A part which remains to be investigated is the effect of pretreatment of carbonate ores i.e., UMK and Kudumane, on the carbon and energy consumption as well as CO_2 emissions. In laboratory scale experiments, it was found that decomposition of carbonate ores is temperature dependent and for UMK, approximately 50 % of the carbonates were decomposed in CO/CO_2 atmosphere at 800 °C. Further work is recommended to pretreat carbonate ores and conduct pilot trials with charge mixtures blended with pretreated UMK and Kudumane. Preheating in air is expected to decompose some carbonates in UMK since the carbonates are mostly in the form of dolomite which has been seen to decompose in 2 step temperatures i.e., at 700 °C and 900 °C. Hence, there exist potential to reduce the specific energy and carbon consumption in SAF when pretreated carbonated ores are used.

Laboratory scale experiments need to be conducted on Kudumane ore to establish the prereduction behavior of this ore. In addition, similar laboratory scale experiments should be conducted on sinter to help establishing the confounding effects of having sinter in charge blends when running pilot experiments.

The specific energy consumption, the specific carbon consumption, and the degree of prereduction for the pilot experiments were calculated. This was based on input (analyses and weights) to the pilot, the off-gas composition, slag, and alloy analyses, as well as an assumed fixed offgas temperature. Improvements should be done to get stable offgas temperature measurements as well as temperature profiles of the reaction zones. This will strengthen mass and energy calculations based on pilot experiments and it will be easier to correlate prereduction behavior of ores as well as slag reduction to prevailing temperature conditions.

In the broader subject on decarbonatization in the ferroalloy industry, investigations focusing on pretreatment with H_2 gas and substituting fossil carbon with biocarbon are highly recommended with particular focus on containment of H_2 gas in pretreatment unit as well as managing carbon balance in the furnace process.

References

[1] H. Aydin, E. Essadiqi, I. H. Jung, and S. Yue, "Development of 3rd generation AHSS with medium Mn content alloying compositions," *Mater. Sci. Eng. A*, vol. 564, pp. 501–508, 2013.

[2] S. E. Olsen, M. Tangstad, and T. Lindstad, *Production of Manganese Ferroalloys*. Trondheim: Tapir Academic Press, 2007.

[3] M. Eissa, H. El-Faramawy, A. Ahmed, S. Nabil, and H. Halfa, "Parameters Affecting the Production of High Carbon Ferromanganese in Closed Submerged Arc Furnace," *J. Miner. Mater. Charact. Eng.*, vol. 11, no. 01, pp. 1–20, 2012.

[4] K. Tang and S. Olsen, "The Effect of Alumina in Ferromanganese Slag," in *The Eleventh International Ferroalloys Congress: Innovations in Ferroalloy Industry*, 2007, pp. 335–343.

[5] P. C. Pistorius, "Reductant selection in ferro-alloy production : The case for the importance of dissolution in the metal," *J. South African Inst. Min. Metall.*, pp. 33–36, 2002.

[6] A. Roine, "HSC Chemistry Software," in *HSC Chemistry Software, v 10.0.4.3*, 2021.

[7] M. Tangstad and S. E. Olsen, "The ferromanganese process – Material and Energy balance," *Seventh Int. Ferroalloys Congr. INFACON VII*, no. June, pp. 621–630, 1995.

[8] O. Biørnstad, "Decrepitation of Comilog, Assmang and UMK manganese ores during prereduction.," *MSc Thesis. Dep. Mater. Sci. Eng. NTNU*, no. July, 2020.

[9] H. S. Reiersen, "Behavior of manganese ores during pre-reduction in small scale furnaces," *MSc Thesis. Dep. Mater. Sci. Eng. NTNU*, no. June, 2021.

[10] ASTM Standards A99-03, "Standard Specifications for Ferromanganese." ASTM International, pp. 1–3, 2009.

[11] J. H. Nam, M. A. Van Ende, and I. H. Jung, "Ferromanganese Production in a Submerged Arc Furnace: Thermodynamic and Energy Balance Analysis," *Jom*, 2022.

[12] K. N. Swamy, D. G. C. Robertson, P. Calvert, and D. Kozak, "Factors Affecting Carbon Consumption in the Production of High Carbon Ferromanganese," in *The 9th International Ferroalloys Congress*, 2001, pp. 293–301.

[13] A. Ahmed, H. Haifa, M. K. El-Fawakhry, H. El-Faramawy, and M. Eissa, "Parameters affecting energy consumption for producing high carbon ferromanganese in a closed submerged arc furnace," *J. Iron Steel Res. Int.*, vol. 21, no. 7, pp. 666–672, 2014.

[14] J. D. Steenkamp, "FactSage-Based Design Calculations for the Production of High-Carbon Ferromanganese on Pilot-Scale," in *11th International Symposium on High Temperature Metallurgical Processing*, 2020, pp. 757–771.

[15] T. Lindstad, M. Syvertsen, R. J. Ishak, H. B. Arntzen, and P. O. Grøntvedt, "the Influence of Alkalis on the Boudouard Reaction," *Tenth Int. Ferroalloys Congr.*, no. February, pp. 261–271, 2004.

[16] M. Tangstad, "The high carbon ferromangese process - Coke bed relations," The Norwegian Institute of Technology, Trondheim, 1996.

[17] R. Ishak and M. Tangstad, “Degree of prereduction without coke consumption in industrial furnaces,” in *The 11th International Ferroalloys Congress*, 2007, pp. 268–280.
[18] M. Kalenga, P. Xiaowei, and M. Tangstad, “Manganese Alloys Production : Impact of Chemical Compositions,” *Thirteen. Int. Ferroalloys Congr.*, vol. 1, no. 1, pp. 647–654, 2013.
[19] B. Sorensen, S. Gaal, M. Tangstad, E. Ringdalen, R. Kononov, and O. Ostrovski, “Properties of Manganese Ores and Their Change in the Process of Calcination,” in *12th International Ferroalloys Congress*, 2010, pp. 439–448.
[20] M. Tangstad, M. Sibony, S. Wasb, and R. Tronstad, “Kinetics of the Prereduction of Manganese Ores,” in *The Nineth International Ferroalloys Congress*, 2001, no. 5, pp. 202–207.
[21] M. Tangstad and S. E. Olsen, “Phase Relations in Ferromanganese Slags during Melting and Reduction,” *5th Int. Conf. Molten Slags, Fluxes Salts 97*, pp. 549–555, 1997.
[22] S. Gaal, K. Berg, G. Tranell, S. E. Olsen, and M. Tangstad, “An investigation into aspects of liquid phase reduction of maganese and silica containing slag,” *VII Int. Conf. Molten Slags Fluxes Salts*, pp. 651–658, 2004.
[23] M. Alam and T. Debroy, “The effects of CO and CO2 on the rate of Na2CO3 catalyzed boudouard reaction,” *Metall. Trans. B*, vol. 15, no. 2, pp. 400–403, 1984.
[24] L. Hongjie and D. G. C. Robertson, “Effect of Moisture, Combined Water and Volatile Elements on Fixed Carbon Required in a Ferromanganese Smelting Furnace,” in *55th Electric Furnace Conference*, 1997, pp. 269–279.
[25] M. Tangstad, K. Ichihara, and E. Ringdalen, “Pretreatment Unit in Ferromanganese Production,” in *The Fourteenth International Ferroalloys Congress: Energy efficiency and environmental friendliness are the future of the global Ferroalloy industry*, 2015, pp. 99–106.
[26] D. P. Crawford, P. L. J. Mayfield, A. D. Brent, and A. H. Olsen, “Direct production of ferromanganese from gemco sand concentrate and coal,” in *7th International Ferroalloys Congress*, 1995, no. June, pp. 239–248.
[27] J. Hamuyuni *et al.*, “Pretreatment of Manganese Ore for Improved Energy Efficiency and Smelting Furnace Stability,” in *16th International Ferroalloys Congress*, 2021, no. September, pp. 27–29.
[28] N. Julia, A. Hecquet, G. Nussbaum, S. Blancher, and A. Amalric, “Pre-Heating Manganese Ore in a Pilot-Scale Rotary Kiln,” in *16th International Ferroalloys Congress*, 2021, no. September, pp. 27–29.
[29] T. Kazdal, R. Haas-Wittmuess, S. Richter, S. Lang, C. Binder, and M. Reuter, “Process Design for the Pre-Treatment of Manganese Ores,” in *16th International Ferroalloys Congress*, 2021, no. September, pp. 27–29.
[30] E. Ringdalen, J. E. Gjøvik, T. A. Larssen, and M. Tangstad, “Pretreatment of Manganese Ores in Different Gas-Atmospheres- a Method to Reduce Energy Consumption and Co2 Emissions in Mn-Alloy Production,” in *16th International Ferroalloys Congress*, 2021, no. September, pp. 27–29.
[31] S. Sambo, L. Hockaday, and T. Seodigeng, “Experimental Study of Packed Bed Heat Transfer in a Shaft Kiln to Pre-Heat Manganese Ore with Hot Air,” in *16th International Ferroalloys Congress*, 2021, no. September, pp. 27–29.
[32] D. Teguri, K. Saito, and Y. Miyauchi, “Manganese ore pre-reduction using a

rotary kiln to manufacture super-low-phosphorus ferromanganese," in *15th international ferroalloys congress*, 2018, no. February, pp. 183–196.
[33] J. E. Post, "Manganese oxide minerals: Crystal structures and economic and environmental significance," *Proc. Natl. Acad. Sci. U. S. A.*, vol. 96, no. 7, pp. 3447–3454, 1999.
[34] J. E. Johnson, S. M. Webb, C. Ma, and W. W. Fischer, "Manganese mineralogy and diagenesis in the sedimentary rock record," *Geochim. Cosmochim. Acta*, vol. 173, pp. 210–231, 2016.
[35] J. Ostwald, "Mineralogy of the Groote Eylandt manganese oxides: A review," *Ore Geol. Rev.*, vol. 4, no. 1–2, pp. 3–45, 1988.
[36] J. Gutzmer and N. J. Beukes, "Mineral paragenesis of the Kalahari manganese field, South Africa," *Ore Geol. Rev.*, vol. 11, no. 6, pp. 405–428, 1996.
[37] F. Ossa Ossa, A. Hofmann, O. Vidal, J. D. Kramers, G. Belyanin, and B. Cavalazzi, "Unusual manganese enrichment in the Mesoarchean Mozaan Group, Pongola Supergroup, South Africa," *Precambrian Res.*, vol. 281, pp. 414–433, 2016.
[38] R. A. Featherstone, "Applications of Mamatwan Manganese Ore.," pp. 263–273, 1975.
[39] N. J. Beukes, E. P. W. Swindell, and H. Wabo, "Manganese deposits of Africa," *Episodes*, vol. 39, no. 2, pp. 285–317, 2016.
[40] A. S. E. Kleyenstuber, "The mineralogy of the manganese/bearing hotazel formation of the proterozoic transvaal sequence in Griqualand West, South Africa," *Trans. Geol. Soc. South Africa*, vol. 87, pp. 257–272, 1984.
[41] M. J. Peterson, J. R. Manuel, and S. Hapugoda, "Geometallurgical characterisation of Mn ores," *Appl. Earth Sci. Trans. Inst. Min. Metall.*, vol. 0, no. 0, pp. 1–21, 2020.
[42] N. Anacleto, O. Ostrovski, and S. Ganguly, "Reduction of manganese oxides by methane-containing gas," *ISIJ Int.*, vol. 44, no. 9, pp. 1480–1487, 2004.
[43] M. S. Fahim, H. El Faramawy, A. M. Ahmed, S. N. Ghali, and A. E. H. T. Kandil, "Characterization of Egyptian Manganese Ores for Production of High Carbon Ferromanganese," *J. Miner. Mater. Charact. Eng.*, vol. 01, no. 02, pp. 68–74, 2013.
[44] D. Chetty and J. Gutzmer, "Quantitative mineralogy to address energy consumption in smelting of ores from the Kalahari Manganese Field , South Africa," in *15th international ferroalloys congress*, 2018, no. February, pp. 25–28.
[45] P. P. Mishra, B. K. Mohapatra, and K. Mahanta, "Upgradation of Low-Grade Siliceous Manganese Ore from Bonai-Keonjhar Belt, Orissa, India," *J. Miner. Mater. Charact. Eng.*, vol. 08, no. 01, pp. 47–56, 2009.
[46] A. Cheraghi, H. Yoozbashizadeh, and J. Safarian, "Chemical, microstructural, and phase changes of manganese ores in calcination and pre-reduction by natural gas," in *15th international ferroalloys congress*, 2018, no. February, pp. 157–168.
[47] J. Ostwald, "Genesis and paragenesis of the tetravalent manganese oxides of the Australian continent," *Econ. Geol.*, vol. 87, no. 5, pp. 1237–1252, 1992.
[48] K. Turkova, D. Slizovskiy, and M. Tangstad, "CO reactivity and porosity of manganese materials," *ISIJ Int.*, vol. 54, no. 6, pp. 1204–1208, 2014.
[49] G. Pochart, L. Joncourt, N. Touchard, and C. Perdon, "Metallurgical benefit of

reactive high grade ore in manganese alloys manufacturing," *Sixth Int. Ferroalloys Congr. Innov. Ferroalloy Ind.*, pp. 217–230, 2007.
[50] G. L. Faria, J. A. S. Tenório, N. Jannotti, and F. G. D. S. Araújo, "A geometallurgical comparison between lump ore and pellets of manganese ore," *Int. J. Miner. Process.*, vol. 137, pp. 59–63, 2015.
[51] G. L. Faria, J. A. S. Tenório, N. Jannotti, and F. G. Da, "Disintegration on heating of a Brazilian manganese lump ore," *Int. J. Miner. Process.*, vol. 124, pp. 132–137, 2013.
[52] G. L. Faria, N. Jannotti, and F. G. D. S. Araújo, "Decrepitation behavior of manganese lump ores," *Int. J. Miner. Process.*, vol. 102–103, pp. 150–155, 2012.
[53] G. L. Faria, J. A. S. Tenório, N. Jannotti, and F. G. D. S. Araújo, "A geometallurgical comparison between lump ore and pellets of manganese ore," *Int. J. Miner. Process.*, vol. 137, pp. 59–63, 2015.
[54] G. L. Faria, J. A. S. Tenório, N. Jannotti, and F. G. Da, "Disintegration on heating of a Brazilian manganese lump ore," *Int. J. Miner. Process.*, vol. 124, pp. 132–137, 2013.
[55] F. N. Siddiquie, J. Alam, and M. Shaif, "Occurrence of Manganese Ore Deposits and Their Mineralogy in Vizianagaram-Visakhapatnam Manganese Ores Belt (Andhra Pradesh) India," *Int. J. Geosci.*, vol. 06, no. 06, pp. 549–566, 2015.
[56] T. Jawed and F. N. Siddiquie, "Mineragraphic Study of Manganese Ore Deposits of Kandri, Mansar, Beldongri and Satak Mines, Nagpur District (Maharashtra) Central India," *Int. J. Geosci.*, vol. 05, no. 07, pp. 710–727, 2014.
[57] M. Tangstad, P. Calvert, H. Brun, and A. G. Lindseth, "Use of Comilog Ore in Ferromanganese Production," in *The Tenth International Ferroalloys Congress: Transformation through Technology*, 2004, no. February, pp. 213–222.
[58] M. Eissa, S. Ghali, A. Ahmed, and H. El-Faramawy, "Optimum condition for smelting high carbon ferromanganese," *Ironmak. Steelmak.*, vol. 39, no. 6, pp. 419–430, 2012.
[59] P. Franke and R. Dieckmann, "Thermodynamics of iron manganese mixed oxides at high temperatures," *J. Phys. Chem. Solids*, vol. 51, no. 1, pp. 49–57, Jan. 1990.
[60] Y. B. Kang and I. H. Jung, "Thermodynamic modeling of oxide phases in the Fe–Mn–O system," *J. Phys. Chem. Solids*, vol. 98, pp. 237–246, Nov. 2016.
[61] L. Kjellqvist and M. Selleby, "Thermodynamic assessment of the Fe-Mn-O system," *J. Phase Equilibria Diffus.*, vol. 31, no. 2, pp. 113–134, 2010.
[62] Y. B. Kang and I. H. Jung, "Critical Evaluations and Thermodynamic Optimizations of the MnO-Mn 2 O 3 -SiO 2 and FeO-Fe 2 O 3 -MnO-Mn 2 O 3 -SiO 2 Systems," *Metall. Mater. Trans. B Process Metall. Mater. Process. Sci.*, vol. 48, no. 3, pp. 1721–1735, 2017.
[63] T. I. Schanche and M. Tangstad, "Isothermal Reduction of Nchwaning Manganese Ore in CO/CO2/H2 Atmospheres," in *16th International Ferroalloys Congress*, 2021, no. September, pp. 27–29.
[64] T. L. Schanche and M. Tangstad, "Prereduction of nchwaning ore in CO/CO2/H2 gas mixtures," *Minerals*, vol. 11, no. 10, 2021.
[65] T. A. Larssen, D. Senk, and M. Tangstad, "Reduction of Manganese Ores in CO-CO2 Atmospheres," *Metall. Mater. Trans. B*, vol. 52, no. 1, pp. 363–381, 2021.

[66] H. S. Reiersen, “Extent of prereduction of manganese ores in small scale experiments,” *Spec. Proj. Dep. Mater. Sceince Eng. NTNU*, no. December, pp. 1–84, 2020.
[67] Y. B. Gao, H. G. Kim, and H. Y. Sohn, “Kinetics of pre-reduction of manganese ore by CO,” *Trans. Institutions Min. Metall. Sect. C Miner. Process. Extr. Metall.*, vol. 121, no. 2, pp. 109–116, 2012.
[68] G. J. W. Kor, “The Thermal Decomposition of Mn2O3 and the Reduction of Mn3O4 by C and CO,” *Metall. Mater. Trans. B*, pp. 1–5, 1978.
[69] L. G. M. de Jesus and M. Tangstad, “CO reactivity of manganese lumps versus briquettes,” *ISIJ Int.*, vol. 60, no. 10, pp. 2129–2133, 2020.
[70] K. S. Abdel Halim, M. Bahgat, M. B. Morsi, and K. El-Barawy, “Pre-reduction of manganese ores for ferromanganese industry,” *Ironmak. Steelmak.*, vol. 38, no. 4, pp. 279–284, 2011.
[71] G. Akdogan and R. H. Eric, “Carbothermic reduction behaviour of wessel manganese ores,” *Miner. Eng.*, vol. 7, no. 5–6, pp. 633–645, 1994.
[72] M. Yastreboff, O. Ostrovski, and S. Ganguly, “Effect of gas composition on the carbothermic reduction of manganese oxide,” *ISIJ Int.*, vol. 43, no. 2, pp. 161–165, 2003.
[73] T. A. Larssen, D. Senk, and M. Tangstad, “Reaction Rate Analysis of Manganese Ore Prereduction in CO-CO2 Atmosphere,” *Metall. Mater. Trans. B*, vol. 52, no. 4, pp. 2087–2100, 2021.
[74] T. A. Larssen, M. Tangstad, and I. T. Kero, “Gaseous Reduction of Mn Ores in CO-CO2 Atmosphere,” *Miner. Met. Mater. Ser.*, pp. 1093–1101, 2018.
[75] T. A. Larssen, “Prereduction of Comilog- and Nchwaning-ore,” 2020.
[76] K. Berg, “Gaseous Reduction of Manganese Ores,” *Ph.D. Thesis*, 1998.
[77] K. L. Berg and S. E. Olsen, “Kinetics of manganese ore reduction by carbon monoxide,” *Metall. Mater. Trans. B Process Metall. Mater. Process. Sci.*, no. 31, pp. 477–490, 2000.
[78] R. Kononov, O. Ostrovski, and S. Ganguly, “Carbothermal solid state reduction of manganese ores: 1. Manganese ore characterisation,” *ISIJ Int.*, vol. 49, no. 8, pp. 1099–1106, 2009.
[79] H. E. Barner and C. L. Mantell, “Kinetics of hydrogen reduction of manganese dioxide,” *Ind. Eng. Chem. Process Des. Dev.*, vol. 7, no. 2, pp. 285–294, 1968.
[80] J. Wiley, *Chemical Reaction Engineering - Boston*. 1982.
[81] R. Kononov, O. Ostrovski, and S. Ganguly, “Carbothermal solid state reduction of manganese ores: 2. Non-isothermal and isothermal reduction in different gas atmospheres,” *ISIJ Int.*, vol. 49, no. 8, pp. 1107–1114, 2009.
[82] R. Kononov, “Carbothermal solid state reduction of manganese oxide and ores in different gas atmospheres,” The Univeristy of New South Wales, Sydney, 2008.
[83] J. Szekely, J. W. Evans, and H. . Sohn, *Gas-Solid Reactions*. New York: Academic Press, 1976.
[84] M. Tangstad, D. Leroy, and E. Ringdalen, “Ferromanganese – Pretreatment for Smelting: Behaviour of Agglomerates in Ferromanganese Production,” *Twelfth Int. Ferroalloys Congr. Sustain. Futur.*, no. October 2014, pp. 457–466, 2010.
[85] M. Visser, H. Smith, E. Ringdalen, and M. Tangstad, “Properties of Nchwaning and Gloria Ore in the Production of Mn Ferro-alloys,” in *The Thirteenth International Ferroalloys Congress: Efficient technologies in ferroalloy industry*,

2013, pp. 553–565.
[86] T. P. Colclough, “A study of the reactions of the basic open-hearth furnace,” *Trans. Faraday Soc.*, pp. 202–223, 1925.
[87] C. W. Bale *et al.*, “Reprint of: FactSage thermochemical software and databases, 2010–2016,” *Calphad Comput. Coupling Phase Diagrams Thermochem.*, vol. 55, pp. 1–19, 2016.
[88] K. Tang and S. Olsen, “The effect of alumina in ferromanganese slag,” *11th Int. Ferroalloys Congr. Ferro Alloy Ind.*, no. May, pp. 335–343, 2007.
[89] S. E. Olsen and T. Lindstad, “Ferromanganese production-process understanding,” in *60 th Electric Furnace Conference*, 2002.
[90] H. Ohta and H. Suito, “Activities of MnO in CaO-SiO2-Al2O3-MnO (<10 Pct)-FetO(<3 pct) slags saturated with liquid iron,” *Metall. Mater. Trans. B*, vol. 26, no. 2, pp. 295–303, 1995.
[91] B. K. D. P. Rao and D. D. R. Gaskell, “The thermodynamic properties of melts in the system MnO-SiO2,” *Metall. Trans. B*, vol. 12, no. 2, pp. 311–317, 1981.
[92] D. H. Woo, Y. B. Kang, and H. G. Lee, “Thermodynamic study of MnO-SiO2-Al2O3 slag system: Liquidus lines and activities of MnO at 1823 K,” *Metall. Mater. Trans. B Process Metall. Mater. Process. Sci.*, vol. 33, no. 6, pp. 915–920, 2002.
[93] T. Coetsee, J. Zietsman, and C. Pistorius, “Predicted effect of ore composition on slag formation in manganese ore reduction,” *Miner. Process. Extr. Metall.*, vol. 123, no. 3, pp. 141–147, 2014.
[94] M. Tangstad, S. Bublik, S. Haghdani, K. E. Einarsrud, and K. Tang, “Slag Properties in the Primary Production Process of Mn-Ferroalloys,” *Metall. Mater. Trans. B Process Metall. Mater. Process. Sci.*, vol. 52, no. 6, pp. 3688–3707, 2021.
[95] X. Li, K. Tang, and M. Tangstad, “Reduction and dissolution behaviour of manganese slag in the ferromanganese process,” *Minerals*, vol. 10, no. 2, pp. 1–16, 2020.
[96] O. I. Ostrovski and T. J. M. Webb, “Reduction of Siliceous Manganese Ore by Graphite.,” *ISIJ Int.*, vol. 35, no. 11, pp. 1331–1339, 1995.
[97] S. Gaal, E. Ringdalen, D. Vaganov, and M. Tangstad, “Melting Phenomenon of Manganese Bearing Ores,” in *8th International Conference on Molten Slags, Fluxes and Salts*, 2009, pp. 101–109.
[98] S. Gaal, D. Lou, S. Wasbø, B. Ravary, and M. Tangstad, “Melting phenomena in ferromanganese production,” in *11th International Ferroalloys Congress*, 2007, pp. 247–257.
[99] E. Ringdalen, S. Gaal, and O. Ostrovski, “Ore Properties in Melting and Reduction Reactions in Silicomanganese Production,” in *The Twelfth International Ferroalloys Congress*, 2010, pp. 249–262.
[100] E. Ringdalen, M. Tangstad, and S. Gaal, “Initial melting and reduction of ore and fluxes at the top of the coke bed during SiMn production,” in *Molten Slags, Fluxes and Salts*, 2009, pp. 1163–1172.
[101] E. Ringdalen, S. Gaal, M. Tangstad, and O. Ostrovski, “Ore melting and reduction in silicomanganese production,” *Metall. Mater. Trans. B Process Metall. Mater. Process. Sci.*, vol. 41, no. 6, pp. 1220–1229, 2010.
[102] E. Ringdalen, M. Tangstad, and T. Brynjulfsen, “Fundamentals, Theory: Melting behaviour of Mn-sources: Effect on furnace performance.,” in *14th International*

Ferroalloys Congress, 2015, no. 1, pp. 436–445.
[103] T. Brynjulfsen and M. Tangstad, "Manganese Alloys Production and Operation: Melting and Reduction of Manganese sinter and pellets," *13th Int. Ferroalloys Congr.*, pp. 137–147, 2013.
[104] B. Sorensen, S. Gaal, E. Ringdalen, M. Tangstad, R. Kononov, and O. Ostrovski, "Phase compositions of manganese ores and their change in the process of calcination," *Int. J. Miner. Process.*, vol. 94, no. 3–4, pp. 101–110, 2010.
[105] T. Coetsee, J. Nell, and P. C. Pistorius, "Phase Characterization of High Basicity Manganese Slags," *Metall. Mater. Trans. B Process Metall. Mater. Process. Sci.*, vol. 48, no. 3, pp. 1463–1485, 2017.
[106] T. Coetsee, "MnO reduction in high carbon ferromanganese production: practice and theory," *Miner. Process. Extr. Metall. Rev.*, vol. 39, no. 5, pp. 351–358, 2018.
[107] Y. E. Lee and L. Kolbeinsen, "Behavior of Slag in Ferromanganese and Silicomanganese Smelting Process," *Metall. Mater. Trans. B*, pp. 1–5, 2021.
[108] L. Holappa and Y. Xiao, "Slags in ferroalloys production - Review of present knowledge," *J. South African Inst. Min. Metall.*, vol. 104, no. 7, pp. 429–437, 2004.
[109] J. Safarian, L. Kolbeinsen, M. Tangstad, and G. Tranell, "Kinetics and mechanism of the simultaneous carbothermic reduction of FeO and MnO from high-carbon ferromanganese slag," *Metall. Mater. Trans. B*, vol. 40, no. 6, pp. 929–939, 2009.
[110] J. Safarian, Ø. Grong, L. Kolbeinsen, and S. E. Olsen, "A process model for the carbothermic reduction of MnO from high carbon ferromanganese slag - The model," *ISIJ Int.*, vol. 46, no. 8, pp. 1120–1129, 2006.
[111] X. Kuangdi, J. Guochang, D. Weizhong, G. Liping, G. Shuqiang, and Z. Baixiong, "The Kinetics of Reduction of MnO in Molten Slag with Carbon Saturated Liquid Iron," *ISIJ Int.*, vol. 33, no. 1, pp. 104–108, 1993.
[112] R. H. Eric and E. Burucu, "The mechanism and kinetics of the carbothermic reduction of mamatwan manganese ore fines," *Miner. Eng.*, vol. 5, no. 7, pp. 795–815, 1992.
[113] T. Coetsee, "The role of manganese ore reduction morphology development in setting reduction mechanisms," *Miner. Eng.*, vol. 137, no. March, pp. 217–231, 2019.
[114] T. Coetsee, C. Reinke, J. Nell, and P. C. Pistorius, "Reduction Mechanisms in Manganese Ore Reduction," *Metall. Mater. Trans. B Process Metall. Mater. Process. Sci.*, vol. 46, no. 6, pp. 2534–2552, 2015.
[115] O. Ostrovski, S. E. Olsen, M. Tangstad, and M. Yastreboff, "Kinetic modelling of MnO reduction from manganese ore," *Can. Metall. Q.*, vol. 41, no. 3, pp. 309–318, 2002.
[116] R. Kononov, O. Ostrovski, and S. Ganguly, "Carbothermal solid state reduction of manganese ores: 3. Phase development," *ISIJ Int.*, vol. 49, no. 8, pp. 1115–1122, 2009.
[117] T. Coetsee, "The Effect of Manganese Ore Iron Content on Carbothermic Reduction Rates at Low Temperatures," *16th Int. Ferroalloys Congr.*, vol. 1, no. September, pp. 27–29, 2021.
[118] M. Yastreboff, O. Ostrovski, and S. Ganguly, "Carbothermic Reduction of Manganese from Manganese Ore and Ferromanganese Slag," in *The Eighth*

International Ferroalloys Congress, 1998, pp. 263–270.
[119] M. Tangstad, E. Ringdalen, E. Manilla, and D. Davila, "Pilot Scale Production of Manganese Ferroalloys Using Heat-Treated Mn-Nodules," *JOM*, vol. 69, no. 2, pp. 358–364, 2017.
[120] T. Brynjulfsen, "Reduction of manganese ore agglomerates," Norwegian University of Science and Technology, 2013.
[121] H. Lagendijk, B. Xakalashe, T. Ligege, P. Ntikang, and K. Bisaka, "Comparing manganese ferroalloy smelting in pilot-scale ac and dc submerged-Arc furnaces," in *Proceedings of the 12th International Ferroalloys Congress: Sustainable Future*, 2010, pp. 497–507.
[122] J. Gundersen and H. Skretting, "Comparison of Electric Smelting on Pilot and Industrial Scale.," *J. South African Inst. Min. Metall.*, vol. 79, no. 1, pp. 18–22, 1978.
[123] P. A. Eidem, "Electrical Resistivity of Coke Beds," Norwegian University of Science and Technology, 2009.
[124] P. A. Eidem, M. Tangstad, and J. A. Bakken, "Electrical conditions of a coke bed in SiMn production," *Can. Metall. Q.*, vol. 48, no. 4, pp. 355–368, 2009.
[125] B. Monsen, M. Tangstad, I. Solheim, M. Syvertsen, R. Ishak, and H. Midtgaard, "Charcoal for manganese alloy production," in *11th International Ferroalloys Congress*, 2007, no. February, pp. 297–310.
[126] E. Ringdalen and M. Tangstad, "Study of SiMn Production in Pilot Scale Experiments - Comparing Carajas sinter and Assmang ore," in *13th International Ferroalloys Congress*, 2013, pp. 195–206.
[127] G. Tranell, M. Andersson, E. Ringdalen, O. Ostrovski, and J. J. Steinmo, "Reaction zones in a FeSi75 furnace-results from an industrial excavation," in *12th International Ferroalloys Congress*, 2010, pp. 709–715.
[128] J. Nell and C. Joubert, "Phase chemistry of digout samples from a ferrosilicon furnace," *13th Int. Ferroalloys Congr.*, no. June 2010, pp. 265–271, 2020.
[129] M. Ksiazek, M. Tangstad, and E. Ringdalen, "Five furnaces five different stories," in *Silicon for the Chemical and the Solar Industry XIII. Kristiansand, Norway*, 2016, pp. 33–42.
[130] N. A. Barcza, A. Koursaris, J. B. See, and W. A. Gericke, "The 'dig out' of a 75 MVA high carbon ferromanganese electric smelting furnace," in *37th Electric Furnace Proceedings*, 1979, no. I, pp. 19–34.
[131] E. A. Nordbø, S. J. Slåtsve Øvrelid, and E. Gridset, "Excavation and Analysis of a 31 MW SiMn-furnace at Eramet Kvinesdal," *SSRN Electron. J.*, no. September, pp. 27–29, 2021.
[132] M. Tangstad, J. E. Olsen, E. Ringdalen, M. Ksiazek, Q. Reynolds, and J. Steenkamp, "Conceptual Tapping Model of Mn-Ferroalloy Furnaces," *Jom*, vol. 74, no. 11, pp. 3962–3970, 2022.
[133] "SINTEF NORLAB," 2019. [Online]. Available: www.sintefnorlab.no. [Accessed: 30-May-2019].
[134] D. Ngoy, D. Sukhomlinov, and M. Tangstad, "Pre-reduction Behaviour of Manganese Ores in H2 and CO Containing Gases," *ISIJ Int.*, vol. 60, no. 11, pp. 2325–2331, 2020.
[135] M. Wojdyr, "Fityk: A General Purpose Peak Fitting Program," *J. Appl. Crystallogr.*, vol. 43, no. 5, pp. 1126–8, 2010.
[136] P. P. Kim, *Reduction Rates of SiMn Slags from Various Raw Materials*, no.

September. 2018.
[137] ASTM E465: 11, "Standard Test Methods for Determination of Manganese (IV) in Manganese Ores by Redox Titrimetry." ASTM International, 2017.
[138] S. Bao, E. Ringdalen, P. Ø. Hanssen, N. Julia, and E. Dabakk, "Evaluation of the analytical technique for determinationof x in MnOx by titration method for Mn ore," *Int. J. Mater. Res.*
[139] T. L. Schanche, "Pretreatment of manganese ores in $CO/CO_2/H_2$ atmospheres," Trondheim, 2022.
[140] K. Tang and S. E. Olsen, "Computer simulation of equilibrium relations in manganese ferroalloy production," *Metall. Mater. Trans. B Process Metall. Mater. Process. Sci.*, vol. 37, no. 4, pp. 599–606, 2006.
[141] V. Oslø, Tangstad, M., and S. E. Olsen, "Reduction kinetics of MnO-saturated slags," in *8th International Ferroalloys Congress*, 1998, pp. 279–283.
[142] M. Tangstad, "Ph.D. Thesis: The high carbon ferromanganese process - Cokebed relations," Ph.D. Thesis, The Norwegian Institute of Technology, Trondheim, Norway, 1996.
[143] D. M. Ngoy, M. Tangstad, and M. Kalenga, "Reduction rate of MnO from two different manganese ores producing ferromanganese," *Proc. 15th Int. Ferro-Alloys Congr. INFACON 2018*, no. February, pp. 207–218, 2018.
[144] M. Ksiazek, "The thermophysical properties of raw materials for ferromanganese production," PhD thesis: NTNU, Trondheim, 2012.
[145] M. Tangstad, "Summary of prereduction experiments in the Disvadri furnaces with industrial materials in Gasferrosil v.2," Trondheim, 2017.
[146] D. Sukhomlinov and M. Tangstad, "Non-isothermal pre-reduction of carbonated manganese ore by carbon monoxide," *Metals (Basel).*, vol. Submitted, pp. 1–15, 2021.
[147] J. Davies, M. Tangstad, T. L. Schanche, and S. . du Preez, "Prereduction of United Manganese of Kalahari ore in CO/CO2, H2/H2O and H2 atmospheres," *Metall. Mater. Trans. B*, vol. Under revi, 2022.
[148] S. Gunasekaran and G. Anbalagan, "Thermal decomposition of natural dolomite," *Bull. Mater. Sci.*, vol. 30, no. 4, pp. 339–344, 2007.
[149] A. I. Rat'Ko, A. I. Ivanets, A. I. Kulak, E. A. Morozov, and I. O. Sakhar, "Thermal decomposition of natural dolomite," *Inorg. Mater.*, vol. 47, no. 12, pp. 1372–1377, 2011.
[150] T. Adamo, "Thermal Conductivity Detector (TCD)," *TRACES Cent.*, vol. 2, no. October, pp. 1–2, 2020.
[151] M. Sparta, V. K. Risinggård, K. E. Einarsrud, and S. A. Halvorsen, "An Overall Furnace Model for the Silicomanganese Process," *Jom*, vol. 73, no. 9, pp. 2672–2681, 2021.

Appendix A: TGA data smoothing in Excel

Raw data mass loss curves from the reduction stage 1200 to 1550 °C were subjected to Gaussian smoothing in Fityk. Initially, the raw data is plotted in Fityk and the Gaussian curves which describe the general outline of the curve are selected in the programm. The Fityk programm utilses the Gaussian equations to calculate the equation which best fits the raw data and generate the equation which can be used to calculate smoothed data from raw data. Figure A1, shows raw TGA reduction curve superimposed with smoothed Fityk curve.

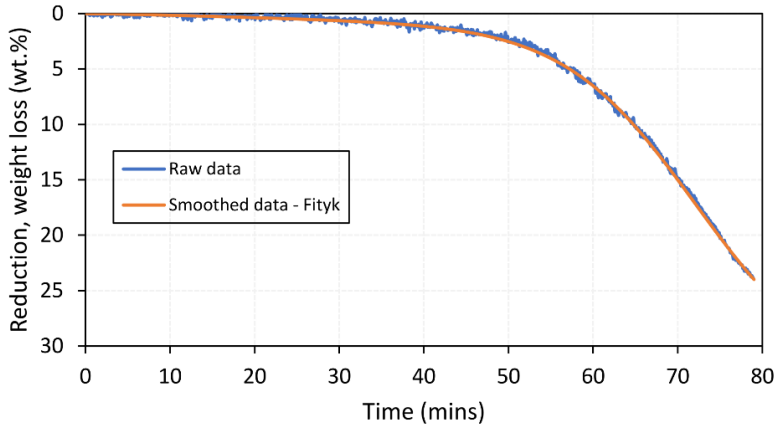

Figure A.1: TGA reduction curve superimposed with smoothed Fityk curve

Appendix B: Calculation of slag composition of reduced charges

The initial rapid heating stage up to 1200 °C represents the prereduction of manganese oxides and iron oxides (MnO_2, Mn_2O_3, Mn_3O_4 to MnO and Fe_2O_3, Fe_3O_4, FeO to Fe, evaporation of bound water and decomposition of carbonates) and the calculated composition of a completely prereduced charge i.e., primary slag, are shown Table 3.5. The composition of the final end slag is calculated based on the TGA data from the reduction stage (i.e., 1200 to 1550 °C) and the chemical compositions of the primary slag. It was assumed that the amount of unreducible oxides (i.e. SiO_2, Al_2O_3, MgO and CaO were constant throughout the entire experiment. The weight loss is attributed to CO and weight loss is mainly from reduction of MnO and C consumed. Hence, the weight of the remaining MnO in slag is the difference from the initial MnO in primary slag. An example of the calculated slag composition using the TGA data in the reduction stage of 'Com 1400 – 30 and Com 1550-30' experiment is shown in Table B1.

Table B.1: Calculated slag composition after reduction of Comilog at 1400 and 1550 °C.

Experiment	Unit	MnO	SiO_2	CaO	MgO	Al_2O_3	Total
Com 1400-30	(g)	6.52	0.43	0.01	0.01	0.70	7.67
	(wt.%)	84.9	5.62	0.16	0.11	9.18	100
Com 1400-30	(g)	0.71	0.43	0.01	0.01	0.70	1.87
	(wt.%)	38.0	23.1	0.68	0.43	37.8	100

Appendix C – Chemical composition of phases measured by EPMA

The detailed EPMA analyses of the slag phases in the Comilog, Nchwaning and UMK charges are described in this section. Each phase was subjected to three-point analysis and the average composition of each phase are presented.

Table C.1: Phase composition for Comilog slags in 'Q1' series analyzed by EPMA.

Phase identity	Experiment	MnO	SiO_2	MgO	K_2O	Al_2O_3	CaO	FeO	Total
Monoxide/ dendritic	Com 1400-0	97.5	0.09	0.15	0.01	0.32	0.01	0.98	99.1
	Com 1400-30	99.1	0.03	0.09	0.00	0.26	0.05	0.38	99.9
	Com 1500-0	98.5	0.12	0.30	0.03	0.47	0.03	0.22	99.8
	Com 1500-30	98.0	0.09	0.37	0.00	0.42	0.03	0.29	99.2
	Com 1550-0	95.5	0.37	0.11	0.02	0.43	0.11	0.26	96.8
	Com 1550-30	93.4	1.04	0.13	1.79	0.60	0.09	0.21	97.2
Light grey	Com 1400-0	62.2	28.0	0.18	0.03	1.09	0.19	1.20	92.9
	Com 1400-30	63.2	27.9	0.19	0.03	1.99	0.59	0.22	94.1
	Com 1500-0	62.1	28.9	0.16	0.05	1.22	0.51	0.20	93.5
	Com 1500-30	62.0	27.8	0.18	0.07	1.44	0.33	0.19	92.0
	Com 1550-0	61.4	29.1	0.24	0.08	1.05	0.79	0.17	92.8
	Com 1550-30	62.3	29.6	0.32	0.04	0.90	0.69	0.18	94.0
Dark grey	Com 1400-0	36.8	0.10	0.46	0.05	55.24	0.02	0.75	93.5
	Com 1400-30	38.1	0.28	0.23	0.02	55.50	0.01	0.23	94.4
	Com 1500-0	36.9	0.17	0.71	0.04	55.03	0.02	0.11	93.4
	Com 1500-30	36.7	0.24	0.76	0.01	55.80	0.00	0.11	93.6
	Com 1550-0	35.3	0.17	1.48	0.01	54.26	0.03	0.10	91.4
	Com 1550-30	35.6	0.08	1.49	0.02	54.72	0.01	0.10	92.0

Table C.2: Phase composition for Nchwaning slags in 'Q2' series analyzed by EPMA

Phase identity	Experiment	MnO	SiO_2	MgO	K_2O	Al_2O_3	CaO	FeO	Total
Monoxide/ dendritic	Nch 1400-0	96.9	0.15	1.34	0.02	0.08	0.77	0.76	100
	Nch 1400-30	96.2	0.08	1.63	0.03	0.15	1.06	0.60	99.8
	Nch 1500-0	93.3	0.14	2.06	0.00	0.07	3.12	0.79	99.5
	Nch 1500-30	95.3	0.08	1.35	0.00	0.06	1.43	0.60	98.8
	Nch 1550-0	87.7	0.24	5.73	0.01	0.11	4.93	0.52	99.2
	Nch 1550-30	85.9	0.59	9.61	0.02	0.19	2.50	0.23	99.1
Mediumt grey	Nch 1400-0	42.3	30.9	1.26	0.01	0.07	19.84	0.28	94.6
	Nch 1400-30	37.4	31.9	1.85	0.00	0.21	24.54	0.51	96.5
	Nch 1500-0	28.1	31.5	1.70	0.02	0.49	33.37	0.46	95.6
	Nch 1500-30	34.5	30.6	1.32	0.01	0.13	27.32	0.50	94.4
	Nch 1550-0	26.0	25.9	1.97	0.03	10.11	22.68	0.60	87.3
	Nch 1550-30	25.0	31.4	3.96	0.00	0.70	33.58	0.12	94.7

Table C.3: Phase composition for UMK slags in 'Q3' series analyzed by EPMA

Phase identity	Experiment	MnO	SiO_2	MgO	K_2O	Al_2O_3	CaO	FeO	Total
Monoxide/ dendritic	UMK 1400-0	90.5	0.29	5.99	0.00	0.11	2.12	0.67	99.7
	UMK 1400-30	82.2	0.24	14.4	0.01	0.06	2.23	0.74	99.9
	UMK 1500-0	89.2	0.20	5.38	0.02	0.14	3.74	0.73	99.4
	UMK 1500-30	85.3	0.26	9.93	0.00	0.22	4.00	0.66	100
	UMK 1550-0	90.0	0.85	5.47	0.00	0.11	3.10	0.27	99.8
	UMK 1550-30	77.3	0.14	19.0	0.04	0.18	3.80	0.63	101
Medium grey	UMK 1400-0	26.4	32.5	3.67	0.03	0.13	33.44	0.40	96.6
	UMK 1400-30	25.0	32.5	4.87	0.00	0.03	33.84	0.44	94.1
	UMK 1500-0	23.4	25.6	1.36	0.09	15.78	24.69	0.82	93.5
	UMK 1500-30	21.0	21.4	1.70	0.04	22.56	26.36	0.48	93.5
	UMK 1550-0	26.3	31.8	2.37	0.01	0.46	34.55	0.11	95.6
	UMK 1550-30	27.7	20.1	1.48	0.06	17.15	26.02	0.14	92.6

Appendix D – Chemical composition of samples from prereduction zone

Samples were excavated from the prereduction of the pilot furnace experiments through digging out procedure presented in section 4.2.5.1 .The chemical composition of prereduced samples from all the pilot experiments and their oxidation levels (i.e., x in MnO_x) are presented in this section.

Table D1: Chemical analysis of ore samples from untreated Comilog experiment

Sample	Depth (cm)	Mn, tot	Fe, tot	MnO_2	Al_2O_3	SiO_2	CaO	MgO	K_2O	CO_2	LOI	**MnO_x**
AO	0	54.6	3.64	78.7	3.57	2.20	0.06	0.15	0.70	0.15	10.5	**1.91**
A1	10	31.1	17.2	24.6	8.56	15.3	0.61	0.50	1.51	4.70	5.99	**1.50**
A2	20	54.6	4.52	35.0	6.62	4.69	0.10	0.25	0.73	5.20	4.92	**1.41**
A3	30	62.5	1.33	24.7	7.00	3.24	0.10	0.21	1.49	0.18	-0.64	**1.25**
A4	40	49.0	11.2	1.80	7.08	3.60	1.53	0.17	1.09	11.0	1.00	**1.02**
A5	50	66.5	2.01	10.8	3.93	2.65	0.07	0.18	1.67	0.48	-3.74	**1.10**
A6	60	60.4	1.89	0.05	6.25	5.85	0.14	0.35	3.42	6.40	-3.49	**1.00**
BO	0	56.1	2.79	79.1	3.45	2.45	0.05	0.09	0.89	0.15	9.21	**1.89**
B1	10	61.2	1.19	63.6	4.16	1.90	0.06	0.17	0.77	0.07	5.57	**1.66**
B2	20	65.4	1.35	24.6	4.96	2.03	0.09	0.29	1.02	0.26	-1.03	**1.24**
B3	30	67.0	1.25	20.4	4.64	2.87	0.09	0.18	0.76	0.15	-3.27	**1.19**
B4	40	58.1	2.52	17.9	10.4	4.03	0.07	0.37	1.79	0.15	-1.46	**1.19**
B5	50	70.2	1.35	5.34	3.51	2.83	0.07	0.14	0.56	0.11	-6.02	**1.05**
B6	60	62.7	3.18	0.05	6.84	5.89	0.55	0.36	1.49	0.62	-6.82	**1.00**
C0	0	48.0	8.90	69.8	4.27	2.49	0.05	0.14	0.39	0.11	10.6	**1.92**
C1	10	54.3	1.60	81.1	5.56	2.60	0.06	0.15	1.19	0.07	10.65	**1.94**
C2	20	52.1	4.91	69.4	6.64	2.71	0.05	0.25	0.71	0.11	8.08	**1.84**
C3	30	60.4	1.62	53.6	5.00	3.25	0.04	0.17	0.82	0.07	2.99	**1.56**
C4	40	61.8	1.02	40.4	3.93	3.58	0.07	0.10	0.80	6.60	4.40	**1.41**
C5	50	63.3	1.51	30.9	5.06	2.68	0.07	0.24	1.47	0.48	0.38	**1.31**
C6	60	53.0	8.01	27.1	6.90	5.10	0.06	0.24	1.04	0.15	-0.23	**1.32**
D0	0	52.6	4.92	70.6	5.10	2.55	0.05	0.21	1.27	0.07	8.47	**1.85**
D1	10	53.3	4.42	61.3	6.22	2.33	0.11	0.37	1.18	0.07	6.74	**1.73**
D2	20	58.2	4.09	34.9	7.04	3.07	0.04	0.16	1.13	0.07	0.69	**1.38**
D3	30	60.1	3.11	27.7	5.28	5.80	0.06	0.21	1.33	0.07	-0.79	**1.29**
B4	40	67.0	2.37	6.49	5.54	2.63	0.09	0.35	0.59	0.04	-5.55	**1.06**
D5	50	67.6	1.81	4.05	5.23	2.78	0.21	0.19	0.98	0.48	-6.15	**1.04**
D6	60	65.5	2.34	0.37	6.62	3.34	0.16	0.32	1.19	0.07	-5.48	**1.00**

Table D2: Chemical analysis of ore samples from preheated Comilog experiment

Sample	Depth (cm)	Mn, tot	Fe, tot	MnO_2	Al_2O_3	SiO_2	CaO	MgO	K_2O	CO_2	LOI	**MnO_x**
AO	0	56.1	4.09	46.2	6.51	3.31	0.08	0.12	1.41	0.66	3.17	**1.52**
A1	10	59.0	2.02	43.2	6.45	4.49	0.08	0.27	0.97	0.33	2.63	**1.46**
A2	20	50.3	8.59	29.7	7.33	5.40	0.07	0.17	1.44	0.48	2.08	**1.37**
A3	30	54.1	4.21	32.2	7.94	6.48	0.32	0.35	1.22	0.48	2.09	**1.38**
A4	40	56.8	3.08	32.8	7.76	3.88	0.59	0.36	1.54	0.92	2.03	**1.36**
A5	50	59.2	1.51	32.3	7.88	4.58	0.06	0.28	1.28	1.10	1.48	**1.34**
A6	60	53.9	4.53	11.5	5.80	4.84	3.26	0.74	2.56	5.50	-0.37	**1.14**
BO	0	55.2	4.61	47.2	7.05	3.96	0.27	0.27	0.93	0.22	2.58	**1.54**
B1	10	60.4	2.87	18.5	6.53	5.21	0.72	0.25	1.15	0.59	-1.39	**1.19**
B2	20	55.9	3.95	26.5	8.44	4.94	0.50	0.30	1.36	0.62	0.52	**1.30**
B3	30	59.7	6.15	4.04	7.00	3.30	0.12	0.14	1.07	0.15	-4.59	**1.04**
B4	40	61.9	4.13	0.31	3.27	3.67	4.53	2.44	0.35	0.18	-5.71	**1.00**
B5	50	63.1	3.75	5.28	5.95	3.52	1.06	0.37	0.95	1.50	-4.76	**1.05**
B6	60	55.7	2.84	6.11	6.18	4.19	8.50	0.53	1.24	2.30	-3.05	**1.07**
C0	0	61.4	1.94	52.1	3.80	2.10	0.36	0.13	1.04	0.22	4.14	**1.54**
C1	10	59.7	2.09	43.7	4.22	3.21	2.19	0.72	1.01	0.40	2.38	**1.46**
C2	20	62.5	1.19	44.3	4.69	2.63	0.07	0.22	1.06	0.37	3.19	**1.45**
C3	30	56.7	2.72	36.5	8.17	3.96	0.12	0.24	1.35	0.33	3.00	**1.41**
C4	40	46.4	6.58	29.6	8.03	9.32	3.73	1.49	1.04	0.26	1.34	**1.40**
C5	50	52.1	6.05	26.6	7.29	6.30	1.73	0.46	1.11	0.37	0.90	**1.32**
C6	60	53.9	8.60	23.0	4.98	5.54	0.81	0.24	0.89	0.22	-1.69	**1.27**
D0	0	56.4	2.36	42.1	9.88	3.84	0.17	0.30	1.12	0.22	1.74	**1.47**
D1	10	61.6	2.38	23.4	6.64	3.59	0.09	0.16	1.18	0.40	-0.69	**1.24**
D2	20	58.7	3.20	21.7	6.87	5.98	0.09	0.13	1.42	0.15	-0.82	**1.23**
D3	30	65.9	1.87	20.3	6.19	2.91	0.08	0.18	0.72	0.40	-1.03	**1.19**
B4	40	65.9	1.87	13.6	6.19	2.91	0.08	0.18	0.72	0.04	-3.31	**1.13**
D5	50	65.3	1.68	6.06	6.32	4.74	0.27	0.30	1.15	0.15	-5.05	**1.06**
D6	60	60.1	2.70	0.05	6.43	6.83	0.82	0.23	1.30	11.0	-2.97	**1.00**

Table D3: Chemical analysis of ore samples from prereduced Comilog experiment

Sample	Depth (cm)	Mn, tot	Fe, tot	MnO_2	Al_2O_3	SiO_2	CaO	MgO	K_2O	CO_2	LOI	**MnO_x**
AO	0	55.9	6.12	40.2	5.57	2.53	0.08	0.03	1.07	0.21	2.26	**1.45**
A1	10	59.6	2.26	40.0	6.82	3.16	0.07	0.03	1.16	0.77	1.66	**1.42**
A2	20	62.2	1.63	38.4	5.74	2.61	0.06	0.03	1.02	0.27	1.24	**1.39**
A3	30	58.7	3.12	24.8	7.01	5.43	0.08	0.06	1.16	0.22	-0.2	**1.27**
A4	40	58.2	1.50	27.7	8.22	6.45	0.09	0.13	1.30	0.21	0.51	**1.30**
A5	50	61.6	1.69	28.3	6.72	2.95	0.07	0.03	1.17	2.2	0.82	**1.29**
A6	60	50.3	3.59	17.0	10.3	10.2	0.11	0.20	1.60	6.3	1.19	**1.21**
BO	0	57.7	1.93	39.8	4.98	2.64	0.07	0.03	0.81	18	7.98	**1.44**
B1	10	53.7	6.31	25.4	7.53	4.95	0.06	0.12	1.37	1.3	0.78	**1.30**
B2	20	58.2	3.95	27.9	6.58	4.22	0.05	0.10	1.29	3.1	-0.4	**1.30**
B3	30	63.2	2.03	17.7	6.81	3.12	0.08	0.03	0.99	2.6	-1.9	**1.18**
B4	40	61.9	2.65	5.35	7.46	5.35	0.18	0.06	1.13	0.17	-4.5	**1.05**
B5	50	61.7	3.43	6.95	5.88	4.28	0.44	0.04	1.04	5.0	-2.6	**1.07**
B6	60	60.7	3.83	0.05	6.78	5.46	0.82	0.10	0.82	12	-4.8	**1.00**
C0	0	59.1	1.99	41.0	5.22	5.89	0.05	0.16	1.12	0.37	2.25	**1.44**
C1	10	60.7	2.46	46.3	4.15	3.70	0.35	0.03	0.86	0.17	2.65	**1.48**
C2	20	56.2	2.39	41.9	7.88	4.25	0.06	0.04	1.82	0.20	2.95	**1.47**
C3	30	53.8	5.81	39.5	6.68	4.37	0.07	0.13	1.33	1.3	2.77	**1.46**
C4	40	60.7	3.31	36.3	4.08	3.35	0.07	0.03	1.03	1.5	1.37	**1.38**
C5	50	23.1	38.8	11.1	2.83	8.61	2.76	0.13	0.54	0.95	0.75	**1.30**
C6	60	63.8	1.54	31.7	2.53	3.10	0.35	0.03	1.62	5.0	1.64	**1.31**
D0	0	62.7	1.18	49.7	3.57	2.27	0.08	0.03	1.38	0.13	3.29	**1.50**

D1	10	43.3	9.71	25.6	6.83	16.5	0.06	0.00	1.03	0.13	1.50	**1.37**
D2	20	50.8	9.29	24.4	4.58	6.10	1.86	0.18	1.12	0.21	0.16	**1.30**
D3	30	61.8	4.55	17.9	4.71	3.07	0.12	0.03	0.82	0.15	-2.1	**1.18**
B4	40	63.0	2.38	7.40	5.53	5.28	0.11	0.04	1.69	0.36	-4.0	**1.07**
D5	50	67.2	1.99	2.27	4.93	3.35	0.11	0.03	0.99	0.095	-5.9	**1.02**
D6	60	62.8	5.17	0.05	3.12	4.97	0.77	0.04	1.66	2.9	-6.8	**1.00**

Table D4: Chemical analysis of ore samples from untreated Nchwaning experiment

Sample	Depth (cm)	Mn, tot	Fe, tot	MnO_2	Al_2O_3	SiO_2	CaO	MgO	K_2O	CO_2	LOI	**MnO_x**
AO	0	48.4	5.65	34.6	0.41	4.56	7.79	1.99	0.03	6.1	6.50	**1.45**
A1	10	48.2	6.57	34.9	0.41	5.04	8.38	1.51	0.03	5.6	5.50	**1.46**
A2	20	46.0	10.0	37.5	0.36	2.62	7.50	0.77	0.06	4.4	5.10	**1.51**
A3	30	46.3	7.77	34.4	0.50	5.76	8.07	2.00	0.03	4.8	5.16	**1.47**
A4	40	48.9	7.89	33.9	0.65	6.23	7.89	1.38	0.03	2.2	1.66	**1.44**
A5	50	51.6	9.87	31.4	0.39	2.96	5.74	0.74	0.03	0.88	-0.2	**1.38**
BO	0	50.9	4.45	35.9	0.39	2.30	9.59	1.69	0.03	5.6	5.45	**1.45**
B1	10	48.6	7.56	39.6	0.63	3.02	6.50	1.54	0.05	4.8	4.84	**1.52**
B2	20	41.0	10.3	28.0	0.85	6.99	8.43	2.00	0.03	8.3	6.92	**1.43**
B3	30	43.0	10.9	27.7	1.28	5.10	8.68	2.75	0.05	6.1	4.32	**1.41**
B4	40	46.4	11.2	21.4	0.64	2.65	10.4	1.25	0.03	2.2	-0.2	**1.29**
B5	50	51.4	10.1	10.9	1.03	4.81	7.18	0.81	0.08	0.33	-3.5	**1.13**
C0	0	49.8	6.42	37.6	0.49	3.23	6.67	1.49	0.03	10	7.93	**1.48**
C1	10	42.5	11.3	34.9	0.40	7.14	7.04	1.04	0.03	4.1	4.80	**1.52**
C2	20	42.8	12.8	31.3	0.47	4.72	6.34	2.18	0.03	5.2	5.40	**1.46**
C3	30	47.0	7.87	34.6	0.24	4.77	7.40	1.72	0.03	6.0	5.13	**1.46**
C4	40	45.54	10.72	37.84	0.46	4.32	7.69	1.59	0.06	2.0	2.64	**1.53**
C5	50	42.46	13.44	31.04	0.31	5.43	9.92	2.02	0.03	0.59	1.21	**1.46**
D0	0	52.38	6.97	39.92	0.36	2.08	7.48	0.51	0.03	1.4	2.23	**1.48**
D1	10	38.14	9.14	29.85	0.43	5.19	11.81	3.16	0.03	7.9	9.21	**1.49**
D2	20	44.71	11.08	35.65	0.52	3.54	7.57	1.14	0.03	4.4	5.65	**1.50**
D3	30	42.26	8.66	27.59	0.52	14.42	6.36	1.20	0.03	3.2	3.19	**1.41**
B4	40	53.3	6.34	31.92	0.44	2.69	8.17	1.93	0.03	2.3	0.86	**1.38**
D5	50	49.95	10.06	11.27	0.94	5.70	7.51	2.70	0.07	0.62	-3.3	**1.14**
D6	60	57.46	6.38	0.9	2.04	7.45	4.82	1.51	0.24	0.29	-6.2	**1.01**

Table D5: Chemical analysis of ore samples from preheated Nchwaning experiment

Sample	Depth (cm)	Mn, tot	Fe, tot	MnO_2	Al_2O_3	SiO_2	CaO	MgO	K_2O	CO_2	LOI	**MnO_x**
AO	0	46.3	8.93	36.8	1.39	5.38	5.89	1.37	0.15	5.00	3.72	**1.50**
A1	10	45.4	10.8	33.9	0.47	4.88	6.36	1.22	0.03	3.80	3.05	**1.47**
A2	20	51.3	7.02	44.7	0.35	1.93	7.02	0.38	0.04	0.99	2.49	**1.55**
A3	30	48.8	9.26	40.1	0.45	4.39	7.24	1.23	0.04	2.00	2.89	**1.52**
A4	40	44.7	16.0	16.1	0.51	3.02	6.06	1.38	0.03	1.60	0.45	**1.23**
A5	50	48.2	10.8	16.8	0.42	5.48	7.08	1.44	0.04	3.20	1.49	**1.22**
A6	60	54.5	7.32	0.05	0.48	6.67	7.65	1.88	0.09	1.70	-4.0	**1.00**
BO	0	37.3	14.9	27.1	0.38	5.47	9.29	3.42	0.11	6.60	6.62	**1.46**
B1	10	46.6	11.0	31.9	0.52	4.99	6.98	1.48	0.03	3.40	3.67	**1.43**
B2	20	53.9	6.68	20.1	0.31	6.26	6.66	0.70	0.03	4.40	0.73	**1.23**
B3	30	51.3	8.43	2.50	0.40	4.53	9.69	1.99	0.04	2.80	-2.3	**1.03**
B4	40	54.6	10.2	0.05	0.31	3.99	6.37	0.15	0.03	0.62	-5.5	**1.00**
B5	50	54.6	8.68	0.05	1.00	4.34	6.68	2.12	0.04	0.76	-5.6	**1.00**
B6	60	52.4	12.0	0.05	0.39	6.08	5.11	0.48	0.17	0.19	-7.8	**1.00**
C0	0	47.1	10.8	33.7	0.29	4.54	7.56	1.09	0.05	3.20	3.44	**1.45**

C1	10	50.9	9.17	36.2	0.36	3.90	5.71	0.46	0.03	1.70	2.84	**1.45**
C2	20	39.4	10.6	27.6	0.61	4.97	11.13	3.93	0.03	6.00	7.03	**1.44**
C3	30	42.7	10.9	32.8	0.59	5.56	8.39	3.02	0.03	3.40	4.97	**1.49**
C4	40	46.3	11.4	38.2	0.41	3.63	7.40	1.84	0.11	1.50	2.29	**1.52**
C5	50	42.4	9.83	28.6	0.50	5.90	8.14	2.68	0.13	15.0	7.81	**1.43**
C6	60	43.6	12.3	18.3	0.41	5.70	9.25	2.20	0.05	2.50	0.87	**1.26**
D0	0	45.8	14.2	35.5	0.42	3.54	4.52	1.46	0.08	1.50	1.77	**1.49**
D1	10	45.5	12.5	35.7	0.81	3.24	6.63	1.49	0.09	1.40	2.67	**1.50**
D2	20	50.7	8.33	9.37	0.65	4.68	7.89	1.75	0.06	3.50	-0.6	**1.12**
D3	30	50.2	10.7	0.05	0.51	4.51	7.51	2.42	0.07	2.50	-3.3	**1.00**
B4	40	49.0	9.57	2.78	1.77	7.82	7.16	2.06	0.20	2.60	-1.6	**1.04**
D5	50	46.9	15.0	0.05	0.54	5.41	8.28	2.66	0.07	0.93	-5.9	**1.00**
D6	60	58.5	7.79	0.05	0.62	4.83	4.45	1.06	0.06	0.39	-6.5	**1.00**

Table D6: Chemical analysis of ore samples from prereduced Nchwaning experiment

Sample	Depth (cm)	Mn, tot	Fe, tot	MnO_2	Al_2O_3	SiO_2	CaO	MgO	K_2O	CO_2	LOI	**MnO_x**
AO	0	37.3	13.3	21.5	0.70	6.54	11.0	1.31	0.03	6.50	5.58	1.36
A1	10	50.0	7.97	41.1	0.38	3.39	6.49	0.69	0.04	2.60	3.12	1.52
A2	20	31.4	27.8	17.4	0.49	5.26	6.42	1.60	0.03	2.60	1.98	1.35
A3	30	52.8	6.88	17.4	0.27	6.01	6.39	0.36	0.08	3.30	1.70	1.21
A4	40	47.9	11.8	28.8	0.45	6.68	5.20	0.44	0.03	2.60	1.61	1.38
A5	50	50.1	8.04	20.9	0.43	8.02	7.38	0.52	0.03	3.40	1.19	1.26
A6	60	52.9	5.82	5.19	0.94	9.09	8.41	2.39	0.07	3.80	-2.7	1.06
BO	0	45.7	9.46	22.2	0.96	10.41	7.46	2.12	0.06	2.80	1.57	1.31
B1	10	47.8	12.7	26.0	0.33	3.88	5.65	0.98	0.04	1.30	0.75	1.34
B2	20	46.8	8.83	16.0	0.58	6.31	9.08	2.90	0.03	3.40	1.32	1.22
B3	30	55.6	8.84	0.05	0.51	8.69	6.18	1.00	0.03	0.51	-6.0	1.00
B4	40	49.4	14.6	0.05	0.40	6.94	5.51	1.45	0.03	1.10	-4.0	1.00
B5	50	56.1	10.3	0.05	0.48	7.97	3.25	0.30	0.04	0.11	-6.3	1.00
B6	60	45.5	17.1	0.05	0.70	9.76	7.88	1.51	0.03	0.22	-8.5	1.00
C0	0	47.2	12.1	30.3	0.47	7.14	4.80	1.86	0.03	1.50	1.60	1.40
C1	10	32.6	27.9	16.0	0.41	7.09	5.54	0.64	0.03	0.44	0.09	1.31
C2	20	47.8	10.3	30.4	0.64	4.91	6.74	1.36	0.03	2.00	1.61	1.40
C3	30	50.0	9.22	34.4	0.52	5.24	5.38	1.05	0.06	1.40	2.01	1.43
C4	40	49.8	10.4	33.8	0.35	6.49	4.40	0.50	0.03	1.10	1.08	1.43
C5	50	43.3	13.0	22.3	0.46	5.46	8.98	0.83	0.03	4.00	2.54	1.33
C6	60	47.2	11.3	12.9	0.33	4.99	7.03	1.15	0.04	3.30	-0.2	1.17
D0	0	49.6	11.5	15.8	0.65	8.09	6.29	0.22	0.03	0.37	-1.8	1.20
D1	10	54.3	6.62	4.68	0.27	5.61	8.58	2.18	0.03	2.50	-2.1	1.05
D2	20	41.5	18.1	12.7	0.66	7.41	5.06	1.54	0.11	0.99	-0.8	1.19
D3	30	55.3	8.43	0.05	0.33	7.10	7.70	0.86	0.03	0.70	-5.3	1.00
B4	40	58.6	7.83	0.05	0.38	5.61	6.81	0.29	0.03	0.11	-6.5	1.00
D5	50	44.2	24.0	0.05	0.63	7.23	5.65	1.19	0.03	0.15	-12	1.00
D6	60	55.8	9.36	0.05	0.32	7.82	5.36	0.77	0.03	0.20	-7.4	1.00

Table D7: Chemical analysis of ore samples from untreated UMK experiment

Sample	Depth (cm)	Mn, tot	Fe, tot	MnO_2	Al_2O_3	SiO_2	CaO	MgO	K_2O	CO_2	LOI	**MnO_x**
AO	0	37.9	5.23	23.7	0.56	6.06	14.09	3.02	0.09	15.0	14.7	**1.39**

A1	10	36.7	4.59	23.5	0.38	5.36	15.67	3.28	0.12	18.0	16.1	**1.40**
A2	20	37.6	5.27	19.3	0.5	6.33	15.23	3.25	0.04	15.0	13.8	**1.33**
A3	30	37.8	4.65	11.6	1.24	8.27	17.77	2.41	0.14	14.0	9.73	**1.19**
A4	40	38.1	5.61	10.4	0.34	6.44	18.31	2.93	0.05	13.0	10.0	**1.17**
A5	50	43.0	5.23	7.27	0.67	6.09	17.88	2.87	0.11	10.0	4.02	**1.11**
A6	60	43.3	5.82	0.05	1.20	7.68	18.51	3.45	1.91	4.80	-3.9	**1.00**
BO	0	36.8	4.42	17.5	0.44	5.26	17.73	2.87	0.05	17.0	14.8	**1.30**
B1	10	39.1	4.81	18.3	0.51	5.69	15.78	3.33	0.05	15.0	12.1	**1.30**
B2	20	41.6	5.05	4.66	0.43	6.37	19.58	3.63	0.02	9.50	3.86	**1.07**
B3	30	50.6	7.17	0.05	0.67	5.12	12.42	2.84	0.13	2.40	-3.8	**1.00**
B4	40	46.8	5.77	0.05	1.21	7.23	19.24	2.99	0.02	1.20	-4.3	**1.00**
B5	50	45.7	6.2	0.05	0.62	6.48	18.26	3.1	0.04	10.0	-1.8	**1.00**
B6	60	42.1	5.77	0.05	1.70	8.88	21.45	3.33	0.33	3.90	-3.1	**1.00**
C0	0	36.1	5.86	21.8	0.50	6.37	14.35	3.17	0.07	14.0	15.5	**1.38**
C1	10	36.5	5.21	21.3	0.42	5.76	14.56	3.5	0.05	15.0	16.2	**1.37**
C2	20	33.2	6.59	20.7	0.41	6.25	16.44	2.65	0.08	16.0	16.9	**1.39**
C3	30	34.5	4.72	20.2	0.55	5.32	17.86	2.43	0.08	18.0	17.3	**1.37**
C4	40	35.4	4.91	19.4	0.50	5.85	17.07	3.01	0.07	16.0	15.8	**1.35**
C5	50	37.4	5.13	18.4	0.40	5.39	17.26	2.38	0.07	14.0	13.8	**1.31**
C6	60	39.8	6.36	9.87	0.90	6.77	18.63	3.48	0.11	7.80	4.51	**1.16**
D0	0	38.2	4.68	24.3	0.53	5.20	15.13	3.24	0.12	14.0	14.1	**1.40**
D1	10	39.5	6.56	13.6	0.52	5.73	16.14	2.93	0.07	11.0	8.49	**1.22**
D2	20	42.4	5.18	4.92	0.38	6.27	19.69	3.17	0.01	7.50	3.16	**1.07**
D3	30	43.4	5.97	1.98	0.57	6.78	18.75	3.55	0.16	5.60	0.46	**1.03**
B4	40	42.0	8.11	0.05	0.68	6.87	19.67	3.98	0.01	2.90	-2.3	**1.00**
D5	50	41.8	7.43	0.05	0.63	7.59	21.87	4.36	0.02	4.20	-3.7	**1.00**
D6	60	45.0	5.91	0.05	2.18	8.57	16.57	4.1	0.37	7.60	-3.5	**1.00**

Table D8: Chemical analysis of ore samples from untreated Mintek mix experiment

Sample	Depth (cm)	Mn, tot	Fe, tot	MnO_2	Al_2O_3	SiO_2	CaO	MgO	K_2O	CO_2	LOI	**MnO_x**
AO	0	36.9	5.52	23.2	0.81	5.73	14.0	2.81	0.10	15	15.1	**1.40**
A1	10	36.9	5.30	24.6	0.41	5.09	15.7	2.19	0.11	16	15.6	**1.42**
A2	20	34.1	7.13	24.9	0.49	6.65	13.8	2.87	0.23	15	16.3	**1.46**
A3	30	36.4	4.63	22.7	0.43	5.55	15.8	2.75	0.15	16	16.1	**1.39**
A4	40	32.1	5.56	15.9	0.50	14.1	14.1	2.50	0.09	20	15.3	**1.31**
A5	50	38.1	6.29	7.45	1.32	6.52	16.1	2.95	0.38	17	9.06	**1.12**
A6	60	39.5	4.83	1.24	0.43	5.82	14.6	2.65	0.39	7.3	-0.1	**1.02**
BO	0	34.2	9.16	15.8	0.39	6.68	18.3	3.57	0.10	24	15.4	**1.29**
B1	10	39.9	5.69	19.9	0.54	4.40	19.9	3.39	0.26	12	10.5	**1.32**
B2	20	39.5	4.83	20.4	0.43	5.82	14.6	2.65	0.39	13	11.9	**1.33**
B3	30	34.2	9.16	8.18	0.39	6.68	18.3	3.57	0.10	12	8.49	**1.15**
B4	40	39.9	5.69	2.89	0.54	4.40	19.9	3.39	0.26	11	5.12	**1.05**
B5	50	45.0	6.66	0.05	0.55	6.97	19.2	3.24	0.16	1.9	-3.9	**1.00**
B6	60	49.6	5.38	0.05	0.59	6.47	17.6	2.60	0.15	0.77	-5.9	**1.00**
C0	0	33.8	5.27	25.8	0.35	5.23	15.1	4.02	0.24	17	19.0	**1.48**
C1	10	33.4	5.46	12.6	0.44	5.18	17.8	2.76	0.03	18	17.4	**1.24**
C2	20	37.7	4.74	25.4	0.62	6.20	15.1	2.92	0.08	15	14.5	**1.43**
C3	30	29.5	6.14	15.7	0.84	15.1	14.8	3.26	0.13	15	15.3	**1.34**
C4	40	37.0	4.89	20.2	0.48	11.9	13.4	2.66	0.25	12	11.6	**1.34**
C5	50	42.7	5.49	4.81	0.50	6.29	16.9	3.00	0.07	8.7	4.41	**1.07**
C6	60	34.6	11.4	0.05	0.48	18.0	16.2	2.14	0.78	1.8	-3.2	**1.00**
D0	0	39.4	8.08	29.7	0.41	4.71	10.8	2.51	0.26	12	12.6	**1.48**
D1	10	39.8	4.83	27.8	0.41	5.30	13.5	3.03	0.06	13	13.5	**1.44**
D2	20	40.5	4.79	23.9	0.27	5.28	14.6	2.05	<0.03	13	12.4	**1.37**
D3	30	36.0	4.31	19.7	0.34	7.12	17.0	2.35	0.04	16	14.9	**1.35**

B4	40	42.3	6.26	2.27	0.41	6.89	19.2	3.95	<0.03	4.8	0.26	**1.03**
D5	50	47.3	5.14	0.05	0.60	8.22	18.0	4.14	0.10	0.62	-5.0	**1.00**
D6	60	52.7	5.09	0.05	0.62	7.61	11.2	3.46	0.23	0.37	-6.2	**1.00**

Appendix F: Material Balances

Material balances from all pilot experiments are calculated in heat and material balance module in HSC Chemistry version 10.0.4.3. The material balances are per 100kg of input material.

Table E1: Material balance for untreated Comilog pilot experiment

Raw Materials	Mass (kg)	MnO_2	Mn_2O_3	Mn_3O_4	MnO	Fe_2O_3	FeO	SiO_2	Al_2O_3	CaO	MgO	K_2O	CO_2	Fix C
UCom	29.33	23.81	0.69			1.38		1.04	1.73		0.35	0.35	-	
Sinter	46.0	-	-	24.3	12.32		2.40	3.08	3.42		0.14	0.34	-	
Limestone	8.67									4.86			3.81	
Coke	16.0							0.68	0.68					14.6
Sum	100	23.81	0.69	24.3	12.32	1.38	2.40	4.80	5.83	4.86	0.49	0.69	-	14.6
Kmol		0.27	0.004	0.11	0.17	0.01	0.03	0.08	0.06	0.087	0.01	0,01	0.087	1.22
Products	Mass (kg)	Mn	Fe	C	Si		MnO	SiO_2	Al_2O_3	CaO	MgO	K_2O	CO	CO_2
HCFeMn	44.14	37.95	2.83	3.09	0.27									
Slag	22.06						5.98	4.23	5.83	4.86	0.49	0.69		
Gas	33.80												21.57	12.24
Sum	100	37.95	2.83	3.09	0.27		5.98	4.23	5.83	4.86	0.49	0.69	21.57	12.24
Kmol		0.69	0.05	0.26	0.01		0.08	0.07	0.06	0.09	0.01	0.01	0.77	0.28
Metal Composition (mass %)						Slag composition (mass %)							Gas composition (%)	
Mn	Fe	C	Si		MnO	SiO_2	CaO	MgO	Al_2O_3	K_2O		CO	CO_2	
86.0	6.4	7.0	0.6		27.1	19.2	22.0	2.2	26.4	3.1		63.8	36.2	

Table E2: Material balance for preheated Comilog pilot experiment

Raw Materials	Mass (kg)	MnO_2	Mn_2O_3	Mn_3O_4	MnO	Fe_2O_3	FeO	SiO_2	Al_2O_3	CaO	MgO	K_2O	CO_2	Fix C
HCom	29.1	5.06	18.9			1.35		1.35	2.03		-	0.34	-	
Sinter	45.5	-	-	23.8	12.1		2.35	3.02	3.36	0.40	0.13	0.34	-	
Limestone	9.2									5.17			4.06	
Coke	16.2							0.69	0.69					14.8
Sum	100	5.06	18.9	23.8	12.1	1.35	2.35	5.06	6.08	5.57	0.49	0.68	-	14.8
Kmol		0.06	0.12	0.10	0.17	0.01	0.03	0.08	0.06	0.10	0.03	0.08	0.09	1.23
Products	Mass (kg)	Mn	Fe	C	Si		MnO	SiO_2	Al_2O_3	CaO	MgO	K_2O	CO	CO_2
HCFeMn	44.0	37.8	2.77	3.08	0.36									
Slag	24.7						6.65	4.30	6.08	5.57	0.13	0.68		
Gas	32.4												25.2	7.46
Sum	100	37.8	2.77	3.08	0.36		6.65	4.30	6.08	5.57	0.13	0.68	25.2	7.46
Kmol		0.69	0.05	0.26	0.01		0.09	0.07	0.06	0.10	0.003	0.01	0.90	0.17
Metal Composition (mass %)						Slag composition (mass %)							Gas composition (%)	
Mn	Fe	C	Si		MnO	SiO_2	CaO	MgO	Al_2O_3	K_2O		CO	CO_2	
85.6	6.9	7.0	0.4		28.4	18.4	23.8	0.56	26.0	2.9		77.1	22.9	

Table E3: Material balance for prereduced Comilog pilot experiment

Raw Materials	Mass (kg)	MnO_2	Mn_2O_3	Mn_3O_4	MnO	Fe_2O_3	FeO	SiO_2	Al_2O_3	CaO	MgO	K_2O	CO_2	Fix C
RCom	28.3	-	23.2			1.35		1.35	2.02		-	0.34	-	
Sinter	46.5	-	-	24.6	12.5		2.43	3.12	3.47		-	0.35	-	
Limestone	9.09									5.09			4.0	
Coke	16.2							0.71	0.35					15.1
Sum	100	-	23.2	24.6	12.5	1.35	2.43	5.18	5.84	5.09	-	0.69	4.0	15.1
Kmol		-	0.15	0.11	0.18	0.08	0.03	0.09	0.06	0.09	-	0.01	0.09	1.26
Products	Mass (kg)	Mn	Fe	C	Si		MnO	SiO_2	Al_2O_3	CaO	MgO	K_2O	CO	CO_2
HCFeMn	46.5	39.8	284	3.26	0.61									
Slag	20.4						4.84	3.89	5.84	5.09	-	0.69		
Gas	33.1												24.9	8.21
Sum	100	39.8	2.84	3.26	0.61		4.84	3.89	5.84	5.09	-	0.69	24.9	8.21
Kmol		0.73	0.05	0.27	0.02		0.07	0.07	0.06	0.09	-	0.01	0.89	0.19
Metal Composition (mass %)						Slag composition (mass %)							Gas composition (%)	
Mn	Fe	C	Si		MnO	SiO_2	CaO	MgO	Al_2O_3	K_2O		CO	CO_2	
85.6	6.1	7.0	1.3		23.8	19.1	25.0	-	28.7	3.39		75.2	24.8	

Table E4: Material balance for untreated Nchwaning pilot experiment

Raw Materials	Mass (kg)	MnO_2	Mn_2O_3	Mn_3O_4	MnO	Fe_2O_3	FeO	SiO_2	Al_2O_3	CaO	MgO	K_2O	CO_2	Fix C
UNch	66.5	-	42.6	2.05	-	10.2	-	2.73	0.23	4.32	0.91	-	3.41	-
Sinter	15.6	-	-	8.26	4.13	-	0.90	0.90	1.20	-	-	0.23	-	-
Coke	17.9	-	-	-	-	-	-	0.91	0.68	-	-	-	-	16.4
Sum	100	-	42.6	10.3	4.13	10.2	0.90	4.54	2.11	4.32	0.91	0.23	3.41	16.4
Kmol		-	0.27	0.05	0.06	0.06	0.01	0.08	0.02	0.08	0.02	0.002	0.08	1.36
Products	Mass (kg)	Mn	Fe	C	Si		MnO	SiO_2	Al_2O_3	CaO	MgO	K_2O	CO	CO_2
HCFeMn	48.1	36.8	7.88	3.37	0.10									
Slag	16.4						4.48	4.34	2.06	4.33	0.91	0.23		
Gas	35.5												27.0	8.49
Sum	100	36.8	7.88	3.37	0.10		4.48	4.34	2.06	4.33	0.91	0.23	27.0	8.49
Kmol		0.67	0.14	0.28	0.004		0.06	0.07	0.02	0.08	0.02	0.002	0.97	0.19
Metal Composition (mass %)						Slag composition (mass %)						Gas composition (%)		
Mn	Fe	C	Si		MnO	SiO_2	CaO	MgO	Al_2O_3	K_2O		CO	CO_2	
76.4	16.4	7.0	0.2		27.4	26.6	26.5	5.6	12.6	1.4		76.1	23.9	

Table E5: Material balance for preheated Nchwaning pilot experiment

Raw Materials	Mass (kg)	MnO_2	Mn_2O_3	Mn_3O_4	MnO	Fe_2O_3	FeO	SiO_2	Al_2O_3	CaO	MgO	K_2O	CO_2	Fix C
HNch	66.7	2.25	42.8	-	-	9.01	-	3.60	0.45	3.91	1.58	-	3.07	-
Sinter	15.7	-	-	8.11	4.05	-	0.90	0.90	1.13	0.27	0.09	0.23	-	-
Coke	17.6	-	-	-	-	-	-	0.91	0.68	-	-	-	-	16.1
Sum	100	2.25	42.8	8.11	4.05	9.01	0.90	5.41	2.26	4.18	1.67	0.23	3.07	16.1
Kmol		0.03	0.27	0.04	0.06	0.06	0.01	0.09	0.02	0.08	0.04	0.002	0.07	1.34
Products	Mass (kg)	Mn	Fe	C	Si		MnO	SiO_2	Al_2O_3	CaO	MgO	K_2O	CO	CO_2
HCFeMn	46.9	36.3	7.0	3.28	0.3									
Slag	18.2						5.05	4.77	2.26	4.18	1.67	0.23		
Gas	34.9												26.2	8.70
Sum	100	36.3	7.0	3.28	0.3		5.05	4.77	2.26	4.18	1.67	0.23	26.2	8.70
Kmol		0.66	0.13	0.27	0.01		0.07	0.08	0.02	0.08	0.04	0.002	0.94	0.2
Metal Composition (mass %)						Slag composition (mass %)						Gas composition (%)		
Mn	Fe	C	Si		MnO	SiO_2	CaO	MgO	Al_2O_3	K_2O		CO	CO_2	
77.4	14.9	7.0	0.6		27.8	26.3	23.0	9.2	12.4	1.3		74.9	25.1	

Table E6: Material balance for prereduced Nchwaning pilot experiment

Raw Materials	Mass (kg)	MnO_2	Mn_2O_3	Mn_3O_4	MnO	Fe_2O_3	FeO	SiO_2	Al_2O_3	CaO	MgO	K_2O	CO_2	Fix C
RNch	75.3	-	15.3	33.6	-	9.15	-	3.89	0.46	5.04	0.92	-	3.95	2.97
Sinter	7.0	-	-	3.62	1.93	-	0.48	0.48	0.48	-	-	-	-	-
Coke	17.7	-	-	-	-	-	-	0.98	0.49	-	-	-	-	16.2
Sum	100	-	15.3	37.3	1.93	9.15	0.48	5.35	1.43	5.04	0.92	-	3.95	19.2
Kmol		-	0.10	0.16	0.03	0.04	0.07	0.09	0.01	0.09	0.02	-	0.09	1.60
Products	Mass (kg)	Mn	Fe	C	Si		MnO	SiO_2	Al_2O_3	CaO	MgO	K_2O	CO	CO_2
HCFeMn	46.2	35.6	6.78	3.23	0.56									
Slag	16.4						4.37	4.14	1.43	5.04	0.92	-		
Gas	35.5												42.7	-4.85
Sum	100	35.6	6.78	3.23	0.56		4.37	4.14	1.43	5.04	0.92	-	42.7	-4.85
Kmol		0.65	0.12	0.27	0.02		0.06	0.07	0.01	0.09	0.02	-	1.53	-0.11
Metal Composition (mass %)						Slag composition (mass %)						Gas composition (%)		
Mn	Fe	C	Si		MnO	SiO_2	CaO	MgO	Al_2O_3			CO	CO_2	
77.1	14.7	7.0	1.2		27.5	26.1	31.7	5.8	9.0			>100		

Table E7: Material balance for untreated UMK pilot experiment

Raw Materials	Mass (kg)	MnO_2	Mn_2O_3	Mn_3O_4	MnO	Fe_2O_3	FeO	SiO_2	Al_2O_3	CaO	MgO	K_2O	CO_2	Fix C
UNch	47.0	-	17.4	9.57	-	3.19	-	3.19	0.29	6.67	1.45	-	5.22	-
Sinter	36.0	-	-	19.0	9.64	-	1.98	2.27	2.83	-	-	0.28	-	-
Coke	17.0	-	-	-	-	-	-	0.86	0.58	-	-	-	-	15.6
Sum	100	-	17.4	28.6	9.64	3.19	1.98	6.32	3.70	6.67	1.45	0.28	3.41	15.6
Kmol		-	0.11	0.13	0.14	0.02	0.03	0.11	0.04	0.12	0.04	0.003	0.12	1.30
Products	Mass (kg)	Mn	Fe	C	Si		MnO	SiO_2	Al_2O_3	CaO	MgO	K_2O	CO	CO_2
HCFeMn	44.6	37.6	3.77	3.13	0.18									
Slag	21.4						3.36	5.94	3.70	6.67	1.45	0.28		
Gas	34.0												29.5	4.51
Sum	100	37.6	3.77	3.13	0.18		3.36	5.94	3.70	6.67	1.45	0.28	29.5	4.51
Kmol		0.68	0.07	0.26	0.006		0.05	0.10	0.04	0.12	0.04	0.003	1.05	0.10
Metal Composition (mass %)						Slag composition (mass %)							Gas composition (%)	
Mn	Fe	C	Si		MnO	SiO_2	CaO	MgO	Al_2O_3	K_2O		CO	CO_2	
84.1	8.5	7.0	0.4		15.7	27.8	31.2	6.8	17.3	1.3		86.7	13.3	

Table E8: Material balance for untreated Mintek mix pilot experiment

Raw Materials	Mass (kg)	MnO_2	Mn_2O_3	Mn_3O_4	MnO	Fe_2O_3	FeO	SiO_2	Al_2O_3	CaO	MgO	K_2O	CO_2	Fix C
UMK	46.3	-	15.0	10.6	-	3.3	-	2.64	0.24	7.28	1.44	0.08	5.76	-
Kudumane	29.3	-	8.7	7.3	-	2.0	-	1.64	0.16	5.01	0.63	-	3.91	-
Quartz	9.7		-		-	-	0.15	8.94	0.22	0.22	-	-	-	
Coke	14.7	-	-	-	-	-	-	0.79	0.47	-	-	-	-	13.4
Sum	100	-	23.8	17.9	-	5.3	0.15	14.0	1.09	12.5	2.07	0.08	9.82	13.4
Kmol		-	0.15	0.08	-	0.03	0.002	0.22	0.01	0.22	0.05	0.001	0.22	1.12
Products	Mass (kg)	Mn	Fe	C	Si		MnO	SiO_2	Al_2O_3	CaO	MgO	K_2O	CO	CO_2
HCFeMn	33.7	26.0	3.79	2.36	1.57									
Slag	30.8						4.42	10.7	1.09	12.5	2.07	0.08		
Gas	35.5												25.9	9.55
Sum	100	26.0	3.79	2.36	1.57		4.42	10.7	1.09	12.5	2.07	0.08	25.9	9.55
Kmol		0.47	0.07	0.20	0.06		0.06	0.18	0.01	0.22	0.05	0.001	0.93	0.22
Metal Composition (mass %)						Slag composition (mass %)							Gas composition (%)	
Mn	Fe	C	Si		MnO	SiO_2	CaO	MgO	Al_2O_3	K_2O		CO	CO_2	
77.1	11.2	7.0	4.7		14.4	34.6	40.6	6.7	3.5	0.3		73.1	26.9	

The degree of prereduction for the charge mixtures was calculated at 0 and 100%. When all the Mn_3O_4 from the reduction of higher manganese oxides is reduced at low temperatures before the Boudouard reaction is activated, the degree of prereduction was defined to be 100%. If all CO_2 from the reduction of Mn_3O_4 is consumed by the Boudoard reaction, the degree of prereduction is 0%. However, the actual degree of prereduction from the charge blends was calculated from the experimental off-gas measurements. Therefore, the variation of carbon consumption with degree of prereduction is illustrated in Figure E1.

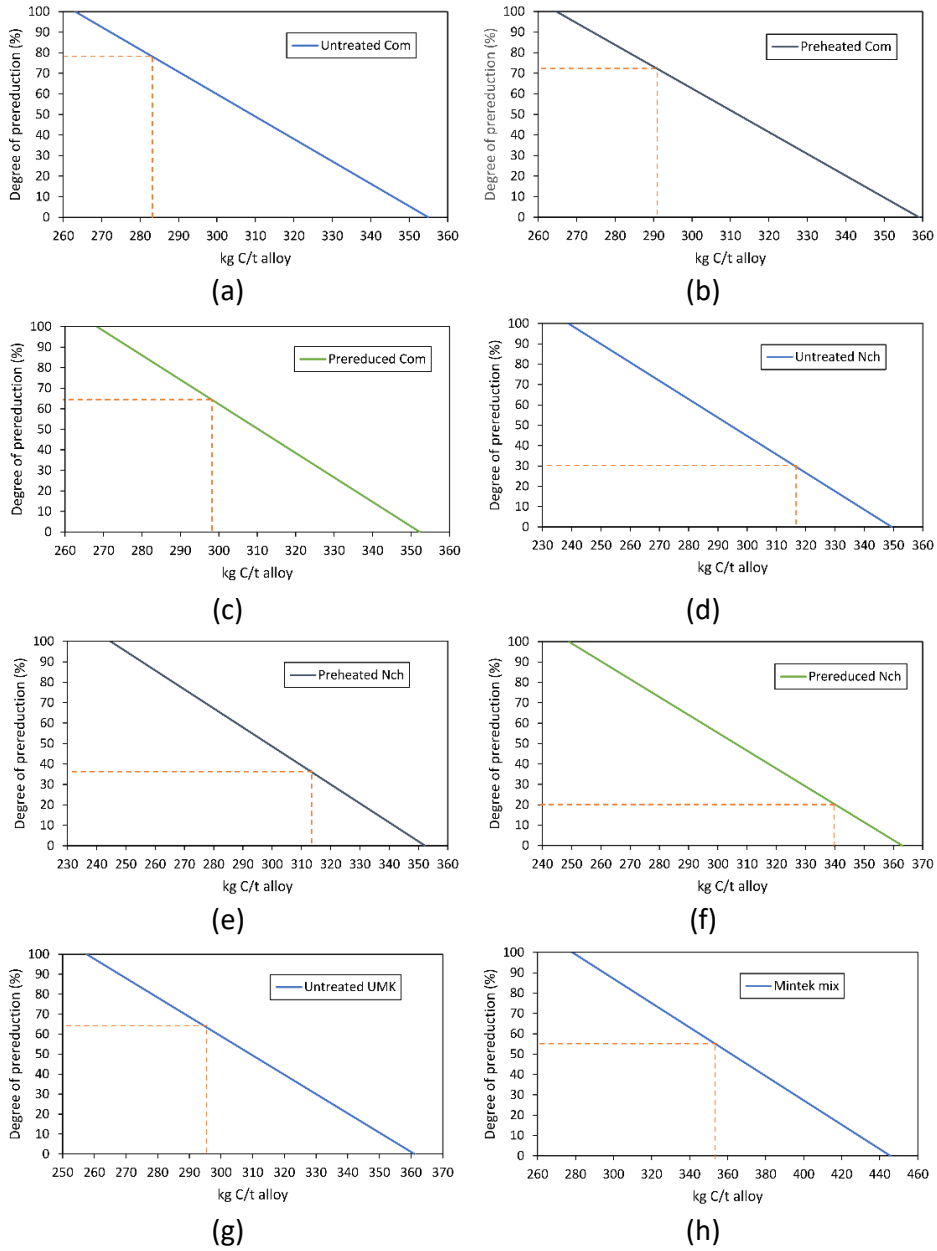

Figure E1: Variation of the degree of prereduction with carbon consumption. The degree of prereduction is estiamted based on the calculated carbon consumption.

ISBN 978-82-326-6532-7 (printed ver.)
ISBN 978-82-326-6929-5 (electronic ver.)
ISSN 1503-8181 (printed ver.)
ISSN 2703-8084 (online ver.)

NTNU
Norwegian University of
Science and Technology